ABSTRACT

SAFAVI ZADEH, SEYED SHAHIN. Evaluating the Effect of MICP Treatment on the Structural and Chemical Stabilization of Coal Ash Impoundments (Under the direction of Dr. Brina M. Montoya and Mohammed A. Gabr).

Coal ash is a by-product of coal combustion process in power plants. A significant portion of the generated coal ash is disposed of in impoundments and landfills. Gradual deposition of coal ash can induce excessive shear stresses and lead to internal and external structural instabilities. Furthermore, the leaching of trace elements from these materials is a concern especially with respect to the potential of increasing the concentrations in the environment above the drinking water or ecological system standards. Interdisciplinary research has revealed new techniques to modify engineering properties of subsurface materials. Microbial induced calcium carbonate precipitation (MICP) is a bio-mediated process that has shown the potential for improving the engineering properties of soils as well as the potential of immobilizing trace elements (e.g., Sr 90). Work in this thesis is focused on evaluating the effect of MICP treatment on Class-F coal ash as a means of addressing the above mentioned concerns. For this purpose, two different areas are investigated, first, the effect of MICP on engineering properties of coal ash, and second, the effect of MICP on leachable trace elements, specifically arsenic and selenium.

Factors affecting the kinetics and chemistry of MICP reactions are studied using chemical equilibrium modeling and experimental batch testing. A column testing program was performed to optimize MICP treatment recipes and to develop MICP treatment protocol. The developed protocol was applied on Class-F coal ash materials from three different sources to evaluate their response to the proposed treatment protocol. Studied factors affecting the MICP treatment of coal ash materials included; a) *S. pasteurii* bacteria activity inhibitors, b) bacteria filtration by coal ash particles, c) particle roughness and its effect on calcium carbonate attachment, d) calcium

carbonate precipitation inhibitors, and e) nucleation sites for calcium carbonate precipitation. A modified consolidation setup was developed and utilized to evaluate the effect of MICP treatment on the compressibility properties of the studied coal ash materials. The treatment protocol was successfully applied to two coal ash materials and the large strain and small strain parameters were evaluated. Finally, the effect of MICP treatment on leaching of arsenic and selenium from the studied coal ash material was studied conducting the chemical equilibrium modeling and batch testing.

Monitoring the shear wave velocity of the MICP treated specimens of the studied coal ash materials showed three different responses, while treated identically. Two of the studied ash materials exhibited significant improvement in stiffness during treatment. However, one of the coal ash materials showed only slight improvement of shear stiffness during treatment. Additionally, the results of acid washing and SEM/EDS analysis indicated a lack of calcium carbonate in the treated coal ash that showed slight improvement in stiffness properties. Evaluating possible causative factors revealed the important role of carbon content in MICP treatment of coal ash material and calcium carbonate precipitation. Given the glassy and spherical nature of the coal ash particles, the carbon content seems to provide initial nucleation sites that are fundamental to the formation of calcium carbonate precipitates.

The large-strain results in modified consolidation setup demonstrated a reduction in compressibility (C_C and m_v) for treated coal ash in comparison to untreated material. This reduction was more at lower levels of applied vertical stresses. The effect of MICP treatment on large-strain parameters (i.e., C_C, m_v, k, C_V, m_v) and small-strain parameters (i.e., α', β') were examined, and the correlations between small-strain parameters (i.e., C_C) and large-strain parameters (i.e., α', β') were determined from experimental data. These correlations can be used

to predict the compressibility behavior of treated and untreated coal ash material while their level of stress and shear wave velocity are known.

Lastly, based on the combined results of adsorption/ desorption chemical equilibrium and batch testing, a backbone curve which correlated the arsenic solubility to pH of the solution was proposed. Comparing the backbone curve and leaching results from MICP treated samples in batch testing seems to indicate that with MICP treatment arsenic was not immobilized through co-precipitation. On the other hand, and based on the results of batch testing, MICP treatment seems to immobilize selenium through co-precipitation. It is therefore suggested that with the knowledge of the effect of pH on leaching behavior response, the MICP treatment can be designed and staged such that the pH of the solution is best suited for decreasing the solubility of the target key elements of concern.

Evaluating the Effect of MICP Treatment on the Structural and Chemical Stabilization of Coal Ash Impoundments

by
Seyed Shahin Safavi Zadeh

A dissertation submitted to the Graduate Faculty of
North Carolina State University
in partial fulfillment of the
requirements for the degree of
Doctor of Philosophy

Civil Engineering

Raleigh, North Carolina

2018

APPROVED BY:

_____	_____
Dr. Brina M Montoya Committee Co-Chair	Dr. Mohammed A Gabr Committee Co-Chair
_____	_____
Dr. Detlef Knappe	Dr. Ashly Cabas

DEDICATION

To my parents,

Without their endless support, love, sacrifice, and encouragement, none of this would have been possible

and

To my lovely wife, Mahboube, who has been incredibly patient and supportive of me while I finish my graduate studies.

BIOGRAPHY

Seyed Shahin (Shahin) Safavi Zadeh was born on July 14, 1987. Shahin is the younger son of two sons born to Ahmad Safavi zadeh and Fariba Bagheri. He was born and grew in Tehran, Iran. Shahin enrolled at Amirkabir University of Technology in Tehran, Iran in summer 2005, where he pursued his Bachelor of science in Civil Engineering, graduating in January 2010. Shahin continued his studies at Amirkabir University of Technology, pursuing a Master's degree in Geotechnical Engineering and focused on his dissertation, titled "Effect of top soil improvement on performance of Rafts and Piled Rafts with different widths in soft clayey soil". He earned his Master of science degree in Jan 2013. In Jan 2014, he moved to the United States and enrolled at North Carolina State University in Raleigh, North Carolina to pursue his Ph.D. degree in Civil Engineering under the guidance of Dr. Brina M Montoya and Dr. Mohammed A Gabr.

.

ACKNOWLEDGMENTS

First, I would like to gratefully and sincerely thank my advisors, Dr. Brina M Montoya and Dr. Mohammed A Gabr, for their support, trust, guidance, understanding, patience, and encouragement throughout my research. I also thank my committee members, Dr. Detlef Knappe and Dr. Ashly Cabas, who supported me through this journey. This work could not have been done without the support from Electrical Power Research Institute (EPRI). I also want to express appreciation to Jake Rhoads and Jerry Atkinson who helped me numerous times to get around the mechanical and equipment related issues in the lab. I also feel grateful for the opportunity to work and interact with all my other colleagues: Ashkan Nafisi, Arash Bozorgi, Kai Feng, Jinung Do, Casey Shanahan, Chien Ting, and Atefeh Zamani.

Last but not least, I would like to thank my parents, Ahamd Safavizadeh and Fariba Bagheri, my lovely wife, Mahboube Ameri, and my brother, Shahyan Safavizadeh, for their unconditional love and support.

TABLE OF CONTENTS

LIST OF TABLES x

LIST OF FIGURES xii

1. CHAPTER 1: Introduction 1

1.1 Introduction 2

1.2 Concerns and issues related to coal ash impoundments 2

1.3 Microbial Induced Calcium Carbonate Precipitation 3

1.4 Outline and Scope of Dissertation 4

1.4.1 Objective 4

1.4.2 Scope 5

1.5 References 7

2. CHAPTER 2: Characteristics of Coal Ashes 8

2.1 Introduction 9

2.2 Material and method 10

2.2.1 X-Ray diffraction (XRD) 10

2.2.2 EPA 3051a (Microwave acid digestion of sediments, sludges, soils, and oils) 11

2.2.3 Carbon Content 12

2.2.4 Scanning electron microscopy (SEM) and energy-dispersive X-Ray Spectroscopy (EDS) 12

2.2.5 Specific Gravity 13

2.2.6 Particle size distribution 13

2.2.7 Liquid Limit 13

2.3 Results 14

2.3.1 X-Ray diffraction (XRD) 14

2.3.2 Microwave acid digestion method (i.e., EPA 3051A) 16
2.3.3 Carbon content 17
2.3.4 Morphology and elemental analysis of particles (SEM/EDS) 18
2.3.5 Specific gravity 21
2.3.6 Particle size distribution 21
2.3.7 Liquid limit 22
2.4 Discussion 23
2.5 References 28
3. Chapter 3: Factors affecting the Kinetics of Urea Hydrolysis via *Sporoscarcina Pasteurii* 29
3.1 Introduction 30
3.2 Material and methods 33
3.2.1 Bacteria and growth condition 33
3.2.2 Evaluating relationship between conductivity and hydrolyzed urea 33
3.2.3 Reaction Modeling 35
3.2.4 Evaluating relationship between cell density and hydrolyzed urea 36
3.2.5 Column Tests 36
3.3 Results and discussion 38
3.3.1 Chemical reactions in MICP 38
3.3.2 Correlation between electrical conductivity and hydrolyzed urea 40
3.3.3 Kinetics of reaction 42
3.3.4 Initial rate of reaction: Bacterial populations and initial concentration of urea 44
3.3.5 Application of monitoring reaction in column test 46
3.4 Conclusion 48
3.5 References 51

4. Chapter 4: Microbial Induced Calcium Carbonate Precipitation on Coal Ash 52
4.1 Introduction 53
4.2 Materials 56
4.2.1 Physiochemical characteristic 56
4.2.2 Engineering characteristics 58
4.3 Methods 59
4.3.1 Bacteria and growth condition 59
4.3.2 Column Test and the Method of Treatment 60
4.3.3 Calcium Carbonate Content 62
4.3.4 Morphology and elemental analysis of particles 62
4.3.5 Bacterial activity 63
4.4 Treatment Protocol and Response 65
4.4.1 MICP and Cementation Mass 68
4.5 Potential factors affecting the MICP treatment process 74
4.5.1 D) Calcium carbonate precipitation inhibitors 80
4.5.2 E) Nucleation sites for calcium carbonate precipitation 83
4.6 Summary and Conclusion 85
4.7 References 88
5. Chapter 5: Effect of MICP Treatment on Engineering Properties of Coal Ash 91
5.1 Introduction 92
5.2 Materials 94
5.2.1 Chemical composition of ash material 94
5.2.2 Particle size distribution of the material 95
5.2.3 Morphology of the particles 97

5.3 Methods 97
5.3.1 Bacteria and growth condition 97
5.3.2 Treatment protocol using modified consolidation test 98
5.3.3 Calcium Carbonate Content 101
5.4 Results and Discussion 101
5.4.1 MICP treatment and its effect on shear wave velocity and hydraulic conductivity 101
5.4.2 Large-strain behavior - Volume change-stress behavior 105
5.4.3 Large strain behavior – hydraulic conductivity (k) and coefficient of consolidation (C_v) 110
5.4.4 Small-strain behavior 113
5.4.5 Correlation between small-strain and large-strain parameters 117
5.5 Summary and conclusions 117
5.6 References 121
6. Chapter 6: Effect of MICP Treatment on Arsenic and Selenium Leaching Behavior of Coal Ash 123
6.1 Introduction 124
6.2 Material and Methods 127
6.2.1 Adsorption/desorption modeling in MINTEQ 128
6.2.2 Bacteria and growth condition 130
6.2.3 Batch testing 131
6.3 Results and Discussion 132
6.3.1 Arsenic adsorption modeling 132
6.3.2 Selenium adsorption modeling 135
6.3.3 Batch testing 136
6.3.4 Results of batch testing on other trace elements 144

6.4 Summary and Conclusions 152
6.5 References 154
7. Chapter 7: Summary, Contribution, and Future work 156
7.1 Introduction 157
7.2 Summary and general discussion 157
7.3 Factors affecting the kinetic of urea hydrolysis via *S. Pasteurii* 160
7.3.1 Summary 160
7.3.2 Contributions 161
7.3.3 Future work 161
7.4 Microbial induced calcium carbonate precipitation on coal ash 162
7.4.1 Summary 162
7.4.2 Contributions 162
7.4.3 Future work 163
7.5 Effect of MICP treatment on engineering properties of coal ash 164
7.5.1 Summary 164
7.5.2 Contributions 164
7.5.3 Future work 165
7.6 Effect of MICP treatment on arsenic and selenium leaching behavior of coal ash 166
7.6.1 Summary 166
7.6.2 Contributions 166
7.6.3 Future work 167
REFERENCES 168

APPENDICES 174

APPENDIX A: Chemical equilibrium modeling of MICP..... 175

APPENDIX B: Adsorption/desorption Modeling……..... 181

LIST OF TABLES

Table 2-1. Data analysis of XRD measurements of three coal ashes using ICDD database..... 14

Table 2-2. Major, minor and trace elements of three coal ash materials in this study..... 16

Table 2-3. Carbon content of three coal ash materials. 17

Table 2-4. D_{10}, D_{30}, D_{50}, D_{60}, coefficient of uniformity (C_u), and coefficient of curvature (C_c) of the studied coal ash materials. 21

Table 2-5. Liquid limit of coal ash materials, using fall-cone and Casagrande method..... 23

Table 2-6. Comparison between results of elements concentrations of three coal ash materials in this study and previously reported data..... 25

Table 2-7. Comparison between physical parameters reported in this study and literature (Bachus and Santamarina 2012). 26

Table 3-1. List of possible solids and their solid equilibrium constants with existence of Ca^{2+}, CO_3^{2-} , OH^-, and O^{2-} (Benjamin 2014). 36

Table 3-2. Ottawa 50-70 grain size characteristic..... 37

Table 3-3. Specifications of columns tests on Ottawa 50-70 37

Table 3-4. Chemical formula and dissociation constants at 25oC of carbonic acid and ammonium ion... 38

Table 3-5. Column test results ([HU] and % of calcite)..... 48

Table 4-1. Results of data analysis of XRD measurements using ICDD database..... 57

Table 4-2. Major, minor and trace elements, results of EPA 3051A method..... 57

Table 4-3. Engineering properties of coal ashes 59

Table 4-4. Recipes of bio-cementation solutions 66

Table 4-5. Recipe of the short column test on three coal ashes (CA1, CA2, CA3)..... 68

Table 4-6. CaCO3 % of the samples in short column test after treatment 71

Table 4-7. PSD characteristics of original coal ashes and modified CA2..... 76

Table 5-1. results of data analysis of XRD measurements using ICDD database. 95

Table 5-2. Engineering properties of coal ashes 96

Table 5-3. Treatment solution recipe. 100

Table 5-4. Summarized results of this study 103

Table 6-1. Results of data analysis of XRD measurements using ICDD database. 127

Table 6-2. Major, minor and trace elements, results of EPA 3051A method. 128

Table 6-3. Recipe of salt solutions in batch testing one. 131

Table 6-4. Recipes of the solutions in batch testing two. 132

Table 6-5. Resultant pH and concentrations (i.e., [As] and [Se]) of batch testing 1 and 2. 137

Table 6-6. Adsorption constants of three fly ashes were used for selenium adsorption/desorption modeling. 141

Table 6-7. pH and trace elements measurements in batch testing 1. 144

Table 6-8. pH and trace elements measurements in batch testing 2. 145

Table 7-1. Chemical solutions in treatment protocol recipes. 158

LIST OF FIGURES

Figure 2-1. General transformation of mineral matter in coal during combustion (Kutchko and Kim 2006). 10

Figure 2-2. X-ray diffraction patterns of three coal ash materials 15

Figure 2-3. Proportional percentage of the main crystals in three coal ash materials using XRD data. 15

Figure 2-4. Samples before and after ignition process for carbon content measurement. 17

Figure 2-5. SEM images of the studied coal ash materials in this research. 19

Figure 2-6. BSE images with elemental spectrum, S1) unburned carbon, S2) Mixed grain, S3) typical coal ash particle 20

Figure 2-7. Comparison between particle size distributions of coal ash materials used in this study. 22

Figure 2-8. Fall-cone test data for three coal ash materials. 23

Figure 2-9. Comparison between particle size distributions of coal ash in this study and previous works (Bachus and Santamarina 2012). 26

Figure 2-10. Coal ash particle size distribution reported by (Bachus and Santamarina 2012). 27

Figure 3-1. LogC-pH for a system containing 333 mM Hydrolyzed Urea 39

Figure 3-2. Precipitated calcium carbonate (a) and pH (b) during hydrolyzed urea titration for solutions with different $[CaCl_2]_{in}$ 41

Figure 3-3. Correlation between electrical conductivity and concentration of hydrolyzed urea. 41

Figure 3-4. Effect of cell population and initial concentration of Urea on the kinetic of hydrolyzing urea 43

Figure 3-5. Measured pH values for the samples with OD =1.16 in batching test program. 43

Figure 3-6. a) Effect of initial urea concentration on initial rate of hydrolysis, b) effect of initial urea concentration on initial rate of hydrolysis. 44

Figure 3-7. Effect of initial substrate (i.e., urea) concentration and enzyme concentration on the rate of urea hydrolysis (Fidaleo and Lavecchia 2003). 45

Figure 3-8. Treatment process, V_S (m/s) vs. Number of injection. 46

Figure 4-1. Particle size distribution of coal ashes. 58

Figure 4-2. Column test details, sample preparation. 61

Figure 4-3. Schematic of devices used for column test. 61

Figure 4-4. Correlation between electrical conductivity and concentration of hydrolyzed urea. 64

Figure 4-5. Shear wave velocity of the specimens at the center height of the columns, optimizing recipe. 67

Figure 4-6. pH (solid line) and Conductivity (dashed line) of the collected effluent after each injection. 67

Figure 4-7. Monitored shear wave velocity during the treatment of short column tests. 70

Figure 4-8. Results of EDS analysis a) on CA1-3 sample b) on CA2-3 sample, both of them were collected from the bottom of the specimen. 72

Figure 4-9. SEM images of CA1 before (left images) and after treatment (right images) with different magnifications. The sample was collected from bottom of CA1-3 specimen. 73

Figure 4-10. Evaluation of bacterial activity in the leachates from coal ashes performing a batch testing. 75

Figure 4-11. a comparison between particle size distribution of the modified CA2 and the original coal ashes. 76

Figure 4-12 . Effect of MICP treatment on VS of modified CA2 77

Figure 4-13. Surface texture of the spherical particles using SEM images; a) CA1, b) CA2. 79

Figure 4-14. a) Agglomerated particles of CA1, b) Typical morphology of CA2. 80

Figure 4-15. Mapping of elements using EDS method; a.1) CA1, EDS image, b.1) CA2, EDS image, c.1) CA3, EDS image, a.2) CA1, iron mapping, b.2) CA2, iron mapping, c.2) CA3, iron mapping a.3) CA1, elemental analysis, b.3) CA2, elemental analysis, c.3) CA3, elemental analysis. 83

Figure 4-16. Effect of decreasing carbon content on MICP treatment 85

Figure 5-1. Particle size distribution of coal ashes. 96

Figure 5-2. Morphology of studied coal ash materials using SEM method 97

Figure 5-3. Schematic diagram of modified consolidation set-up..... 100

Figure 5-4. Components of modified odometer test 101

Figure 5-5. Monitored shear wave velocity during treatment for both CA1 and CA3 specimens..... 102

Figure 5-6. SEM images of treated CA1 and CA4 material..... 103

Figure 5-7. Semi-log correlation between VS and a) CaCO3 content, and b) Void ratio (e) for CA1 and CA3 specimens. 104

Figure 5-8. Hydraulic conductivity as a function of a) CaCo3 content, b) Void ratio, e..... 105

Figure 5-9. Variation of void ratio with vertical effective stress in modified oedometer set up..... 106

Figure 5-10. A comparison between the resultant compression index of the untreated material of this study with the range of previously reported data (Modified from (Bachus and Santamarina 2012)..... 107

Figure 5-11. Strain and shear wave velocity response of CA1 material specimens with different level of cementation while loading-unloading cycles were applied on. 109

Figure 5-12. Strain and shear wave velocity response of CA1 material specimens with different level of cementation while loading-unloading cycles were applied on. 110

Figure 5-13. Effect of incremental loading on a) hydraulic conductivity (a), b) coefficient of volume change (m_v), c) coefficient of consolidation (c_v)..... 112

Figure 5-14. Parametric study on the effect of φ on α factor and β exponent of studied coal ash materials. 114

Figure 5-15. Effect of cementation and loading on small strain behavior of CA1 and CA3 material..... 116

Figure 5-16. Correlation between α' factors and β'exponents for all the studied specimens. 116

Figure 5-17. Correlation between CC and small strain parameters; a) β'exponents and b) α' factors..... 117

Figure 6-1. Validation of arsenic modeling in chemical equilibrium model using the reported data and parameters by Wang et al. 2008..... 134

Figure 6-2. Validation of selenium modeling using the reported data and parameters by Wang et al. 2007 for FA#1008 fly ash. 136

Figure 6-3. Effect of salts on arsenic solubility in batch testing based on the suggested background pH-[As] curve. 139

Figure 6-4. Effect of MICP treatment on arsenic solubility in batch testing based on the suggested background pH-[As] curve. 139

Figure 6-5. Results of batch testing 1 and curve fitting using three different fly ashes' parameter... 143

Figure 6-6. Results of the samples were treated using different MICP treatment recipes. 143

Figure 6-7. [B] vs. pH of the samples in batch testing 1. 146

Figure 6-8. [B] vs. pH of the samples in batch testing 2. 146

Figure 6-9. [Cr] vs. pH of the samples in batch testing 1. 147

Figure 6-10. [Cr] vs. pH of the samples in batch testing 2. 147

Figure 6-11. [Mo] vs. pH of the samples in batch testing 1. 148

Figure 6-12. [Mo] vs. pH of the samples in batch testing 2. 148

Figure 6-13. [V] vs. pH of the samples in batch testing 1. 149

Figure 6-14. [V] vs. pH of the samples in batch testing 2. 149

Figure 6-15. [Sr] vs. pH of the samples in batch testing 1. 150

Figure 6-16. [Sr] vs. pH of the samples in batch testing 2. 150

1. CHAPTER 1: Introduction

1.1 Introduction

Coal is one of the primary sources of energy to produce electricity in the United States. Coal combustion generates about 110 million tons of coal combustion residuals (CCRs) annually (CCRs Rules 2015). Although there has been an increased utilization of CCRs, more than half of the produced by-products are disposed as waste (Harkness et al. 2016a). These wastes are usually deposited in surface impoundments and landfills. Coal ash is often disposed of in wet impoundments, and there are over 500 of them across the country.

1.2 Concerns and issues related to coal ash impoundments

Coal ash is a unique sediment compared to natural soils because of its distinct particle and bulk scale characteristics (Bachus and Santamarina 2015), and its chemical composition. This uniqueness leads to challenging stability related issues. From a mechanical stability perspective, global and internal stability issues are the points of concern. Saturated coal ash has the potential to be liquefied under self-weight while the additional waste is deposited and the induced shear stress overwhelm the shear strength. On December 22, 2008, the Tennessee Valley Authority (TVA) Kingston Fossil Plant experienced a coal ash slurry spill due to saturated coal ash losing shear strength and liquefying as additional material was deposited and stored in the storage pond. The failure of the storage pond led to contamination of an area of about 300 acres, which included two tributaries to the Tennessee River, Emory River, and Clinch River. The spill of coal ash in Dan River, Eden, North Carolina is an example of internal stability issues. On February 2nd, 2014, a 48-inch storm water pipe that was located beneath a storage pond broke which allowed ash and water from the impoundment to flow into the Dan River. The spill into the Dan River compromised the water quality of the river, which in turn jeopardized wildlife and drinking water. In addition, leaching of trace elements within the stored coal ash into surface water and groundwater has also

increased awareness of the environmental and human health risk of CCR disposal and storage. Reports of 40 confirmed and 113 potential damage cases of storage and disposal of CCRs has been documented in the EPA CCR Management Rule. 60% of these damage cases are surface water and groundwater contamination (CCRs Rules 2015). The concentration of chemical elements such as arsenic (As), boron (B), molybdenum (Mo), strontium (Sr), chromium (Cr), selenium (Se) are usually higher than leachate from natural soil sediment, and these elements might put risk into the health of human being and wildlife. The concentration of leaching elements depends on the source of coal and the combustion process of the power plant. Based on the composition of coal ash and solution condition, the concentration of major, minor and trace elements could be different. Several factors are affecting both chemical and mechanical stability of coal ash ponds, and its level could be highly variable from one coal ash impoundment to another. With increased legislature pressure to close coal ash ponds in the near future, such as the current environment in North Carolina, appropriate technology should be developed to safely and more efficiently close the ponds and prevent the likelihood of heavy metal leaching and mechanical instability, which can lead to contamination of the surrounding environment.

1.3 Microbial Induced Calcium Carbonate Precipitation

Interdisciplinary research has given rise to innovative methods to improve subsurface material (DeJong et al. 2010). Subsurface microbes can promote calcium carbonate precipitation by increasing the subsurface alkalinity (DeJong et al. 2010) utilizing several biogeochemical reactions such as urea hydrolysis, nitrate reduction, sulfate reduction and iron reduction (DeJong et al. 2010). The hydrolysis of urea by the widely distributed microbes is one of the new biologically occurring reactions that can generate carbonate ions without an associated production of protons (Whiffin 2004), and most of the current studies on microbial induced calcite precipitation (MICP) focus on

hydrolyzing urea. The employed microbes break down the urea into carbonate and ammonium in MICP reaction. This reaction will lead to saturation of solution while enough calcium ions present in the solution. Precipitation of calcium carbonate crystals is one of the products. These crystals precipitate between soil particles and bond them together which increases the strength and stiffness of the soil (Mortensen et al. 2011). The primary properties of the soil that can be changed significantly during MICP treatments include permeability, stiffness, compressibility, shear strength, and volumetric behavior (DeJong et al. 2010). The ability to change these soil properties provide numerous possibilities for applications (DeJong et al. 2010). Increasing shear strength for different purposes (Lin et al. 2015), and decreasing the erodability (Shanahan and Montoya ; Shanahan and Montoya 2016) and liquefaction potential(Zamani and Montoya 2015; Montoya et al. 2012) are some of the applications of this approach. MICP has been used not only for improving strength and stiffness of the soil, but also for capturing the solid-phase of contaminations (Warren et al. 2001a).

MICP is a novel approach to improve the stability of the coal ash sediments by using a natural, biological process to cement the particles together. Bio-cementation (another name of MICP) seems to be ideal because the cementation may increase the strength of the coal ash and prevent particle migration while maintaining the permeability of the sediment to allow for drainage. On the other hand, the bio-cementation process tends to capture heavy metals into the calcite cement through co-precipitation and may prevent the heavy metals from migrating.

1.4 Outline and Scope of Dissertation

1.4.1 Objective

The primary objective of this research is evaluating the effect of MICP treatment on coal ash impoundments. For this purpose, two different areas are considered to be investigated, first, the

effect of MICP on engineering properties of coal ash, second, its effect on leachable trace elements. This research is the first study has investigated the effect of MICP treatment on the coal ash material.

1.4.2 Scope

The variability in the morphology and chemical composition of coal ash sediments lead to different behaviors, not only in comparison to natural sediments but also between power plant sources. Different characteristics of the coal ashes cause different geochemical behavior. To understand and predict the response of coal ash in different conditions, a proper and adequate knowledge of chemical and mechanical properties is necessary. Three coal ash materials from three different coal power plants are used in this study. In **Chapter 2**, "Characteristics of Coal Fly Ashes", the results of a wide variety of tests for characterization of physical properties and chemical compositions are presented.

To optimize the treatment process of MICP, a proper understanding of the principles controlling the biochemical reaction is necessary. In this process, there are chemical and biological factors affecting the concentration, rate, and crystallization of products. Microbes are the main reason for controlling the rate of urea hydrolysis in MICP treatment. In **Chapter 3**, "Factors affecting the Kinetics of Urea Hydrolysis via", the influential parameters affecting the equilibrium chemical reactions and kinetics of MICP treatment are evaluated.

The particle size distribution, morphology and chemical composition of coal ash render a different behavior in comparison to the previously MICP treated materials. In **Chapter 4** "Microbial Induced Calcium Carbonate Precipitation on Coal Ash", the MICP treatment protocol for coal ash material is developed and different possible factors affecting the MICP treatment of this material are investigated.

The impact of MICP treatment on engineering properties of coal material is unknown. In **Chapter 5**, "Effect of MICP Treatment on Engineering Properties of Coal Ash", the developed treatment protocol is implemented in the coal ash specimens in a modified oedometer setup to evaluate the effect of MICP treatment on small-strain and large-strain parameters.

One of the main concerns regarding coal ash impoundments is trace elements leaching into nearby surface waters and groundwater. Based on the hypothesized statements, MICP has the potential of immobilization of some trace elements. In order to assess this theory, in **Chapter 6**, "Effect of MICP Treatment on Arsenic and Selenium Leaching Behavior of Coal Ash", the effect of MICP treatment of coal on mobilization/immobilization of selenium and arsenic are explored through sets of batch testing and adsorption/desorption chemical equilibrium modeling.

Finally, in chapter 7, "Summary, Contribution, and Future work", the conducted work is summarized, the contributions from the work are explicitly discussed, and the future work of each chapter are presented.

1.5 References

Bachus, R. C., and Santamarina, J. C. (2015). "Geotechnical Properties and Diagenesis of Ponded Fly Ash." 326-333.

CCRs Rules. (2015). "Hazardous and Solid Waste Management System; Disposal of Coal Combustion Residuals From Electric Utilities: Final Rule." United States Environmental Protection Agency, Washington, DC.

DeJong, J. T., Mortensen, B. M., Martinez, B. C., and Nelson, D. C. (2010). "Bio-mediated soil improvement." *Ecol.Eng.*, 36(2), 197-210.

Harkness, J. S., Sulkin, B., and Vengosh, A. (2016). "Evidence for coal ash ponds leaking in the southeastern United States." *Environ.Sci.Technol.*, 50(12), 6583-6592.

Lin, H., Suleiman, M. T., Brown, D. G., and Kavazanjian Jr, E. (2015). "Mechanical behavior of sands treated by microbially induced carbonate precipitation." *J.Geotech.Geoenviron.Eng.*, 142(2), 04015066.

Montoya, B. M., DeJong, J. T., Boulanger, R. W., Wilson, D. W., Gerhard, R., Ganchenko, A., and Chou, J. (2012). "Liquefaction mitigation using microbial induced calcite precipitation." *GeoCongress 2012: State of the Art and Practice in Geotechnical Engineering*, 1918-1927.

Mortensen, B. M., Haber, M. J., DeJong, J. T., Caslake, L. F., and Nelson, D. C. (2011). "Effects of environmental factors on microbial induced calcium carbonate precipitation." *J.Appl.Microbiol.*, 111(2), 338-349.

Shanahan, C., and Montoya, B. M. (2016). "Erosion Reduction of Coastal Sands Using Microbial Induced Calcite Precipitation." *Geo-Chicago 2016*, 42-51.

Shanahan, C., and Montoya, B. M. "Erosion Reduction of Coastal Sands Using Microbial Induced Calcite Precipitation." *Geo-Chicago 2016*, 42-51.

Warren, L. A., Maurice, P. A., Parmar, N., and Ferris, F. G. (2001). "Microbially mediated calcium carbonate precipitation: implications for interpreting calcite precipitation and for solid-phase capture of inorganic contaminants." *Geomicrobiol.J.*, 18(1), 93-115.

Whiffin, V. S. (2004). "Microbial CaCO3 precipitation for the production of biocement". Murdoch University.

2. CHAPTER 2: Characteristics of Coal Ashes

2.1 Introduction

Coal is composed of combustible organic matter with a variable amount of inorganic elements. The coal combustion process produces solids coal combustion residuals (CCRs). The physical and chemical behavior of coal ashes is controlled by the source of coal, boiler and its operating conditions, and post-combustion condition (Kim 2002). During combustion, minerals in coal become fluid at high temperature and are then cooled. In a pulverized coal (PC) fire boiler, the furnace operating temperatures are typically more than 1400^0c (Kutchko and Kim 2006). At these temperatures, the mineral matter within the coal may oxidize, decompose, fuse, disintegrated or agglomerate (i.e., illustrated in Figure 2-1). Rapid cooling in the post-combustion zone results in the formation of spherical, amorphous particles. Expansion of trapped volatile matter can cause the particles to form a hollow cenosphere. Minerals with high melting points may remain relatively unchanged. The heating and cooling have a significant effect on the composition and morphology of each particle (Clarke 1993). Therefore, the physiochemical properties of fly ash are not unique and can be significantly different from various sources of power plants (Kutchko and Kim 2006).

The characteristics of three coal ashes from three different power plants, which are the studied material of this research, are evaluated in this chapter. These physicochemical properties are used in the next chapters to discuss the reason for different behavior during MICP treatment process.

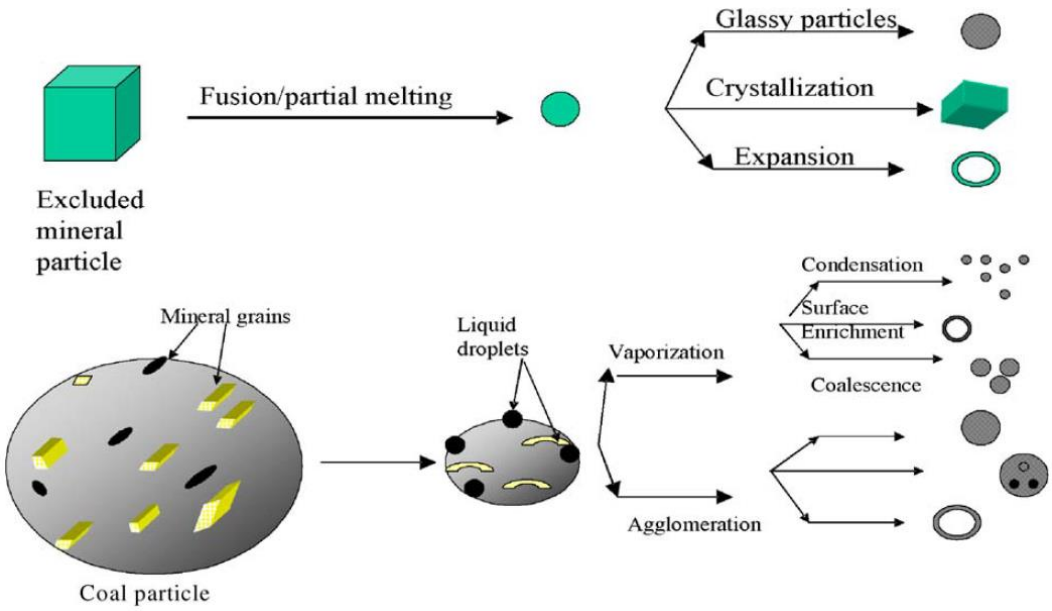

Figure 2-1. General transformation of mineral matter in coal during combustion (Kutchko and Kim 2006).

2.2 Material and method

Three coal ash materials are studied in this research, and they are referred as CA1, CA2, and CA3 materials. Their physiochemical properties are widely investigated, and the results are presented in this chapter. For this purpose, their chemical composition are determined using X-Ray diffraction, EPA 3051 method (i.e., microwave assisted acid digestion) and Carbon content measurement. The morphology, surface texture, as well as the elemental composition of particles are analyzed using SEM (i.e., scanning electron microscopy) method. Pycnometer, hydrometery, sieve analysis, and fall-cone method were the tools to measure specific gravity, particle size distribution and liquid limit of coal ashes.

2.2.1 X-Ray diffraction (XRD)

X-ray diffraction (XRD) qualitatively identifies the crystalline phases of the coal ash sample. In this machine, electrons hit a solid sample and x-rays are emitted. When the x-rays hit a crystal

structure, some x-rays diffract based on this crystal structure, but other x-rays penetrate further into the sample until colliding into a crystal. The machine reads all of the angles of diffracted, scattered x-rays and their intensities to create a pattern. These patterns are plotted, creating a diffractogram relating diffracted intensity to diffraction angle.

PANalytical Empyrean X-ray diffractometer with a cukα radiation was used to perform the XRD test in the analytical instrumentation facility, North Carolina State University. The step size was 0.026 degree, the counting time per step was 447 seconds, and the scan angle was from 10 to 90^0. High Score Plus software is used with an International Centre for Diffraction Data (ICDD) XRD database to analyze the data.

2.2.2 EPA 3051a (Microwave acid digestion of sediments, sludges, soils, and oils)

The major, minor, and trace elements concentrations in the coal ash samples were determined using EPA microwave-assisted acid digestion method 3051A (Link et al. 1998). Element One, Inc in Wilmington, NC, performed this test. In EPA 3051A method, half a gram of each of the coal ash samples was digested in duplicate with 10 ml concentrated reagent grade nitric acid in Teflon reaction vessels using a PerkinElmer Multiwave 3000 Anton Paar Microwave Reaction System. After the digestions was completed, the supernatant solutions were extracted and filtered through 0.2 ml syringe filters and were analyzed for metals on a PerkinElmer Elan 6100 Inductively coupled plasma mass spectrometry (ICP-MS) according to EPA Method 6020A. Samples were analyzed for mercury on a PerkinElmer FIMS-100 CVAA mercury analyzer according to EPA Method 7470A. Samples were analyzed for silicon on a PerkinElmer AAnalist 200 according to Standard Methods 3111D.

2.2.3 Carbon Content

To measure carbon content of coal ashes, the crucible was heated to 1000^0C for three hours, and after cooling them down to 110^0C, their dry weight was measured. Around 20 gr of coal ash was placed in a crucible, and it was held in 110^0c for 24 hours. Its dried mass was measured, and then its temperature raised to 500^0c for 24 hours. The ignition temperature of carbon is around 400^0c, and 500^0c is a proper temperature to ignite the carbon parts while maintaining other minerals in the solid phase (Styszko-Grochowiak et al. 2004). The mass of carbon is the subtraction of dried mass before putting and after holding the samples for 24 hours in the furnace.

2.2.4 Scanning electron microscopy (SEM) and energy-dispersive X-Ray Spectroscopy (EDS)

The coal ash samples were analyzed at the Analytical instrumentation facility at NCSU using the SEM equipped with backscattered and secondary electron detectors coupled (BSE) with EDS. The SEM-EDS provides detailed imaging information about the morphology and surface texture of individual particles, as well as the elemental composition of samples. BSE provides visual information based on gray-scale intensity between chemical phases. Backscattered electrons are high-energy electrons that are reflected directly from the specimen surface. The number of electrons backscattered correlates to the atomic number (Kutchko and Kim 2006). For example, a particle consisting of iron (atomic number 26) will be significantly brighter than a particle of carbon (atomic number 6). This phenomenon generates a contrast between phases of different atomic numbers that can easily be distinguished in the backscattered electron image. The elemental composition of a sample is determined using characteristic X-ray spectrum of the specimen being examined. The elemental analysis was performed in a ‘‘spot mode’’ in which the beam is localized on a single area manually chosen within the field of view. The location is represented by a ‘‘+’’

on the provided SEM images. The EDS detector was capable of detecting elements with atomic number equal to or greater than six. The intensity of the peaks in the EDS is not a quantitative measure of elemental concentration, although relative amounts can be inferred from relative peak heights (Kutchko and Kim 2006).

2.2.5 Specific Gravity

Pycnometers were used to determine the specific gravity of the coal ash specimen. Specific gravity is the ratio of the mass of the unit volume of soil to the mass of the same volume of gas-free distilled water at a stated temperature. ASTM Standard Test for Specific Gravity of Soil Solids by Water Pycnometer (ASTM D 854-00 2000) was followed to perform the test. Solids and liquid were under laboratory temperature condition (20^{o}c).

2.2.6 Particle size distribution

A hydrometer analysis was used to determine the grain size distribution of the fine-grained (e.g., < 75 microns) portion of the coal ash, following ASTM D422-63 (ASTM D422-63 2007). The hydrometer test was run in duplicate to evaluate the variability of the coal ash material. Mechanical sieving was also performed on the coal ash material to characterize the course grained (e.g., > 75 microns) ash, following ASTM D422-63.

2.2.7 Liquid Limit

Two common standard methods to measure the liquid limit of soils are Casagrande cup (ASTM D4318-10) and fall-cone (ISO/TS 17892-6:2004) method. The plastic index of the coal ash is small, and it was not possible to measure the plastic limit by using Casagrande method.

To measure the liquid limit of the material using standard fall-cone test, the samples were prepared following the mentioned standard method and placed in the cylindrical cups, with a diameter greater than of 55 mm and depth of at least 30 mm, the depth of penetration of cone was measured for different levels of water content. The depth of penetration versus water content data points were plotted, and the water content corresponding to 20 mm depth of penetration is representing the liquid limit of the material.

2.3 Results

2.3.1 X-Ray diffraction (XRD)

X-Ray diffraction patterns of three coal ash materials are shown in Figure 2-2. These results indicated the existence of expected major elements in all of the coal ashes; Aluminum Silicon Oxide, Silicon Oxide, Iron Oxide, Aluminum Oxide. Quantification of minerals using ICDD database indicated the proportion of each of the mentioned elements in examined samples (i.e., presented in Table 2-1). Figure 2-3 provides a visual percentage chart of different crystals. It should be considered, the presented percentages are dependent on the selected crystals during the analysis, and their summation must be 100%, which does not include all the present crystals.

Table 2-1. Data analysis of XRD measurements of three coal ashes using ICDD database.

Crystal	Formula	Relative Percentage (%)		
		CA1	CA2	CA3
Aluminum Silicate	Al_2SiO_5	53.5	36	44.4
Silicon Oxide	SiO_2	36.4	36	37.4
Iron Oxide	Fe_2O_3	5.1	14	9.1
Calcium Oxide	CaO	1	2	0
Aluminum Oxide	Al_2O_3	4	12	9.1

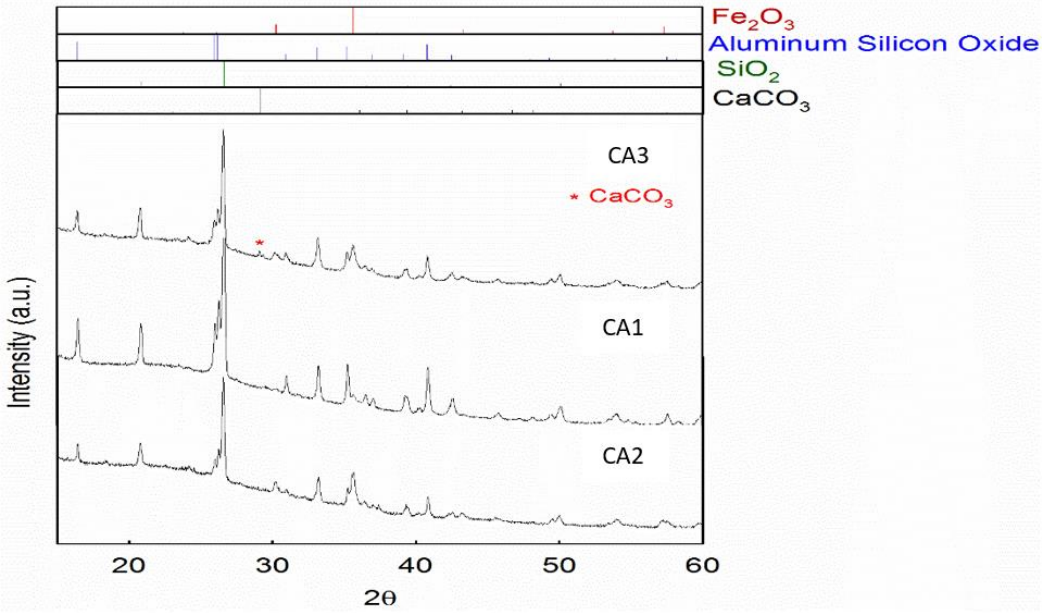

Figure 2-2. X-ray diffraction patterns of three coal ash materials

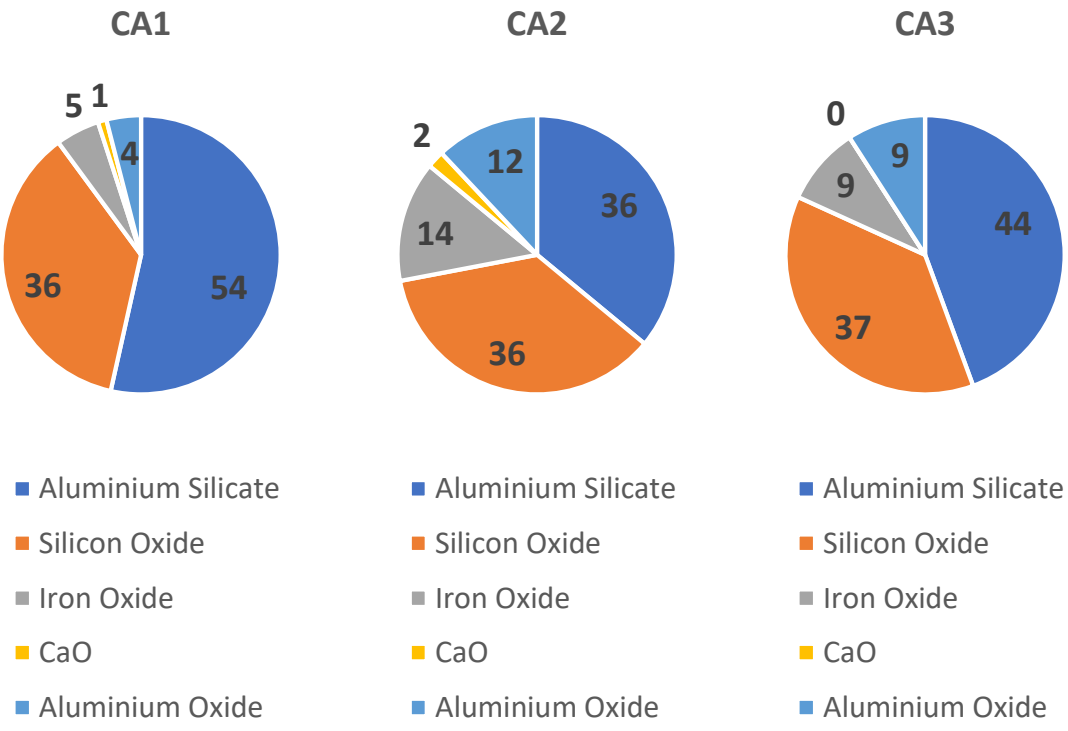

Figure 2-3. Proportional percentage of the main crystals in three coal ash materials using XRD data.

2.3.2 Microwave acid digestion method (i.e., EPA 3051A)

Table 2-2 Provides the results of EPA 3051A method on three coal ash materials including major, minor, and trace elements. These concentrations are the soluble concentration in reagent Nitric acid. The presented concentrations are not representing the total concentration of matters because this reagent is not able to solve all the solids. Silicon crystals are very stable, and to measure its concentration, triple digestion method was used. The presented concentrations of trace elements are almost maximum levels that can be expected in leachate because of the high solubility of Nitric Acid reagent in comparison to usual fluids passing through coal ash in impoundments.

Table 2-2. Major, minor and trace elements of three coal ash materials in this study.

Type	Element	CA1	CA2	CA3
			mg/kg	
Major	Silicon	103011	113698.5	95193
	Iron	19856	72657	62504
	aluminum	14271	17884	22861
	Calcium	5689	9276.5	5117
Minor & Trace elements	potassium	2021	2429.5	3126
	Magnesium	995	891	1654
	Sodium	406	1424	558
	Barium	377	185	447
	Strontium	178	123	285
	Boron	77.9	383	88.5
	Manganese	77.8	66.6	101
	Vanadium	70.5	147	87.6
	Copper	50.3	39.5	56.6
	Arsenic	42.8	33.6	69.4
	Nickel	37.9	45.7	48.7
	Zinc	36.5	146.5	56.4
	Chromium	36.3	95.4	51
	Lead	18.9	44.6	18.3
	Molybdenum	8.76	99.4	4.42
	Selenium	6.01	5.24	6.31
	Cadmium	0.764	2.33	1.07
	Mercury	< 0.193	< 0.197	< 0.200

2.3.3 Carbon content

Carbon content measurements of three coal ash materials were duplicated, and the results, as presented in Table 2-3, covered a wide range of carbon contents, from 0.45% on CA2 coal ash to 8.46% on CA3 coal ash. The photos of the samples before and after putting them into the furnace were taken and the difference between colors is evident in Figure 2-4. The reason is converting black carbon particles to carbon dioxide during ignition and removing them by evaporation.

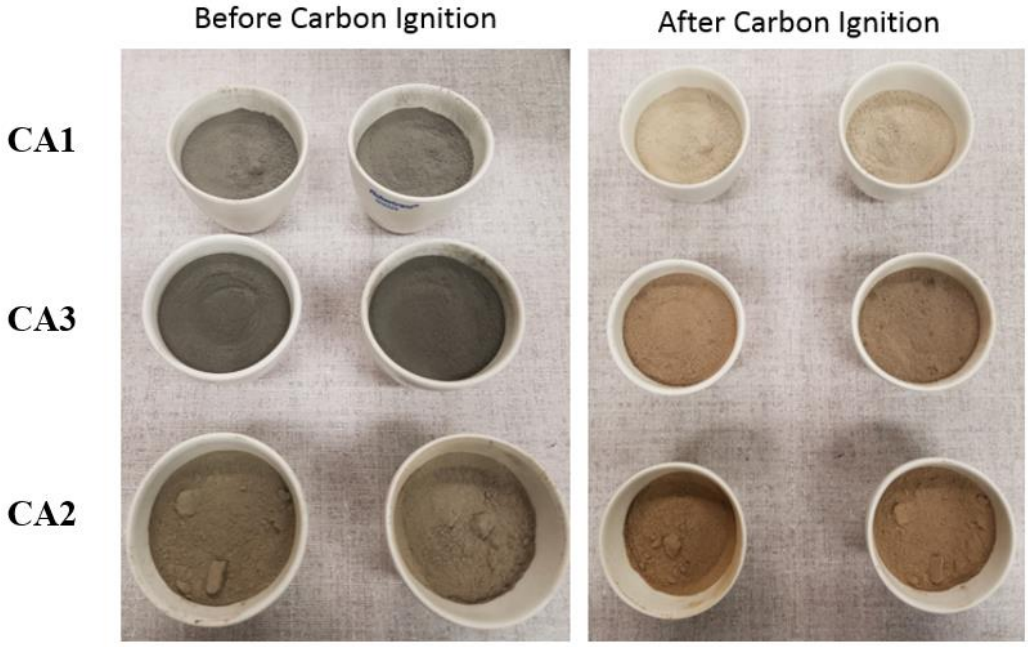

Figure 2-4. Samples before and after ignition process for carbon content measurement.

Table 2-3. Carbon content of three coal ash materials.

Source	% Carbon	% Carbon (Average)
CA1	3.47%	3.42%
	3.36%	
CA2	0.44%	0.48%
	0.53%	
CA3	8.90%	8.46%
	8.02%	

2.3.4 Morphology and elemental analysis of particles (SEM/EDS)

The morphology of coal ash was investigated using SEM images. The results, as presented Figure 2-5, confirm the existence of typical coal ash spheres, cenospheres, unburned carbon, mineral aggregate, agglomerated aggregates, and irregular shaped amorphous particles in all three coal ash materials. The images of CA1 and CA2 coal ash show denser particles in Figure 2-5, which is related to the sample preparation. These pictures are representing some random samples, and they cannot be used quantitatively.

EDS method was used beside SEM images to analyze the matters in some random particles (i.e., demonstrated in Figure 2-6). Based on energy-dispersive X-Ray analysis, brighter particles represent the elements with the higher atomic number, and darker points are related to lower atomic number (Kutchko and Kim 2006). The spectrum-1 (S1) is an irregular particle with a dark color. The EDS analysis revealed that it is mostly an unburned carbon particle. Most of the spheres like spectrum-3 are typical coal ash particles containing mainly silicon and aluminum. The brighter points are, the higher atomic number matters which might be mixed with Aluminum Silicate or might be pure (e.g., Spectrum-2 in Figure 2-6).

CA1

CA2

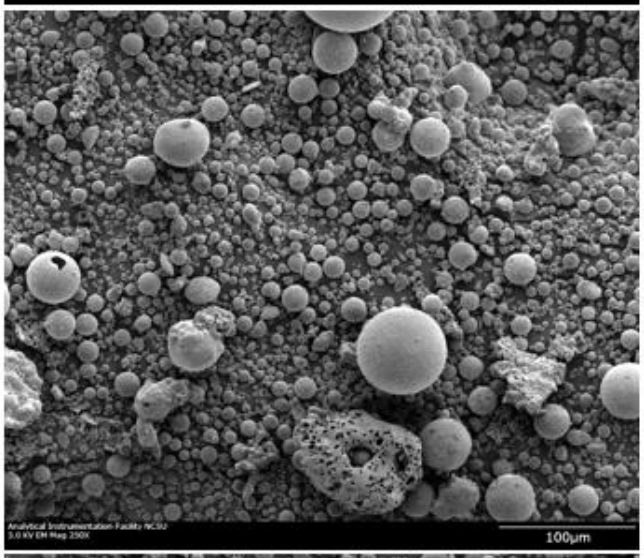

CA3

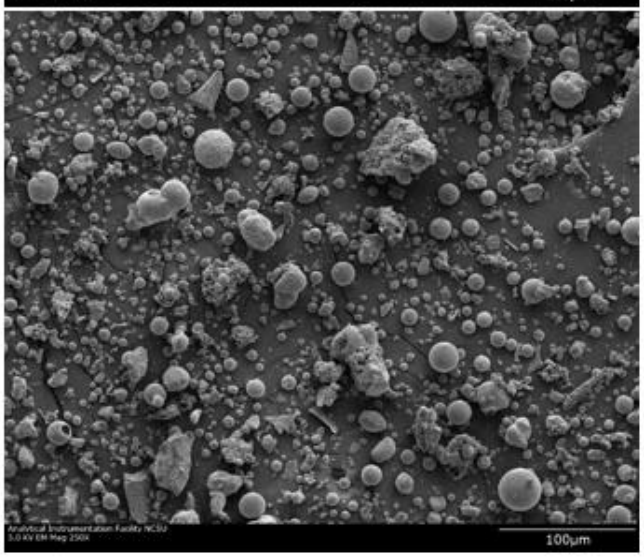

Figure 2-5. SEM images of the studied coal ash materials in this research.

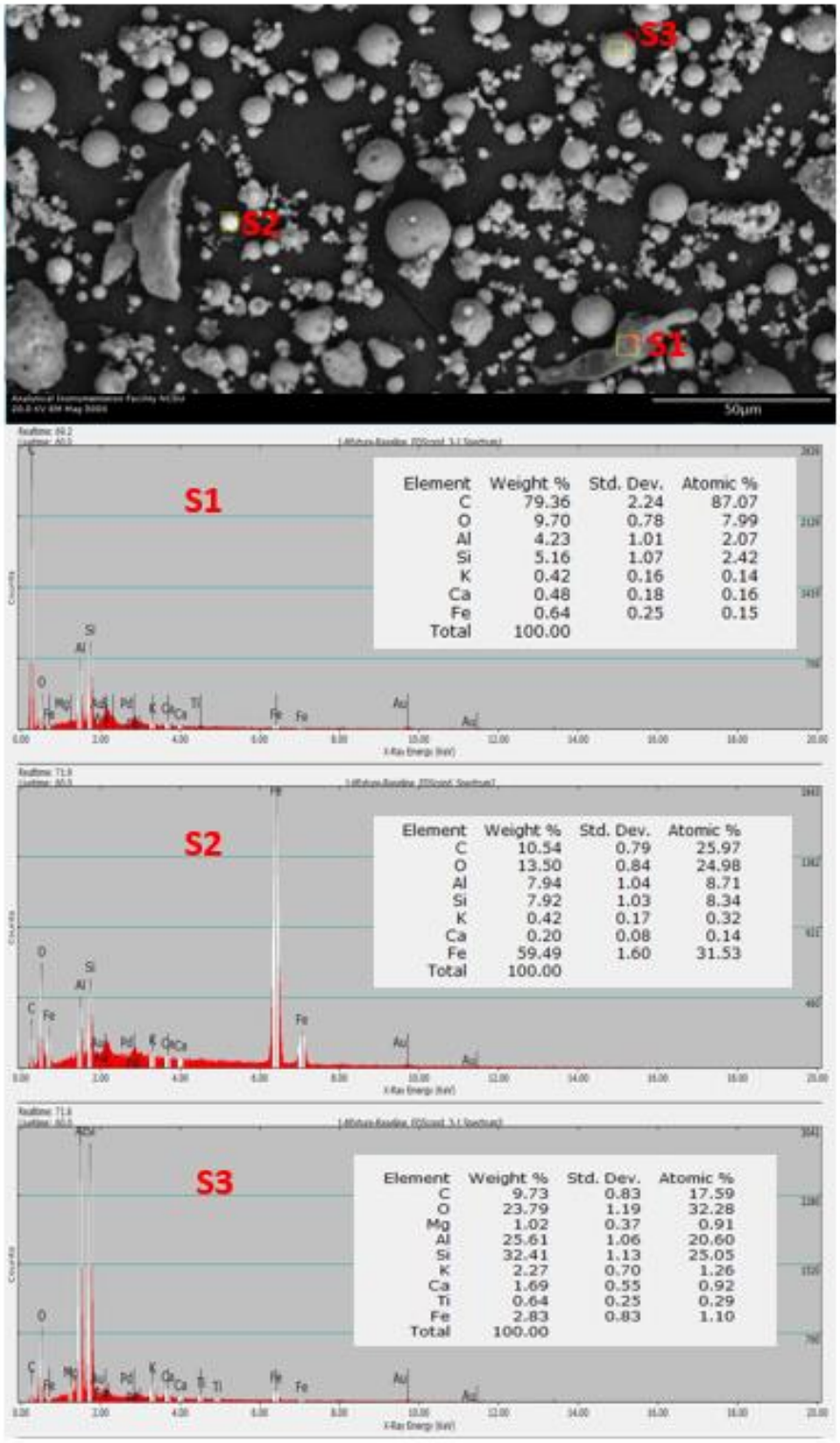

Figure 2-6. BSE images with elemental spectrum, S1) unburned carbon, S2) Mixed grain, S3) typical coal ash particle

2.3.5 Specific gravity

The measurements and calculations showed different values of specific gravity for three coal ash materials. CA1 coal ash has a specific gravity of 2.00, and it is lower than other two coal ash materials' specific gravities, which are 2.34, and 2.35 for CA2 and CA3 coal ash, respectively. These values are in the range of the reported values in previous studies (Bachus and Santamarina 2012).

2.3.6 Particle size distribution

The particle size distribution results, which are a combination of the hydrometer and mechanics sieving tests results, are presented in Figure 2-7 for three studied coal ash materials. All the tests were performed in duplicate, and the reported data are the average values. D-values (i.e., D_{10}, D_{30}, D_{50}, and D_{60}) were extracted from particle size distribution graphs, the coefficient of uniformity (C_u) and coefficient of curvature (C_c) were calculated, and the values are presented in Table 2-4. The CA2 material has the finest grain size distribution in comparison to the other two materials. The percentages of particles greater than sieve #200 (0.075mm) are 35%, 18%, and 8% for CA1, CA2, and CA3 material, respectively. The CA2 material contains 32% of the particles less than 10 um while it is 6% for CA1 material and 14% for CA3 material.

Table 2-4. D_{10}, D_{30}, D_{50}, D_{60}, coefficient of uniformity (C_u), and coefficient of curvature (C_c) of the studied coal ash materials.

Coal ash	D60 (Micron)	D50 (Micron)	D30 (Micron)	D10 (Micron)	Cu	Cc
CA1	48.6	32.3	21.9	13.7	3.6	0.7
CA2	18.7	14.2	9.4	3.8	4.9	1.2
CA3	23.1	20.5	16.0	9.0	2.6	1.2

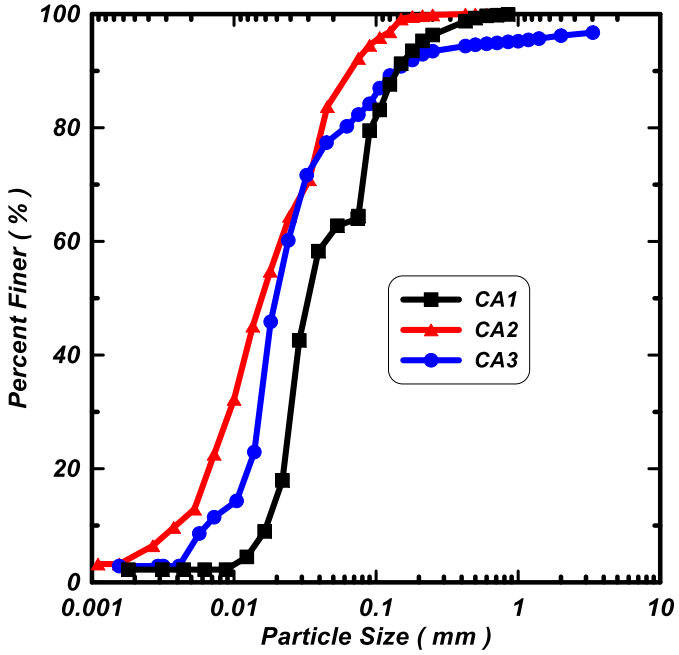

Figure 2-7. Comparison between particle size distributions of coal ash materials used in this study.

2.3.7 Liquid limit

Atterberg limits and indices correlate the state of soil to its water content. There are two methods to measure the liquid limit of the soils: Casagrande cup (ASTM D4318-10) and fall-cone (ISO/TS 17892-6:2004). The plastic index of the coal ash is small, and it was not possible to measure it by Casagrande method. The Casagrande cup method was successfully conducted only on the CA2 material. The fall-cone test was successfully performed on the all three coal ash materials. A summary of the liquid limit measurements is presented in Figure 2-8and Table 2-5.

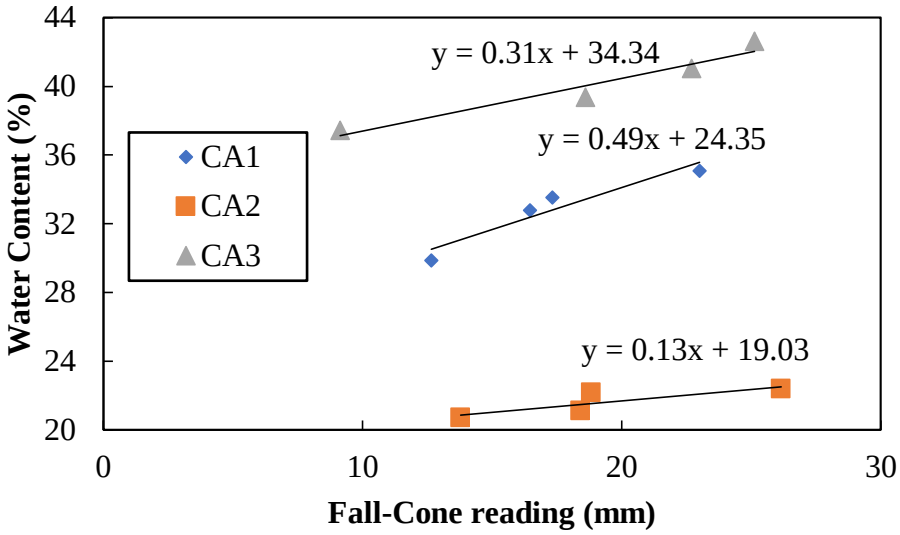

Figure 2-8. Fall-cone test data for three coal ash materials.

Table 2-5. Liquid limit of coal ash materials, using fall-cone and Casagrande method.

Coal Ash Source	LL (Fall-Cone) (%)	LL (Casagrande Cup) (%)
CA1	34	---
CA2	22	21
CA3	41	---

2.4 Discussion

Within this section, a comparison between reported data in this chapter and the previously reported data in literature is presented, and the results are summarized. XRD method assesses the crystalline component of the material; elements on amorphous solids are not detectable with this method. The data percentages reported are proportional, and the results are highly dependent on the predetermined crystals in the analysis. For example, by considering five crystal's compositions in a data analysis, the summation of the percentages is 100%. Adding a new composition to the system will decrease the other crystals' proportional percentage while the summation of

percentages of 6 crystals remains 100%. By comparing the XRD results of the coal ash materials in this study to the previously reported data (i.e., the reported in 2012 EPRI report (Bachus and Santamarina 2012)) all the percentages are in the range of previously reported data.

There are different methods for analyzing the soluble matters of solids, and the total soluble concentrations are highly dependent on the selected method. These methods are developed to simulate different conditions. EPA 3051A, which has been developed for measuring total soluble elements, was used in this study. Although there are some methods which lead to higher element's concentration, results of EPA 3051A method can be a proper representative of maximum soluble trace elements in a solution because of strong acidity of the solution, and it has a solid mass to solution volume ratio of 1:20. The concentrations of different elements using the mentioned method in this study as well as results of three other papers are compared in Table 2-6. The last column of this table is the concentrations of elements of a Type-F coal ash provided using triple digestion method. In this approach, three different acids are used to digest the compositions and extract elements. As expected, the reported concentrations performing triple digestion method are higher than results of EPA 3051A because of using three different acids. By comparing the results of this study with the reported data from other studies were used the same method, the solubility of elements in this study seems to be in acceptable range.

SEM and EDS results confirmed previous observations regarding morphology and surface texture and elemental compositions (Kutchko and Kim 2006). All the reported shapes of particles (e.g., typical coal spheres, cenospheres, unburned carbon, mineral aggregate, agglomerated aggregates, and irregular shaped amorphous particles) were observed in the studied coal ash materials, and the majority of the elements were Si, Al, Fe, Ca.

Table 2-6. Comparison between results of elements concentrations of three coal ash materials in this study and previously reported data.

Source of data		1*			2*		3*	4*
Element type	Element	CA1	CA2	CA3	Min	Max		
		mg/kg						
Major	Silicon	103011	113699	95193	0	0	NR	229743
	Iron	19856	72657	62504	12108	19588	71167	102805
	Aluminum	14271	17884	22861	9305	21801	35333	130276
	Calcium	5689	9276.5	5117	4860	32348	NR	22520
Minor & Trace elements	potassium	2021	2429.5	3126	638	3161	NR	16187
	Magnesium	995	891	1654	1127	5060	NR	5702
	Sodium	406	1424	558	460	1910	2383	3631
	Barium	377	185	447	NR	NR	802	889
	Strontium	178	123	285	287	557	NR	NR
	Boron	77.9	383	88.5	117	903	NR	NR
	Manganese	77.8	66.65	101	NR	NR	NR	272
	Vanadium	70.5	147	87.6	56	120	81	NR
	Copper	50.3	39.5	56.6	NR	NR	98	163
	Arsenic	42.8	33.6	69.4	17	167	41	116
	Nickel	37.9	45.7	48.7	7.5	37	57	153
	Zinc	36.5	146.5	56.4	NR	NR	671	158
	Chromium	36.3	95.45	51	18	52	53	154
	Lead	18.9	44.6	18.3	NR	NR	33	77
	Molybdenum	8.76	99.45	4.42	5.4	20	12	NR
	Selenium	6.01	5.24	6.31	7.7	23	6	8.97
	Cadmium	0.764	2.33	1.07	NR	NR	3	10.79
	Mercury	< 0.193	< 0.197	< 0.200	NR	NR	NR	NR
	1*	Results of this study, EPA 3051 method						
	2*	(Bhattacharyya et al. 2009), EPA 3051 method						
	3*	(Jankowski et al. 2006), EPA 3051 method						
	4*	(Kim and Hesbach 2009), triple digestion method						
	NR	Not reported						

Bachus and Santamarina (2012) had a comprehensive study on engineering properties of coal ash materials which were collected from different power plants' sources in the USA, and the results of this study are reported in EPRI report (Bachus and Santamarina 2012). A comparison has been made on the particle size distribution (i.e., PSD) of the studied coal ash materials and all the particle size distribution curves are reported in the mentioned report (Bachus and Santamarina 2012) in Figure 2-9. The mean D50 of 42 reported particle size distributions in EPRI report is 0.033 with a standard deviation and coeefficient of variation of 0.032 and 95.4%, respectively. D50 of CA1,

CA2, and CA3 materials was, respectively, 0.032, 0.014, 0.02, which were lower than mean D50 of reprted data and in the range of one standard deviation below the mean value.

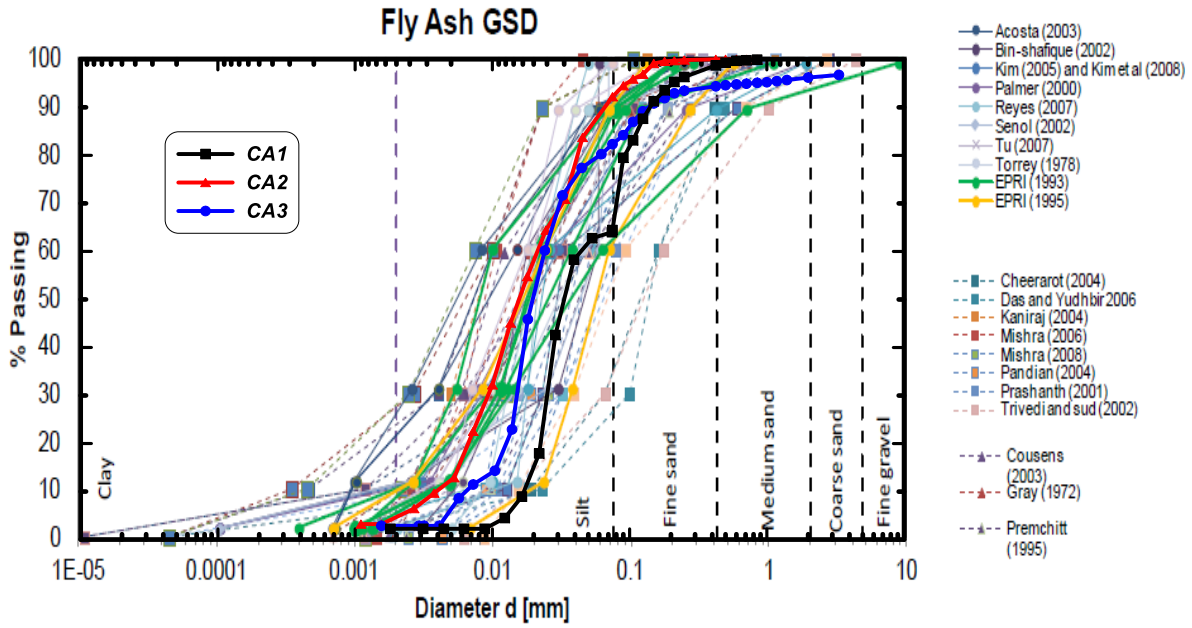

Figure 2-9. Comparison between particle size distributions of coal ash in this study and previous works (Bachus and Santamarina 2012).

Table 2-7. Comparison between physical parameters reported in this study and literature (Bachus and Santamarina 2012).

	Reported		This Study		
	Minimum	Maximum	CA1	CA2	CA3
Specific Gravity	1.25	3.05	2	2.34	2.35
D50 (mm)	0.004	0.15	0.032	0.014	0.0205
D10 (mm)	0.00035	0.025	0.013	0.0038	0.009
Liquid Limit (%)	28	55	34	22	41

The maximum and minimum values of Specific Gravity, D50 (mm), D10 (mm), Liquid Limit (%) are extracted from EPRI report (Bachus and Santamarina 2012) and presented in Table 2-7. All the reported parameters' values are in the range of previously reported data in EPRI report except the CA2 material's liquid limit. Liquid limit of CA2 coal ash is lower than minimum value is reported in that report. The specific gravity of CA1 coal ash is in the lower band of USA coal ash

materials (i.e., minimum of 1.98), and the specific gravity of other two coal ash materials are at the mid-range. Figure 2-10 shows the frequency of having different ranges of the coefficient of uniformity (C_u) and curvature (C_c) from the results of several studies in different points of the world (Bachus and Santamarina 2012). It shows C_c and C_u of the coal ash materials in this study (Table 2-4) are in the most frequent ranges presented in the literature.

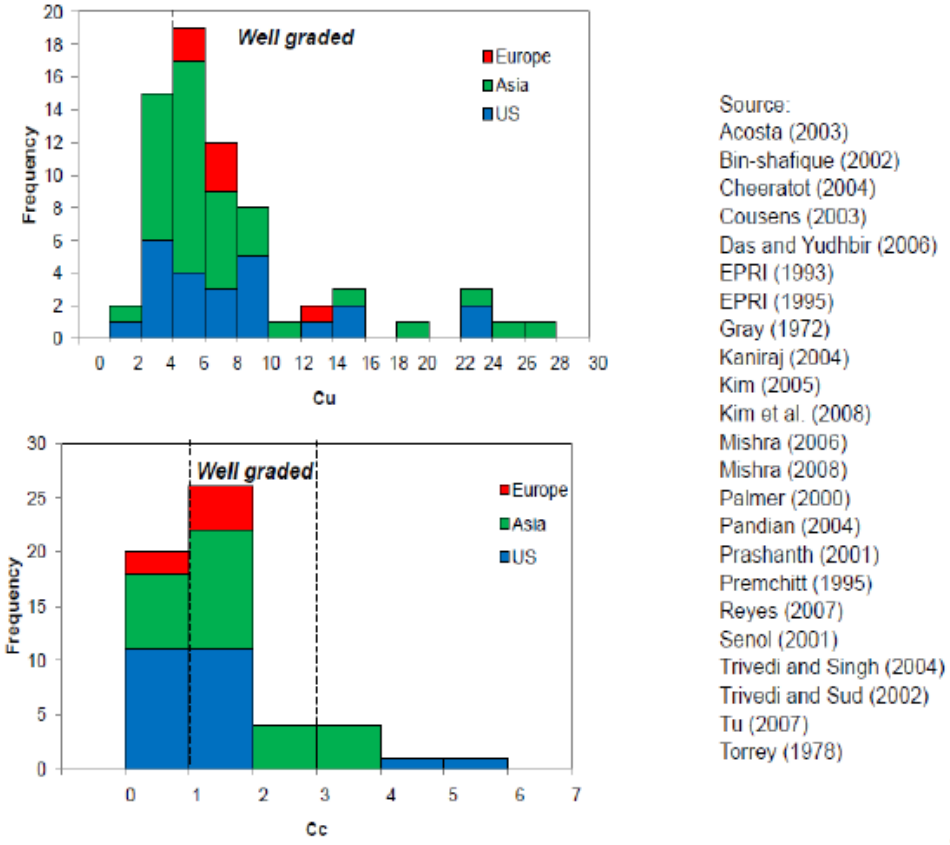

Figure 2-10. Coal ash particle size distribution reported by (Bachus and Santamarina 2012).

2.5 References

ASTM D 854-00. (2000). "Standard Test for Specific Gravity of Soil Solids by Water Pycnometer." ASTM International, West Conshohocken, PA.

ASTM D422-63. (2007). "D422–63 (2007) Standard test method for particle-size analysis of soils." ASTM International, West Conshohocken.Doi, 10 1520.

Bachus, R., and Santamarina, C. (2012). "Geotechnical Properties of Fly ASH and Potential for Static Liquefaction: Volume I–Summary and Conclusions." EPRI, Palo Alto, CA.

Bhattacharyya, S., Donahoe, R. J., and Patel, D. (2009). "Experimental study of chemical treatment of coal fly ash to reduce the mobility of priority trace elements." Fuel, 88(7), 1173-1184.

Clarke, L. B. (1993). "The fate of trace elements during coal combustion and gasification: an overview." Fuel, 72(6), 731-736.

Jankowski, J., Ward, C. R., French, D., and Groves, S. (2006). "Mobility of trace elements from selected Australian fly ashes and its potential impact on aquatic ecosystems." Fuel, 85(2), 243-256.

Kim, A. G. (2002). "Physical and chemical characteristics of CCB." Proceedings of Coal Combustion By-Products and Western Coal Mines: A Technical Interactive Forum. Allton, IL: US Department of the Interior, Office of Surface Mining, 25-42.

Kim, A. G., and Hesbach, P. (2009). "Comparison of fly ash leaching methods." Fuel, 88(5), 926-937.

Kutchko, B. G., and Kim, A. G. (2006). "Fly ash characterization by SEM–EDS." Fuel, 85(17–18), 2537-2544.

Link, D. D., Walter, P. J., and Kingston, H. M. (1998). "Development and validation of the new EPA microwave-assisted leach method 3051A." Environmental Science and Technology, 32(22), 3628-3632.

Poykio, R., Manskinen, K., Nurmesniemi, H., and Dahl, O. (2011). "Comparison of trace elements in bottom ash and fly ash from a large-sized (77 MW) multi-fuel boiler at the power plant of a fluting board mill, Finland." Energy Explor.Exploit., 29(3), 217-233.

Styszko-Grochowiak, K., Gołaś, J., Jankowski, H., and Koziński, S. (2004). "Characterization of the coal fly ash for the purpose of improvement of industrial on-line measurement of unburned carbon content." Fuel, 83(13), 1847-1853.

3. Chapter 3: Factors affecting the Kinetics of Urea Hydrolysis via *Sporoscarcina Pasteurii*

Shahin Safavizadeh

Graduate Student, North Carolina State University, Department of Civil, Construction, and Environmental Engineering, Raleigh, NC 27695; email: ssafavi2@ncsu.edu

Brina M. Montoya

Assistant Professor, North Carolina State University, Department of Civil, Construction, and Environmental Engineering, Raleigh, NC 27695; email: bmmorten@ncsu.edu

Mohammed A. Gabr

Professor, North Carolina State Univ., Department of Civil, Construction, and Environmental Engineering, Raleigh, NC 27695; email: gabr@ncsu.edu

Abstract

Interdisciplinary research has revealed new techniques to modify engineering properties of subsurface material. Microbial induced calcium carbonate precipitation (MICP) is a bio-mediated process which has shown the potential for improving the engineering properties of soil, it has also the potential of immobilizing trace elements. MICP depends upon microbial induced urea hydrolysis, which produces carbonate, bicarbonate, carbonic acid, ammonia, and ammonium. Carbonate content. super saturation index and alkalinity of the solution determine the rate and type of calcium carbonate (CaCO3) precipitation. The chemistry of the MICP reactions is modeled using MINTEQ 3.1, and the effect of different parameters in MICP chemical reaction are investigated. There are several studies that have observed the effect of enzyme concentration on the kinetics of hydrolyzing urea. Few studies have observed the bacteria as the agent. Microbial precipitation is favored to loose enzyme precipitation due to the enzyme cost and accessibility to in-situ bacteria. A urea hydrolyzing bacterium, *Sporosarcina pasteurii* (ATCC 11859) was cultured and used for this study. The effects of the cell population and initial concentration of urea, and the kinetics of urea hydrolysis were evaluated using electrical conductivity as a monitoring method. The correlation between conductivity and hydrolyzed urea was found and used to monitor urea hydrolysis and bacteria activity. Results from this study can be used in understanding the population of active ureolytic bacteria and to design the timing of MICP treatments based on microbial activity. This was demonstrated in an experiment which was designated to exemplify the practicality of microbial monitoring during the MICP process using electrical conductivity.

3.1 Introduction

Interdisciplinary research has given rise to innovate methods for improving soil engineering properties (e.g., strength, stiffness, permeability). Synthetic methods can be costly, impractical and

may introduce hazardous substances (DeJong et al. 2010). Microbial induced calcium carbonate precipitation (MICP) is an emerging innovative bio-geochemical process for stabilization of unbound materials. This process induces the precipitation of calcium carbonate between soil particles and cements them together which increases the material's strength and stiffness (Mortensen et al. 2011). MICP has been used not only for improving strength and stiffness of the soil but also has been investigated for the solid-phase capture of trace elements (Warren et al. 2001a). Subsurface microbes can promote calcium carbonate precipitation by increasing the subsurface alkalinity, which may be accomplished by several bio-geochemical reactions (e.g., urea hydrolysis, nitrate reduction, sulfate reduction and iron reduction) (DeJong et al. 2010). Urea hydrolysis is unique in that it can generate carbonate ions without an associated production of protons (Whiffin 2004), and recent studies on bio-mediated soil improvement have mostly focused on urea hydrolysis. There are several bacteria which contain urease in nature. Sporosarcina pasteurii (formerly known as *Bacillus pasteurii*) is a common bacterium in soil, and it has a high activity on urea hydrolysis. The chemical process of MICP includes breaking down the aqueous urea into ammonium and carbonate in a solution consisting of calcium ions, as shown in Equation (1). Increasing the concentration of carbonate saturates the solution and calcium carbonate precipitates per the reaction is shown in Equation (2).

$$\begin{array}{l} CO(NH_2)_2 + H_2O \rightarrow NH_2COOH + NH_3 \\ NH_2COOH + H_3O \rightarrow NH_3 + H_2CO_3 \end{array}$$

$$CO(NH_2)_2 + 2H_2O \rightarrow 2NH_3 + H_2CO_3 \rightarrow 2NH_4^+ + CO_3^{2-} \quad (1)$$

$$CO_3^{2-} + Ca^{2+} \leftrightarrow CaCO_3(s) \quad (2)$$

Calcium concentration, total carbonate concentration, pH level (alkalinity), and presence of nucleation site are the governing factors of CaCO3 precipitation (Van Paassen 2009). Bacterial cells provide nucleation sites on the soil particles for CaCO3 precipitation (Warren et al. 2001a). The concentration of calcium can be easily controlled by adding a salt into the solution (e.g., CaCl2, Ca(NO3)2). The products of hydrolyzing urea can increase the pH level with a corresponding increase of the percentage of carbonate in comparison to total dissolved carbonate based on acid-base reactions (Benjamin 2014), which is ideal for calcium carbonate precipitation.

For optimal design and analysis of MICP process, a proper knowledge of chemistry and enzyme kinetics is necessary. In the past, the catalytic properties of urease and reaction kinetics have been covered in the literature (Fidaleo and Lavecchia 2003; Bachmeier et al. 2002) and the parameters needed for applying the Michaelis-Menten equation (Fidaleo and Lavecchia 2003) have been well studied. Enzymes are protein molecules in cells which catalyze the biochemical reactions. Whiffin (2004) reported a study on the effect of PH and pre-exposure on urease activity by using two different bacteria (*S. pasteurii* and *Proteus vulgaris*) (Whiffin 2004). Hammad et al. (2013) demonstrated the level urease activity and calcium carbonate precipitation via *S. pasteurii* (Hammad et al. 2013). What seems to be lacking, however, is the availability of an expression for the dependency of the hydrolysis rate on the solution properties and cell population. The factors governing the rate of hydrolyzing urea consist of enzyme concentrations which is a function of the cell population, type of enzyme, concentration of reactant and product, pH of the system, and temperature (Fidaleo and Lavecchia 2003).

In the scope reported herein, the ureolytic chemical reactions were modeled in MINTEQ 3.1 (Gustafsson 2013) to study the effect of different parameters including pH, initial concentrations, and concentration of hydrolyzed urea on the chemical equilibrium of the reactions. Electrical

conductivity measurements were developed as a monitoring method to assess the kinetics of the MICP reactions after the implementation of proper calibration approach. Effect of thr population of bacteria and initial concentration of urea is also assessed. An experimental study was designed using a set of column tests and utilizing Ottawa 50-70 sand in order to investigate the applicability of using electrical conductivity as a monitoring method during the MICP soil stabilization process.

3.2 Material and methods

3.2.1 Bacteria and growth condition

Sporosarcina pasteurii (ATCC 11859), a urease containing bacterium, was grown and used in this study. For this purpose, ammonium yeast extract medium (ATCC 1376) was used to grow the bacteria at 30 ^{o}C. Each ingredient was autoclaved and mixed after sterilization. The growth medium was inoculated with the *S. pasteurii* stock culture and incubated aerobically at 30 ^{o}C with 200 revolutions per minute until the sample reached the desired cell population. Incubation stopped before reaching the stationary phase of bacteria growth curve in order to assure having healthy and active bacteria. Cultures were centrifuged at 4000 g for 20 minutes in 15 ml vials. The spent supernatant medium was replaced with fresh growth medium and centrifuged a second time after the complete mixing of cells and growth medium. Harvested bacteria were saved at 4 ^{o}C to minimize bacterial activity. The population of bacteria was assessed using optical density (i.e., OD_{600}).

3.2.2 Evaluating relationship between conductivity and hydrolyzed urea

Electrical conductivity evaluates composite parameters in solution. The electrical conductivity of a solution is measured by imposing an electrical field and establishing a flow current (I) based on

migration of ions toward the opposite charged electrodes (Benjamin 2014; Rhoades 1996). As the concentration of ions increases in a solution, the solution would be more conductive of electrical flow current which corresponding to a higher electrical conductivity. The following two equations are used to correlate the electrical conductivity (κ) to ion concentration (c_i), ion charge (z_i), and equivalent ionic conductance (λ_i) (Benjamin 2014).

$$\lambda_{ave} = \frac{\sum \lambda_i c_i z_i}{\sum c_i z_i} \tag{3}$$

And,

$$\kappa = \lambda_{ave} \sum c_i z_i \tag{4}$$

The values of λ_i is specific for each ion. It is designated to $\lambda_{i,0}$ in the case of the infinitely dilute solution. In real solutions, λ_i for any ion is less than $\lambda_{i,0}$, because its mobility is reduced due to interaction with species other than water molecules. This leads to a non-linear correlation between the concentration of hydrolyzed urea and electrical conductivity.

In order to evaluate the concentration of hydrolyzed urea on the conductivity of solution, batch testing program was conducted. In this case, 10 different concentrations of Urea (CH_4N_2O) were prepared in 0.1 M to 1 M with 0.1 M increment, considering volume of bacteria vials. Sealed containers were used to prevent gas exchange between the atmosphere and the solution. One 15 ml vial of solution containing *S. pasteurii* (OD_{600}=1.18) was added to each container and the initial conductivity and pH was measured right after mixing. The conductivity of each sample was measured after three days, allowing the bacteria to hydrolyze all of the urea in the solution. Conductivity of the samples was measured after 3 days and 6 hours since mixing again to check

the completeness of urea hydrolysis. This electrical conductivity was used to correlate electrical conductivity and hydrolyzed urea concentration (i.e., [HU]).

3.2.3 Reaction Modeling

The chemical reactions were modeled using the chemical equilibrium program MINTEQ 3.1 (Gustafsson 2013). To understand the equilibrium state, equations including mass balances, chemical equilibrium expressions, and a charge balance, proton condition, or total hydrogen (TOTH) are used. Two types of model configurations were defined. In the first, the concentration of all the chemicals to prepare the systems are known, and the final equilibrium condition is the outcome of interest. In the second, the final state of the system is defined (e.g., pH) and the chemical input is sought (Benjamin 2014)

The effect of pH on the concentration of different possible elements of a system containing only hydrolyzed urea were modeled to understand the mechanism of MICP. For this purpose, the pH of a solution containing 333 mM hydrolyzed urea was varied in the range of 0 to 14, and the chemical inputs including NH_4^+, NH_3, CO_2/H_2CO_3, HCO_3^-, CO_3^{2-}, H^+, and OH^- are sought.

The calcium carbonate precipitation in solutions with different initial concentration of $CaCl_2$ is simulated by titration of hydrolyzed urea. 1 M CO_3^{2-} and 2 M NH_4^- are equivalent to 1 M hydrolyzed urea based on Equation 1, and these ratios were used to input hydrolyzed urea in the program. The range of concentration of $CaCl_2$ and hydrolyzed urea is 0 to 1000 mM. This range covers the concentrations in the most current published studies ((Martinez et al. 2013), (Van Paassen 2009)) . Different possible solid crystals might precipitate with the existence of Ca^{2+}, CO_3^{2-}, OH^-, and O^{2-}. Their name, formula, and equilibrium Constants are listed in Table 3-1. Further details about the steps to model MICP reaction are explained in Appendix A.

Table 3-1. List of possible solids and their solid equilibrium constants with existence of Ca^{2+}, CO_3^{2-} , OH^-, and O^{2-} (Benjamin 2014).

Name	Formula	$LogK_{so}$
Calcite	$CaCO_{3(S)}$	-8.48
Aragonite	$CaCO_{3(S)}$	-8.34
Vaterite	$CaCO_{3(S)}$	-7.91
Calcium Carbonate Hydrate	$CaCO_{3(S)}.H_2O$	-7.14
Portlandite	$Ca(OH)_{2(s)}$	27.74
Aragonite	CaO	32.7

3.2.4 Evaluating relationship between cell density and hydrolyzed urea

In order to evaluate the effects of initial concentration of urea and cells population, 15 samples were prepared while mixing urea, deionized water, and bacteria solution. The urea concentrations were 50 mM, 100 mM, and 200 mM. Five populations of bacteria were assessed (i.e., OD_{600} of 15 ml vials were 0.225, 0.603, 0.893, 1.065, 1.16). In order to minimize the presence of dead bacteria, incubation of bacteria stopped at OD around 0.22, which is far from plateau OD (i.e., ~1 to 1.2) of bacteria growth curve. The bacterial population increased while centrifuging and mixing after removing supernatant. The electrical conductivities of the solutions were measured until reaching the plateau in the time-conductivity curve. This measurement was conducted in an open system, and CO_2 gas was in exchange with atmosphere. Such an exchange could decrease the conductivity by revealing CO_2 gas to the atmosphere and this reduction of conductivity decreases as the rate of reaction is higher (less time for gas exchange). The conductivity of solution was converted to concentration of hydrolyzed urea using the derived equation in batching test program (i.e., discussed in results section).

3.2.5 Column Tests

A set of column tests were performed to assess the applicability of using conductivity measurements as a monitoring method. Ottawa 50-70 sand was used to construct the samples in

the columns. The sand grain size characteristics are presented in Table 3-2. Two short columns and one long column were prepared using air pluviation method along with vibration to attain the desired density. The specification of the specimens are summarized in

Table 3-3.

Table 3-2. Ottawa 50-70 grain size characteristic

D_{50} (mm)	e_{min}	e_{max}
0.22	0.55	0.87

Table 3-3. Specifications of columns tests on Ottawa 50-70

Specifications	Short Column, 100 mM CaCl2	Short Column, 200 mM CaCl2	Long Column , 100 mM CaCl2
Void ratio, e	0.59	0.60	0.59
Height (cm)	5.33	5.38	9.81
Diameter (cm)	5	5	5
Volume of voids	38.7	39.7	71.5

A vertical stress of 100 kPa was applied on top of the specimens using a frame load. Cementation solutions contained: 400 mM urea, 100 mM NH_4Cl and two different concentrations of $CaCl_2$; 100, and 200 mM. One of the short columns and the long column were treated with 0.1 M $CaCl_2$ recipe, and 0.2 M $CaCl_2$ recipe was used for the other short column. One 15 mL vial of bacteria (OD~1) was mixed with 100 ml of the cementation solution to make treatment solution before injection. Two pore volumes of treatment solution were injected into the bottom of the test specimens using a peristaltic pump at a rate of 8 ml/min. Shear wave velocity (V_s) of the specimens were measured before each injection to monitor the calcium carbonate precipitation. Three pore volumes of 1 M urea solution were injected into the specimens again and retained for 5 hours. After the retention time, another 1 M urea solution injected into the specimens again, and a predetermined volume of effluent (based on pore volume of the specimens) was collected to

measure the electrical conductivity. At the end, de-ionized water passed through the columns to stop further ureolytic reactions.

After treatment was completed, the specimens were extracted and divided into several sections. The mass of $CaCO_{3(s)}$ was measured per section using gravimetric acid washing method (Mortensen et al. 2011).

3.3 Results and discussion

3.3.1 Chemical reactions in MICP

Acid-Base reactions of ammonia and carbonic acid were assessed using MINTEQ 3.1 (Gustafsson 2013). The pH of a system contained 333 mM hydrolyzed urea (333 mM of $TOTCO_3$ and 666 mM of $TOTNH_3$) was numerically increased using virtual acid and base. The concentrations of the elements (H_2CO_3, HCO_3^-, CO_3^{2-}, NH_3, NH_4^+, H^+, OH^-) in the close system were the output of the modeling, as shown in

Figure 3-1. These results illustrate the chemical equilibrium condition; for solving relevant equations, dissociation constants of carbonic acid (i.e., di-protonic acid) and Ammonia (i.e., mono-protonic acid) are used (Table 3-4).

Table 3-4. Chemical formula and dissociation constants at 25°C of carbonic acid and ammonium ion.

Name	Formula	pK_{a1}	pK_{a2}
Carbonic acid	H_2CO_3	6.35	10.33
Ammonium ion	NH_4^+	9.24	-

The products of hydrolyzing 1 M of urea solution are 1 M of total carbonate and 2 M of total ammonia. The release of these elements into the system increases the pH to approximately 9.3. By assessing the dissociation constants of carbonate system, this level of pH is between pK_{a1} and pK_{a2}

of carbonic acid and more close to pK_{a2}. Therefore, the concentration of carbonate is higher than two other possible acids. Increasing the concentration of hydrolyzed urea also increases the concentration of total dissolved carbonate and correspondingly increases the concentration of carbonate. In this condition, and in the presence of the calcium or other divalent cations, the system would saturate and precipitation would occur at the soil's nucleation points.

Figure 3-1 shows the sensitivity of concentration of different possible solutes in a close system. Since pH decreases when an acid is added into the system, the concentration of carbonic acid increases while the concentration of the carbonate decreases (total dissolved carbonic is constant) and it makes the system unsaturated which result in dissolving calcium carbonate in the system. This concept is applied during gravimetric acid washing.

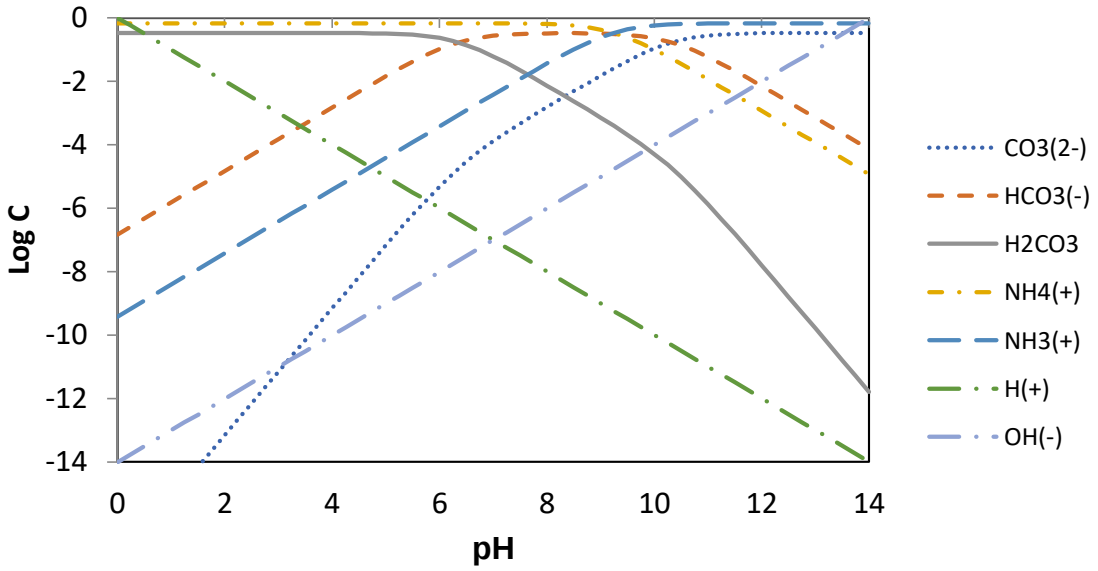

Figure 3-1. LogC-pH for a system containing 333 mM Hydrolyzed Urea

To understand the process of calcium carbonate precipitation ($CaCO_{3(s)}$), solutions with different concentration of calcium chloride ([$CaCl_2$]) were modeled to be titrated by a solution containing high concentration of hydrolyzed urea [HU] using MINTEQ 3.1. pH and the precipitated calcite

are the output parameters of interest, as presented in Figure 3-2. Results showed a linear correlation between [HU] and [$CaCO_{3(s)}$] while [HU] is less than initial [$CaCl_2$] (i.e., in the range of study, 0 to 1 M). For the case of having higher [HU] than initial [$CaCl_2$] (i.e., [$CaCl_2$]$_{in}$), the graph reached a plateau. In theory, the solubility of the solids increases while the salinity of the system increases because of decreasing the activity of the elements. Based on the same criteria, after reaching the maximum precipitated $CaCO_{3(s)}$ ([HU]=[$CaCl_2$]$_{in}$), as shown in Figure 3-2-a, the [$CaCO_{3(s)}$] decreases because of increasing the salinity of solution but the dissolution is not noticeable. The variation of pH during titration of HU in solutions with different initial concentration of $CaCl_2$ is plotted in Figure 3-2-b. Releasing the products of hydrolyzing urea in a solution has a tendency to increase the pH to 9.3. Existence of Ca^{2+} in the system buffers such increase. The carbonate product reacts with Ca^{2+} to precipitate calcium carbonate. This reaction consumes the CO_3^{2-}, which is the reason of increasing pH while NH^{4+} is released into the system as a urea hydrolysis product. NH^{4+} is an acid and decreases the pH level as demonstrated in Figure 3-2-b. The pH of the system starts increasing while the level of saturation is getting equal or lower than saturation index by consuming Ca^{2+}, the [HU] is close to initial [$CaCl_2$] at this point.

These results illustrate that the level of hydrolyzing urea can be monitored by measuring the pH when the initial concentrations of species in the solutions are known. While these results represent systems consisting of only HU and $CaCl_2$, similar results can be produced for other recipes conducting chemical equilibrium modeling.

3.3.2 Correlation between electrical conductivity and hydrolyzed urea

Batch testing was conducted in duplicates and the results are presented in Figure 3-3. A second order polynomial was fitted to the measured data (i.e., Equation 5) and will be used to convert the conductivity to the hydrolyzed urea concentration.

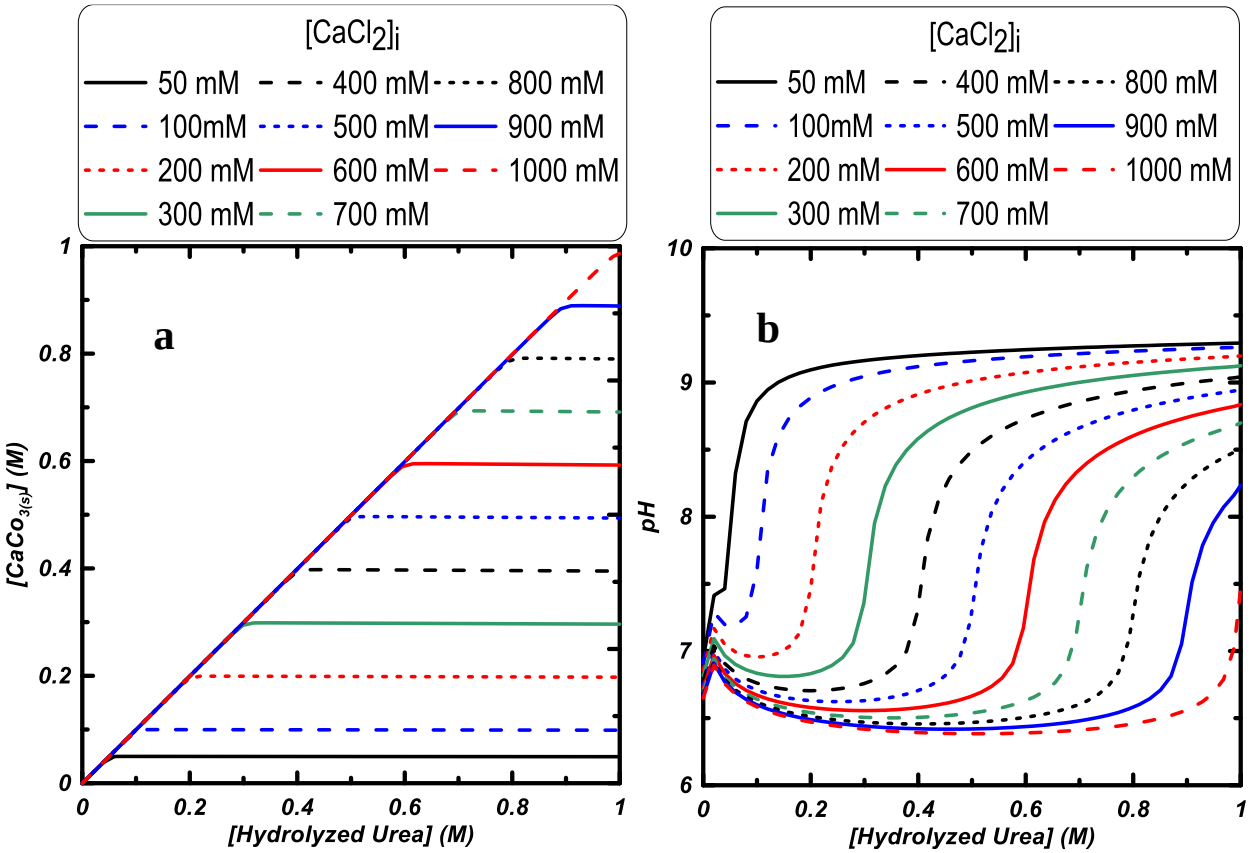

Figure 3-2. Precipitated calcium carbonate (a) and pH (b) during hydrolyzed urea titration for solutions with different $[CaCl_2]_{in}$.

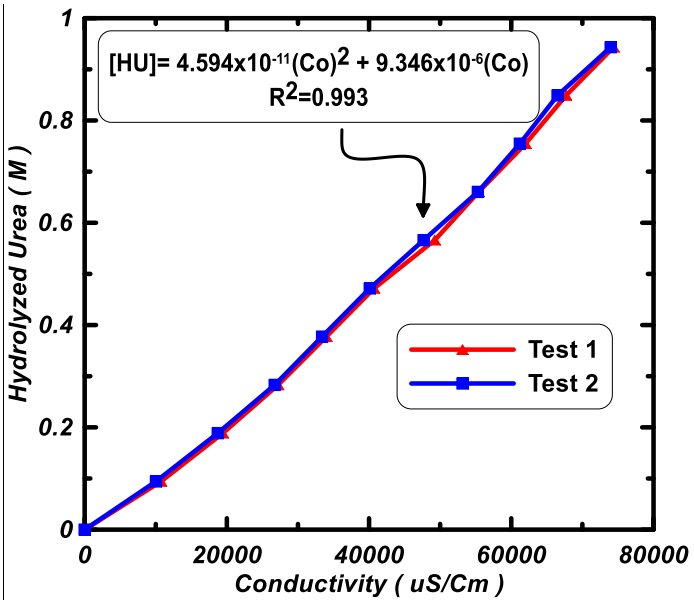

Figure 3-3. Correlation between electrical conductivity and concentration of hydrolyzed urea.

$$[HU]=4.594x10^{-11}(Co)^2+9.346x10^{-6}(Co) \quad (5)$$

3.3.3 Kinetics of reaction

The electrical conductivity was measured during the hydrolysis of urea for 15 batch samples, consisting of 5 populations of bacteria and 3 different initial concentration of urea. The measured electrical conductivities were converted to concentration of hydrolyzed urea using Equation 5, and the results are presented in Figure 3-4. The results indicated that increasing the bacteria cell population increased the rate of hydrolyzed urea, and such increase caused reaching to the curve plateau (i.e., maximum hydrolyzed urea) in a shorter period regardless of the initial urea concentration.

By comparing the shape of graphs in Figure 3-4 against the shape of graphs developed using the Michaelis-Menten equation (i.e., shown in Figure 3-7), here is an obvious difference. The slopes of these graphs show the rate of urea hydrolysis. Based on Michaelis-Menten equation, by having a constant concentration of enzyme in the system, the rate of the reaction decreases as time passes. The results in Figure 3-4 indicated that the concentration of enzyme is not constant likely due to the bacteria processes; therefore, the initial increase in rate of reaction could be caused by the increasing of enzyme concentration. On the other hand, increasing the pH can increase the rate of urea hydrolysis based on Michaelis-Menten equation, and the pH of the tested samples were increased while urea was hydrolyzed in solutions (e.g., the measured pH values for the samples with OD = 1.16 are demonstrated in Figure 3-5). Therefore, both the effect of pH and the urea hydrolysis mechanism with bacteria could be the reason for having this upward concaves in Figure 3-4' curves.

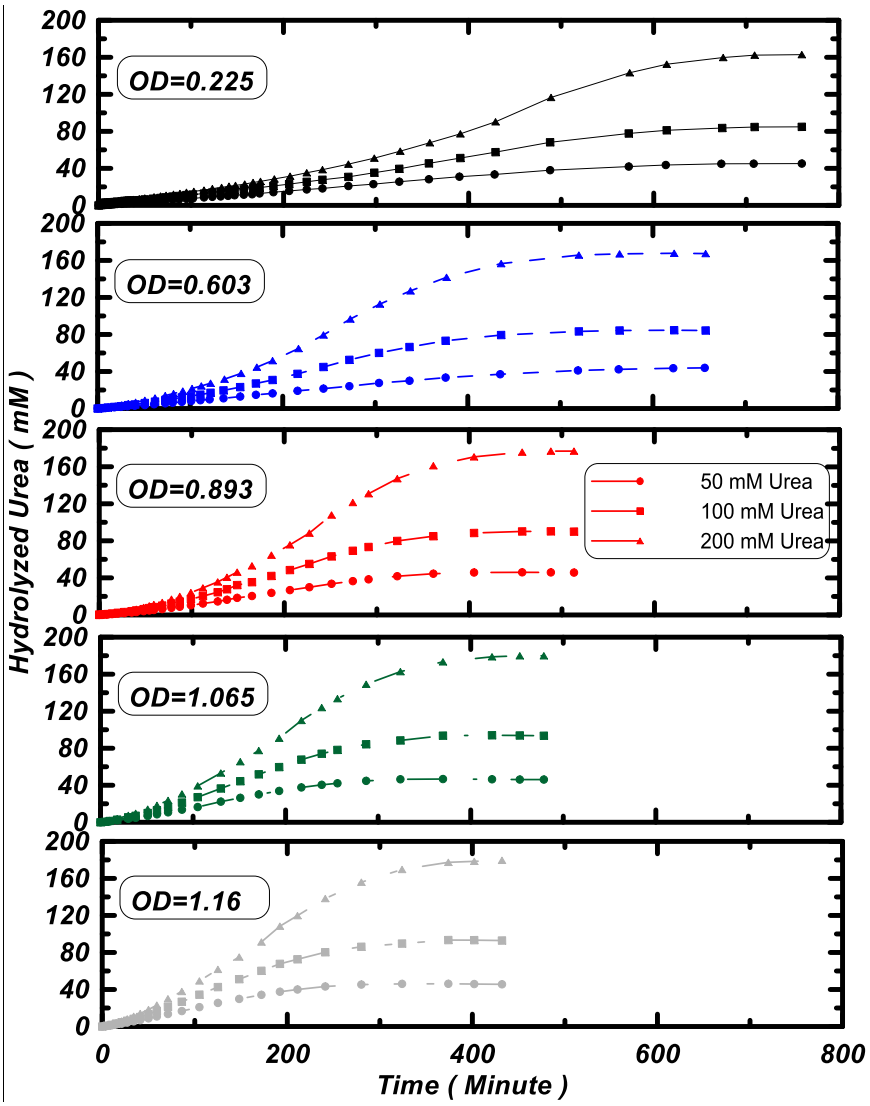

Figure 3-4. Effect of cell population and initial concentration of Urea on the kinetic of hydrolyzing urea

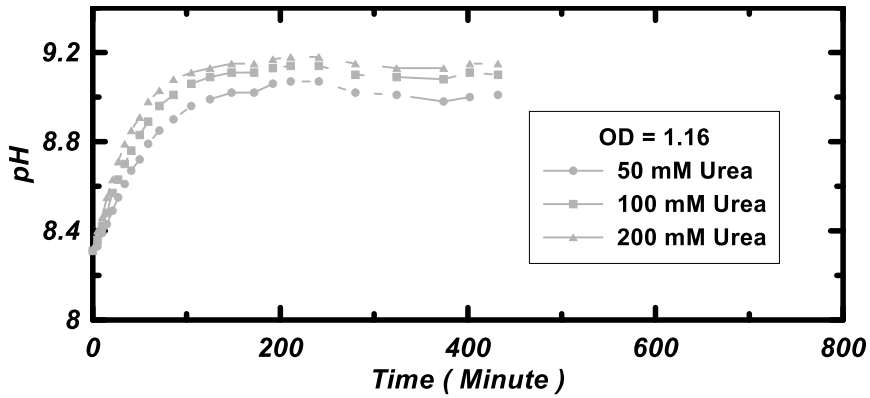

Figure 3-5. Measured pH values for the samples with OD =1.16 in batching test program.

There is a difference between the values of hydrolyzed urea concentration at the plateau for different population of bacteria (Figure 3-4). For example, the hydrolyzed urea concentration at the plateau for the solutions with initial urea concentration of 200 mM are 163 and 180 mM for the solutions with OD = 0.225 and OD = 1.16, respectively. The samples were monitored in an open system and the CO_2 gas was in exchange with atmosphere, therefore, as the rate of reaction decreases (lower population of bacteria), CO_2 gas has more time to be released into the atmosphere, which led to lower conductivity.

3.3.4 Initial rate of reaction: Bacterial populations and initial concentration of urea

The initial rate of reaction is defined as the rate of urea hydrolysis during the first 60 minutes. This parameter is extracted from the kinetic graphs in Figure 3-4 to evaluate the effect of initial urea concentration ($[U]_0$) with constant optical density (Figure 3-6-a) and effect of cell population with constant initial urea concentration (Figure 3-6-b).

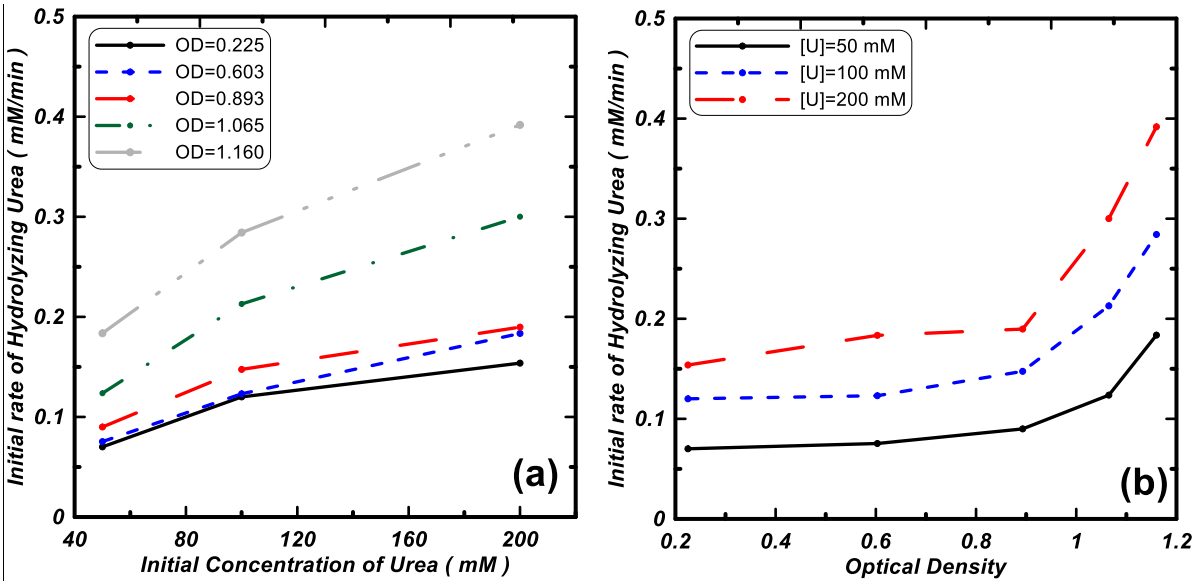

Figure 3-6. a) Effect of initial urea concentration on initial rate of hydrolysis, b) effect of initial urea concentration on initial rate of hydrolysis.

Higher initial urea concentration results in a higher rate of reaction for the first hour. The trend shows the slope of these graphs are decreasing with increasing the $[U]_0$. Fidaleo and Marcello (2003) showed that the initial rate of urea hydrolysis would decrease while the $[U]_0$ increases and it would not be a function of $[U]_0$ while $[U]_0$ is higher than a specific value for jack bean enzyme study (as demonstrated in Figure 3-7). Considering the trend of the curves in Figure 3-6-a, the curves might reach the plateau if the $[U]_0$ is increased beyond the 200 mM. Further investigation is needed to conclude such a statement.

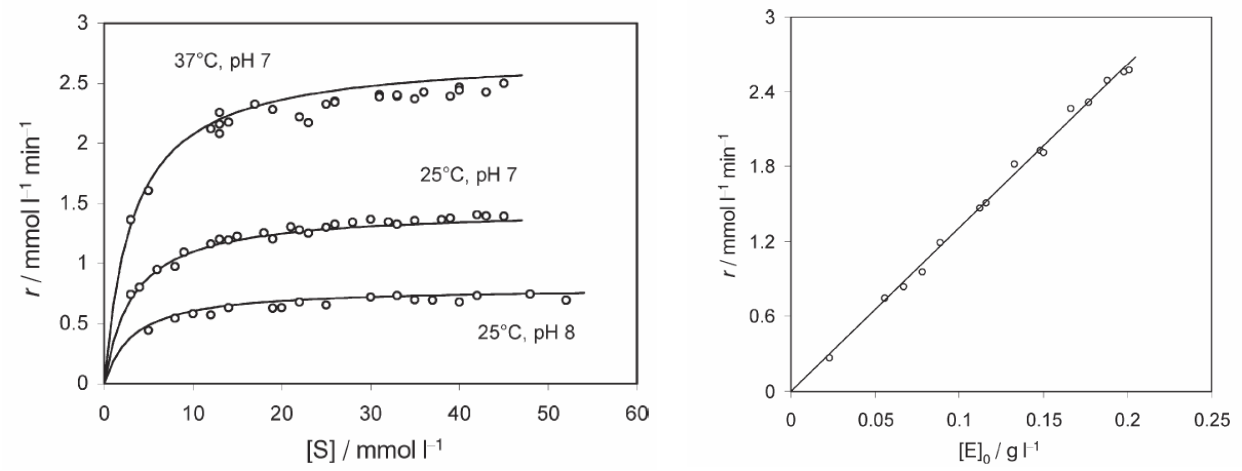

Figure 3-7. Effect of initial substrate (i.e., urea) concentration and enzyme concentration on the rate of urea hydrolysis (Fidaleo and Lavecchia 2003).

On the other hand, and as shown in Figure 3-6-b, the initial rate of reaction is increasing slightly when the OD increased between 0.22 to 0.89. This rate increased significantly after OD of 0.89. There is a linear correlation between the concentration of enzyme and initial rate of reaction based on results reported in Fidaleo and Marcello's study in 2003 (Figure 3-7). The correlation between optical density and cell population of a solution is not linear. Montoya 2006 showed there is a logarithmic correlation between OD and cell population. Therefore, a similar correlation, which is developed with the same OD meter is usded in this study, is needed to see if the initial rate of reaction and cell population has a linear relationship too.

3.3.5 Application of monitoring reaction in column test

A set of column tests were prepared to assess the feasibility of using electrical conductivity as a monitoring method during the MICP process. Three soil columns were prepared using air pluviation method. After applying 100 kPa and measuring initial shear wave velocity, the samples were treated and the shear wave velocities (Vs) were measured before each treatment injection to monitor the progress of the treatment process (Figure 3-8). The trends of increasing the shear wave velocity of the two short and the long columns, which were treated with the same recipe, were shown to be very similar. It can be concluded that the increase of calcite content in the middle of these two columns is the same. The short column with higher [CaCl2] concentration in treatment recipe showed a faster increase in shear wave velocity, which indicating higher precipitated calcium carbonate content.

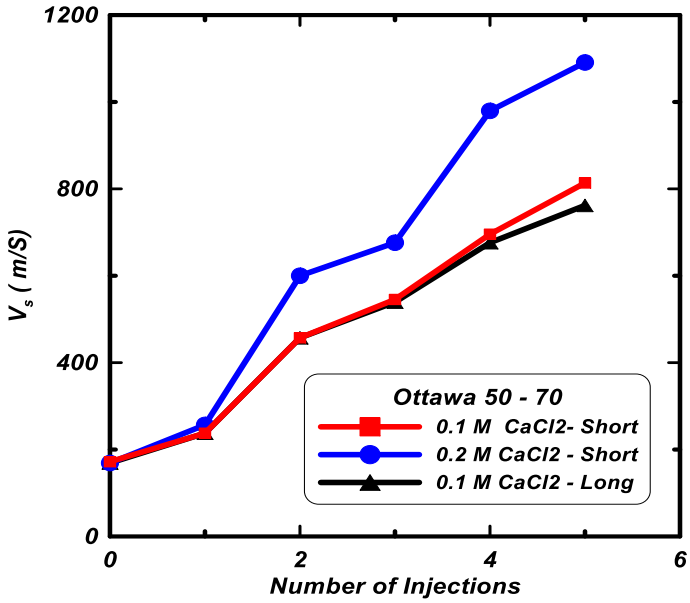

Figure 3-8. Treatment process, Vs (m/s) vs. Number of injection.

The electrical conductivity of the solution containing only urea is 0 and it increases by hydrolyzing the urea and corresponding concentration of ions. In order to explore the activity of the bacteria at

different locations of the column tests, the electrical conductivity measurements were conducted. For this purpose, a solution containing 1 M urea was injected into the specimens and after 5 hours' retention time, the same solution was injected, in the meantime, the effluent was collected for electrical conductivity measurement. The volume of void of the short columns was 40 ml, and 2-20 ml samples were collected to cover 1 pore volume. The volume of void was 72 ml for long column specimen and 3-24 ml samples were the volume divisions for 1 pore volume. The electrical conductivity of the effluent is converted to [Hydrolyzed Urea] using Equation 5 and the results are shown in Table 3-5. The height level 1 is representing the top of the specimen and height level 2 is the lower part (the point of injection) for the short columns specimen. The height level 1, 2, and 3 are representing the top, middle, and bottom of the long column specimen, respectively. $[HU]/[U]_0$ is the concentration of hydrolyzed urea over the initial concentration of urea (1 M) in Table 3-5. The distribution of $[HU]/[U]_0$ is expressing the population of the bacteria at different specimens' sections. The results indicated that the activity (population) of the bacteria is higher at injection points and it decreased by taking distance from injection point.

The long column specimen was divided into three parts and the short columns were divided into two parts similar to divisions for conductivity measurements. Samples were extracted to determine mass of calcium carbonate using gravimetric acid washing method (Table 3-5). The mass of calcium carbonate of 0.2 M calcium chloride recipe is approximately twice of the mass of calcium carbonate of 0.1 M recipe. On the other hand, the percent of the calcium carbonate at the injection point is maximum (i.e., bottom of the soil column) and carbonate content was lowest in the location of discharge (i.e., top of the soil column).

The results of shear wave velocity and mass of calcite support the current knowledge that higher the mass of calcite increases shear wave velocity. Distribution of mass of calcite and [HU] based

on conductivity measurement is also in agreement with the current literature. These results confirm the potential for using electrical conductivity as a monitoring technique for the assessment of bacterial population and kinetics.

Table 3-5. Column test results ([HU] and % of calcite)

Height level		1	2	3
Short Column, 0.1 M CaCl2	% of $CaCO_3$	1.66	2.18	-
	Effluent Volume	20	20	-
	$[HU]/[U]_0$ (M)	0.21	0.38	-
Short Column, 0.2 M CaCl2	% of $CaCO_3$	2.73	4.22	-
	Volume	20	20	-
	$[HU]/[U]_0$ (M)	0.33	0.62	-
Long Column, 0.1 M CaCl2	% of $CaCO_3$	1.33	1.85	2.81
	Volume	24	24	24
	$[HU]/[U]_0$ (M)	0.17	0.39	0.51
Level 1 is the top of the specimen				
HU = Hydrolyzed Urea				

3.4 Conclusion

The chemical reactions of urea hydrolysis and calcium carbonate precipitation were modeled using MINTEQ. The modeling results indicated that the concentration of different possible species strongly depends on the pH level of the system based on their equilibrium constants. In a system containing a certain total carbonate, by increasing pH higher than pK_{a1} (dissociation constant), the concentration of carbonate increased while the concentration of the other two species (H_2CO_3 and HCO_3^-) decreased. The products of hydrolyzing urea increased the pH level and also the total dissolved carbonate of the system. These two factors increased the concentration of carbonate which results in saturation, nucleation, and precipitation of $CaCO_3$ under the presence of calcium ion. The modeling of calcium carbonate precipitation revealed that there is a linear correlation between the concentration of precipitated calcium carbonate and the concentration of hydrolyzed urea. This linear correlation continued until the concentration of hydrolyzed urea is close to initial

concentration of calcium chloride and then it reached a plateau in $CaCO_{3(S)}$-[HU] curves. Monitoring the pH of the system revealed that while there is Ca^{2+} in the system, the level of pH decreased because of consumption of produced carbonate by Ca^{2+} while NH_4^+ is released, which is an acid. After consuming all of Ca^{2+}, further urea hydrolysis increased the level of pH.

The correlation between electrical conductivity and concentration of hydrolyzed urea was successfully determined conducting a batch testing. The developed equation (6) was used in another batch testing program to evaluate the effect of cell population and initial urea concentration on the kinetic of hydrolyzed urea.

The kinetics of hydrolyzing urea with *S. pasteurii* has a different behavior in comparison to the results of using enzyme. The maximum rate of reaction does not occur initially which is observed in the enzyme kinetics study (Fidaleo and Lavecchia 2003). The gradual increase of pH and the mechanism of urea hydrolysis with bacteria are the two possible reasons for this difference. For the solutions with the same bacteria population, the initial rate of reaction increased by increasing the $[U]_0$, and the slope $[U]_0$ - initial rate of urea hydrolysis decreased while the $[U]_0$ decreased. However, trend of graphs showed a tendency to reach a plateau, it needs further investigation to conclude such statement.

Increasing the OD of the solutions, which represents the cell population, increased the rate of urea hydrolysis. The correlation between OD and the initial rate of hydrolyzing urea was not linear. The correlation between OD and cell population is needed to see if there is a linear correlation between initial rate of urea hydrolysis and cell population.

The results from this study can be used for monitoring MICP treatment and for understanding the population and activity of bacteria in soil. For this purpose, the soil must be saturated by pre-determined concentration of urea and after scheduled time the solution should be collected. The

conductivity of the solution must be measured and converted to [U] using equation (6). The last step is going back to the kinetic graphs and based on the [U] and time, the cell population can be determined.

A set of column test was performed to explain the applicability of electrical conductivity method as a monitoring approach in MICP treatment. The electrical conductivity measurements of different specimens' sections could show the bacteria activity distribution at different specimens' points. The results of electrical conductivity measurements indicated higher bacteria activity at the injection points, and the bacteria activity decreased by taking distance from injection point. The results of electrical conductivity were confirmed presenting the calcium carbonate distribution along the specimens' height.

3.5 References

Bachmeier, K. L., Williams, A. E., Warmington, J. R., and Bang, S. S. (2002). "Urease activity in microbiologically-induced calcite precipitation." *J.Biotechnol.,* 93(2), 171-181.

Benjamin, M. M. (2014). *Water chemistry*. Waveland Press.

DeJong, J. T., Mortensen, B. M., Martinez, B. C., and Nelson, D. C. (2010). "Bio-mediated soil improvement." *Ecol.Eng.,* 36(2), 197-210.

Fidaleo, M., and Lavecchia, R. (2003). "Kinetic study of enzymatic urea hydrolysis in the pH range 4-9." *Chemical and Biochemical Engineering Quarterly,* 17(4), 311-318.

Gustafsson, J. P. (2013). "Visual MINTEQ version 3.1, department of sustainable development." *Environmental Science and Engineering, KTH, Stockholm*.

Hammad, I. A., Talkhan, F. N., and Zoheir, A. E. (2013). "Urease activity and induction of calcium carbonate precipitation by Sporosarcina pasteurii NCIMB 8841." *Journal of Applied Sciences Research,* 9(3), 1525-1533.

Martinez, B. C., DeJong, J. T., Ginn, T. R., Montoya, B. M., Barkouki, T. H., Hunt, C., Tanyu, B., and Major, D. (2013). "Experimental optimization of microbial-induced carbonate precipitation for soil improvement." *J.Geotech.Geoenviron.Eng.,* 139(4), 587-598.

Mortensen, B. M., Haber, M. J., DeJong, J. T., Caslake, L. F., and Nelson, D. C. (2011). "Effects of environmental factors on microbial induced calcium carbonate precipitation." *J.Appl.Microbiol.,* 111(2), 338-349.

Rhoades, J. D. (1996). "Salinity: electrical conductivity and total dissolved solids." *Methods of Soil Analysis Part 3—Chemical Methods,* (methodsofsoilan3), 417-435.

Van Paassen, L. A. (2009). "Biogrout, ground improvement by microbial induced carbonate precipitation.".

Warren, L. A., Maurice, P. A., Parmar, N., and Ferris, F. G. (2001). "Microbially mediated calcium carbonate precipitation: implications for interpreting calcite precipitation and for solid-phase capture of inorganic contaminants." *Geomicrobiol.J.,* 18(1), 93-115.

Whiffin, V. S. (2004). "Microbial CaCO3 precipitation for the production of biocement". Murdoch University.

4. Chapter 4: Microbial Induced Calcium Carbonate Precipitation on Coal Ash

Shahin Safavizadeh

Graduate Student, North Carolina State University, Department of Civil, Construction, and Environmental Engineering, Raleigh, NC 27695; email: ssafavi2@ncsu.edu

Brina M. Montoya

Assistant Professor, North Carolina State University, Department of Civil, Construction, and Environmental Engineering, Raleigh, NC 27695; email: bmmorten@ncsu.edu

Mohammed A. Gabr

Professor, North Carolina State Univ., Department of Civil, Construction, and Environmental Engineering, Raleigh, NC 27695; email: gabr@ncsu.edu

Abstract

There are two main concerns regarding the coal ash impoundments. Gradual deposition of coal ash can cause the induced shear stress overwhelm the shear strength under the self-weight condition and corresponds to structural instability. The other concern is trace elements leaching from these material and the potential of increasing the concentrations above the drinking water or ecological system standards. Microbial induced calcium carbonate precipitation (MICP) offers the solution to a wide range of geo-environmental problems, from improving soil properties by calcite cementation to capturing heavy metals during co-precipitation. In this study, the protocol of coal ash treatment using the MICP method has been experimentally developed for the first time. The protocol is applied to three coal ashes from different powerplant sources, and their response to treatment is assessed. The various behavior of the materials while treating by developed protocol lead to a comprehensive study on several possible factors that may affect the MICP treatment of coal ash, and the results are discussed.

4.1 Introduction

Coal provides more than 40 percent of the world's electricity (Nijhuis and Kendrick 2014). Despite increasing the availability of alternatives, the coal-burning power plants have been one of the primary sources of electricity generation in the United States (DOE/EIA-0035 (2017/04)). To produce electricity, coal is combusted in the coal-burning plants, and it generates coal combustion residuals (CCRs). There are more than one thousand power plants nationwide that produce an estimated 140 million tons of CCRs per year in the United States (Daniels 2016). While some coal ash is recycled in industrial applications, the majority is disposed of in landfills and impoundments (i.e., ash ponds) (Harkness et al. 2016b).

On December 2008, a coal ash impoundment at the Kingston fossil plant, holding coal ash generated over five decades (more than one billion gallons) failed under self-weight deposition. The accumulation of coal ash layers under undrained loading condition led to global slope instability (Walton and Butler 2009). This collapse resulted in the contamination of over three acres of the land and cost more than 1.2 billion dollars to clean up (Daniels 2016). Another incident occurred in February 2014, when a stormwater pipe burst under a 27-acre coal ash pond in Eden, North Carolina. Consequently, over 39000 tons of coal ash spilled into the Dan River, and around 90% of the spill is still remained in the Dan River (Daniels 2016). Trace elements' concentration (e.g., Arsenic, Selenium, Chromium) in monitoring wells close to impoundments have been reported to be higher than background levels and even higher than drinking water and ecological standards in some cases (Harkness et al. 2016b). In summary, global stability, internal stability, and release/leaching of trace elements into the natural environment are primary engineering concerns regarding the coal ash impoundments.

One of the novel approaches to improve the engineering properties of unbound media is microbial induced calcium carbonate precipitation (MICP). This approach has the potential of providing a natural and sustainable solution to improve the engineering properties of soils, and unbound materials in general, and research on the subject has gained momentum in recent years (DeJong et al. 2010). In this approach, a type of urea hydrolyzing bacteria is employed to break down the urea in the solution. The products of this biochemical reaction are carbonic acid (H_2CO_3), Bicarbonate (HCO_3^-), Carbonate Ion (CO_3^{2-}), Ammonia (NH_3), and Ammonium (NH_4^+), with pH level of the solution being the determinative factor of the dominant element based on the acid-base reactions. This reaction increases the level of pH and carbonate portion, correspondingly. In a solution containing calcium ions, increasing the carbonate concentration leads to saturation, nucleation, and

finally calcium carbonate precipitation (Benjamin 2014). The precipitated calcium carbonate bonds the particles together. Several factors control the feasibility and efficiency of MICP treatment approach. These include the activity of the bacteria, pH level, the composition of the treatment recipe, frequency of treatment, number of nucleation sites, bacterial filtration, and inhibitors of calcite crystal growth (Van Paassen 2009).

Results from previous studies indicated that MICP treatment of sand has the potential to increase its shear modulus and stiffness (Martinez et al. 2013), to decrease its compressibility and hydraulic conductivity (DeJong et al. 2010), and to change its volumetric behavior from contractive to dilative (Feng and Montoya 2015). On the other hand, from a water quality perspective, MICP treatment has been used for immobilization of strontium 90 (Fujita et al. 2010). The potential ability of MICP treatment to improve the engineering properties and to immobilize trace elements lead to the hypothesis that this approach may possibly be used to address the aforesaid concerns regarding coal ash impoundments. The distinction between coal ash and natural soils necessitate a comprehensive study on the method of treatment and possible MICP treatment inhibitors.

In this study, the effect of MICP treatment on the coal ash material is investigated. A soil column testing program is performed on coal ash from different power plants. The testing program encompassed the development and optimization of the treatment process. Shear wave velocity, calcium carbonate content, and microscale images are utilized to assess the response of coal ash to the MICP treatment. To optimize the treatment recipe, different approaches are explored, and the best treatment process is recommended. Possible factors affecting the MICP treatment process on coal ashes are examined and discussed.

4.2 Materials

Three different coal ash materials (i.e., referred to as CA1, CA2, and CA3) are used in this study. The physiochemical and engineering properties of the study materials are summarized herein.

4.2.1 Physiochemical characteristic

The crystalline phases of the three fly ash test materials were identified using X-ray diffraction method (XRD). PANalytical Empyrean X-ray diffractometer with a cukα radiation was used to perform the XRD test in the Analytical Instrumentation Facility at North Carolina State University. The step size is 0.026 degree, the counting time per step is 447 seconds, and the scan angle is from 10 to 90^0. To analyze the data, High Score Plus software is used with an International Centre for Diffraction Data (ICDD) XRD database. As shown in

Table 5-1, the results of analysis determined the existence of the aluminum silicate, silicon oxide, aluminum oxide, and iron oxide as the major crystalline part of these fly ashes.

The major, minor and trace element concentrations are measured using standard microwave acid digestion method EPA 3051A (Link et al. 1998) and the results are presented in

Table 4-2. In this process, the solids are dissolved in reagent nitric acid with a solution to mass ratio of 20. Silicon crystals are very stable, and therefore triple digestion method was used to measure its concentration. The presented concentration of trace elements are viewed as the maximum level that can be expected in leachate because of the high solubility of the nitric acid reagent in comparison to usual fluids passing through fly ash.

The samples were placed in a furnace with 500^0c temperature for one 24 hrs to measure the carbon content of the coal ashes. The mass lost is considered as the burnt mass of carbon. The results of

carbon content measurements indicated 3.42%, 0.48%, and 8.46% by weight for CA1, CA2, and CA3, respectively.

Table 4-1. Results of data analysis of XRD measurements using ICDD database.

Crystal	Formula	Relative Percentage		
		CA1	CA2	CA3
Aluminum Silicate	Al_2SiO_5	53.5	36	44.4
Silicon Oxide	SiO_2	36.4	36	37.4
Iron Oxide	Fe_2O_3	5.1	14	9.1
Calcium Oxide	CaO	1	2	0
Aluminum Oxide	$Al2O_3$	4	12	9.1

Table 4-2. Major, minor and trace elements, results of EPA 3051A method

Type	Element	CA1	CA2	CA3
		mg/kg		
Major	Silicon	103011	113698.5	95193
	Iron	19856	72657	62504
	aluminum	14271	17884	22861
	Calcium	5689	9276.5	5117
Minor & Trace elements	potassium	2021	2429.5	3126
	Magnesium	995	891	1654
	Sodium	406	1424	558
	Barium	377	185	447
	Strontium	178	123	285
	Boron	77.9	383	88.5
	Manganese	77.8	66.6	101
	Vanadium	70.5	147	87.6
	Copper	50.3	39.5	56.6
	Arsenic	42.8	33.6	69.4
	Nickel	37.9	45.7	48.7
	Zinc	36.5	146.5	56.4
	Chromium	36.3	95.4	51
	Lead	18.9	44.6	18.3
	Molybdenum	8.76	99.4	4.42
	Selenium	6.01	5.24	6.31
	Cadmium	0.764	2.33	1.07
	Mercury	< 0.193	< 0.197	< 0.200

4.2.2 Engineering characteristics

The hydrometer test (e.g., < 75 microns) and sieve analysis were performed to determine the grain size distribution of the material, following (ASTM D422-63 2007). The results of the hydrometer test and sieve analysis of the three coal ashes are shown in Figure 5-1. The CA2 material has the finest grain size distribution in comparison to the other two materials. The percentages of particles greater than sieve #200 (0.075mm) are 35%, 18%, and 8% for CA1, CA2, and CA3 material, respectively. CA2 material contains 32% of the particles less than 10 um while it is 6% for CA1 material and 14% for CA3 material.

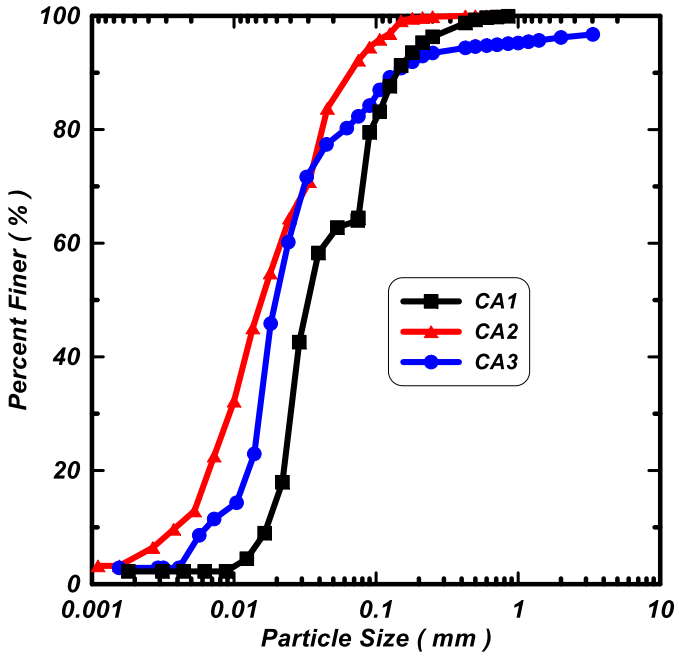

Figure 4-1. Particle size distribution of coal ashes.

To determine the specific gravity (G_S) and liquid limit (LL) of the material, the standard pycnometer (ASTM D 854-00 2000) and fall-cone test (ISO/TS 17892-6:2004) were conducted in duplicates, respectively. Based on Bachus and Santamarina's (2012) recommendation, the falling head test was performed to assess the hydraulic conductivity of the material under minimum

relative density condition (maximum hydraulic conductivity). The assessed properties of the three coal ash materials are summarized in Table 5-2.

Table 4-3. Engineering properties of coal ashes

Characteristic	Material		
	CA1	CA2	CA3
D50 (Micron)	31.6	15.8	19.9
CU	3.3	5.5	3.7
CC	0.7	1.0	1.5
GS	2	2.34	2..35
LL (%)	34	22	41
k (cm/s)	1.95E-04	9.20E-05	1.95E-04

4.3 Methods

4.3.1 Bacteria and growth condition

Sporosarcina pasteurii (ATCC 11859), a urea hydrolyzing bacterium, was grown and used in this study. For this purpose, ammonium yeast extract medium (ATCC 1376) was used to grow the bacteria at 30 ^{o}C. Each ingredient was autoclaved and mixed after sterilization. The growth medium was inoculated with *S. pasteurii* stock culture and incubated aerobically at 30 ^{o}C with 200 revolutions per minute till the desired population of cells was reached assessed using optical density (i.e., OD_{600}). Incubation stopped before reaching the plateau of the growth curve to avoid dead bacterial cells. Cultures were centrifuged at 4000 g for 20 minutes in 15 ml vials. The old supernatant medium was replaced with fresh growth medium and centrifuged a second time after the complete mixing of cells and growth medium. Harvested bacteria were saved at 4 ^{o}C to minimize their activity.

4.3.2 Column Test and the Method of Treatment

The column tests are performed to investigate the method of treatment of the study coal ashes. Sample preparation followed recommendations in the literature (Bachus and Santamarina 2012). The dry fly ash was mixed with deionized water into a slurry using a water content twice the liquid limit. The slurry was allowed to consolidate under its own weight for 24 hours. The remaining supernatant fluid was drained from the soil column (Figure 4-2). This process simulates the deposition of particles in a pond. A water-tight column extension is added to the soil column during the slurry placement; once the slurry has deposited and excess water drained, the extension is removed and the top cap is placed onto the top of the fly ash (Figure 4-2). Once the filter and top cap are placed, additional overburden is added to the coal ash by placing a point-load frame onto the top cap. Bender elements were added at the middle of the columns' height to monitor the trend of calcium carbonate precipitation as indicated by the change in the shear wave velocity with the precipitation of calcium carbonate. The applied vertical overburden stress increases the intensity of the shear wave velocity readings, as well as provides sufficient effective stress to inject the treatment solution without sample disturbance. The weight of load frame was set to apply a 100 kPa vertical pressure to the top of the specimens. Treatment solution was injected using a peristaltic pump with a specified injection rate. Certain volume of treatment solution was injected once a day until a desired level of treatment, assess using shear wave velocity, was reached. Deionized water was injected into the treated specimens after treatments were terminated in order to investigate the leaching of trace elements and to cease further biochemical reactions.

The diameter of the columns was 5 cm, and two different specimens' heights of 10 cm (long column) and 5 cm (short column) were used (i.e., 2:1 and 1:1 are sample height:diameter, respectively). Reducing the effect of filtering on bacterial distribution through the height of sample

was the reason for shortening the height from 10 cm to 5 cm. Figure 4-3 illustrates the column and instrumentation setup used during testing.

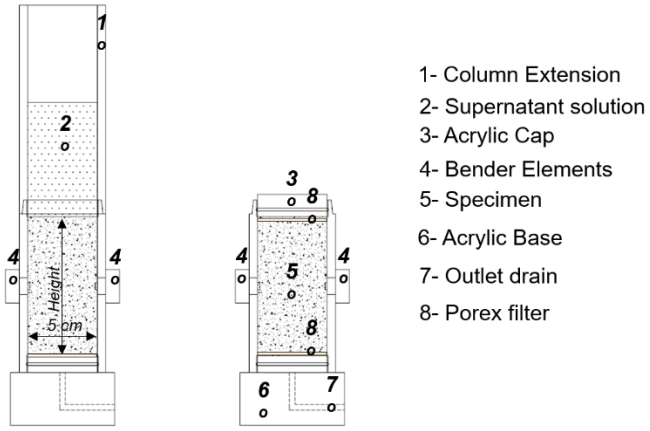

Figure 4-2. Column test details, sample preparation.

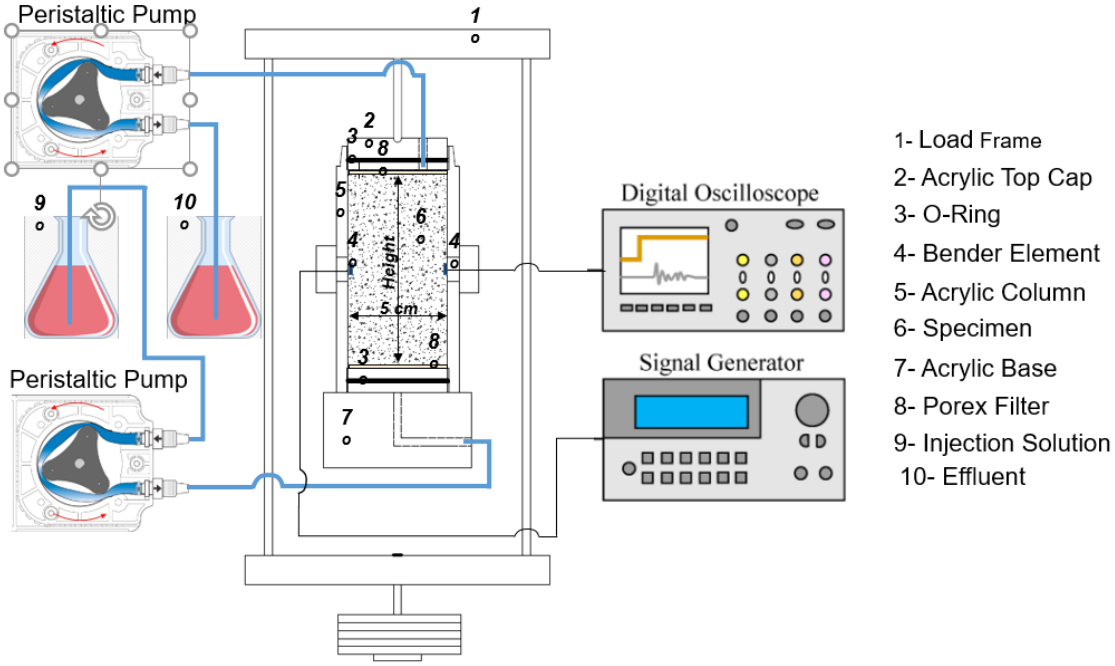

Figure 4-3. Schematic of devices used for column test.

4.3.3 Calcium Carbonate Content

To measure the mass of calcite, gravimetric acid washing of the samples was performed with the assistant of a centrifuge in order to accelerate coal ash deposition. The oven-dried mass of each sample section was recorded before and after washing with 1 M of HCl. The dissolved calcium carbonate and acid solution were rinsed multiple times allowing the dissolved salts to be washed from the sample. The difference between the two oven dried masses was taken as the mass of calcium carbonate. The calcium carbonate percentage is calculated by dividing the mass of calcium carbonate by the mass of soil (Mortensen et al. 2011).

4.3.4 Morphology and elemental analysis of particles

The fly ash samples were analyzed at the Analytical instrumentation facility (AIF) at NCSU using the scanning electron microscope (SEM) equipped with backscattered and secondary electron detectors (BSE) coupled with energy dispersive X-ray spectroscopy (EDS). The SEM–EDS provides detailed imaging information about the morphology and surface texture of individual particles, as well as the elemental composition of samples. BSE provides visual information based on gray-scale intensity between chemical phases. Backscattered electrons are high-energy electrons that are reflected directly from the specimen surface. The number of electrons backscattered correlates to the atomic number. For example, a particle consisting of iron (atomic number 26) will be significantly brighter than a particle of carbon (atomic number 6). This phenomenon generates a contrast between phases of different atomic numbers that can easily be distinguished in the backscattered electron image (Kutchko and Kim 2006). The elemental composition of a sample is determined using characteristic X-ray spectrum of the specimen being examined. The EDS detector was capable of detecting elements with atomic number equal to or

greater than six. The intensity of the peaks in the EDS is not a quantitative measure of elemental concentration, although relative amounts can be inferred from relative peak heights (Kutchko and Kim 2006).

X-Ray Photoelectron Spectroscopy (XPS) is a second method used in this study to provide elemental and chemical bonding information from the very top surface of a specimen; therefore, the cleanliness of the sample and the storage container is important. The specimen is bombarded with X-Rays, and emitted electrons are energy analyzed. Most of the signal arises from the first few monolayers (Moulder 1995).

4.3.5 Bacterial activity

Electrical Conductivity is often used to monitor biochemical processes because it is sensitive to the ionic concentration in solution. As the concentration of ions increases in a solution, the solution would be more conductive of electrical flow current. To find the correlation between hydrolyzed urea concentration and the electrical conductivity of the solution, a batch testing was conducted. Sealed containers were used to prevent the gas exchange between atmosphere and the solution. Ten different concentrations of urea (CH_4N_2O) were prepared in the range of 0.1 M to 1 M with 0.1 M increments. One 15 ml vial of the solution containing *S. pasteurii* bacteria (OD_{600}=1.18) was added to each container, and the initial conductivity and pH were measured. The conductivity of each sample was measured after 3 days to allow sufficient time for hydrolyzing the urea. The final electrical conductivity measurement was taken after an additional 6 hours to ensure the urea was completely hydrolyzed. This batch testing was duplicated and the results are presented in Figure 4-4. A second-order polynomial equation (6) was fitted to the measured data, as presented in Figure 4-4 and will be used to assess the concentration of hydrolyzed urea (HU) from the electrical conductivity measurements (Co).

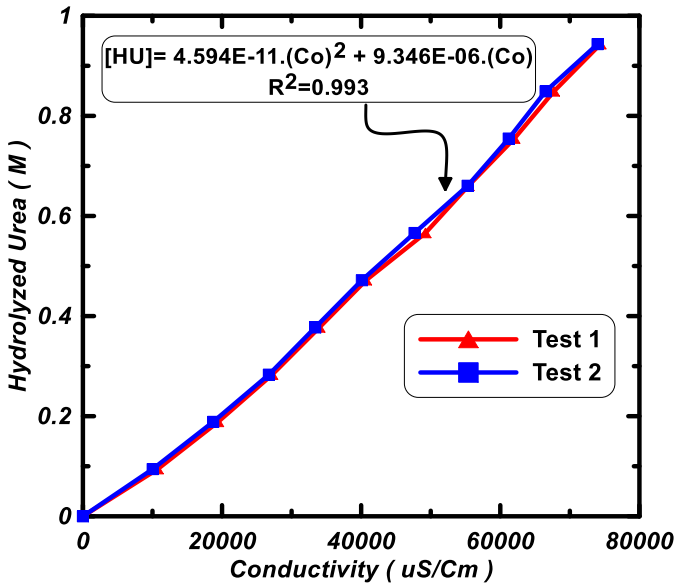

Figure 4-4. Correlation between electrical conductivity and concentration of hydrolyzed urea.

$$[HU]=4.594x10^{-11}.\ (Co)^2+9.346x10^{-06}.\ (Co) \quad \textbf{(6)}$$

To evaluate the effect of trace elements toxicity on the bacteria within different ashes, a second series of batch testing was conducted on three different coal ashes. Samples were prepared by mixing 200 gr of deionized water with 40 gr oven dried coal ash, and then incubated for 48 hours at 200 rpm and lab temperature. The mix was seated for 72 hours to allow solid particles to settle. The supernatant was collected and poured into the 60 ml vials and mixed with treatment recipe. The mix solution consists of 1 M urea, supernatant solution from the coal ash, and 5 grams of bacteria solution with OD=1.2 in total volume of 40 ml. Deionized water was used in baseline samples instead of coal ash supernatant solution for the sake of comparison. The conductivity of the solutions was measured after adding bacteria into the solution, and it was converted to hydrolyzed urea concentration using Equation (6).

4.4 Treatment Protocol and Response

Two-phase injection method has been used in past bio-treatment studies of sandy and silty soils (Martinez et al. 2013). In this approach, the biological media is injected into the specimen from bottom to top, and after sufficient retention time for attaching the bacteria to the soil particles, cementation media is injected. The biological solution comprised the bacteria's nutrition (i.e., urea) and microbe cells (*S. Pasteurii*). The cementation media have the salt (i.e., $CaCl_2$) in addition to microbe nutrition. To evaluate the effect of this approach on coal ash, four test samples with H/D=2 were prepared using the CA1 material. Three pore volumes of the biological solution, including 0.3 M urea and one-15 ml bacteria solution (OD~1.1), were injected into the columns; 4 hours of retention time was given to the bacteria for attaching to the particles. Different recipes of cementation solutions (i.e., three columns with 0.3 M urea and 0.1, 0.2, and 0.3 M $CaCl_2.2H_2O$ and one column with 0.5 M urea and $CaCl_2.2H_2O$) were injected into the specimens, and the shear wave velocity of each specimen was monitored using bender elements. The V_S of the specimens did not show a noticeable increase after four injections. The test was duplicated and the validation of such results was confirmed. Possible explanations could be a lack of active bacteria in coal ash (i.e., attachment did not occur within the retention time, or the coal ash environment is not proper for bacteria activity) or behavior of the coal ash particles that is different from sand during MICP because of filtering, shape, size, roughness, and composition of particles.

To ensure the presence of bacteria in the pore volume during the treatment, the bacteria culture is mixed with cementation media right before each injection. Five long columns (i.e., 10cm height) were prepared using the CA1 material to investigate the efficacy of the treatment method. The recipes of the bio-cementation solution are presented in Table 4-4. Three specimen's pore volumes (75 ml) of the bio-cementation solution were injected into the specimens from bottom to top at a

rate of 7 ml/min. The shear wave velocity (V_S) of the specimens was measured before each injection, and the results are plotted in Figure 4-5 in terms of V_S / V_{Si} (i.e., V_S normalized to the initial shear wave velocity, V_{Si}) of the specimens. The monitored V_S of the column 1 (C1) specimen increased after second injection while such an increase occurred for the column 2 (C2) specimen after seven injections. However, the rate of V_s increase for C2 specimen was higher than for C1 and the magnitude of V_S for these two specimens is nearly equal at the end of treatment. Recipe [1:1] used in column 3 Specimen (C3) did not yield noticeable increase in shear wave velocity, which was confirmed with duplication. There was a slight V_S increase at the last treatments for C4 column, but it was negligible in comparison to the increase in V_S observed for C1 and C2 specimens. The baseline (i.e., BL) specimen did not show any noticeable shear wave velocity variation while deionized water was injected during treatments. The high induced pressure during the twelfth injection detached the shaft from the bottom base of the MICP treated columns and the treatment was ceased due to suspected clogging.

Table 4-4. Recipes of bio-cementation solutions

Column	[Urea] (M)	[$CaCl_2$] (M)	NH_4Cl (M)
BL	0	0	0
C1	0.4	0.1	0.1
C2	0.4	0.2	0.1
C3	0.4	0.4	0.1
C4	0.8	0.4	0.1

The pH and conductivity of the effluent were measured right after each injection to monitor the bacteria activity and changes in treatment solution (Figure 4-6). During the MICP process, the pH will increase above neutrality when the concentrations of the products from hydrolyzed urea increase above the concentration of initial $CaCl_2$. By comparing the results of pH, which are presented in Figure 4-6, and shear wave velocity (Figure 4-5), a jump in pH level can be observed at the onset of V_S increase and this jump is showing higher hydrolyzed concentration in

comparison to initial $CaCl_2$ concentration. Electrical conductivity is produced by the summation of the conductivity of different ions (e.g., Ca^{2+}, Cl^-, NH_4^+, CO_3^{2-}, etc.). Results of electrical conductivity shown in Figure 4-6 confirm the concentration validity of injected solutions.

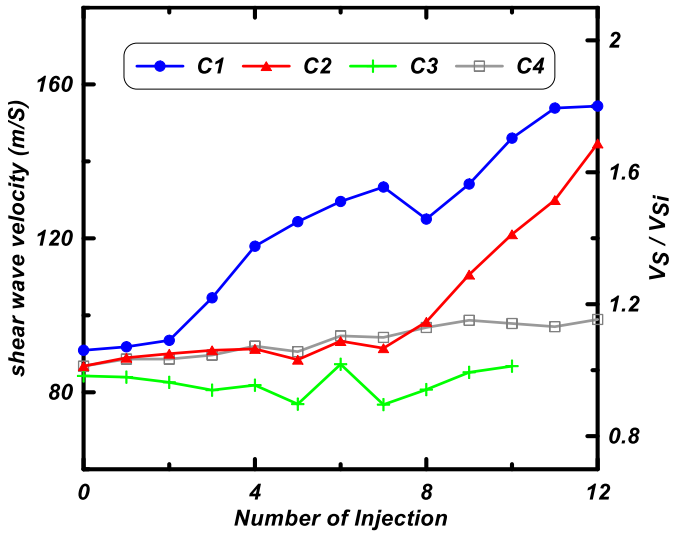

Figure 4-5. Shear wave velocity of the specimens at the center height of the columns, optimizing recipe.

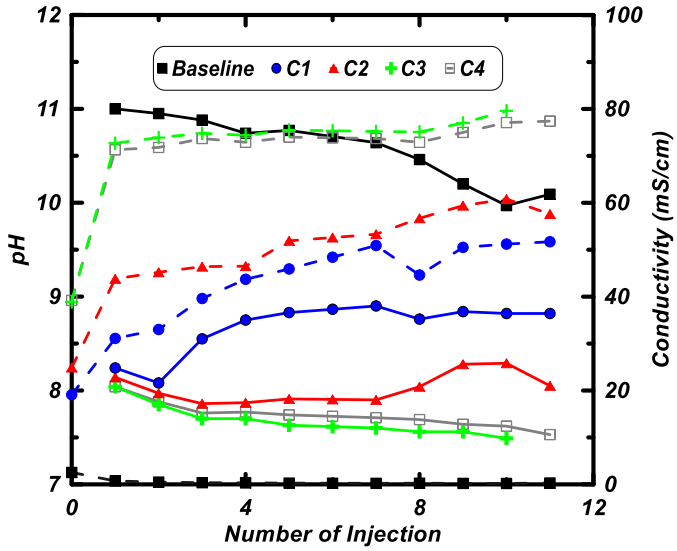

Figure 4-6. pH (solid line) and Conductivity (dashed line) of the collected effluent after each injection.

4.4.1 MICP and Cementation Mass

For this part of the study, the height of columns was shortened to decrease the effect of filtering on bacterial distribution and its effect on the corresponding calcium carbonate precipitation within the ash. Based on the results of shear wave velocity on long column test, 0.1 M and 0.2 M $CaCl_2$ recipes (i.e., shown in Table 4-4) yielded consistent increase in shear wave velocity, and these recipes were selected for further investigation.

Nine column specimens were designated to evaluate the effect of MICP treatment on the material of this study; three columns for each coal ash (i.e., CA1, CA2, and CA3). The name of the column and their treatment recipes are presented in Table 4-5. Both diameter and height of the specimens were both 5 cm. Based on the results of previously discussed column testing as well as results in literature (Martinez et al. 2013), decreasing the volume of injection while increasing the frequency of injection helps to minimize clogging, and have more uniformly distributed bacteria. Therefore, the rate of injection was raised to 11 ml/min instead of 7 (ml/min), and the volume of injection was decreased to 2 pore volumes (instead of 3).

Table 4-5. Recipe of the short column test on three coal ashes (CA1, CA2, CA3)

Column and material	[Urea] (M)	[CaCl2] (M)	NH4Cl (M)
CA1-1, CA2-1, CA3-1	0	0	0
CA1-2, CA2-2, CA3-2	0.4	0.1	0.1
CA1-3, CA2-3, CA3-3	0.4	0.2	0.1

Shear wave velocity (V_S) of the specimens was measured before each injection. Figure 4-7 shows both V_s and normalized V_s with respect to the initial shear wave velocity (V_{si}). MICP treatment showed the highest V_S increase in CA1 material. The rate of V_S increase for CA1, using 0.2 M recipe, is higher than the case of using the 0.1 M recipe. The initial shear wave velocity of CA1 material under 100 kPa is approximately 85 m/s, and it was increased to 550 and 840 m/s after 16

injections for CA1-2 and CA1-3 columns, respectively. The average increase of V_S per injection for CA1-2 column was 28 m/s (0.1 M $CaCl_2$), and it was 41 m/s or CA1-3 column (0.2 M $CaCL_2$) for total 16 number of injections. The V_S measurements of short column test indicated higher levels of improvement in comparison to the results of long column (10 cm) test. The potential reasons include: a) shortening of column's height decreased the effect of bacteria filtering, and it was easier for bacteria and media to reach to the center of column where the pair of benders are installed, b) increasing the rate of injection, albeit with lower volume, allowed for more injections with no clogging and to push the bacteria further along the column's height. On the other hand, the result of MICP treatment on CA2 showed slight V_S increase in comparison to CA1 and CA3. The V_{Si} of the CA2 columns was approximately 115 m/s under 100 kPa pressure. After 15 injections, the V_S increased to 150 m/s for CA2-2 and it was increased to 195 m/s for CA2-3, when the samples clogged and the treatment was stopped. There could be several possible reasons for not improving the V_S during treatment, which will be discussed later. The CA3 material was successfully treated. The V_{Si} of the CA3 columns was nearly 70 m/s under 100 kPa pressure. The resultant V_S of CA3 specimens indicated that the average rate of increasing V_S of CA3-3 (0.2 M $CaCl_2$) is 16 m/s for total 14 injections and it is 8.2 m/s for CA3-2.

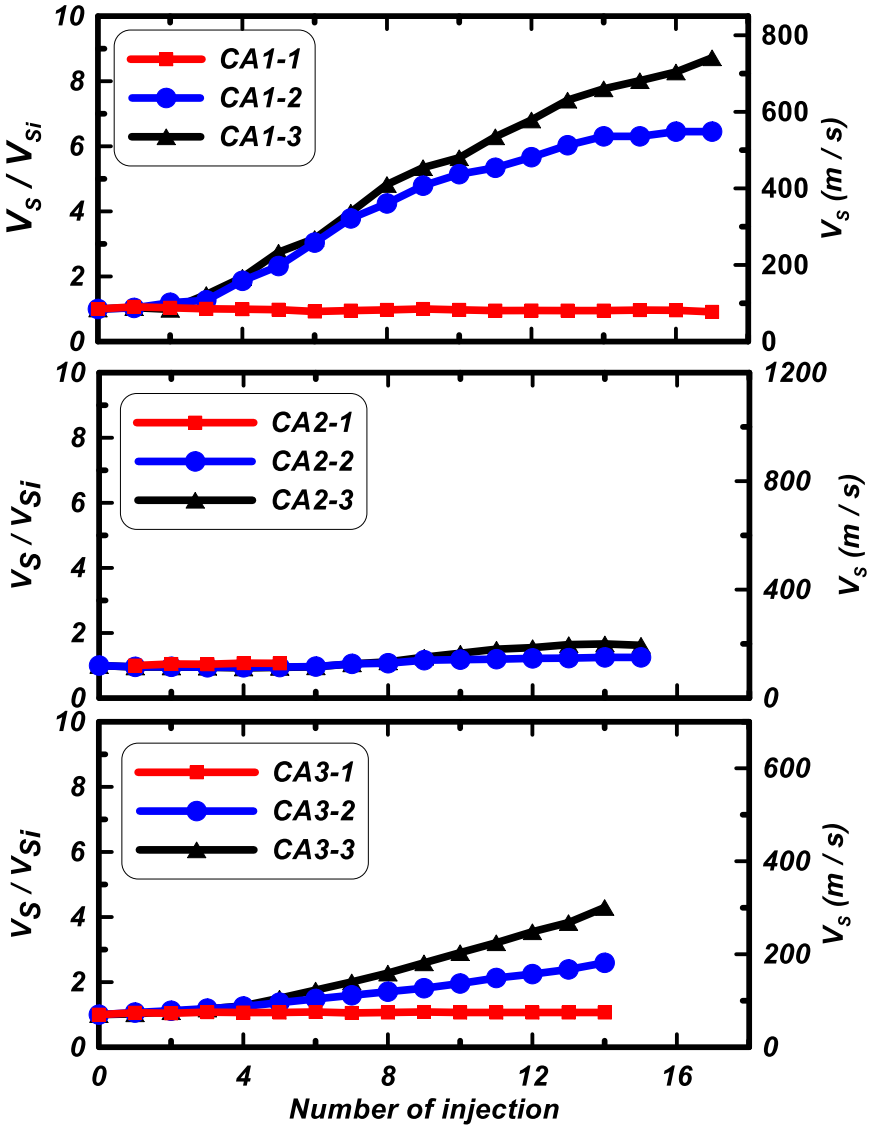

Figure 4-7. Monitored shear wave velocity during the treatment of short column tests.

In summary, the V_S results of CA2 material did not show a noticeable increase in comparison to the other two materials. The CA1 experienced an increase in V_S of about 6-8 times the initial V_S value within 16 treatments. CA3 also increased 2.5-4 times the initial V_S within 14 treatments. The treated coal ash specimens were extracted from the columns and sectioned into three parts. The calcium carbonate of the samples from each part was measured using gravimetric acid washing method with the assistance of a centrifuge. To consider the effect of acid digestion during acid washing and corresponding mass lost, the same acid washing method was performed on a baseline

(untreated) specimen. The results indicated that the baseline CA1, CA2 and CA3 material have, respectively, 2, 3.5 and 3 % of mass loss and these values are subtracted from total mass loss. The $CaCO_3$ percentages of the samples are presented in Table 4-6.

Table 4-6. $CaCO_3$ % of the samples in short column test after treatment

Column	Position	CaCO3 (%)
CA1-2	Bottom	17.20
	Middle	8.80
	Top	3.20
CA1-3	Bottom	20.20
	Middle	12.40
	Top	8.30
CA3-2	Bottom	11.60
	Middle	5.20
	Top	3.10
CA3-3	Bottom	13.90
	Middle	10.90
	Top	9.70

The pattern of calcium carbonate precipitation is further investigated using SEM images of the CA1 and CA3 samples before and after treatment. SEM images of the samples with various magnification levels are presented in Figure 4-9. The observed pattern was the same for both treated CA1 and CA3 materials. Therefore, only SEM images of the CA1-3 sample (i.e., collected from the bottom section of CA1-3 specimen) is presented. It shows the $CaCO_3$ bonds between coal ash particles, which explains the increase in the shear wave velocities while treating the columns. Energy dispersive X-ray spectroscopy (EDS) mapping was performed in addition to the SEM analysis to confirm that the precipitated crystals were $CaCO_3$. Figure 4-8-a shows the elemental analysis performed on a preselected line to determine the type and intensity of the elements. The results indicated that the most dominant elements on the exhibited line are silicon, aluminum, and calcium. The calcium herein proves that the crystalline shapes in the SEM images are precipitated calcium carbonate crystals. The results of V_S measurements of CA2 columns'

treatment indicated no to slight increase in shear modulus after 14 times treatment solution injection. Figure 4-8-b shows the result of EDS analysis on the sample collected from the bottom of CA2-3 column. These results and additional SEM images demonstrated the absence of calcium carbonate precipitation during the MICP process.

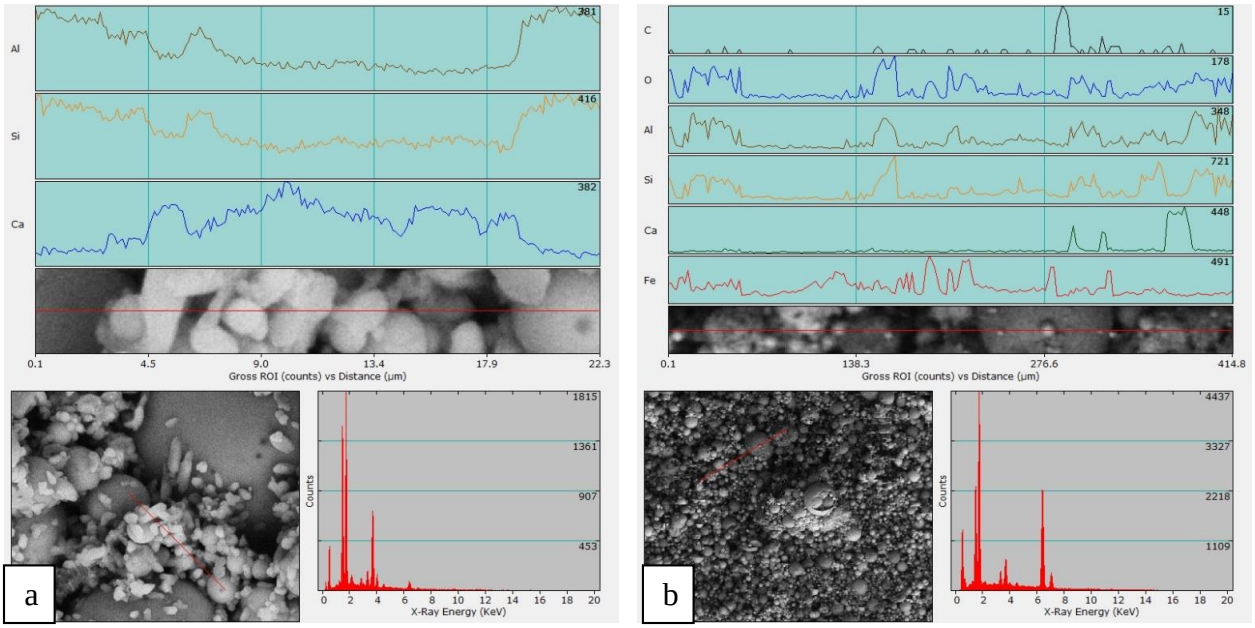

Figure 4-8. Results of EDS analysis a) on CA1-3 sample b) on CA2-3 sample, both of them were collected from the bottom of the specimen.

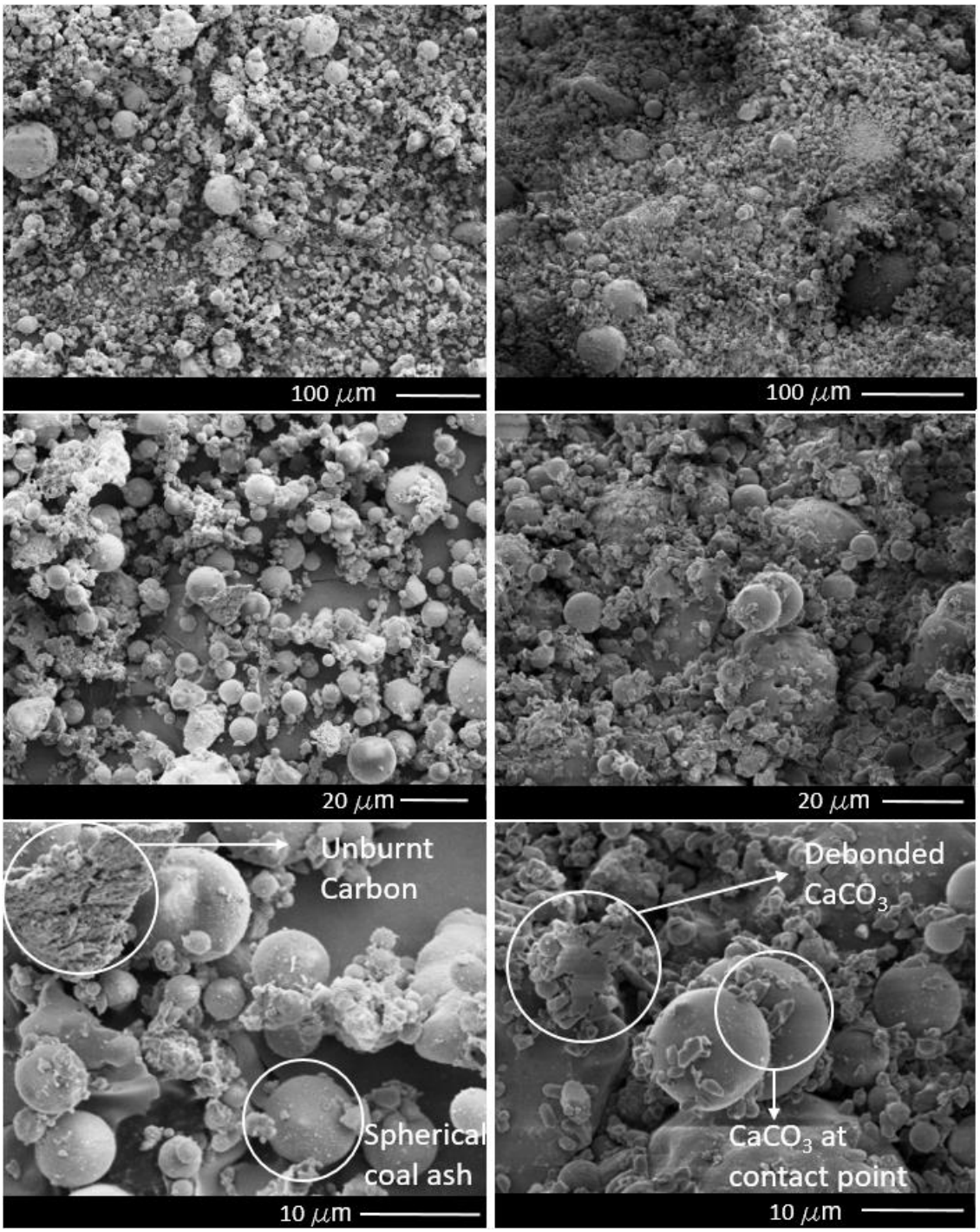

Figure 4-9. SEM images of CA1 before (left images) and after treatment (right images) with different magnifications. The sample was collected from bottom of CA1-3 specimen.

4.5 Potential factors affecting the MICP treatment process

The results of short column testing on three coal ash materials indicated that their shear wave velocity response and the calcium carbonate precipitation's percent were different while they were identically treated. Several possible factors are considered to further the understanding of such different responses. These factors include: A) *S. Pasteurii* bacteria activity inhibitors, B) bacteria filtration by coal ash particles C) particle roughness and its effect on calcium carbonate attachment, D) calcium carbonate precipitation inhibitors, E) nucleation site for calcium carbonate precipitation.

Sporosarcina pasteurii's urease inhibitors. Urease activity has been found to be highly dependent on the existence of heavy metal ions (Upadhyay 2012). It was demonstrated that these ions reacted on the active sites of the enzyme in a manner similar to the formation of metal sulfide. These insoluble sulfide metals have been shown to highly inhibit the urease activity and corresponding urea hydrolysis (Shaw 1954). The relative inhibitory efficiency of the studied metals has been reported to be; $Ag^{+} \sim Hg^{2+} > Cu^{2+} > Cd^{2+} > Ni^{2+} > Co^{2+} > Fe^{2+} > Mn^{2+}$ (Upadhyay 2012). The results of EPA 3051A standard test method on CA1, CA2 and CA3 indicated the existence of the mentioned heavy metals with different quantities. Therefore, a batch testing was performed to evaluate the toxicity of the trace element on the activity of the bacteria.

After incubating the material with deionized water for 48 hrs to solubilize the trace elements, the leachate was collected and mixed with urea to have 1 M urea concentration. The bacteria activity was monitored by tracking the concentration of hydrolyzed urea using conductivity measurements. The testing was performed in duplicate for each coal ash material. The results of batch testing are shown in Figure 4-10 and indicated that the soluble trace elements in the leachates collected from the three test coal ashes could not cease the bacterial activity, and urea was hydrolyzed in a trend

similar to the baseline. While the results for the leachate solution were slightly lower than the baseline, the difference is negligible. Therefore, it can be concluded that the soluble heavy metals in deionized water did not hinder the activity of the bacterium and as such it is not the reason for the lack of calcium carbonate precipitation in CA2 material.

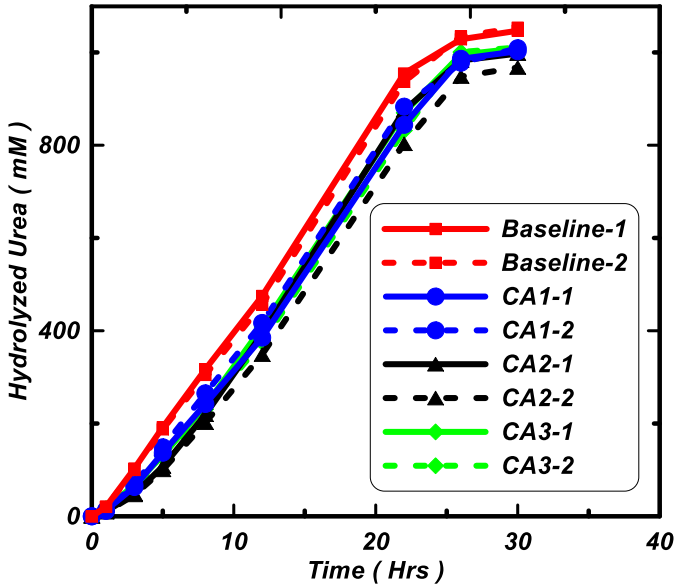

Figure 4-10. Evaluation of bacterial activity in the leachates from coal ashes performing a batch testing.

Bacteria filtration by coal ash particles. Based on the results of particle size distribution and characteristics (Table 4-7), the CA2 material has significant fines content compared to the other ash materials. In CA2, 92% of the particles are finer than 0.075 mm, while it is 65% and 82% for CA1 and CA3 materials, respectively. One of the hypotheses to explain the lower improvement in V_S is the fines content of the ash filtered the bacteria more significantly during the pumped flow inoculation, resulting in an inadequate distribution of bacteria within the soil column to induce MICP. To test this hypothesis, the fines content was reduced by removing the supernatant during the hydrometer test. The resultant particle size distribution (i.e., PSD) of the Modified CA2 is

presented in Figure 4-11. The particle size characteristics of three original coal ashes and Modified CA2 are presented in Table 4-7.

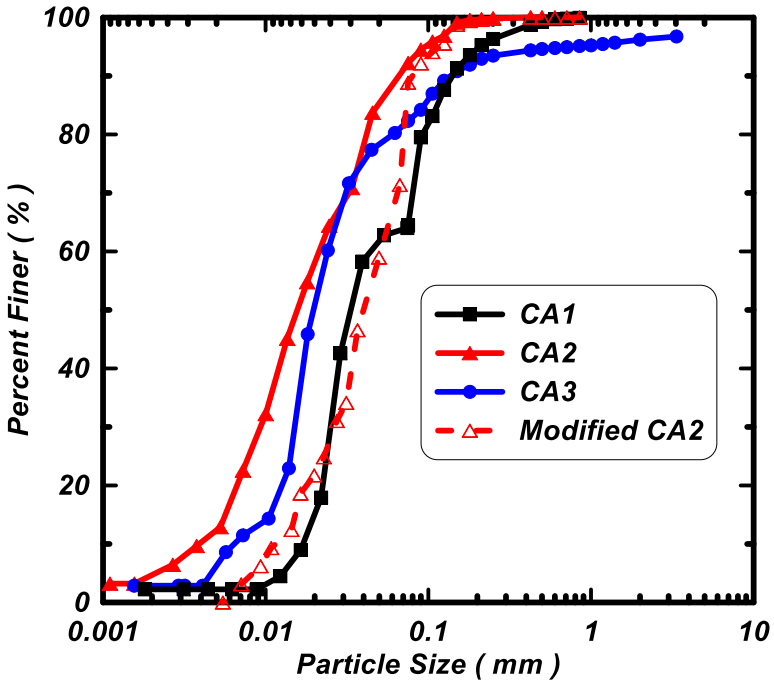

Figure 4-11. a comparison between particle size distribution of the modified CA2 and the original coal ashes.

Table 4-7. PSD characteristics of original coal ashes and modified CA2.

Characteristic	CA1	CA3	CA2	Modified CA2
D85 (Micron)	120.8	94.6	49.8	73.2
D60 (Micron)	46.4	24.0	21.5	51.2
D50 (Micron)	31.6	19.9	15.8	40.3
D30 (Micron)	21.9	15.2	9.4	26.6
D15 (Micron)	17.2	10.7	5.7	15.2
D10 (Micron)	14.0	6.4	3.9	11.2
D15/5 (Micron)	3.4	2.1	1.1	3.0
Cu	3.3	3.7	5.5	4.6
Cc	0.7	1.5	1.0	1.2

An approximate relationship for determining the pore opening size of material is D_{15} / 5 (Giroud 2010). There are several factors such as uniformity, particle shape and roughness of both filter and retained material affecting the filter's opening size (Giroud 2010). Therefore, while the D_{15} / 5 criterion does not provide the actual opening size, it can be used to compare the different coal ash

materials. The resultant particle size distribution (PSD) of the modified CA2 material showed that removing some portion of the fine particles produced a material with PSD closer to CA1 and CA3 (i.e., the PSD curve of modified CA2 material is located between CA1 and CA3 PSD (Figure 4-11)). Therefore, it should have a behavior similar to CA1 and CA3 from a filtration perspective. The MICP treatment worked on CA1 and CA3 materials (Figure 7); hence bacteria filtration is likely not an MICP treatment inhibitor given the modified PSD of CA2.

To investigate the effect of MICP treatment on the modified CA2 material, two short columns were prepared using modified CA2 material. After applying 100 kPa pressure to the top of the columns, two pore volumes of the bio-cementation solution (0.1 M $CaCl_2$ as shown in Table 4-5) were injected into the columns and the V_S was monitored. Even though the CA2's PSD was modified, the shear wave velocity of the specimens did not noticeably increase after 14 injections (Figure 4-12) (i.e., from V_{Si} = 100 m/s to 130 m/s). These results indicated that in this case the PSD and bacteria filtration are not the controlling factors of MICP treatment inhibitions for CA2 material.

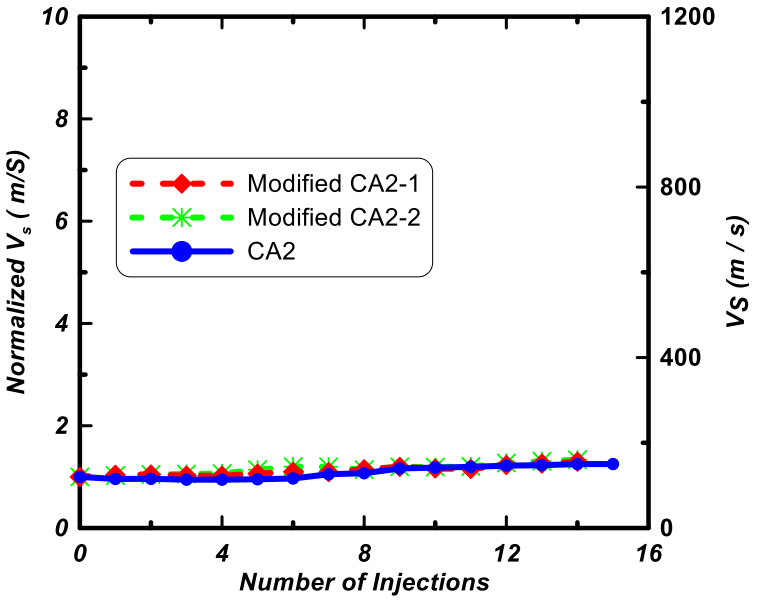

Figure 4-12 . Effect of MICP treatment on V_S of modified CA2

Particle roughness and its effect on calcium carbonate attachment. Roughness of the particles is a factor controls the attachment of precipitated calcium carbonate to particle surfaces. The heat energy when the coal is combusted and the ash is generated can affect the melting process of mineral matter in coal. The high heat energy level results in melting minerals (Clarke and Sloss 1992) and based on the cooling operation system, the surface of the particle could have different texture and different levels of roughness (Kutchko and Kim 2006). Lower carbon content is an evidence of exposing the coal to higher heat energy (Xiao et al. 2005). The coal ash evaluated in the current study has varying levels of carbon content (3.42%, 0.48%, and 8.46% by weight for CA1, CA2, and CA3, respectively), indicating that the ash may also have varying particle surface roughness. In order to explore the particles' surface, morphology and texture, the SEM images of untreated CA1 and CA2 matrial are compared in Figure 4-13. As mentioned earlier, treatment of CA1 yielded the maximum level of improvement while the same treatment of CA2 did not show any noticeable V_S increase.

Two main differences were observed by comparing the SEM images: 1) the spherical particles of CA2 include higher percentage of bright material (Figure 4-13) which indicates a higher iron content (Kutchko and Kim 2006), 2) the number of agglomerated particles in CA1 material is much higher than CA2 as indicated in Figure 4-14.

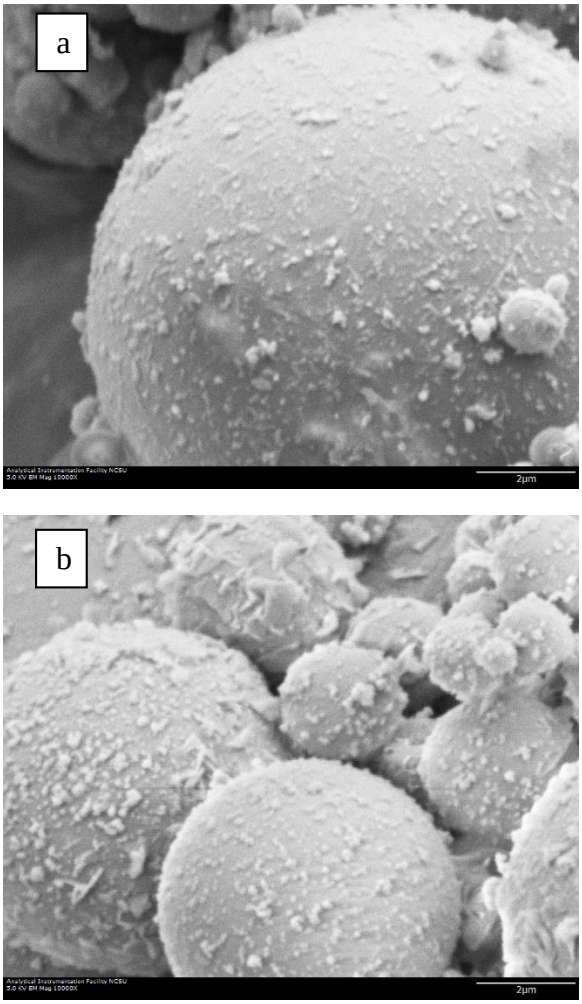

Figure 4-13. Surface texture of the spherical particles using SEM images; a) CA1, b) CA2.

The SEM images did not indicate that CA1 particles are rougher than CA2, and they confirmed the higher percentage of iron in the CA2 material, which was also previously shown from EPA 3051 results. A hypothesis that can be advanced here is the agglomerated particles provide enough roughness as nucleation sites for calcium carbonate precipitation, but such hypothesis needs further investigation.

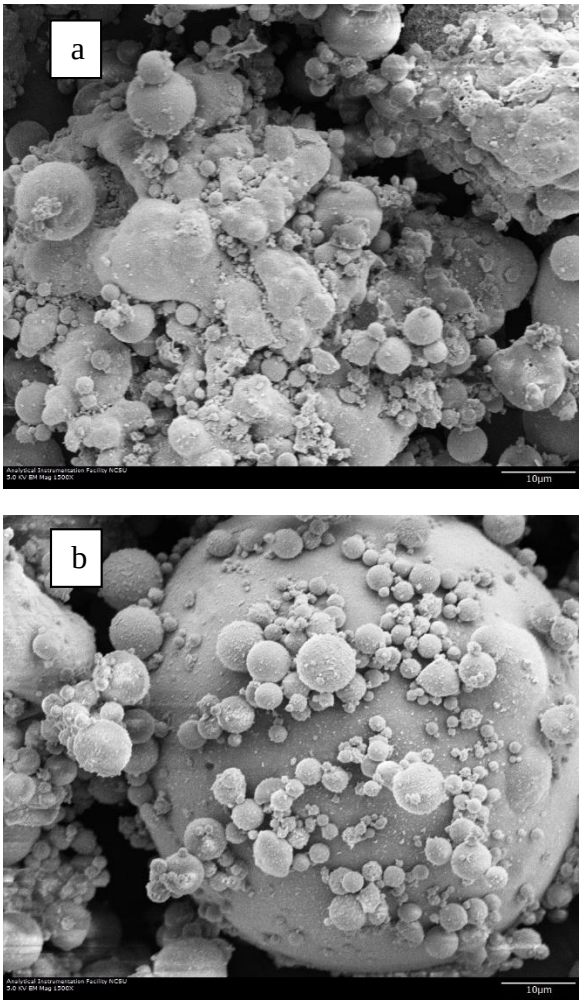

Figure 4-14. a) Agglomerated particles of CA1, b) Typical morphology of CA2.

4.5.1 D) Calcium carbonate precipitation inhibitors

While the concentration of CO_3^{2-} ion in a solution containing Ca^{2+} is steadily increased, the concentration of $CaCO_{3(aq)}$ complex increases and the solution goes to a supersaturation state. The polymerization, nucleation, and precipitation are the steps for calcium carbonate crystallization (Benjamin 2014). There are three main types of imperfections in crystal: point, line and surface imperfections. These imperfections have the ability to change the crystal growth structure and even to inhibit crystal growth (Mullin 2001). Impurity of the ions in the solution is one of the reasons leading to imperfections. Divalent cations have been the main focus of the studies on inhibition of

calcite crystallization (e.g., iron (Katz et al. 1993), magnesium (Berner 1975), cadmium and strontium (De Leeuw 2002)). The results of microwave acid digestion test (Table 4-2) and XRD method (Table 4-1) indicated that the concentration of iron in CA2 material is higher than for CA1 and close to the concertation in CA3. (Katz et al. 1993)) showed that existence of Fe (II) and Fe(III) could decrease the rate and efficiency of calcite precipitation, and Fe(II) is a stronger calcite inhibitor in comparison to Fe(III). To investigate the effect of iron on calcite precipitation, two approaches were considered; a) performing a short column test to assess the effect of retention time, allowing more time for calcium carbonate to precipitate if indeed the precipitation rate is decreased due to the presence of iron, ,and b) conducting elemental analysis on CA2 and CA3 using EDS and XPS approach to find the iron content and type of iron (i.e., Fe(II) or Fe(III)).

Three short coal ash columns of CA2 material were prepared to investigate the effect of retention time on calcium carbonate precipitation after bio-cementation solution injection. Two of the columns were designated to look at the effect of retention time, and the third was used as baseline test. The 0.1 M $CaCl_2$ recipe in Table 4-5 was used as the treatment solution while deionized water was injected into the baseline specimen. The V_S of the specimens were monitored for 3 days after each injection and the solution was injected into each column for four times. The tracked V_S of the treated columns followed the V_S of the baseline specimen. The V_S results showed three days of retention time to the treated columns did not change the V_S response, and the treatment did not improve the V_S noticeably.

The elemental mapping was conducted on the three coal ashes (CA1, CA2, and CA3) using EDS method in AIF at NCSU. This method provides the percentage of different elements in each coal ash material, but it cannot determine the valance of the elements (e.g., Fe(II) or Fe(III)). The results (i.e., shown in Figure 4-15) indicated that the iron percentage in CA2 and CA3 is close (i.e.,

approximately 13%) and higher than CA1 (i.e., 6.5%). The CA2 and CA3 materials have roughly the same iron percentage. To explore the type of formed crystals, particularly iron, XPS was performed on CA2 and CA3 materials. Analysis of the results indicated that the Fe signal was very similar for both samples and the peak for Fe was at 712 eV which is more likely Fe_2O_3 (Fe(III)) than FeO (Fe(II)). Therefore, the main iron composition of these coal ashes are likely Fe_2O_3 (Fe(III)), which is a weaker calcite inhibitor in comparison to Fe(II). Therefore, it seems that iron is not the reason of calcite crystal inhibition in CA2 material.

The XPS results pointed out the existence of Sulfur on CA2 which was not detected in the CA3 material. Previous studies on the effect of sulfur/sulfate on inhibition of calcite precipitation indicated that low concentration of sulfate ions (i.e., up to 3 mM) did not sufficiently interact with calcite surfaces as a substitute of carbonate to retard or inhibit calcite crystal growth ((Vavouraki et al. 2008; Reddy and Nancollas 1976). Moreover, CA3 material has two carbon peaks while only one is detected form the XPS results on CA2, and it matched with a carbide peak. Carbide is a compound of carbon and a less electronegative element (Greenwood and Earnshaw 1984). The existence of carbide confirms the results of carbon content and indicates an incomplete burn of carbon during coal combustion process for CA3 material.

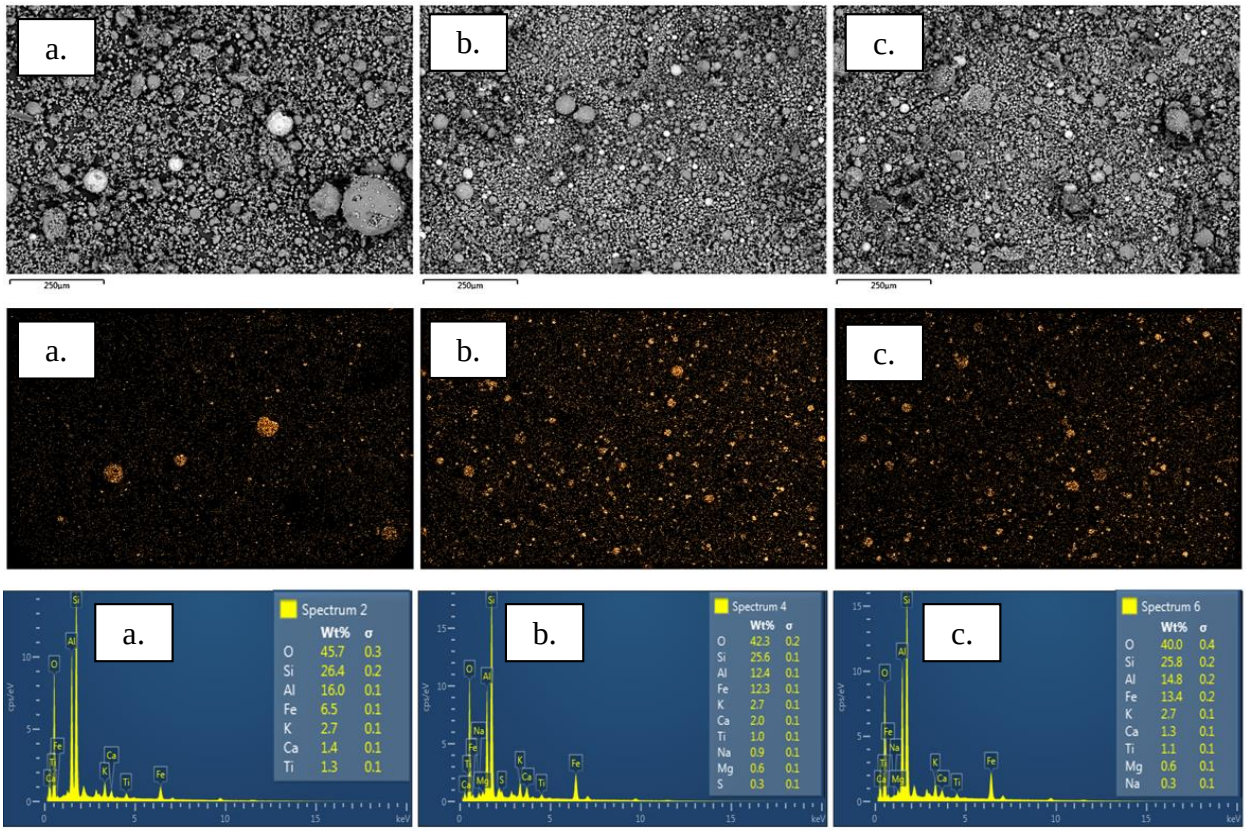

Figure 4-15. Mapping of elements using EDS method; a.1) CA1, EDS image, b.1) CA2, EDS image, c.1) CA3, EDS image, a.2) CA1, iron mapping, b.2) CA2, iron mapping, c.2) CA3, iron mapping a.3) CA1, elemental analysis, b.3) CA2, elemental analysis, c.3) CA3, elemental analysis.

4.5.2 E) Nucleation sites for calcium carbonate precipitation

Nucleation sites have an important role in calcium carbonate precipitation. They are the area that the chemical complexes nucleate and crystal growth takes place. Lack of nuclei can lead to an inhibition of crystallization. The carbon content results indicated that the carbon content of the CA2 material is quite small (i.e., ~0.5%) compared to the other two materials (i.e., 3.42% and 8.46% for CA1 and CA3, respectively). The mapping on SEM images revealed that CA1 and CA3 material have a large number of agglomerated particles while most of the CA2 material is spherical and glassy. Furthermore, the results of XPS on CA2 and CA3 material showed the existence of

carbide on CA3 material which was not in CA2. This collective evidence points to the hypothesis that the carbon content could be the reason that the MICP treatment did not work on CA2 material.

Activated carbon has been used in filtration system to adsorb inorganic content of water for improving water quality (Mohan and Singh 2002). Because of high adsorption potential of this material, it can be considered as a nucleation site for calcite growth. On the other hand, dissolved inorganic carbon in solution can cause inhibition of calcite growth (Lebron and Suarez 1996).

In order to assess the effect of carbon content on the MICP treatment process, the carbon content of CA3 material was removed by exposing CA3 material to heat in a furnace at two different temperatures of 500^{o}c and 700^{o}c for 24 hours and they referred to modified CA3-500^{0}c and modified CA3-700^{0}c material, respectively. The mass reduction was measured to be 8.3% and 9.3%, respectively. Five Short columns were then prepared using the original CA2 and CA3, and modified CA3 materials. One column specimen was prepared for original CA2, original CA3, and modified CA3-700^{0}c, and two column specimens were prepared using modified CA3-500^{0}c material. The 0.1 M bio-cementation solution (Table 4-5) was injected into the columns while monitoring the V_S. Results of V_S measurements are shown in Figure 4-16. The initial V_S of the columns was decreased by removing the carbon content and the initial value was different for CA3 and CA2 material. Therefore, the shear wave velocity normalized with respect to the initial shear wave velocity is presented to compare their behavior. Results of monitoring shear wave velocity of the CA3 and CA2 material are similar to what has been observed during the first short column testing (Figure 4-7 and Figure 4-16). The results indicated the lack of carbon in the ash inhibits calcium carbonate precipitation. The V_S of the original CA3 material increased to 3.5(V_{Si}) after 12 times injection, and it was 1.3(V_{Si}) for original CA2 material. Carbon content reduction changed the behavior of CA3 material significantly while exposed to MICP treatment. The V_S increase of

modified CA3 material decreased significantly in comparison to original material and its trend was more similar to V_S trend of original CA2 material. It is therefore concluded that carbon content of coal ash has a significant impact on MICP treatment. The hypothesis here is that the carbon and carbide material in coal ash can provide the nucleation site for calcium carbonate crystal growth and the lack of this material would inhibit calcium carbonate precipitation.

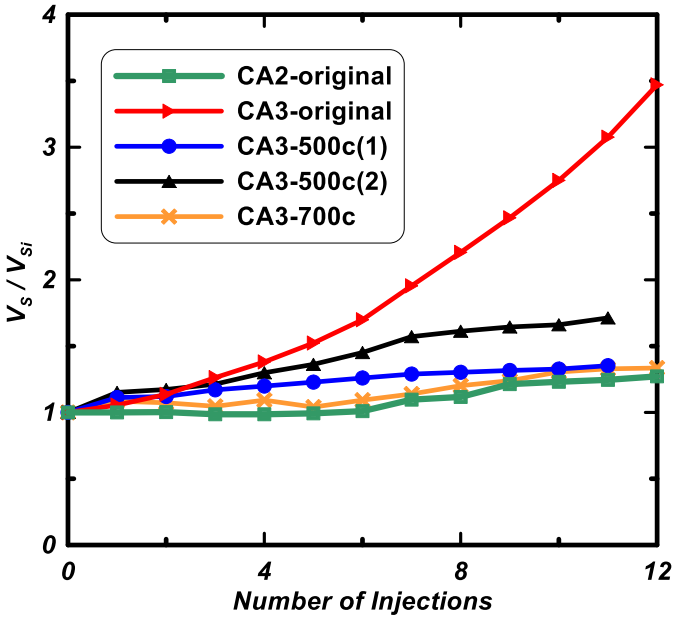

Figure 4-16. Effect of decreasing carbon content on MICP treatment

4.6 Summary and Conclusion

In this study, the effect of MICP treatment on the coal material was investigated for the first time. The protocol of treatment was developed after looking at different methods and recipes. The bio-cementation method increased the shear stiffness (assessed via shear wave velocity) for the CA1 and CA3 materials and the 4:1 (urea(M): $CaCl_2.2H_2O$(M)) and 4:2 recipes showed the best improvement on shear stiffness. The pattern of calcium carbonate precipitation on the treated material was explored using SEM/EDS method, and it was different from typical solid calcium carbonate patterns between sand particles using same treatment method. The MICP treatment did

not work on one of the coal ashes (CA2) and accordingly, different possible factors potentially affecting the MICP treatment of coal ash were studied: A) *Sporosarcina pasteurii* bacteria activity inhibitors, B) bacteria filtration by coal ash particles C) particle roughness and its effect on calcium carbonate attachment, D) calcium carbonate precipitation inhibitors, E) nucleation site for calcium carbonate precipitation.

The results indicated that the leachate from the coal ashes and the soluble trace elements did not decrease the urealytic activity of the *S. pasteurii* bacteria noticeably. The effect of bacteria filtration of CA2 material was studied by removing a fraction of the finest ash particles using the hydrometer method. The results of the corresponding short column test with the modified coal ash particles size distribution showed that filtration is not the reason MICP did not work on CA2 material. Roughness of particles can help the attachment of calcium carbonate. The SEM/EDS images showed that the roughness of spherical particles in CA1 and CA2 are similar and it is even higher in CA2 material. There were more agglomerated particles in CA1 and CA3 compared to CA2, which is related to coal combustion and cooling process, and they may provide nucleation sites for calcium carbonate precipitation. This study didn't cover the effect of agglomerated particles, and it should be studied further. The existence of soluble calcium carbonate precipitation inhibitors in coal ashes has the potential to cease the crystal growth. Iron is a calcite inhibitor, and the CA2 and CA3 have high iron percentage based on the results of SEM/EDS, acid digestion and XRD. The percentage and type of iron within CA2 and CA3 were mapped using EDS and XPS methods, respectively. The results showed the iron percentage is similar in the two ash materials and the majority of the iron present is Fe_2O_3 in both. The retarder effect of iron or other possible elements were explored by allowing for extended treatment retention time of the specimens in short column while monitoring shear wave velocity. The V_S results did not show improvement.

The last hypothesis for the lack of calcium carbonate precipitation in CA2 was providing the nucleation site for calcium carbonate precipitation by carbon and carbide material in coal ash, which was absent in CA2. The carbon content of CA3 material was removed by exposing it to high heat. An additional column test was performed on the modified ash material and the V_S results indicated that carbon and carbide content has an impact on MICP treatment of coal ash. Tracking the normalized V_S of the material showed the similar trend between modified CA3 and CA2.

In summary, the protocol of coal ash treatment using MICP approach was developed and applied to three coal ash material with different physiochemical and engineering characteristic. The results of column test indicated that the studied material responded differently while treated similarly. Two of coal ash material (i.e., CA1 and CA2) were successfully treated and MICP treatment increased the shear wave velocity (represented the shear modulus). Presence of calcium carbonate was proved using SEM/EDS analysis and measuring the $CaCO_3$ content. The treatment protocol did not improve the shear response of one of coal ash materials (i.e., CA2), and the possible reasons were investigated running different tests. The carbon content was found to have an important role in calcium carbonate precipitation of coal ashes. The hypothesis is the carbon and carbide material in coal ash can provide the nucleation site for calcium carbonate crystal growth and the lack of this material would inhibit calcium carbonate precipitation.

4.7 References

ASTM D 854-00. (2000). "Standard Test for Specific Gravity of Soil Solids by Water Pycnometer." *ASTM International, West Conshohocken, PA,* .

ASTM D422-63. (2007). "D422–63 (2007) Standard test method for particle-size analysis of soils." *ASTM International, West Conshohocken.Doi,* 10 1520.

Bachus, R., and Santamarina, C. (2012). "Geotechnical Properties of Fly ASH and Potential for Static Liquefaction: Volume I–Summary and Conclusions." *EPRI, Palo Alto, CA,* .

Benjamin, M. M. (2014). *Water chemistry.* Waveland Press, .

Berner, R. A. (1975). "The role of magnesium in the crystal growth of calcite and aragonite from sea water." *Geochim.Cosmochim.Acta,* 39(4), 494504.

Clarke, L. B., and Sloss, L. L. (1992). *Trace elements-emissions from coal combustion and gasification.* IEA Coal Research, .

Daniels, B. L. (2016). "Caution: Hazards Ahead: How the EPA's Refusal to Classify Coal Ash as Hazardous Waste Fuels Environmental and Public Health Concerns." *Vill.Envtl.LJ,* 27 93.

De Leeuw, N. H. (2002). "Molecular dynamics simulations of the growth inhibiting effect of Fe2 , Mg2 , Cd2 , and Sr2 on calcite crystal growth." *The Journal of Physical Chemistry B,* 106(20), 5241-5249.

DeJong, J. T., Mortensen, B. M., Martinez, B. C., and Nelson, D. C. (2010). "Bio-mediated soil improvement." *Ecol.Eng.,* 36(2), 197-210.

Feng, K., and Montoya, B. M. (2015). "Drained shear strength of MICP sand at varying cementation levels." *IFCEE 2015,* 2242-2251.

Fujita, Y., Taylor, J. L., Wendt, L. M., Reed, D. W., and Smith, R. W. (2010). "Evaluating the potential of native ureolytic microbes to remediate a 90Sr contaminated environment." *Environ.Sci.Technol.,* 44(19), 7652-7658.

Giroud, J. P. (2010). "Development of criteria for geotextile and granular filters." *Proceedings of the 9th International Conference on Geosynthetics, Guaruja, Brazil,* 4564.

Greenwood, N. N., and Earnshaw, A. (1984). "Chemistry of the Elements." .

Harkness, J. S., Sulkin, B., and Vengosh, A. (2016). "Evidence for Coal Ash Ponds Leaking in the Southeastern United States." *Environ.Sci.Technol.,* 50(12), 6583.

Katz, J. L., Reick, M. R., Herzog, R. E., and Parsiegla, K. I. (1993). "Calcite growth inhibition by iron." *Langmuir,* 9(5), 1423-1430.

Kutchko, B. G., and Kim, A. G. (2006). "Fly ash characterization by SEM–EDS." *Fuel,* 85(17–18), 2537-2544.

Lebron, I., and Suarez, D. L. (1996). "Calcite nucleation and precipitation kinetics as affected by dissolved organic matter at 25 C and pH> 7.5." *Geochim.Cosmochim.Acta,* 60(15), 2765-2776.

Link, D. D., Walter, P. J., and Kingston, H. M. (1998). "Development and validation of the new EPA microwave-assisted leach method 3051A." *Environmental Science and Technology,* 32(22), 3628-3632.

Martinez, B. C., DeJong, J. T., Ginn, T. R., Montoya, B. M., Barkouki, T. H., Hunt, C., Tanyu, B., and Major, D. (2013). "Experimental optimization of microbial-induced carbonate precipitation for soil improvement." *J.Geotech.Geoenviron.Eng.,* 139(4), 587-598.

Mohan, D., and Singh, K. P. (2002). "Single-and multi-component adsorption of cadmium and zinc using activated carbon derived from bagasse—an agricultural waste." *Water Res.,* 36(9), 2304-2318.

Mortensen, B. M., Haber, M. J., DeJong, J. T., Caslake, L. F., and Nelson, D. C. (2011). "Effects of environmental factors on microbial induced calcium carbonate precipitation." *J.Appl.Microbiol.,* 111(2), 338-349.

Moulder, J. F. (1995). *Handbook of x-ray photoelectron spectroscopy : a reference book of standard spectra for identification and interpretation of XPS data.* Physical Electronics, Eden Prairie, Minn.

Mullin, J. W. (2001). *Crystallization.* Butterworth-Heinemann, .

Nijhuis, M., and Kendrick, R. (2014). "Can coal ever be clean." *Retrieved October,* 7 2015.

Reddy, M. M., and Nancollas, G. H. (1976). "The crystallization of calcium carbonate: IV. The effect of magnesium, strontium and sulfate ions." *J.Cryst.Growth,* 35(1), 33-38.

Shaw, W. H. (1954). "The inhibition of urease by various metal ions." *J.Am.Chem.Soc.,* 76(8), 2160-2163.

Upadhyay, L. S. B. (2012). "Urease inhibitors: A review." .

Van Paassen, L. A. (2009). "Biogrout, ground improvement by microbial induced carbonate precipitation." .

Vavouraki, A. I., Putnis, C. V., Putnis, A., and Koutsoukos, P. G. (2008). "An atomic force microscopy study of the growth of calcite in the presence of sodium sulfate." *Chem.Geol.,* 253(3), 243-251.

Walton, W. H., and Butler, W. (2009). "Root Cause Analysis of TVA Kingston Dredge Pond Failure on December 22, 2008." *Vernon Hills,* .

Xiao, X., Yang, H., Zhang, H., Lu, J., and Yue, G. (2005). "Research on carbon content in fly ash from circulating fluidized bed boilers." *Energy Fuels,* 19(4), 1520-1525.

5. Chapter 5: Effect of MICP Treatment on Engineering Properties of Coal Ash

Shahin Safavizadeh

Graduate Student, North Carolina State University, Department of Civil, Construction, and Environmental Engineering, Raleigh, NC 27695; email: ssafavi2@ncsu.edu

Brina M. Montoya

Assistant Professor, North Carolina State University, Department of Civil, Construction, and Environmental Engineering, Raleigh, NC 27695; email: bmmorten@ncsu.edu

Mohammed A. Gabr

Professor, North Carolina State Univ., Department of Civil, Construction, and Environmental Engineering, Raleigh, NC 27695; email: gabr@ncsu.edu

Abstract

In this study, the MICP treatment protocol was experimentally implemented on two coal ash materials (i.e., CA1 and CA3) to investigate the efficacy of such approach on engineering properties. For this purpose, a modified oedometer device was developed to enable the injection of treatment solutions and to provide the ability to monitor shear wave velocity. The coal ash specimens were treated to reach different levels of shear wave velocity, which corresponded to varying amounts of $CaCO_3$ content. The large-strain and small-strain parameters were investigated by conducting oedometer tests; the hydraulic conductivity and shear wave velocity were also estimated throughout the loading process. Results indicate that the MICP treatment decrease the compressibility (compression index decreased up to a factor of about 0.5), hydraulic conductivity (up to a factor of about 0.05), coefficient of consolidation, and the slope of line in $\log(\sigma'_V)$-V_S (i.e. β') of the treated specimens (β' decreased up to 0.01 from 0.31 of untreated material) , and it increased the shear wave velocity after treatment and intersection of the line in $\log(\sigma'_V)$-V_S (i.e., α', and it increased up to 383 m/s from 38 m/s for untreated material). The correlation between small-strain and large-strain parameters are explored and discussed.

5.1 Introduction

Coal power plants have been one of the primary sources of electricity generation in the United States (DOE/EIA-0035 (2017/04)) and worldwide (Nijhuis and Kendrick 2014). Coal combustion residuals (CCRs) are the byproduct of coal burning in power plants, and over 140 million tons of CCRs are produced in United States yearly (Daniels 2016). Despite all the effort to recycle the coal ash in industrial application, most of CCRs are disposed of in monofills and impoundments (Harkness et al. 2016b), with over 500 ash impoundments across the United States.

Gradual disposal of coal ash in impoundments leads to elevating the height and corresponding increase of stress for the bottom layers of ash. The relatively low permeability and high compressibility of coal ash (Bachus and Santamarina 2014) can result in an undrained condition under high rate of loading (e.g., high rate of coal ash disposal, dewatering, and increasing the pond water level). Increasing the level of stress and changing the loading condition from drained to undrained condition can lead to global instability of ash ponds. This scenario was the reason for the Kingston power plant spill in 2008 (Walton and Butler 2009), which resulted in contamination of 300 acres of the land (Daniels 2016). In 2014, increasing the level of load above a stormwater pipe located beneath the impoundment in Eden North Carolina caused the pipe to break and spill of over 39,000 tons of coal ash into the Dan River (Daniels 2016). On the other hand, trace elements' concentration (e.g., arsenic, selenium, chromium) in monitoring wells close to impoundments have been reported to be above the background levels and even higher than drinking water and ecological standards in some cases (Harkness et al. 2016b). The structural stability and release/leaching of trace elements are the primary concerns regarding the coal ash impoundment.

A novel approach to improve the engineering properties of unbound media is microbial induced calcium carbonate precipitation (MICP). This approach has the potential of providing a natural and sustainable solution to improve the engineering properties of soils, and unbound materials in general, and research on the subject has gained momentum in recent years (DeJong et al. 2010). Results from previous studies indicated that MICP treatment of sand has the potential to increase its shear modulus (Martinez et al. 2013), to decrease its compressibility (Lin et al. 2015) and hydraulic conductivity (DeJong et al. 2010), and to change its volumetric behavior from contractive to dilative (Feng and Montoya 2015). On the other hand, from a water quality

perspective, MICP treatment has been used for immobilization of strontium in the ground water (Fujita et al. 2010). All the potential abilities of MICP treatments lead to the hypothesis that this method could be applied to coal ash material to minimize its related concerns. The results of column test on coal ash material revealed that MICP treatment could increase the shear wave velocity and calcium carbonate content of the specimens (i.e., discussed in chapter 4), but its effect on engineering properties of coal ash is unknown.

The objective of this study is to experimentally explore the effect of MICP treatment on engineering properties of coal ash material. Compressibility, hydraulic conductivity, and shear wave velocity are the target parameters to be investigated. Traditional odometer testing equipment is modified to provide the ability to inject treatment solution and to measure shear wave velocity. The large-strain and small-strain parameters are extracted from the experimental data for untreated and treated specimens, and a discussion is provided on the level of cementation's effect on different parameters.

5.2 Materials

5.2.1 Chemical composition of ash material

Two different coal ash materials (i.e., referred to as CA1 and CA3) are used in this study. The crystalline phases of the two coal ash test materials were identified using X-ray diffraction (XRD). PANalytical Empyrean X-ray diffractometer with a cukα radiation was used to perform the XRD analysis in the Analytical Instrumentation Facility at North Carolina State University. The step size is 0.026 degree, the counting time per step is 447 seconds, and the scan angle is from 10 to 90^0. High Score Plus software is used with an International Centre for Diffraction Data (ICDD) XRD database to analyze the data. As shown in Table 5-1, the results of analysis determined the

existence of the aluminum silicate, silicon oxide, aluminum oxide, and iron oxide as the major crystalline part of these coal ashes.

The samples of coal ash materials were placed in a furnace with 500^0c temperature for 24 hours to measure their carbon content. The mass lost is considered as the burnt mass of carbon. The results of carbon content measurements indicated 3.42% and 8.46% by weight for CA1and CA3, respectively.

Table 5-1. results of data analysis of XRD measurements using ICDD database.

Crystal	Formula	Relative Percentage	
		CA1	CA3
Aluminum Silicate	Al_2SiO_5	53.5	44.4
Silicon Oxide	SiO_2	36.4	37.4
Iron Oxide	Fe_2O_3	5.1	9.1
Calcium Oxide	CaO	1	0
Aluminum Oxide	Al_2O_3	4	9.1

5.2.2 Particle size distribution of the material

The hydrometer test (e.g., < 75 microns) and sieve analysis were performed to determine the grain size distribution of the material, following (ASTM D422-63 2007). The results of the hydrometer test and sieve analysis of two coal ash materials are shown in Figure 5-1. The CA3 material is finer in comparison to the CA1 material. The percentages of particles greater than sieve #200 (i.e., 0.075mm) are 35% and 18% for the CA1 and CA3 materials, respectively. The CA3 material contains 14% of the whole grains less than 10 μm while it is 6% for CA1 coal ash. Although CA1 material has smaller particle size distribution than CA3, all the CA1 particles are smaller than 1 mm while about five percent of the CA3 material is larger than 1 mm.

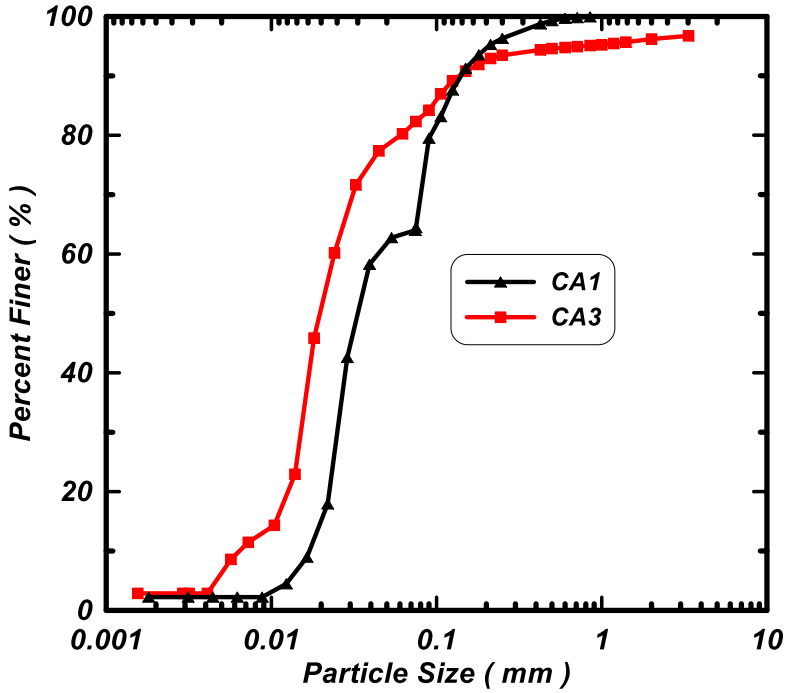

Figure 5-1. Particle size distribution of coal ashes.

To determine the specific gravity (G_S) and liquid limit (LL) of the material, the standard Pycnometer (ASTM D 854-00 2000) and Fall-cone test (ISO/TS 17892-6:2004) were conducted in duplicates, respectively. Based on Bachus and Santamarina's (2012) recommendation, the falling head test was performed to assess the hydraulic conductivity (k) of the material under minimum relative density condition (maximum k). The assessed properties of the two coal ashes are summarized in Table 5-2.

Table 5-2. Engineering properties of coal ashes

Characteristic	Material	
	CA1	CA3
D50 (Micron)	31.6	19.9
C_U	3.3	3.7
C_C	0.7	1.5
G_S	2	2..35
LL (%)	34	41
k (cm/s)	1.95E-04	1.95E-04
Carbon content (%)	3.42	8.46

5.2.3 Morphology of the particles

The morphology of coal ash particles was explored using SEM images, as presented in Figure 5-2. The images confirm the existence of typical fly ash spheres, cenospheres, unburned carbon or carbide, mineral aggregate, agglomerated aggregates, and irregular shaped amorphous particles in both coal ash materials. The image of CA1 material shows denser particles which are related to the sample preparation. These images represent some random samples, and they cannot be used quantitatively.

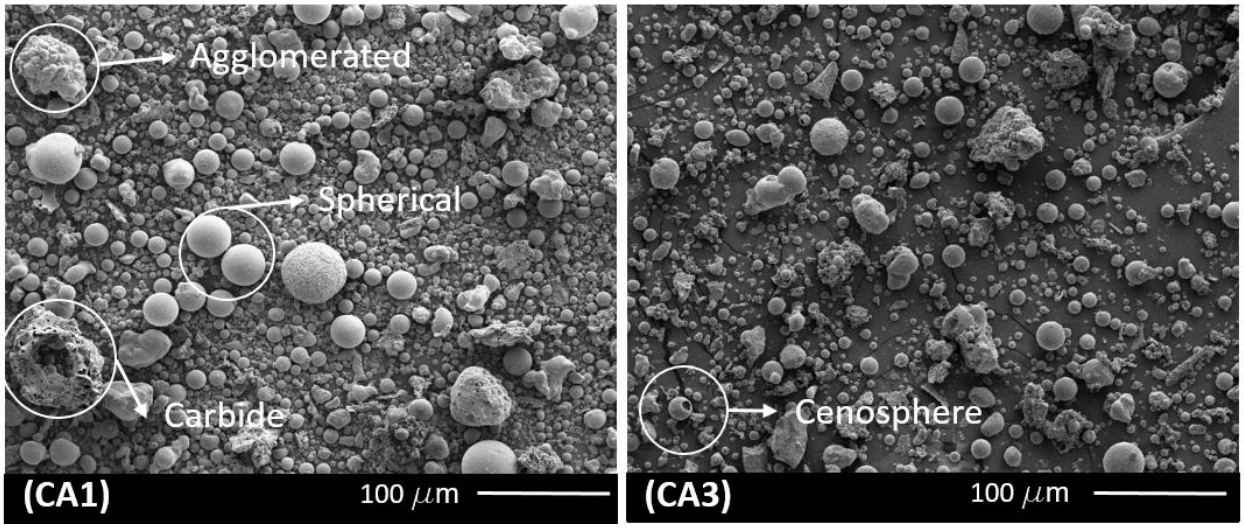

Figure 5-2. Morphology of studied coal ash materials using SEM method

5.3 Methods

5.3.1 Bacteria and growth condition

Sporosarcina pasteurii (ATCC 11859), a urea hydrolyzing bacterium, was grown and used in this study. For this purpose, ammonium yeast extract medium (ATCC 1376) was used to grow the bacteria at 30 ^{o}C. Each ingredient was autoclaved and mixed after sterilization. The growth medium was inoculated with *S. pasteurii* stock culture and incubated aerobically at 30 ^{o}C with 200

revolutions per minute till the desired population of cells was reached assessed using optical density (i.e., OD_{600}). Incubation stopped before reaching the plateau of the growth curve to avoid dead bacterial cells. Cultures were centrifuged at 4000 g for 20 minutes in 15 ml vials. The spent supernatant medium was replaced with fresh growth medium and centrifuged a second time after the complete mixing of cells and growth medium. Harvested bacteria were saved at 4 ºC to minimize their activity.

5.3.2 Treatment protocol using modified consolidation test

A modified odometer set up was developed to evaluate the effect of MICP treatment on coal ash material's characteristics. A schematic diagram of the new set up and a photograph of the odometer cells are demonstrated in Figure 5-3 and Figure 5-4, respectively. The bottom acrylic base of each cell has a port for injecting bio-treatment media; it is also equipped with a bender element sensor at the center to monitor the change in the stiffness of the specimens during treatment (i.e., caused by cementation process) and consolidation. A stainless steel ring provides confinement; it also has the advantage of being electrically accessible to the specimen to reduce electrical crosstalk during shear wave velocity measurements by grounding the specimen. The acrylic top cap is equipped with the paired bender element sensor. An electrical pulse is sent to the bender element to make it vibrate which cause a shear wave propagation in the target material using a signal generator. The paired bender element sensor receives the shear wave and triggers an electrical signal due to piezoelectric properties of the transducer. The travel time of shear wave between the two benders is recorded using a digital oscilloscope. Shear wave velocity (V_s) is computed by dividing the tip to tip distance of the benders over the travel time. The top cap has two holes to remove the effluent during the treatment solution injection. A Porex high-density polyethylene filter material is fixated to the bottom and top caps to prevent migration of coal ash fines. The port of the bottom cap is

connected to a burette with a tube to keep the specimen saturated by leveling the burette's water to the level of specimen.

Four specimens were prepared for each ash source using water pluviation, recommended by (Bachus and Santamarina 2012), to simulate the deposition of coal ash in impoundments. Coal ash was mixed with water at twice of its liquid limit to prepare a slurry, and it was poured into the consolidation ring containing 75 ml deionized water. The particle deposition was allowed for twenty-four hours, and after draining the supernatant solution, the top cap was placed on the top of the specimen. The specimen was preloaded with 500 psf (~24 kPa) and initial hydraulic conductivity (k) and initial shear wave (V_{Si}) velocity were estimated. To estimate the hydraulic conductivity, water was passed through the specimen at a prescribed rate from the bottom port and the corresponding induced water pressure was measured at the injection point using a digital pressure meter. The hydraulic conductivity was calculated using constant rate equation and knowing the total head difference after reaching steady state condition, flow rate, and specimens' length and surface area. One of the specimens was the baseline which represents the behavior of untreated coal ash, and the rest of the specimens were treated to have different levels of calcium carbonate content. A comprehensive study was performed on the MICP treatment of coal ash (i.e., discussed in chapter 4) and the presented recipe in Table 5-3 was chosen from the results of that study to treat the specimens. Treatment was performed by injecting 75 ml (~two pore volumes of the specimen) of bio-cementation media at a rate of 11 ml/min from bottom to top using a syringe pump. One 15 ml vial of bacteria solution was used for each 100 ml treatment solution to prepare bio-cementation solution. Twenty-four hours of retention time was allowed between each injection, and the shear wave velocity was measured before each injection. Treatment stopped after reaching the target shear wave velocity (taken as 2, 3, and 4 times of the initial shear wave

velocity). 75 ml (~two pore volumes of the specimen) of deionized water were passed through the specimen to stop bio-cementation reaction and to measure the hydraulic conductivity after treatment. The specimen was unloaded, and the initial height of the specimen was measured. This height was used to calculate the vertical strain and initial void ratio.

Finally, an incremental load consolidation test was conducted and the deformation of the specimen was recorded for each loading sequence. After reaching the plateau in the time-deformation curve for each loading increment, shear wave velocity was measured, and then de-ionized water was pumped into the specimen to measure the hydraulic conductivity. After reaching the maximum vertical effective stress (i.e., 1530 kPa), unloading-loading cycles were applied on the specimens to explore decementation.

Table 5-3. Treatment solution recipe.

Chemical Component	Urea (CH_4N_2O)	$CaCl_2.2H_2O$	NH_4Cl
Concentration (mM)	400	100	100

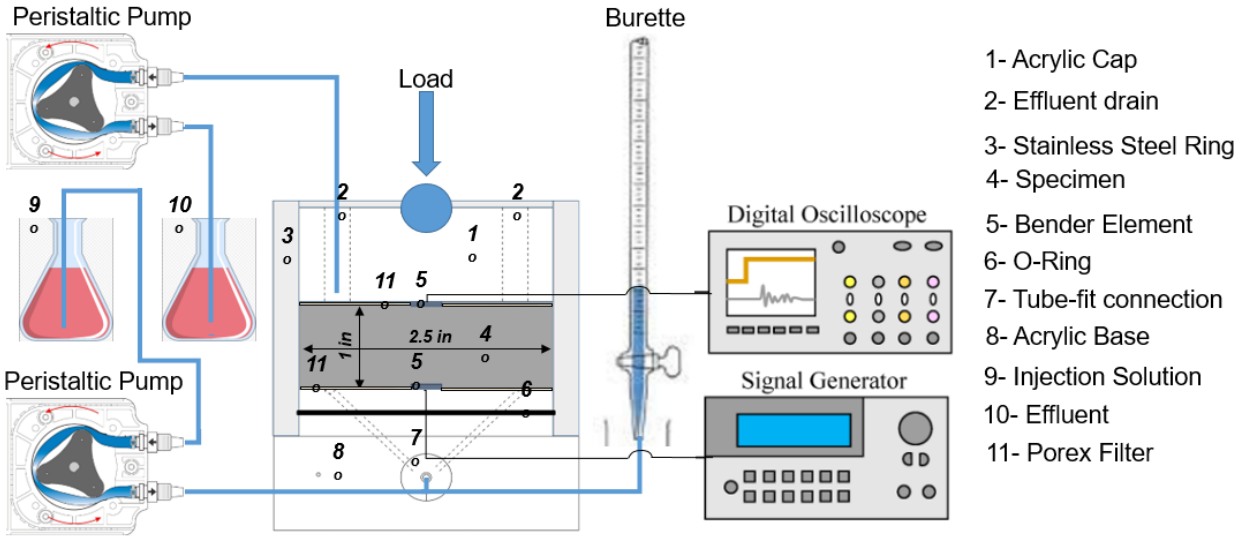

Figure 5-3. Schematic diagram of modified consolidation set-up

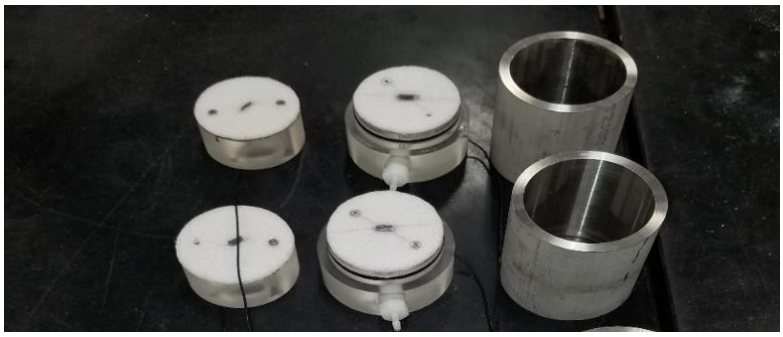

Figure 5-4. Components of modified odometer test

5.3.3 Calcium Carbonate Content

To measure the mass of calcite, gravimetric acid washing of the samples was performed with the assistance of a centrifuge. The oven-dried mass of each sample section was recorded before and after washing with 1 M of HCl. The dissolved calcium carbonate and acid solution were rinsed multiple times allowing the dissolved salts to be washed from the sample. The difference between the two oven dried masses was taken as the mass of calcium carbonate. The calcium carbonate percentage is calculated by dividing the mass of calcium carbonate by the mass of soil (Mortensen et al. 2011). The centrifuge was used in acid washing process to speed up the ash deposition process.

5.4 Results and Discussion

5.4.1 MICP treatment and its effect on shear wave velocity and hydraulic conductivity

Four specimens were prepared using water pluviation method for each coal ash (CA1 and CA3). A vertical stress of 500 psf (~24kPa) was applied to the top of each specimen, and the initial shear wave velocity (V_{Si}) was measured after completing primary consolidation. The hydraulic conductivity was estimated measuring the induced pore water during deionized water injection. The resultant V_{Si} and k_i of the specimens are presented in Table 5-4. The bio-cementation

treatment solution was injected into the specimens once per day, and the treatment process was monitored using shear wave velocity (V_S) measurements before each injection. The results of V_S and normalized shear wave velocity (V_S/V_{Si}) for both coal ash materials are demonstrated in Figure 5-5. The initial shear wave velocity of CA1 at 24 kPa vertical effective stress is higher than the V_{Si} of the CA3, which indicates different fabric and contact level deformation (Cha et al. 2014); the initial shear wave velocity of the material will be further assessed and discussed later in this paper. The CA1 specimens were treated to target V_S of two, three, and four times the V_{Si}, and the average increase of V_S per injection was 17 m/s. For CA3 material, the specimens were treated to target V_S of two and three times the V_{Si}, and the average increase of V_S was 9-10 m/s per injection.

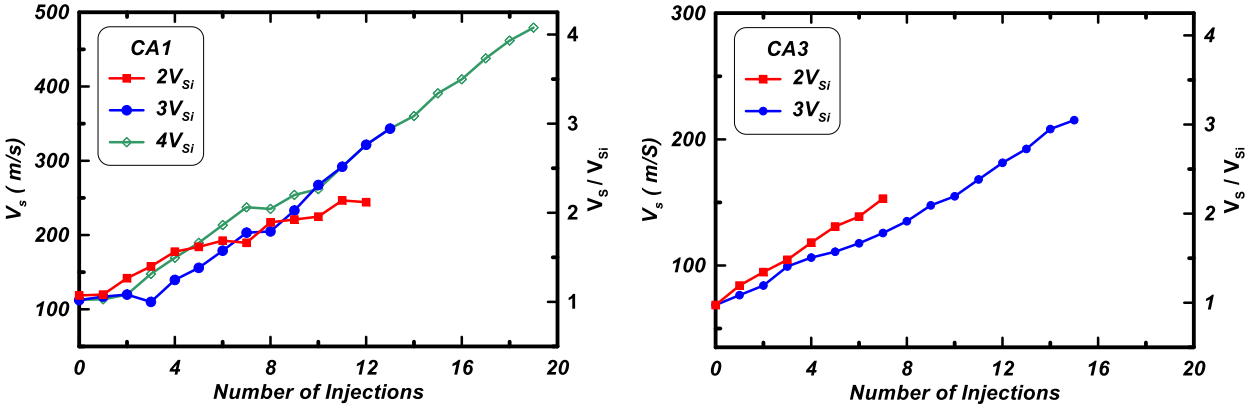

Figure 5-5. Monitored shear wave velocity during treatment for both CA1 and CA3 specimens.

The calcium carbonate content of the specimens were measured using gravimetric acid washing and the percentages are presented in Table 5-4. Acid washing of coal ash material dissolves some soluble elements, and this mass loss must be considered in $CaCO_3$ calculation. It was 2 and 3 percent for CA1 and CA3 materials, respectively.

Table 5-4. Summarized results of this study

Parameter	Unit	CA1				CA3		
		Baseline	2Vsi	3Vsi	4Vsi	Baseline	2Vsi	3Vsi
CaCO3	(%)	0	3.3	4.2	7	0	2.66	5.1
V_{Si}	m/s	103.50	199.66	269.38	391.43	89.1	145.1	208.2
e_{at}	-	0.65	0.63	0.60	0.57	0.76	0.71	0.69
Cc	-	0.110	0.081	0.078	0.057	0.118	0.104	0.074
k_i	cm/s	1.16E-04	6.60E-05	9.23E-05	7.63E-05	7.84E-05	8.91E-05	9.09E-05
k_{at}	cm/s	1.16E-04	2.01E-05	1.68E-05	5.50E-06	7.84E-05	1.47E-05	4.42E-06
k_{at}/k_i	1.0	1.00	0.30	0.18	0.07	1.00	0.17	0.05
α' factor	m/s	38.5	118.6	199.9	372.6	31.7	72.3	129.4
β' exponent	-	0.31	0.17	0.10	0.01	0.32	0.19	0.13

The SEM/EDS images were used to explore the existence and the pattern of $CaCO_3$ precipitation. The EDS analysis confirmed the presence of $CaCO_3$. The pattern of $CaCO_3$ in both MICP treated materials are demonstrated in Figure 5-6. As shown, calcium carbonate bonds the coal ash particles, and its morphology is not the same at different points (e.g., it has sharp edges at some points while it is rounded in others).

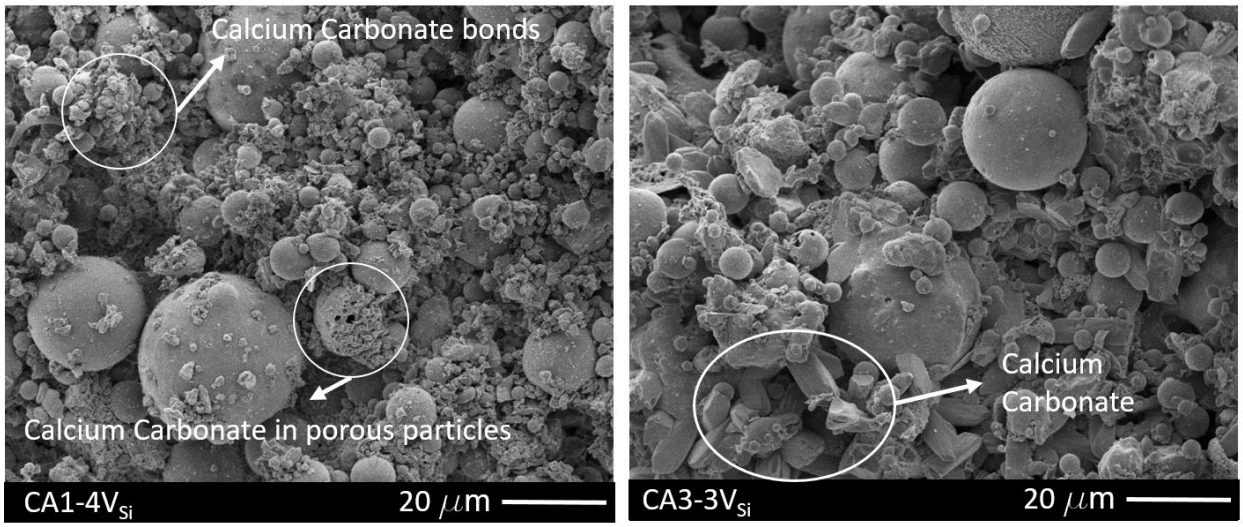

Figure 5-6. SEM images of treated CA1 and CA4 material.

Void ratio of the specimens is the volume of void over the the volume of solid, which includes coal ash particles and precipitated $CaCO_3$. The void ratio of the specimens is computed knowing the height, coal ash mass, the specific gravity of coal ash and $CaCO_3$ (i.e. $CaCO_3$ crystals are assumed to have G_S = 2.71 (DeBoer 1977), and the calcium carbonate mass. The computed void

ratio (e_{at}) of the specimens under 24 kPa vertical stress and after treatment can be found in Table 5-4.

The results of $CaCO_3$ content versus shear wave velocity after treatment (V_{Si}) are plotted in Figure 5-7, and there is a semi-log correlation between these two parameters, the same correlation can be observed between the void ratio after treatment (e) and shear wave velocity after treatment (V_{Si}).

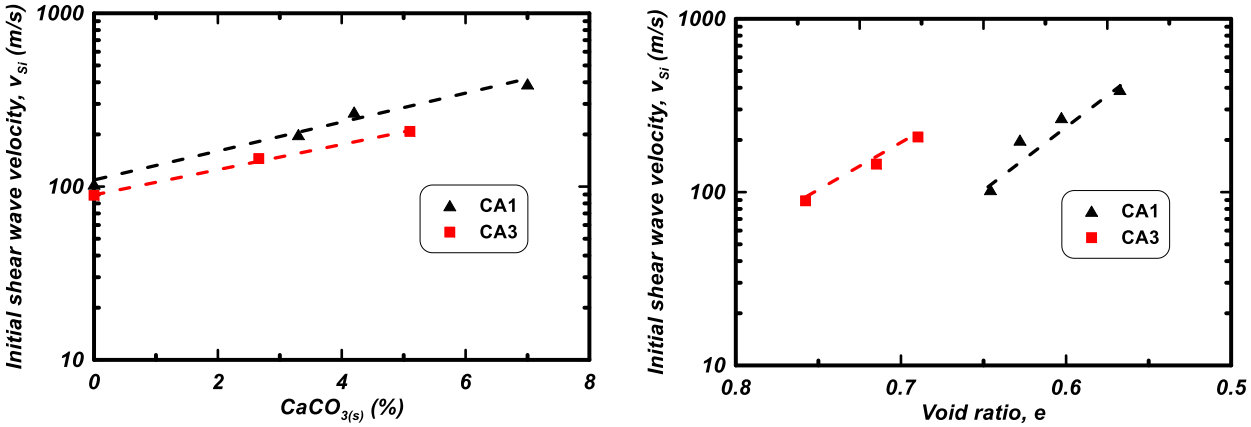

Figure 5-7. Semi-log correlation between V_S and a) $CaCO_3$ content, and b) Void ratio (e) for CA1 and CA3 specimens.

Hydraulic conductivity of the specimens were estimated using constant rate method after treatment to assess the effect of MICP treatment, and the hydraulic conductivities before (k_i) and after treatment (k_{at}) are presented in Table 5-4. Increasing the level of cementation decreased the hydraulic conductivity of the specimens. The maximum level of cementation for CA1 material (i.e. 7.0% of $CaCO_3$ precipitation) resulted in a k reduction to 0.07 of k_i. It is 0.05 of k_i for CA3 material while the $CaCO_3$ is 5.1%. The bio-cementation decreased the CA3 material's hydraulic conductivity more in comparison to CA1 material. The reason is related to the finer particle sizes of CA3, and the corresponding smaller pore throat sizes within the specimen. Therefore, filling the void spaces with $CaCO_3$ precipitation can decrease the hydraulic conductivity more for CA3 material.

The effect of cementation and the associated void ratio reduction on hydraulic conductivity of the specimens are illustrated in Figure 5-8. Increasing the calcium carbonate content of the specimens decreased the void ratio and hydraulic conductivity. The correlation between $CaCO_3$-k and e-k are linear in a semi-logarithmic scale. The slope of this line for the CA3 material is steeper than the slope of the line for CA1 material, which again expresses higher decreases of k values by increasing the $CaCO_3$ content.

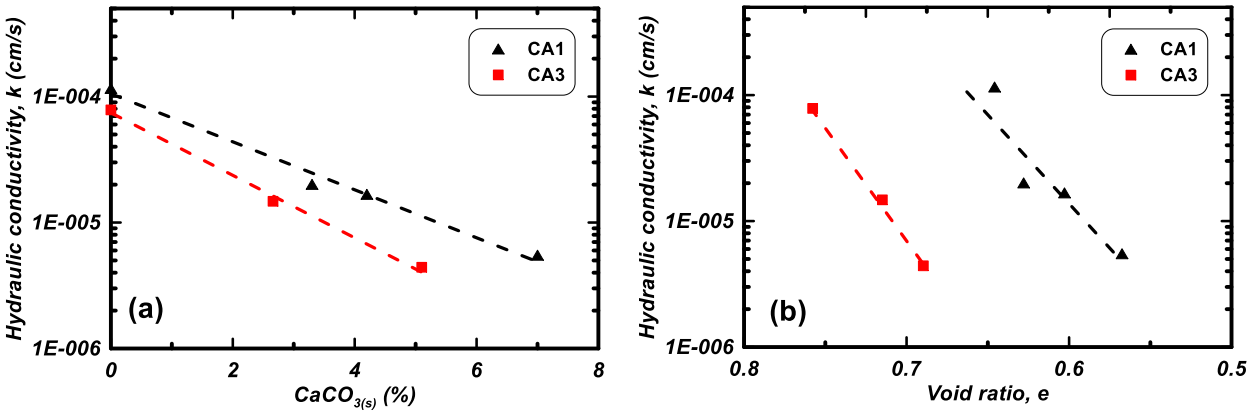

Figure 5-8. Hydraulic conductivity as a function of a) $CaCo_3$ content, b) Void ratio, e

5.4.2 Large-strain behavior - Volume change-stress behavior

The variation of void ratio (e) with increase of vertical effective stress (σ'_V) of the specimens in the modified oedometer set up can reveal the effect of bio-cementation on the volumetric behavior of cemented and uncemented specimens (as data are presented in Figure 5-9). The produced $CaCO_3$ during the treatment process decreased the initial void ratio of the treated specimens (as presented in Table 5-4). Increasing the level of applied σ'_V decreased the void ratio of the specimens, however, this reduction was lower while the specimens had higher $CaCO_3$ content. The range of the void ratio of the specimens got narrower as the σ'_V increased, and finally, the void ratio of the specimens converged to a similar value for each material at 1530 kPa. There is not an instant drop similar to the reported data by (Yun and Santamarina 2005), who studied the large

strain-volume change behavior of cemented sand using Portland cement. The reason for having such a collapse was related to a very loose particle structure (e.g., e=1.1) using the capillary forces during Portland cement mixing (Feng and Montoya 2014). However, the trends of results are similar to reported data for MICP treated sands (Lin et al. 2015; Feng and Montoya 2014).

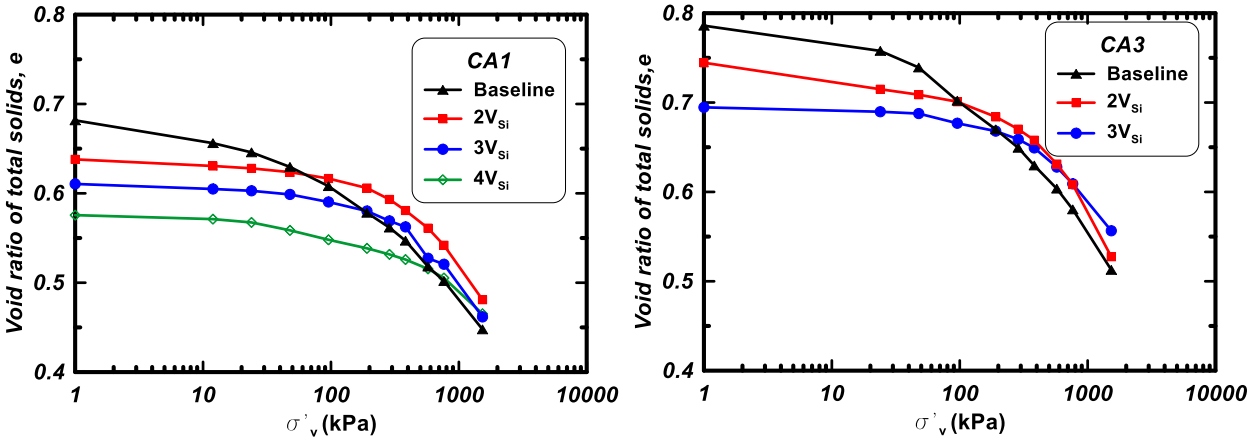

Figure 5-9. Variation of void ratio with vertical effective stress in modified oedometer set up.

The compression index (C_C) of untreated and treated specimens are derived from the e-log(σ'_V) graph for a range of σ'_V between 24 kPa to 1530 kPa, and they are presented in Table 5-4. The C_C of the untreated specimens are 0.11 and 0.12 for CA1 and CA3, respectively, which is right in the middle range of previously reported data (Bachus and Santamarina 2012) (as shown in Figure 5-10).

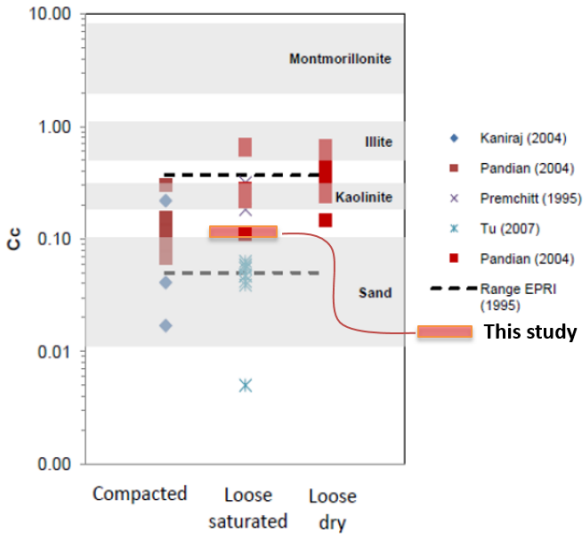

Figure 5-10. A comparison between the resultant compression index of the untreated material of this study with the range of previously reported data (Modified from (Bachus and Santamarina 2012).

Unloading-loading cycles were applied to the specimens to explore the effect of decementation of the treated material. The deformation and the shear wave traveling time between benders of the specimens were recorded for each incremental vertical stress, and the corresponding strain and shear wave velocities were estimated (as manifested in Figure 5-11 and Figure 5-12 for CA1 and CA2, respectively).

The resultant strain values of MICP treated specimens are smaller than the baseline at the same load condition. For example, the strain level at σ'_V =1530 kPa for untreated CA1 specimen is 15%, and it decreased to 10% for $2V_{Si}$ and $3V_{Si}$ specimens, and there was a further reduction to 7% strain for the $4V_{Si}$ specimen. The strain level at the same load for the untreated CA3 specimen is approximately 16%, and it decreased to 12% and 8% for the $2V_{Si}$ and $3V_{Si}$ specimens, respectively.

The effect of bio-cementation on compressibility reduction is more at lower levels of vertical effective stresses and its effect decreased while the applied stress increased. The coefficients of volume change ($m_v = \frac{\Delta\varepsilon}{\Delta\sigma'_V}$) for different cementation levels are derived from σ'_V-strain results

(i.e., Figure 5-11 and Figure 5-12) and are plotted in Figure 5-13-b, which confirms a higher compressibility reduction of the treated material at lower load levels.

Calcium carbonate precipitation bonds the ash particles together, which increases the small-strain stiffness and shear wave velocity of bio-cemented material as shown in Figure 5-5. For a treated specimen, increasing the vertical effective stress increases the level of induced shear stress on the cementation bonds and may break them. This breakage can be monitored exploring the V_S of the specimens during unloading. The lower shear wave velocity during unloading in comparison to loading is an indicator of cementation bond breakage (Yun and Santamarina 2005). On the other hand, a higher shear wave velocity during unloading compared to loading can represent the effect of load history (i.e., over consolidation) and plastic deformation.

The unloading curves of the untreated specimens for both materials in σ'_v-V_S are above the loading curves, which indicated the effect of over consolidation and residual stresses. In Figure 5-11, all the unloading curves for the treated CA1 material are beneath the loading curve. Therefore, 1530 kPa vertical effective stress can break some calcium carbonate bonds even for the specimen with the highest level of cementation. Please note the bender sensors in the CA1-2V_{Si} specimen did not work after increasing the σ'_V from 765 kPa to 1530 kPa in the first loading, its shear wave velocity measurement is not complete in Figure 5-11.

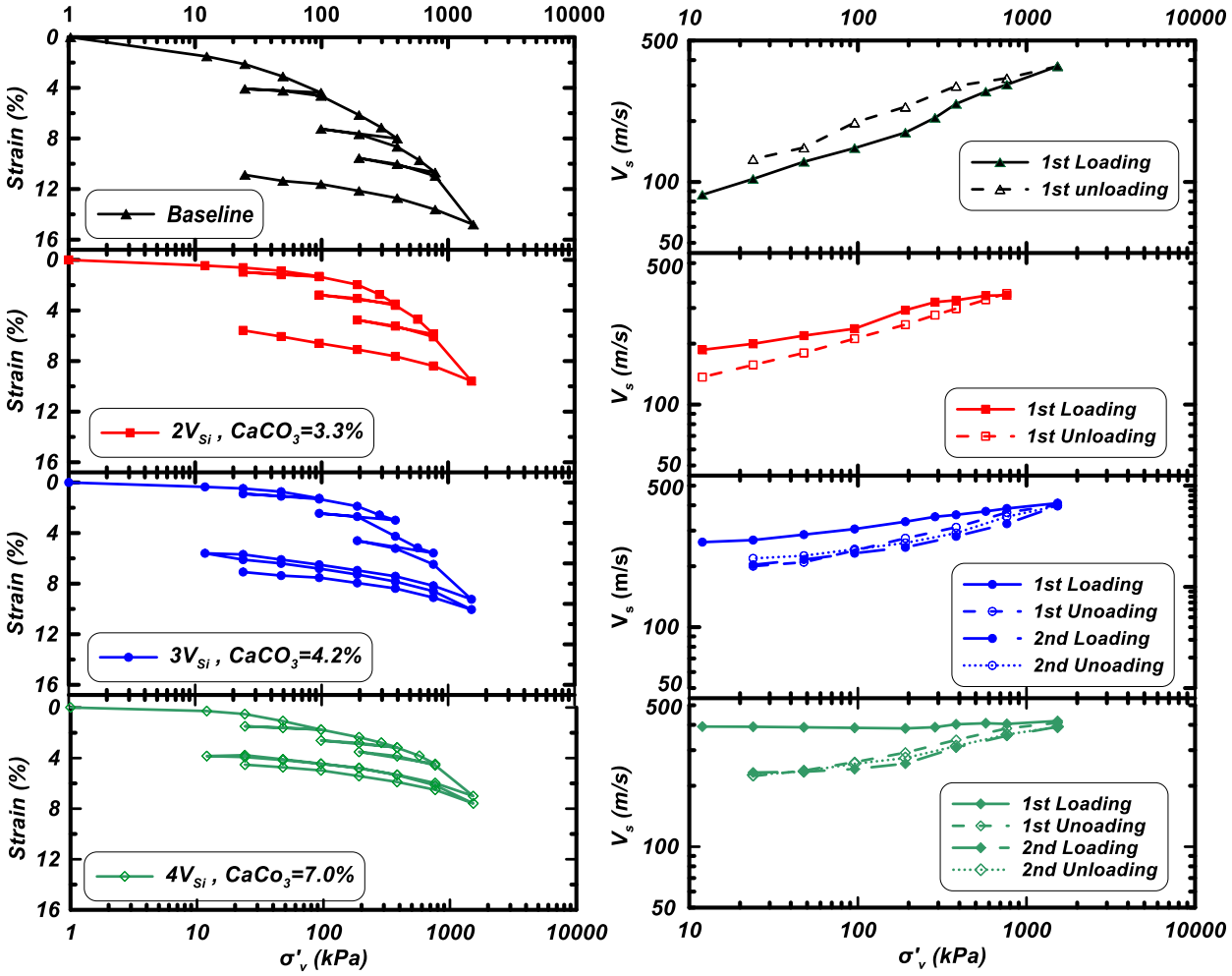

Figure 5-11. Strain and shear wave velocity response of CA1 material specimens with different level of cementation while loading-unloading cycles were applied on.

The unloading curves of both treated CA3 specimens (as shown in Figure 5-12) are above the loading curve for a limited range of vertical effective stress. It is from 1530 to 96 kPa for $2V_{si}$ specimen and from 1530 to 192 kPa for $3V_{si}$ specimen, but they are beneath the loading curve for the vertical stresses below the mentioned range. It shows that loading and the induced residual stresses overwhelmed the effect of decementation for the specified range, even though the lower unloading V_S curve than loading curve at the lower vertical effective stresses expressed specimens' decementation.

The resultant shear wave velocity of the second unloading curve for all the treated specimens for both CA1 and CA3 materials are equal or higher than second loading curve. Therefore this level of loading had broken all the cementation bonds or could not break anymore.

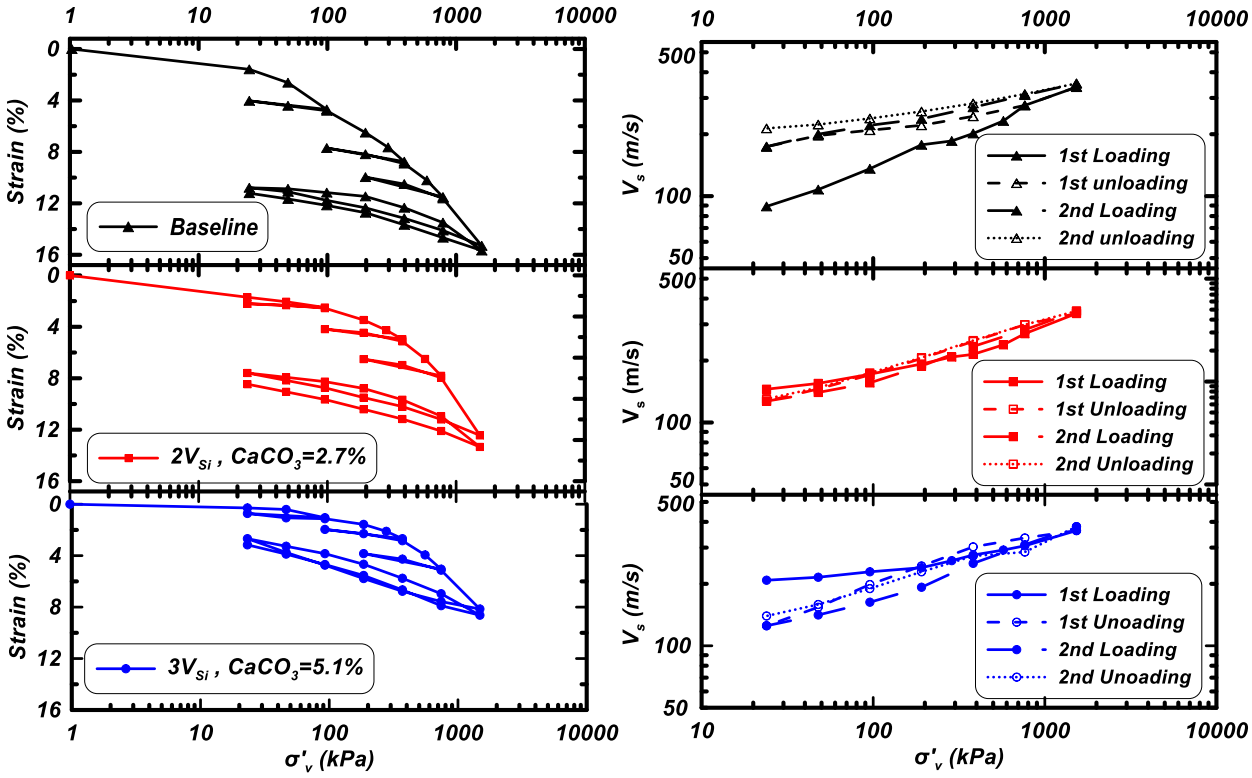

Figure 5-12. Strain and shear wave velocity response of CA1 material specimens with different level of cementation while loading-unloading cycles were applied on.

5.4.3 Large strain behavior – hydraulic conductivity (k) and coefficient of consolidation (C_v)

After completing the primary consolidation of each incremental load, deionized water was injected into the specimen and hydraulic conductivity was estimated knowing the induced water pressure at injection point, and the results are presented in Figure 5-13-a. Two factors are governing the hydraulic conductivity of the specimens; 1) increasing the amount of applied stress decreases the volume of void which leads to a reduction in the hydraulic conductivity of the specimens, 2) breaking the cementation bonds between particles provides preferential flow pathways which

result in an increase in hydraulic conductivity. There is no cementation in the untreated specimens (Baseline), so increasing the stress level reduces the hydraulic conductivity of them. The decrease of hydraulic conductivity of CA3-Baseline is more than CA1-Baseline, especially at lower stress levels. An increase in the hydraulic conductivity for all treated specimens was observed at a stress level between 200 and 800 kPa, which could be explained by cementation breakage.

The coefficient of consolidation (C_v) is computed using values of hydraulic conductivity and coefficient of compressibility in $C_v = k/(m_v . \gamma_w)$ equation, and resultant C_v is presented in Figure 5-13-c. The C_v of untreated specimens increased as the σ'_v increased, which is in agreement with the previous reported data (Kaniraj and Gayathri 2004). These Results indicated that C_v decreased with increasing the level of cementation. However, it did not increase while the σ'_v increased all the times for treated specimens because of decementation effect. E.g., k of CA1-Baseline specimen decreased from 1.16E-04 cm/s to

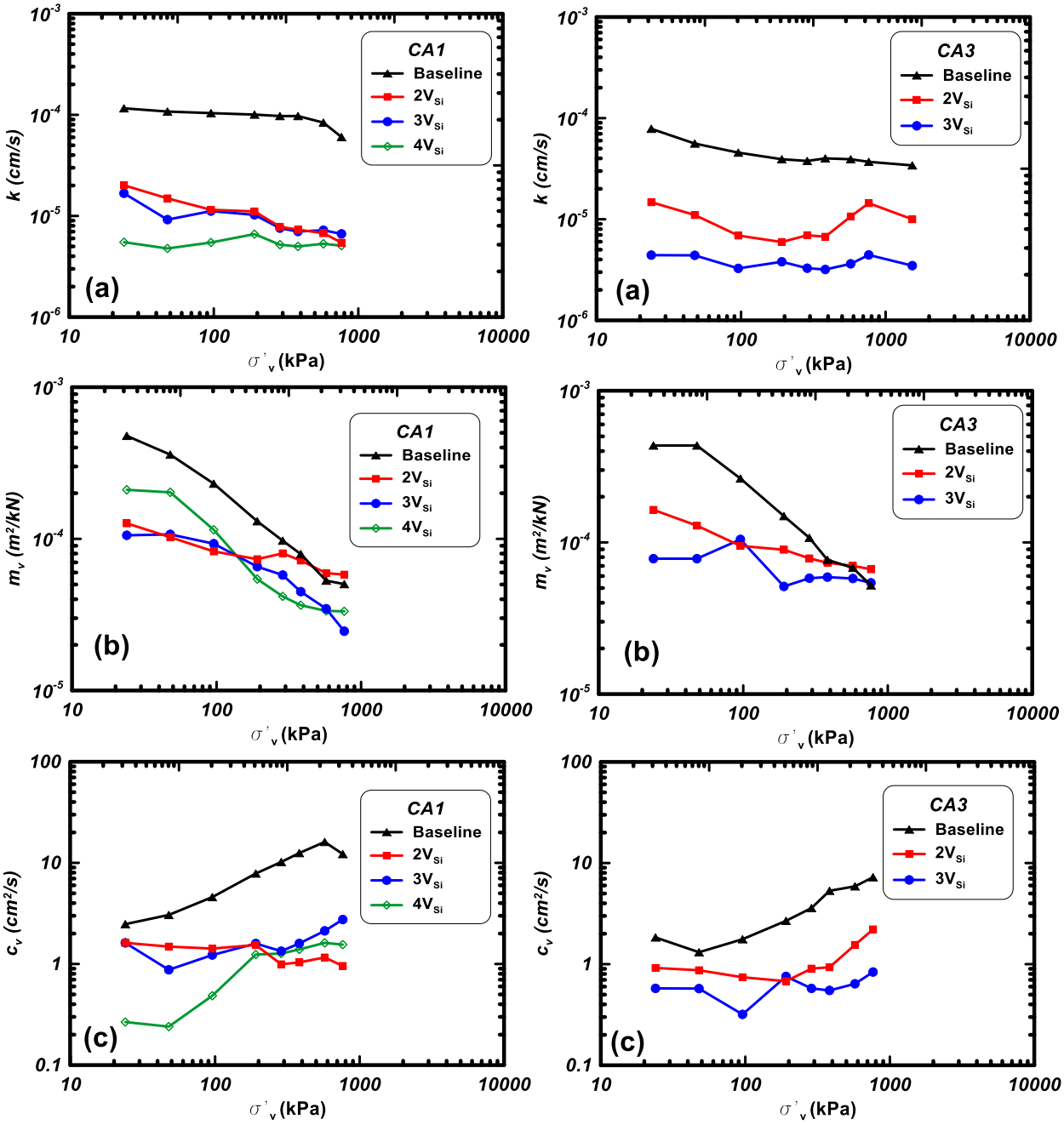

Figure 5-13. Effect of incremental loading on a) hydraulic conductivity (a), b) coefficient of volume change (m_v), c) coefficient of consolidation (c_v)

5.4.4 Small-strain behavior

The small strain shear stiffness (i.e., G) reflects particle contact shear stiffness (Cha et al. 2014), and it is a function of mean effective stress for granular material as illustrated in Equation (1) (Cascante and Santamarina 1996; Hardin and Drnevich 1972).

$$V_S = \sqrt{\frac{G}{\rho}} = \alpha\left(\frac{\sigma'_{\perp} + \sigma'_{II}}{2kPa}\right)^{\beta} = \alpha\left(\frac{\sigma' z(1+k_0)}{2kPa}\right)^{\beta} = \alpha\left(\sigma'_m\right)^{\beta} \quad (1)$$

Where the $\sigma'_{\perp}$ is the in direction of particle motion and σ'_{II} is in direction of wave propagation. α factor is the shear-wave velocity at a mean effective stress (σ'_m) equal to 1 kPa, and the β exponent captures the sensitivity of the skeletal shear stiffness to the applied effective stress (Cha et al. 2014). The α factor represents the grain packing and fabric characteristic of the material while β exponent reflects both the nature of interparticle contacts and fabric changes during loading (Cha et al. 2014; Santamarina et al. 2001). With the extent of cementation, α factor increases and β exponent decreases. The β exponent can reach to 0 value for highly cemented material and it could also be as high as 0.7 for very soft, high-specific surface soils (Yun and Santamarina 2005).

Initially, the constant parameters of the equation (1) are investigated using the data points of untreated coal ash material. The OCR of the specimens is equal to 1 for the first loading curves because of sample preparation method (i.e., water pluviation method). To compute the horizontal effective stress, K_0 was estimated using the equation $K_0 = 1 - \sin(\varphi)$ for an OCR=1 (Mayne and Kulhawy 1982). The friction angles of the studied coal ash materials are unknown. Hence a parametric study was conducted on the effect of friction angle (φ) within the range of previously reported data (i.e., reported between 25^0 to 45^0 in Bachus and Santamarina 2012) on the constant parameters (i.e., α and β). The results (as presented in Figure 5-14) revealed that the φ variation

would result in α factor of 42.7±1.3 m/s and 35.2±1.1 m/s for CA1 and CA3, respectively. The φ variation did not change the β exponent, and it was 0.31 for CA1 and 0.32 for CA3 coal ashes.

The equation $\beta = 0.73 - 0.27\log(\frac{\alpha}{m/s})$ is recommended by (Cha et al. 2014) to correlate the α factor and β exponent for soils. Using the mentioned range of α factors in this study, especially the lower range (i.e., 41.4 m/s for CA1 and 34.1 for CA3 material), resulted in β exponent values pretty close to the experimental values (e.g., using α values of 34.1 and 36.4 for CA3 material gives β exponent equal to 0.32 and 0.31, respectively).

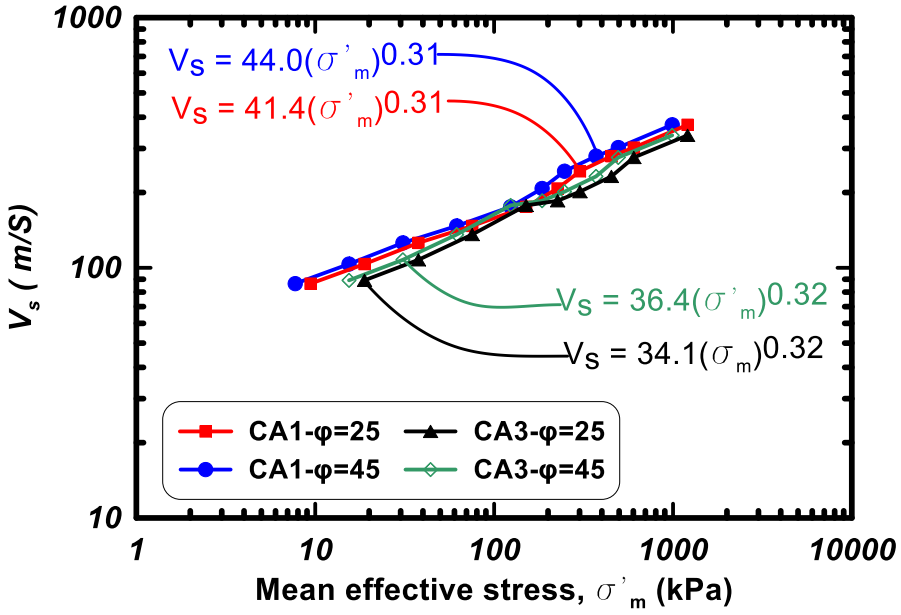

Figure 5-14. Parametric study on the effect of φ on α factor and β exponent of studied coal ash materials.

(Yun and Evans 2011) study on the at-rest lateral stress for cemented sand revealed that cementation decreases the at-rest lateral stress coefficient (K_0) value compared to uncemented sand, increasing the load and the associated decementation cause increasing K_0 toward the uncemented sand's K_0. Therefore, K_0 of cemented sand is highly variable, and without having the proper equipment, it is not possible to estimate the horizontal effective stress and mean effective

stresses for the cemented material. Accordingly, vertical effective stress (σ'_v) is considered instead of the mean effective stress (σ'_m) in equation 1 to compare the effect of cementation on the coal ash material's properties. α' and β' are placed instead of α and β, as presented in Equation 2.

$$V_S = \alpha'\left(\sigma'_v\right)^{\beta'} \quad (2)$$

The shear wave velocities of the specimens for each loading increment are demonstrated in Figure 5-15. The α' factor and β' exponent of each curve is estimated performing a regression analysis on V_S- σ'_v data points and the values are provided in Figure 5-15 and Table 5-4. The β' exponent values of untreated specimens are the same as β exponent (i.e., β'= β =0.31 for CA1 material and β'= β =0.32 for CA3 material), and α' factor values are slightly smaller than α values for both material (i.e., α'=38.5 m/s for CA1 material and α'=31.7 m/s for CA3 material). Increasing the bio-cementation content reduced the slope of data points for each specimen in Figure 5-15 (i.e., β' exponent) and increased the α' for both material (e.g., the β' exponent factor decreased from 0.31 for CA1-Baseline to 0.01 for CA1-4V_{Si}, and the α' values for the same specimens enhanced to 372.6 m/s from 38.5 m/s).

Higher calcium carbonate content in the specimens resulted in higher initial V_S and decreasing the β', which represents the variation of V_S while σ'_v increases. Such β' reduction led to having the same V_S for all the specimens with the same material at σ'_v =1530 kPa. Similar trend was observed on e-σ'_v for the specimens with the same material, and void ratios converged to the same values.

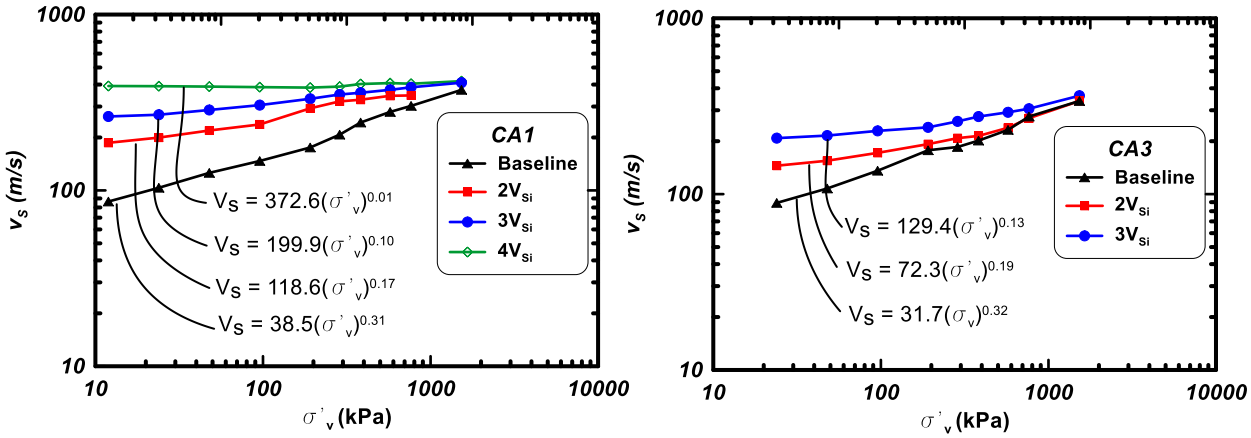

Figure 5-15. Effect of cementation and loading on small strain behavior of CA1 and CA3 material.

All the α' factors and β'exponents values of treated and untreated specimens for both materials (i.e., CA1 and CA3) were placed in the same graph (as presented in Figure 5-16) and the correlation was found performing regression analysis. The resultant correlation is $\beta = 0.75 - 0.29\log(\alpha')$ which is similar to the correlation suggested by (Cha et al. 2014) between α factors and β exponents (i.e., $\beta = 0.73 - 0.27\log(\alpha)$).

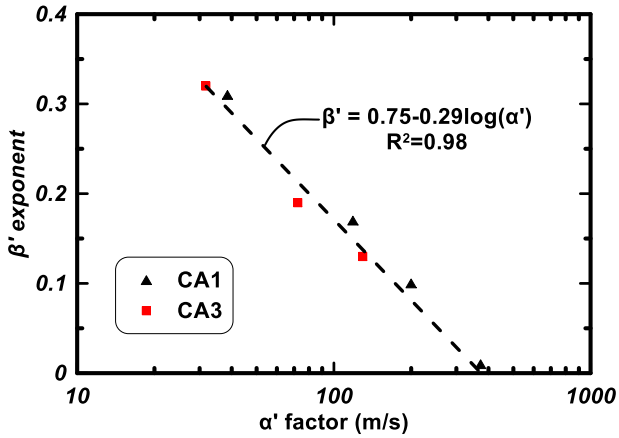

Figure 5-16. Correlation between α' factors and β'exponents for all the studied specimens.

5.4.5 Correlation between small-strain and large-strain parameters

The α' factors and β'exponents were estimated from the results of shear wave velocity (i.e., small strain analysis) while the vertical effective stress varied from 24 kPa (500 psf) to 1530 kPa (32000psf). The compression indexes (C_C) were derived from the σ'_v-strain results also from the same range of loading. Finding the correlation between these parameters may be used to predict the behavior of the uncemented and cemented material in the laboratory and in the field (e.g., using the cross hole, SCPT, and surface waves to estimate V_S). There is a semi-log correlation between C_C and β'exponents (i.e., $\beta' = 0.94 \log(C_C)+1.17$), and it is demonstrated in Figure 5-17-a. The correlation between α' factors and C_C is presented in Figure 5-17-b on a log-log scale, and i.e., $\alpha' = 0.03 C_C^{-3.27}$.

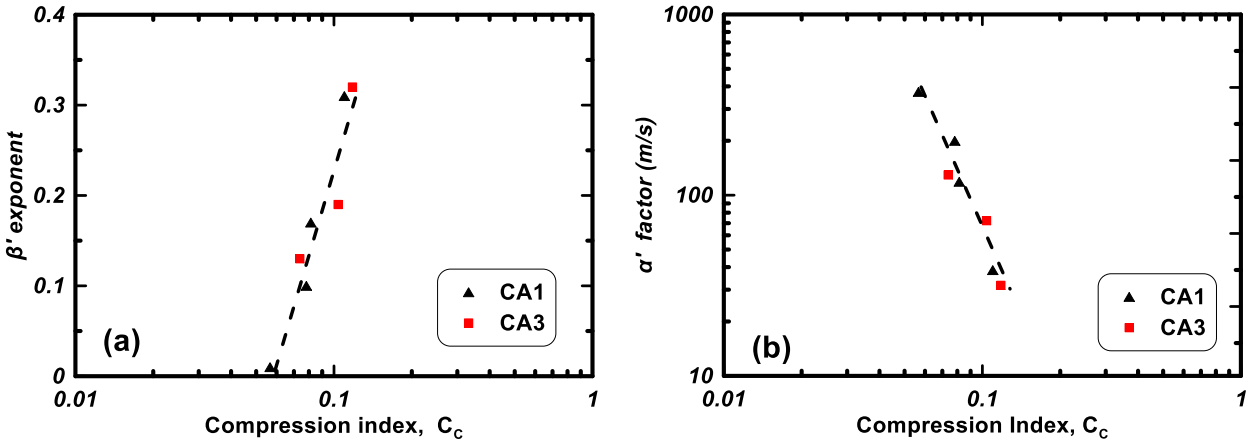

Figure 5-17. Correlation between C_C and small strain parameters; a) β'exponents and b) α' factors.

5.5 Summary and conclusions

In the study presented herein, the effect of MICP treatment on engineering properties of two coal ash materials was investigated. For this, purpose, a modified oedometer equipment was developed to allow for the ability to inject solution into the specimen, to measure the corresponding induced

fluid pressure, while to monitoring the shear wave velocity. The specimens were MICP treated to reach different target shear wave velocities, which corresponded to different levels of bio-cementation. The effect of MICP treatment on large-strain (i.e., compressibility, hydraulic conductivity, coefficient of consolidation) and small-strain parameters (i.e., β' and α') of the studied material was explored. Two coal ashes with different engineering characteristics were successfully treated using MICP to reach different levels of cementation. The acid washing results and SEM/EDS images confirmed the $CaCO_3$ existence.

Based on the results reported in this study, and following conclusions are advanced;

1. Increasing the calcium carbonate content decreased the initial void ratio of the total solids in the treated coal ash. Higher levels of cementation reduced the reduction in void ratio as a function of increasing vertical stress. The void ratio of the specimens with different levels of cementation converged to nearly the same value with increasing the applied vertical stress.
2. The large-strain results demonstrated a reduction in compressibility (C_C and m_v) for treated coal ash in comparison to untreated material. This reduction is more at lower levels of applied vertical stresses.
3. Bio-cementation decreased the initial hydraulic conductivity (k_i) of the studied material. The results indicated that maximum level of cementation of these tests could decrease the hydraulic conductivity to 0.07 and 0.05 of initial hydraulic conductivity for CA1 and CA3 matrials, respectively.
4. Shear wave velocity was monitored during loading-unloading cycles to look at the decementation (bond breakage). Higher shear wave velocity of unloading curve in comparison to the loading curve demonstrated the effect of over consolidation or load

history, on the other hand, the bio-cementation increased the V_S compared to uncemented material. The second unloading curve of shear wave velocity was equal or above the second loading curve for all the specimens, which indicated that this level of vertical stress could not break the cementation bonds anymore, or all of them are already broken.

5. Increasing the vertical load on top of the specimens decreased the hydraulic conductivity of the untreated specimens because of decreasing void spaces. The level of reduction is a function of compressibility and particle size distribution. The criteria was the same for bio-cemented material except while the loading condition breaks the cemented bonds and provides preferential flow pathways. This is observed in the treated specimens with a rapid increase in hydraulic conductivity with respect to the effective vertical stress.
6. C_v is a function of both hydraulic conductivity and compressibility (or coefficient of volume change). The computed C_v of untreated coal ashes revealed an increase as the vertical stress increased, and is related to the $CaCO_3$ content of treated specimens. The effect of increasing vertical load on C_v for treated specimens showed more scatter compared to untreated specimens. This is likely due to decementaion, breaking of bonds, and creation of preferential flow paths.
7. The sensitivity of "α" and "β" parameters in shear wave velocity-mean effective stress equation ($V_S=\alpha(\sigma'_m)^{\beta}$) to variation of friction angle (within the reported range in literature) was explored. The results indicated that the friction angle variation between 25 to 45^0 would lead to an average α factor of 42.7±1.3 m/s and 35.2±1.1 m/s for Ca1 and CA3, respectively. This variation did not change the β value, and it was 0.31 for CA1 and 0.32 for CA2 coal ashes.

8. Increasing the calcium carbonate of the specimens increased the initial shear wave velocity (α' factor) and decreased the slope of shear wave velocity-vertical effective stress (β' exponent).
9. Increasing the level of load to 1530 kPa converged the void ratio and shear wave velocity of all the specimens to the same void ratio and shear wave velocity.
10. The β' exponent (the slope of $\log(\sigma_v')$-$\log(V_S)$) is an indicator of compressibility and the correlation between β' and C_C is extracted from experimental results. Also, the correlation between C_C and α' factor (i.e., representing the fabric and grain packing of material) is derived and presented.

5.6 References

ASTM D 854-00. (2000). "Standard Test for Specific Gravity of Soil Solids by Water Pycnometer." ASTM International, West Conshohocken, PA, .

ASTM D422-63. (2007). "D422–63 (2007) Standard test method for particle-size analysis of soils." ASTM International, West Conshohocken.Doi, 10 1520.

Bachus, R., and Santamarina, C. (2012). "Geotechnical Properties of Fly ASH and Potential for Static Liquefaction: Volume I–Summary and Conclusions." EPRI, Palo Alto, CA, .

Bachus, R. C., and Santamarina, J. C. (2014). "Geotechnical Properties and Diagenesis of Ponded Fly Ash." Geo-Congress 2014: Geo-characterization and Modeling for Sustainability, Geo-Congress 2014, 326-333.

Cascante, G., and Santamarina, J. C. (1996). "Interparticle contact behavior and wave propagation." J.Geotech.Eng., 122(10), 831-839.

Cha, M., Santamarina, J. C., Kim, H., and Cho, G. (2014). "Small-strain stiffness, shear-wave velocity, and soil compressibility." J.Geotech.Geoenviron.Eng., 140(10), 06014011.

Daniels, B. L. (2016). "Caution: Hazards Ahead: How the EPA's Refusal to Classify Coal Ash as Hazardous Waste Fuels Environmental and Public Health Concerns." Vill.Envtl.LJ, 27 93.

DeBoer, R. B. (1977). "Influence of seed crystals on the precipitation of calcite and aragonite." Am.J.Sci., 277(1), 38.

DeJong, J. T., Mortensen, B. M., Martinez, B. C., and Nelson, D. C. (2010). "Bio-mediated soil improvement." Ecol.Eng., 36(2), 197-210.

Feng, K., and Montoya, B. M. (2015). "Drained shear strength of MICP sand at varying cementation levels." IFCEE 2015, 2242-2251.

Feng, K., and Montoya, B. M. (2014). "Behavior of Bio-Mediated Soil in k 0 Loading." New Frontiers in Geotechnical Engineering, 1-10.

Fujita, Y., Taylor, J. L., Wendt, L. M., Reed, D. W., and Smith, R. W. (2010). "Evaluating the potential of native ureolytic microbes to remediate a 90Sr contaminated environment." Environ.Sci.Technol., 44(19), 7652-7658.

Hardin, B. O., and Drnevich, V. P. (1972). "Shear modulus and damping in soils: design equations and curves." Journal of Soil Mechanics & Foundations Div, 98(sm7),.

Harkness, J. S., Sulkin, B., and Vengosh, A. (2016). "Evidence for Coal Ash Ponds Leaking in the Southeastern United States." Environ.Sci.Technol., 50(12), 6583.

Kaniraj, S. R., and Gayathri, V. (2004). "Permeability and consolidation characteristics of compacted fly ash." J.Energy Eng., 130(1), 18-43.

Lin, H., Suleiman, M. T., Brown, D. G., and Kavazanjian Jr, E. (2015). "Mechanical behavior of sands treated by microbially induced carbonate precipitation." J.Geotech.Geoenviron.Eng., 142(2), 04015066.

Martinez, B. C., DeJong, J. T., Ginn, T. R., Montoya, B. M., Barkouki, T. H., Hunt, C., Tanyu, B., and Major, D. (2013). "Experimental optimization of microbial-induced carbonate precipitation for soil improvement." J.Geotech.Geoenviron.Eng., 139(4), 587-598.

Mayne, P. W., and Kulhawy, F. H. (1982). "Ko- OCR Relationships in Soil." Journal of the Soil Mechanics and Foundations Division, 108(6), 851-872.

Mortensen, B. M., Haber, M. J., DeJong, J. T., Caslake, L. F., and Nelson, D. C. (2011). "Effects of environmental factors on microbial induced calcium carbonate precipitation." J.Appl.Microbiol., 111(2), 338-349.

Nijhuis, M., and Kendrick, R. (2014). "Can coal ever be clean." Retrieved October, 7 2015.

Santamarina, J. C., Klein, A., and Fam, M. A. (2001). "Soils and waves: Particulate materials behavior, characterization and process monitoring." Journal of Soils and Sediments, 1(2), 130.

Walton, W. H., and Butler, W. (2009). "Root Cause Analysis of TVA Kingston Dredge Pond Failure on December 22, 2008." Vernon Hills.

Yun, T. S., and Evans, T. M. (2011). "Evolution of at-rest lateral stress for cemented sands: experimental and numerical investigation." Granular Matter, 13(5), 671-683.

Yun, T. S., and Santamarina, J. C. (2005). "Decementation, softening, and collapse: changes in small-strain shear stiffness in k 0 loading." J.Geotech.Geoenviron.Eng., 131(3), 350-358.

6. Chapter 6: Effect of MICP Treatment on Arsenic and Selenium Leaching Behavior of Coal Ash

Abstract

Coal power plants are one of the primary sources of electricity generation worldwide. Coal ash is the by-product of coal combustion process in power plants, and the unutilized component is disposed of in impoundments and landfills. The chemical leaching from coal ash impoundments into the ground and surface water is the main environmental concerns regarding coal ash impoundments. Microbial induced calcium carbonate precipitation (MICP) has the potential to immobilize trace elements through calcium carbonate co-precipitation, and it has been used to immobilize strontium-90 in experimental and field scale. The objective of this study is to investigate the effect of MICP treatment on arsenic and selenium leaching behavior from fly ash material. For this purpose, chemical equilibrium modeling and batch testing were utilized to explore the effect of pH, different salts, and MICP treatment. A background curve which demonstrates the effect of pH on solubility of the mentioned elements was suggested for arsenic, and it was used to explore the effect of MICP treatment on immobilization/mobilization of the trace elements based on batch testing results. This method did not decrease the arsenic solubility; however, the treatment recipe can be designed to decrease the pH of the solution which leads to solubility reduction during treatment. The results of batch testing indicated that MICP treatment immobilized selenium through co-precipitation.

6.1 Introduction

Coal power plants produce over 750 megatons of fly ash globally with less than 50 percent of this by-product utilized in industry (Izquierdo and Querol 2012a). The rest of the produced fly ash is stored in lagoon impoundments and landfills. The organic matter of coal is burnt during the combustion process, and inorganic elements remain in the coal ash. Therefore, the concentration of the inorganic matters is higher than the source coal (Bhattacharyya et al. 2009). The phase

transformation of the mineral matter in the coal during high-temperature combustion may render trace elements in the ash matrix susceptible to leaching (Jones 1995). The source of coal, the type of combustion system, and the post-combustion conditions are factors affecting the mineralogy of fly ash. Therefore, fly ash from different power plants across the county will have different levels of elements concentrations (Izquierdo and Querol 2012a).

The US EPA limited the maximum contaminant level of arsenic to 10 ug/l in drinking water and it is 50 ug/l for selenium (EPA 2003). These two elements may originate from coal ash impoundments. The concentration of arsenic in a bituminous fly ash can be in a range of 1 mg/kg to 1000 mg/kg (Ainsworth and Rai 1987). The content of selenium in coal ash can be as high as 200 mg/kg, however, it is usually less than 50 mg/kg and is typically in the range of 10 to 20 mg/kg (Wang et al. 2007). Predominant form of arsenic and selenium in fly ashes were reported to be As(V) and Se(IV), respectively (Narukawa et al. 2005; Huggins et al. 2007). The previous studies reported the association of arsenic with aluminum and iron oxide and these two oxides are considered as the main adsorbent of arsenic (Silberman and Harris 1984; Xu et al. 2001). Many factors have been shown to influence the leaching of arsenic from fly ash, such as pH level, calcium, magnesium, reducing or oxidizing conditions, solid-to-liquid (S/L) ratio, leaching time, temperature, and anionic constituents such as sulfate and phosphate (Lecuyer et al. 1996; Praharaj et al. 2002). Different metal-selenite (SeO_3^{2-}) forms can be in a solution and they have different solubility constants (e.g., $pK_s(CaSeO_3)$=5.53, $pK_s(MnSeO_3)$=6.9, $pK_s(FeSeO_3)$=9.99, $pK_s(K_2SeO_3)$=1.48) (Aurelio et al. 2010). The primary factors controlling the adsorption of selenium in coal ash are the existence of iron hydroxide and aluminum oxide (Hansen and Fisher 1980), calcium precipitation and calcium oxide (Van der Hoek, Eline E and Comans 1996; Lecuyer et al. 1996). Retention of selenite in the calcite crystals through co-precipitation has been reported

by different authors (Aurelio et al. 2010; Reardon et al. 1993). Aurelio et al. 2010 reported up to 27.6 mmole se/kg of solid (i.e., Ca^{2+}, CO_3^{2-}, and SeO_3^{2-}) by isomorphic substitution of carbonate ions by selenite ions. Lower solubility constant of calcite (i.e., pK_s(calcite)=8.48) than calcium selenite indicates more stable structure of calcite and less solubility, which is desire for immobilizing selenium through calcite co-precipitation.

Microbial induced calcium carbonate precipitation (MICP) method has the potential of capturing trace elements into the calcite mineral through co-precipitation and therefore minimizing heavy metal migration into the ground and surface water. Carbonate is one of the resultant anions of hydrolyzing urea, and calcium carbonate would start nucleation and crystallization as the concentration of calcium ions satisfies the saturation condition (Benjamin 2014). In this process, some elements (i.e., more likely divalent cations) might co-precipitate and be captured in solid crystals. This method has been used to capture Sr90, which is a divalent cation, in experimental (Warren et al. 2001b) and field (Fujita et al. 2010) scales testing projects. The effect of MICP treatment on leaching behavior of coal ash is however unknown at present.

The objective of this study is investigating the use of the MICP process to specifically minimize arsenic and selenium leaching potential. To find an optimized protocol to reduce the concentration of the elements of concerns in leachate, factors affecting the solubility of the elements and the chemical reactions occurring during MICP treatment are investigated. Chemical equilibrium modeling and batch testing are used to evaluate the effect of pH, salts, and MICP treatment on leaching behavior of arsenic and selenium in a Class-F fly ash. Results are presented and the potential of using the MICP process to minimize the leaching potential of arsenic and selenium is discussed.

6.2 Material and Methods

A Class-F fly ash was studied (will be referred to as CA1 material herein). The carbon mass of the test samples was measured by placing the oven-dried samples in a furnace at 500^0c for 24 hours and measuring the mass lost. The CA1 carbon content, which is the mass of carbon over the mass of fly ash, was found to be 3.42%.

The crystalline phases of the test fly ash were identified using X-ray diffraction method (XRD). PANalytical Empyrean X-ray diffractometer with a cukα radiation was used to perform the XRD test. The step size used in testing is 0.026 degree, the counting time per step is 447 seconds, and the scan angel is from 10 to 90^0. To analyze the data, High Score Plus software is used with an International Centre for Diffraction Data (ICDD) XRD database. As shown in Table 6-1, the results from the testing and analysis showed the existence of the aluminum silicate, silicon oxide, aluminum oxide, and iron oxide as the major crystalline part of this fly ash.

Table 6-1. Results of data analysis of XRD measurements using ICDD database.

Crystal	Formula	Relative Percentage
Aluminum Silicate	Al_2SiO_5	53.5
Silicon Oxide	SiO_2	36.4
Iron Oxide	Fe_2O_3	5.1
Aluminum Oxide	Al_2O_3	4
Calcium Oxide	CaO	1

The major, minor and trace element concentrations are measured using standard microwave acid digestion method EPA 3051A (Link et al. 1998). The results are presented in Table 6-2. In this process, the solids are dissolved in reagent nitric acid with a solution to mass ratio of 20. Silicon crystals are very stable, and therefore triple digestion method was used to measure its concentration. The obtained concentrations of trace elements from this approach are vewed as the

maximum level that can be expected in leachate because of high solubility of the nitric acid reagent in comparison to usual fluids passing through fly ash.

Table 6-2. Major, minor and trace elements, results of EPA 3051A method.

Type	Element	mg/kg
Major	Silicon	103011
	Iron	19856
	aluminum	14271
	Calcium	5689
Minor & trace elements	potassium	2021
	Magnesium	995
	Sodium	406
	Barium	377
	Strontium	178
	Boron	77.9
	Manganese	77.8
	Vanadium	70.5
	Copper	50.3
	Arsenic	42.8
	Nickel	37.9
	Zinc	36.5
	Chromium	36.3
	Lead	18.9
	Molybdenum	8.76
	Selenium	6.01
	Cadmium	0.764
	Mercury	< 0.193

6.2.1 Adsorption/desorption modeling in MINTEQ

Adsorption is the accumulation of molecules at the interface between two solid and fluid phases, and the adsorption density (q) is the amount of material sorbent per unit amount of adsorbent (e.g., mg/g) (Benjamin 2014). In this study, the physical adsorption, which is a result of electrostatic interaction between the solid surface and the adsorbent is considered as the predominant adsorption condition. There are several models which have been suggested for modeling the adsorption/desorption of solids. Langmuir isotherm and Freundlich isotherm models are the base

of more complicated models. Herein, competitive Langmuir adsorption model was used to evaluate adsorption/desorption of arsenic and selenium elements on fly ash surface. In this model, a single adsorbent with multiple sorbates can be considered. The simplest way to present this model is having one sorbate, which converts the model to basic Langmuir isotherm model. The competitive Langmuir adsorption model to estimate each sorbent density (q_i) is presented in Equation 1 (Benjamin 2014).

$$q_i = \frac{K_{ads,i}\cdot[i]}{1+\sum_{all\ j} K_{ads,j}\cdot[j]} q_{max} \quad (1)$$

q_{max} is total adsorption density of the solid (mole/gr or mole/L), $K_{ads,j}$ is the adsorption constant of the sorbate j, and [j] is the concentration of sorbent j in the solution.

Equations 2, 3, and 4 demonstrated the pH dependency of different As (V) forms in a solution (Wang et al. 2008; Gustafsson 2013);

$H_3AsO_4 \Leftrightarrow H_2AsO_4^- + H^+$, $pK_{a1} = 2.26$ (2)

$H_2AsO_4^- \Leftrightarrow HAsO_4^{2-} + H^+$, $pK_{a2} = 6.76$ (3)

$HAsO_4^- \Leftrightarrow AsO_4^{3-} + H^+$, $pK_{a3} = 11.29$ (4)

Equation 5 and 6 show different forms of selenium ion in a solution and its pH dependency (Wang et al. 2007; Gustafsson 2013). All the acid-base constants in Equations 2 – 6 are in agreement with the MINTEQ 3.1 data base.

$H_2SeO_3 \Leftrightarrow HSeO_3^- + H^+$, $pK_{a1} = 2.64$ (5)

$HSeO_3^- \Leftrightarrow SeO_3^{2-} + H^+$, $pK_{a2} = 8.36$ (6)

The chemical reactions were modeled using the chemical equilibrium program MINTEQ 3.1 (Gustafsson 2013). In order to understand the equilibrium state, equations including mass balances,

chemical equilibrium expressions, and a charge balance, proton condition, or total hydrogen (TOTH) equation were used (Benjamin 2014). Based on data from previous studies, which will be discussed later in the "Results" section, the adsorption constants of the As and Se, and total adsorption density (q_{tot}), were defined in the program. The pH level of the system was varied between 4 to 12 in 0.5 pH increments to explore the solubility of the mentioned elements in different systems. At first, the model was validated based on data reported in literature, and then, it was used to suggest the pH-solubility dependence of the elements for the studied material. The steps for modeling adsorption/desorption of arsenic are explained in Appendix B, and the same steps are performed for selenium adsorption/desorption modeling.

6.2.2 Bacteria and growth condition

Sporosarcina pasteurii (ATCC 11859), a urea hydrolyzing bacterium, was grown and used in this study. For this purpose, ammonium yeast extract medium (ATCC 1376) was used to grow the bacteria at 30 °C. Each ingredient was autoclaved and mixed after sterilization. The growth medium was inoculated with *S. pasteurii* stock culture and incubated aerobically at 30 ºC with 200 revolutions per minute till the desired population of cells was reached assessed using optical density (i.e., OD_{600}). Incubation stopped before reaching the plateau of the growth curve to avoid dead bacterial cells. Cultures were centrifuged at 4000 g for 20 minutes in 15 ml vials. The spent supernatant medium was replaced with fresh growth medium and centrifuged a second time after the complete mixing of cells and growth medium. Harvested bacteria were stored at 4 ºC to minimize their activity.

6.2.3 Batch testing

Two batch testing programs were designed to explore the effect of MICP treatment on leaching behavior of fly ah. 10-gr oven-dried mass of solid (i.e., fly ash) was mixed with 200 ml of solution (i.e., Liquid/Solid ratio = 20) in an incubator with 200 revolutions per minute at 21^0C for 4 to 24 hours. The pH of the supernatant solution was measured during incubation once per day and again right after incubation (i.e., the final pH). The aqueous samples were collected using a syringe and 30 μm syringe filter. The inductively coupled plasma mass spectroscopy (ICP-MS) was conducted to measure trace elements' concentrations.

During the first batch testing program, the effect of components in $CaCl_2$ salt (i.e., Ca^{2+} and Cl^-) was investigated by performing the testing with seven different solutions in duplicate (i.e., batch testing 1). One of them was deionized water and the recipes of the rest are presented in Table 6-3. $CaCl_2.2H_2O$ was considered the base of the other salts concentration, the concentration of the NaCl ([NaCl]) is twice of [$CaCl_2.2H_2O$] and it is equal for [$Ca(NO_3)_2.4H_2O$] in molar unit. The maximum and minimum concentrations were chosen to bracket typical treatment recipes used in experimental studies (Martinez et al. 2013; Mortensen et al. 2011; Bothe and Brown 1999).

Table 6-3. Recipe of salt solutions in batch testing one.

Chemical	Min		Max	
	mg/L	mM	mg/L	mM
$CaCl_2.2H_2O$	400	2.72	58804	400
NaCl	263.6	5.44	38752	800
$Ca(NO_3)_2.4H_2O$	642.5	2.72	94456	400

The second batch testing program was performed to investigate the effect of MICP treatment on immobilization/mobilization of arsenic and selenium. Several [urea(mM):Ca^{2+} (mM)] ratios were used in this batch testing, as presented in Table 6-4.

Table 6-4. Recipes of the solutions in batch testing two.

Sample's name	Salt		Urea
	name	(mM)	(mM)
[4:0]	-	-	4
[40:0]	-	-	40
[400:0]	-	-	400
[4:4], Cl	$CaCl_2$	4	4
[40:40], Cl	$CaCl_2$	40	40
[400:400], Cl	$CaCl_2$	400	400
[400:100], Cl	$CaCl_2$	100	400
[400:100], NO3	$Ca(NO_3)_2$	100	400
[400:400], NO3	$Ca(NO_3)_2$	400	400

Three of the recipes had only urea (i.e., 1:0 recipe), four of them had molarity ratio ([Urea]/[Salt]) of 1 (i.e., 1:1 recipe), and two of them had the molarity ratio of 4 (i.e., 4:1 recipe). The *S. Pasteurii* bacteria hydrolyzes urea during MICP reaction. In order to mix *S. Pasteurii* bacteria in solutions, 11 ml of 15 ml supernatant solution in the bacteria vials were first removed, and the centrifuged culture was mixed with the remained solution. This 4 ml bacteria solution was combined with the specified solutions to form 200 mg of the recipes in. The samples were incubated and tested with the same method was mentioned for the first batch testing program. Based on the activity of the bacteria, four days were enough for urea hydrolysis of all testing solutions.

6.3 Results and Discussion

6.3.1 Arsenic adsorption modeling

Results of a study on adsorption of arsenic (V) onto fly ash by Wang et al. 2008 was used to validate chemical equilibrium modeling with MINTEQ. Based on their report, the curve fitting on results of batch acidimetric-alkalimetric titration on a Class- F fly ash identified three types of monoprotic acid sites on the ash surface (i.e., called α, β, and γ). The reported results of arsenic adsorption modeling explained that the arsenic is adsorbed only on site α; considering the other

two sites would result in arsenic adsorption levels that are more than batch test results. The curve fitting results revealed the pK_H of the studied fly ash was 3.5 for L/S=10 and 3.3 for L/S=20. Equation 7 correlates the positively and neutrally charged surface hydroxyl groups and pH (Wang et al. 2008).

$$SOH + H^+ \Leftrightarrow SOH_2^+,\ K_H = 10^{3.5\ (\text{or } 3.3)} \quad (7)$$

The adsorption reaction of different arsenic species were expressed as presented in equation 8, 9, and 10 (Wang et al. 2008).

$$SOH_2^+ + H_2AsO_4^- \Leftrightarrow S\text{-}H_2AsO_4 + H_2O; K_{S1} \quad (8)$$

$$SOH_2^+ + HAsO_4^{2-} \Leftrightarrow S\text{-}HAsO_4^- + H_2O;\ K_{S2} \quad (9)$$

$$SOH_2^+ + AsO_4^{3-} \Leftrightarrow S\text{-}H_2AsO_4 + H_2O;\ K_{S3} \quad (10)$$

The reported values for K_{S1} and K_{S2} were, respectively, 4.4 (or 5.9 kcal mol^{-1}) and 7.9 (or 10.6 kcal mol^{-1}), and the maximum arsenic adsorption density was $7.5x10^{-6}$ mole/(gr ash). At pH of 10 and lower, the AsO_4^{3-} concentration is low, so the adsorption constant of AsO_4^{3-} (i.e., K_{S3}) was not reported.

Based on Equation 2 – 9, Equations 11 and 12 are obtained to be the input of the adsorption parameters in MINTEQ.

$$SOH + 3H^+ + AsO_4^{3-} - H_2O \Leftrightarrow S\text{-}H_2AsO_4,\ K_{ads,1} = 10^{25.95} \quad (11)$$

$$SOH + 2H^+ + AsO_4^{3-} - H_2O \Leftrightarrow S\text{-}HAsO_4,\ K_{ads,1} = 10^{22.69} \quad (12)$$

The mentioned parameters and total arsenic concentration of 11.2 mg/l were the input of chemical equilibrium modeling. pH titration was performed, and total dissolved arsenic ($[As(V)]_D$) was

obtained from the modeling results. The arsenic adsorption ratio (i.e., equation 13) was computed form the results of modeling and compared with the reported data to validate the model.

$$R = 1 - \frac{[As]_D}{[As]_{add} + [As]_b} \qquad (13)$$

Where, $[As]_D$, $[As]_{add}$, and $[As]_b$ are the soluble, added and background arsenic concentrations. $[As]_b$ was 1.2 mg/l and $[As]_{add}$ was 10 mg/l in modeling for validation.

The results shown in Figure 6-1indicated that arsenic adsorption modeling using maximum adsorption density (i.e., q in the figure) of $7.5x10^{-06}$ mole/gr resulted in an adsorption ratio lower than reported data. Therefore, the maximum site density was varied to explore its effect on matching the data by Wang et al. 2008. Increasing the maximum site density from $7.50x10^{-06}$ mole/gr to 3.05 $x10^{-05}$, better matched the reported data points, as demonstrated in Figure 6-1. These results showed that chemical equilibrium modeling with MINTEQ can be used to predict the effect of pH on arsenic adsorption/desorption behavior.

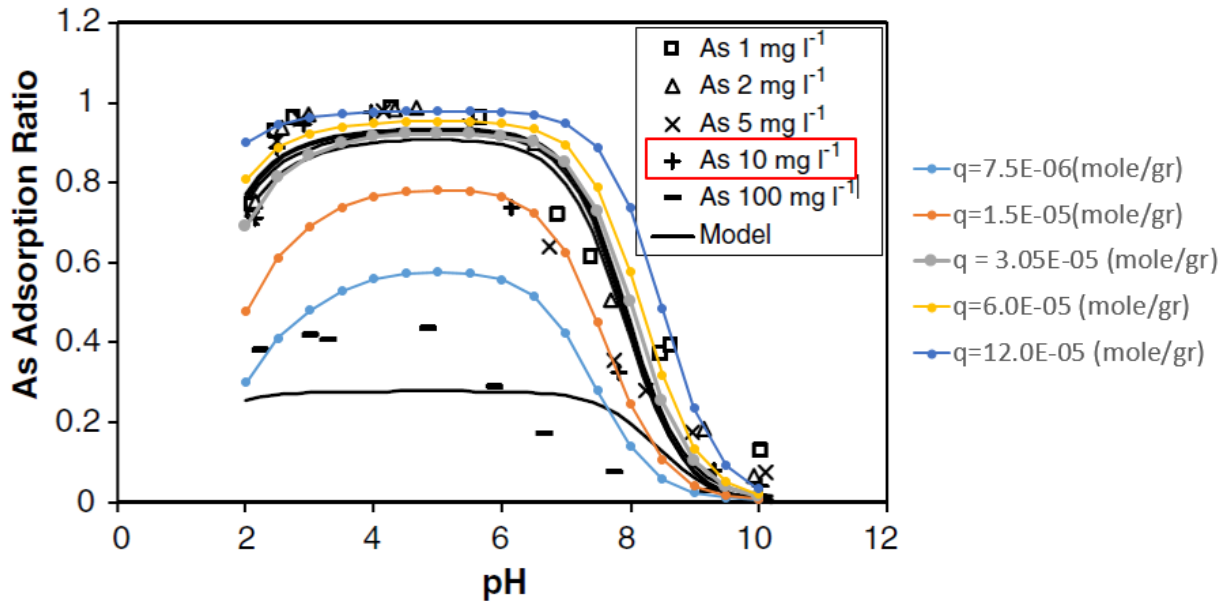

Figure 6-1. Validation of arsenic modeling in chemical equilibrium model using the reported data and parameters by Wang et al. 2008.

6.3.2 Selenium adsorption modeling

The results of a study on selenium adsorption/desorption were used to validate the chemical equilibrium modeling (Wang et al. 2007). The study was conducted on two Class-F fly ashes, and the data points and resultants parameters of one of them (i.e., FA#1008) are provided here to validate the modeling. Based on the reported data, the curve fitting on results of batch acidimetric-alkalimetric titration identified three types of monocratic acid sites (i.e., called α, β, and γ) on the ash surface similar to the previous reported data for arsenic. Only the α site was used to derive the adsorption parameters again, which has a pK_H of 3.2 in Equation 7. Equations 14 and 15 present the reported adsorption reactions of different selenium (IV) species. The K_{S1} and K_{S2} values for fly ash #1008 were reported to be $10^{3.6}$ and $10^{6.3}$, respectively. The maximum α site density and maximum selenium concentration of this fly ash were reported to be $39x10^{-5}$ mole/gr (i.e., equal to 39 mmole/l for L/S=10) and 3.5 mg/kg, respectively,

$$SOH_2^+ + HSeO_3^- \Leftrightarrow S\text{-}HSeO_3 + H_2O;\ K_{S1} \quad (14)$$

$$SOH_2^+ + SeO_3^{2-} \Leftrightarrow S\text{-}AsO_3^- + H_2O;\ K_{S2} \quad (15)$$

The results of soluble selenium concentration under addition of 5 gr Se(IV) for FA#1008 (Wang et al. 2007) were used in chemical equilibrium modeling. The adsorption ratio was extracted from modeling output using Equation (16).

$$R = 1 - \frac{[Se]_D}{[Se]_{add} + [Se]_b} \quad (16)$$

Where $[Se]_D$, $[Se]_{add}$, and $[Se]_b$ are the soluble, added and background selenium concentrations.

The pH of the solution was varied along with using different site densities (i.e., q in Figure 6-2) and the soluble selenium and the associated adsorption ratio were monitored, as demonstrated in

Figure 6-2. The results showed increasing the site density and approaching the reported site density values (i.e., 39 mmoles/gr) resulted in a curve closer to the data by Wang et al. 2007. Therefore, the selenium adsorption/desorption can be modeled using chemical equilibrium modeling (i.e., competitive Langmuir isotherm) in MINTEQ.

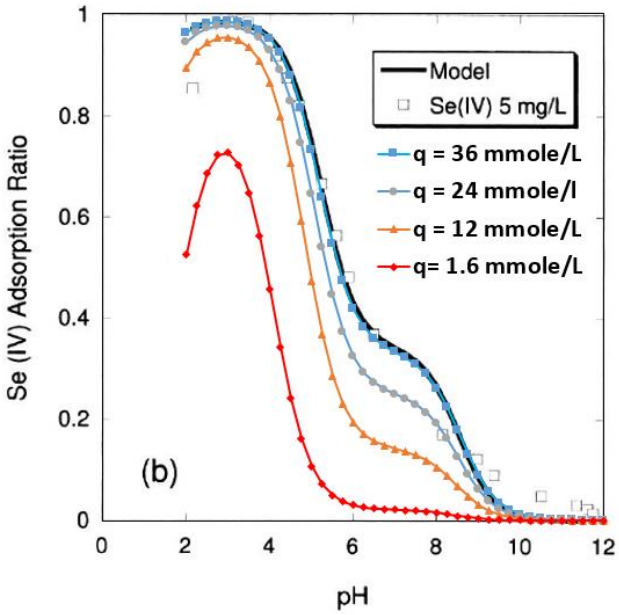

Figure 6-2. Validation of selenium modeling using the reported data and parameters by Wang et al. 2007 for FA#1008 fly ash.

6.3.3 Batch testing

Batch testing "1" was conducted on CA1 fly ash to look the effect of salts on arsenic and selenium adsorption/desorption behavior. The pH of the solution was measured after four days of incubation. Arsenic and selenium concentrations of the collected aqueous samples were measured using ICP-MS method. A summary of the pH and concentrations for each salt solution is presented in Table 6-5. A comparison between the results of arsenic and selenium concentrations of all the incubated samples and the concentration from microwave acid digestion method (EPA3051A) show the

concentrations of all the batch testing samples to be lower than data from microwave acid digestion method.

Table 6-5. Resultant pH and concentrations (i.e., [As] and [Se]) of batch testing 1 and 2.

Sample	pH	Arsenic		Selenium	
		(ug/L)	(mg/kg)	(ug/L)	(mg/kg)
Baseline	8.39	336.8	6.74	258.0	5.16
Min $CaCl_2$	8.17	194.8	3.90	162.9	3.26
Max $CaCl_2$	7.42	154.8	3.10	209.7	4.19
Min NaCl	8.46	249.5	4.99	147.5	2.95
Max NaCl	8.44	681.0	13.62	183.0	3.66
Min $Ca(NO_3)_2$	8.22	163.5	3.27	156.5	3.13
Max $Ca(NO_3)_2$	7.51	142.0	2.84	181.0	3.62
[4:0]	8.48	373.1	7.46	161.8	3.24
[40:0]	9.17	733.3	14.67	243.4	4.87
[400:0]	9.33	1237.4	24.75	278.0	5.56
[4:4], $CaCl_2$	8.17	317.7	6.35	120.6	2.41
[40:40], $CaCl_2$	7.97	219.0	4.38	53.7	1.07
[400:400], $CaCl_2$	7.70	122.1	2.44	39.5	0.79
[400:100], $CaCl_2$	9.15	662.0	13.24	84.5	1.69
[400:100], $Ca(NO_3)_2$	9.19	939.3	18.79	102.7	2.05
[400:400], $Ca(NO_3)_2$	7.47	46.6	0.93	18.0	0.36

The adsorption/desorption of fly ash is highly dependent on the pH of the solution. Increasing pH level increases the solubility of both arsenic and selenium in the studied fly ashes (Izquierdo and Querol 2012b). Therefore, the effect of salts and MICP treatment cannot be determined without considering the pH effect. Chemical equilibrium modeling is utilized to suggest an arsenic and selenium background pH-[element] curve for CA1 fly ash. Results of batch testing for arsenic and selenium, are discussed separately.

Results of arsenic modeling. To develop the background pH-[As] curve, which represents the effect of pH on solubility, the data points obtained for deionized water and minimum salts (i.e., $CaCl_2.2H_2O$, $Ca(NO_3)_2,.4H_2O$, NaCl) samples in batch testing 1 were used to calibrate the arsenic adsorption/desorption modeling. For this purpose, the same acid/base constants and adsorption

constants, which were obtained during the validation part, were defined in MINTEQ. The resultant arsenic concentration from microwave acid digestion method (i.e., 42.8 mg/kg or 2.14 mg/l while L/S was 20 in batching test) was considered as the total arsenic (V) of the system. The surface site density was varied to assess the background curve based on the mentioned data points. The maximum surface site density was increased from the validation model's maximum site density (i.e., q=3.05 mmole/gr) to 24 mmole/gr to have a best fitting curve, shown in Figure 6-3. The background curve (i.e., "Modeling" curve in Figure 6-3) shows a good match with data points from samples that were incubated with deionized water and minimum salt concentration solutions. It is used herein as the baseline curve for exploring the effect of treatment solutions on mobilization/immobilization of arsenic. Comparing the results of the baseline curve and the maximum salt concentration samples showed that all these solutions increased the solubility of the arsenic. Increasing the salinity of a solution increases the solubility of the system because of elemental activity reduction (Benjamin 2014) which could be the reason of increasing the arsenic concentration in maximum salt solutions. Increasing the concentration of calcium salts decreased the final pH values after four days of incubation, and led to having lower [As] in comparison to the [As] in deionized water sample.

In Figure 6-4, the results of batch testing 2 are compared with the suggested baseline curve to explore the effect of MICP treatment on solubility of arsenic. The results indicated that using 1:1 recipe (i.e., [4:4], [40:40], and [400:400]) decreased the pH level (i.e., compared to deionized water sample) and this reduction was higher as the urea and salts concentrations were increased. Therefore, increasing the salt concentration in 1:1 recipe decreased the [As] while it is higher than baseline curve. The decrease of pH and [As] were higher in [400:400], $Ca(NO_3)_2$ samples as compared with [400:400], $CaCl_2$ solution. On the other hand, 4:1 recipes (i.e., [400:100], $CaCl_2$

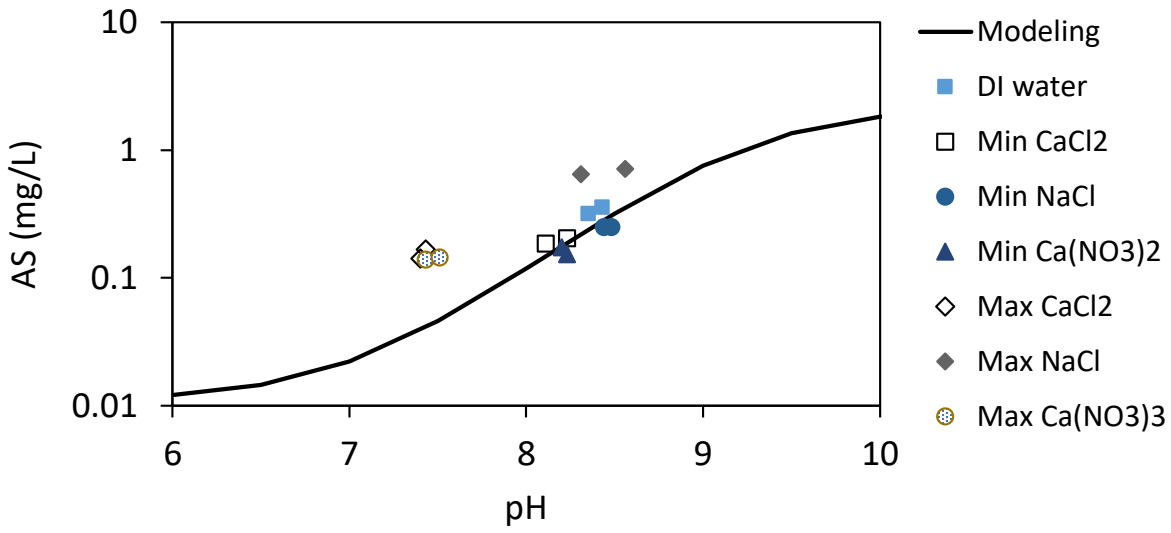

Figure 6-3. Effect of salts on arsenic solubility in batch testing based on the suggested background pH-[As] curve.

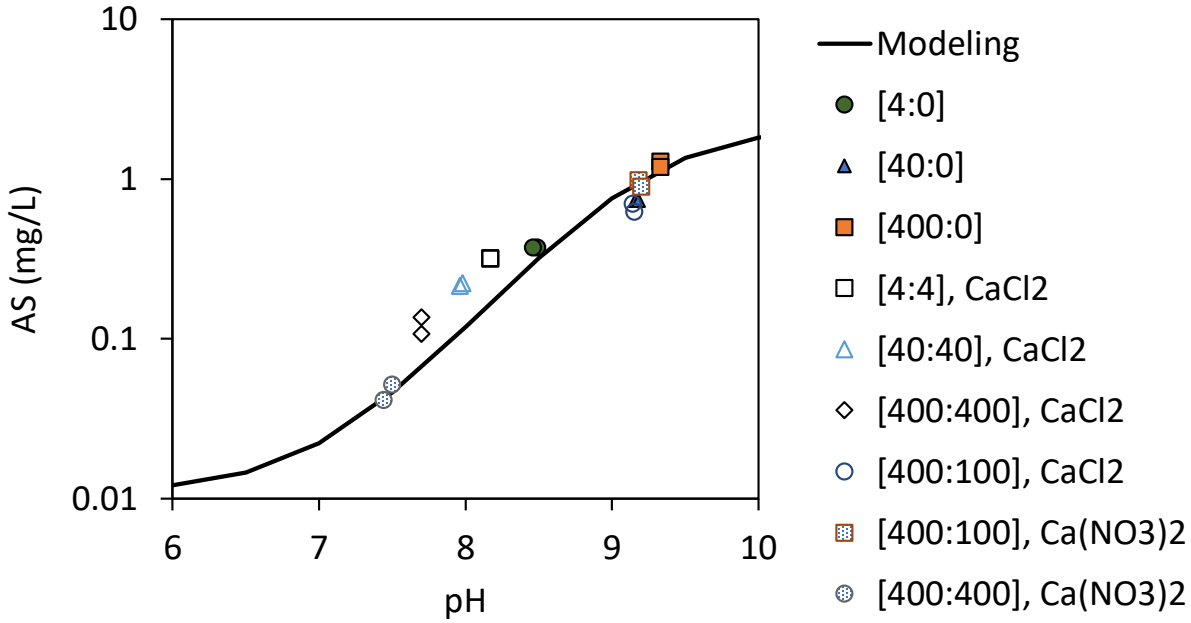

Figure 6-4. Effect of MICP treatment on arsenic solubility in batch testing based on the suggested background pH-[As] curve.

and [400:100], $Ca(NO_3)_3$) increased the final pH values, therefore, it mobilized the arsenic in solution. Comparing the results of 4:1 recipe solutions with baseline curves showed this recipe did not decrease the solubility of arsenic. In summary, the studied MICP treatment recipes did not

decrease the arsenic solubility through MICP co-precipitation in relation to the solubility with the suggested baseline curve.

Results of Se modeling. To find the baseline curve of pH-[Se] the parameters obtained from the validation section (i.e., FA #1008) were defined in MINTEQ. Maximum selenium concentration was considered to be 6.01 mg/kg (i.e., 0.3 mg/L) based on the results of microwave acid digestion method. The maximum adsorption site density was varied to fit the baseline curve to the results of [Se] from deionized water and minimum salts concentration samples. The results showed variation of site density would not lead to a curve which is fit to the resultant [Se] of the mentioned samples. The effect of salts is unknown, therefore, only [Se] concentration of deionized water samples used for curve fitting. For this purpose, the maximum site density was decreased from 39 mmole/l (i.e., the reported and also validated site density) to 24 mmole/l to have the best match. The resultant baseline curve fitting using the FA#1008 parameters did not match with the [Se] in minimum salt concentration samples. This could be due to the effect of salts or using wrong adsorption constants. The adsorption constants of two other fly ashes were reported by Su and Wang 2011 (i.e., presented in Table 6-6), which were named FA#034 and FA#094, and used in adsorption/desorption modeling. The maximum site density was varied to have the best match with the results of deionized water samples and also to assess whether using adsorption constants of the other fly ashes leads to having a fit to the results of samples with minimum salts concentrations. The results of curve fitting for all three fly ashes are demonstrated in Figure 6-5. All three background curves (which were fitted with the results of deionized water samples) show the same [Se] trend and values for the pH=7 and above, and none of them is close to the results of the samples with the minimum salts concentrations. The baseline curves presented in Figure 6-5 is based on only two

data points (i.e., for deionized water samples) and further study on the effect of pH is necessary to be able to suggest the baseline or background curve.

The minimum salts concentrations slightly decreased the pH of the solutions in the cases of having calcium in salts (i.e., maximally from 8.46 to 8.17 for minimum $CaCl_2$ sample) and the pH was almost constant for minimum NaCl concentration sample (i.e., varied from 8.39 to 8.46). However, all the minimum salts concentration samples have [Se] lower than values obtained for the deionized water samples. Increasing the concentration of the calcium salts (i.e., $CaCl_2$ and $Ca(NO_3)_2$) to maximum decreased the level of pH to 7.42 and 7.51, respectively, for $CaCl_2$ and $Ca(NO_3)_2$ samples. However, the [Se] of maximum salt concentration samples were higher than [Se] in the minimum salt concentrations samples with the same salt material (e.g., [Se] = 163 ug/L while pH=8.17 for minimum $CaCl_2$ sample and it increased to 210 ug/L while pH=7.42 for maximum $CaCl_2$ sample). Decreasing the pH reduces the selenium solubility (Izquierdo and Querol 2012a). On the other hand, increasing the salinity raises the solubility of selenium (Benjamin 2014). For the mentioned samples the effect of salinity overwhelmed the effect of pH, and it increased the selenium solubility while the salt concentration was raised from minimum to maximum.

Table 6-6. Adsorption constants of three fly ashes were used for selenium adsorption/desorption modeling.

Fly ash	pK_H	$Logk_{S1}$	$logk_{S2}$
FA#1008	3.2	3.6	6.3
FA#034	3.5	2.86	7.86
FA#094	3.2	4.68	6.75

The results for samples which were treated with the MICP process and different recipes are presented in conjunction with the background curves in Figure 6-6. Three of the recipes contained only urea which resulted in hydrolyzed urea after bacteria activity. These solutions were chosen to

explore the effect of hydrolyzed urea (HU) without any salt on mobilization /immobilization of elements. The samples that were treated with recipe [4:0] have the lower [Se] than deionized water, [40:0], and [400:0] samples. Increasing the [HU] in the solutions resulted in increasing the pH and [Se] of the incubated solutions (e.g., [Se] of the samples treated with [400:0] recipe was 278 ug/l while it was 162, 243, and 258 ug/l for [4:0], [40:0], and deionized water sample, respectively). Using 1:1 recipes decreased the [Se] concentration. Increasing the concentrations in 1:1 recipes resulted in higher reduction in pH and [Se] (e.g., [Se]=120.6 ug/l and pH=8.17 for [4:4], CaCl2 samples, these values decreased to [Se]=39.5 ug/l and pH=7.7 for [400:400], CaCl2 samples). Comparing the results of 1:1 recipes to salt recipes indicated that the [Se] was lower in 1:1 recipes (e.g., [Se]=18 ug/l and pH=7.47 for [400:400], Ca(NO3)2 sample while [Se]=181ug/gr and pH=7.51 for Max Ca(NO3)2 samples). It can be concluded that MICP treatment (e.g., co-precipitation) may be the reason for this reduction as the pH is almost the same value for both recipes. The [Se] and pH of [400:100], CaCl2 samples were, respectively, 84.5 ug/l and 9.15, these values were, respectively, 9.19 and 103 ug/l for [400:100], $Ca(NO_3)_2$. The pH values are higher than the pH of the deionized water and maximum and minimum salts concentrations samples while the [Se] were lower than [Se] in all the mentioned samples. Therefore, the effect of MICP treatment and co-precipitation can again explain this reduction in [Se] concentration.

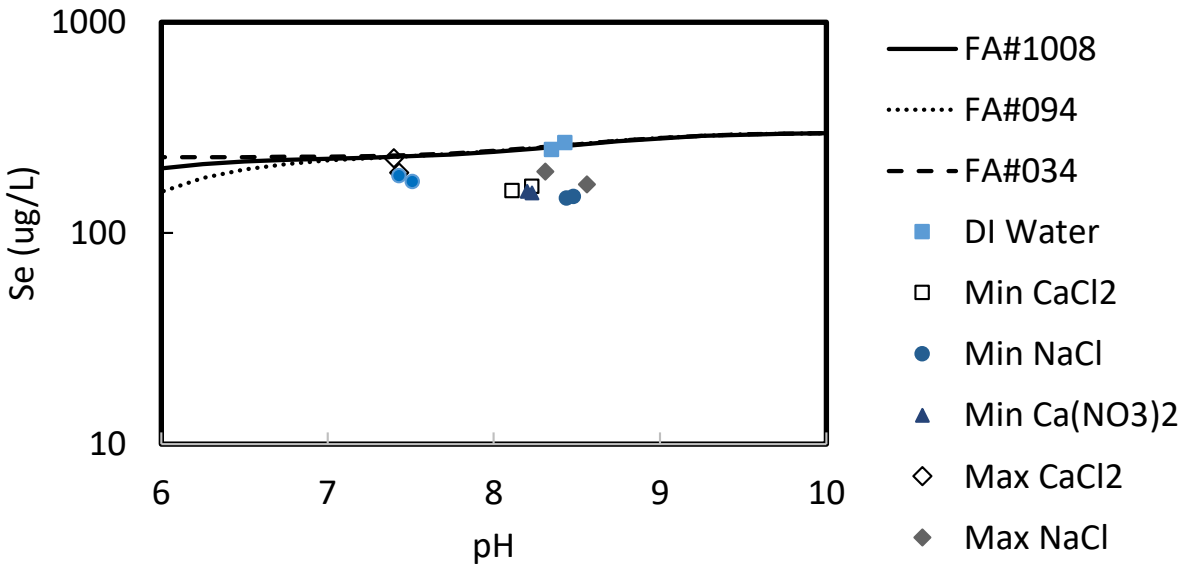

Figure 6-5. Results of batch testing 1 and curve fitting using three different fly ashes' parameter.

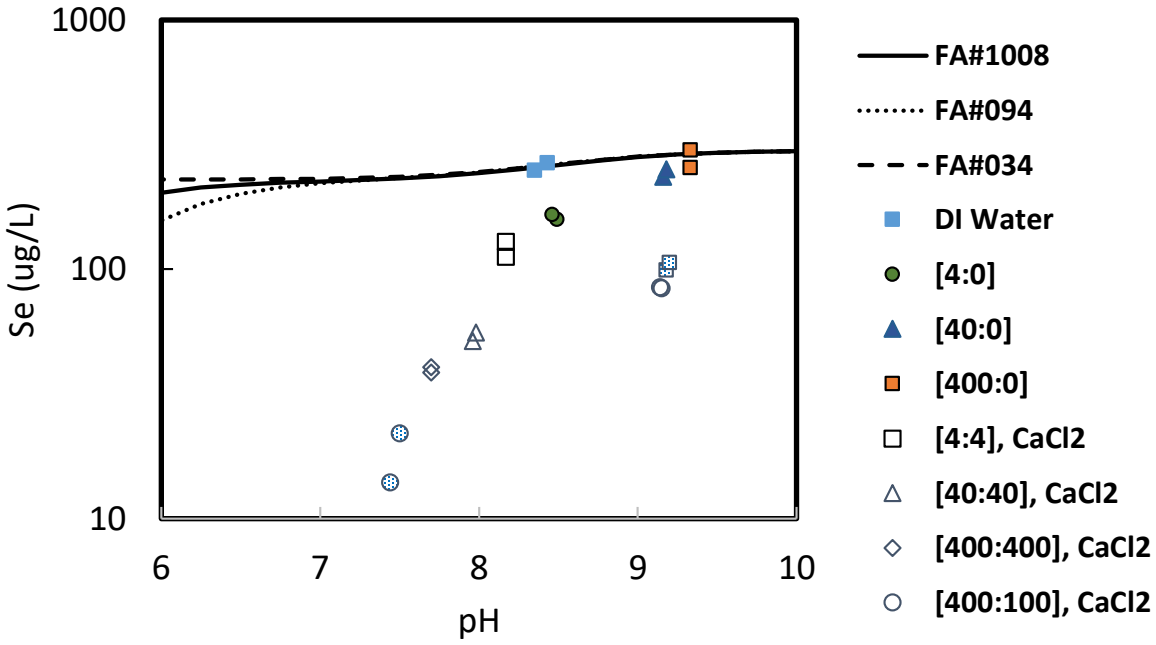

Figure 6-6. Results of the samples were treated using different MICP treatment recipes.

6.3.4 Results of batch testing on other trace elements

The concentration of some other trace elements of concern including boron (B), chromium (Cr), molybdenum (Mo), strontium (Sr), vanadium (V), zinc (Zn), beryllium (Be), cadmium (Cd), cupper (Cu), and nickel (Ni) were measured in the samples of batch testing 1 using ICP-MS method for future study. A Summary of all the pH and trace elements measurements are presented in Table 6-7. Results of batch testing 1 indicated that some of the trace elements' concentrations including Zn, Be, Cd, Cu, and Ni were lower than detection limit of measurement device, therefore, they were removed from the list for further analysis in batch testing 2. The pH and trace elements measurement results of the batch testing 2 can be found in Table 6-8.

Table 6-7. pH and trace elements measurements in batch testing 1.

Sample	pH	As	B	Cr	Mo	Se	Sr	V	Zn	Be	Cd	Cu	Ni
		ug/L											
DI water-1	8.43	357	2,272	62.5	190	267	501	182	18.9	<1.00	0.79	0.93	6.88
DI water-2	8.35	317	2,381	61.5	205	249	499	159	13.4	<1.00	0.81	0.53	6.87
Min $CaCl_2$-1	8.11	185	1,334	59.3	193	159	495	118	5.9	<2.00	<2.00	<2.00	<2.00
Min $CaCl_2$-2	8.23	205	1,445	58.7	189	167	518	133	<5.00	<2.00	<2.00	<2.00	<2.00
Min NaCl-1	8.44	250	761	53.9	179	146	472	156	<5.00	<2.00	<2.00	<2.00	<2.00
Min NaCl-2	8.48	249	893	54.4	182	149	468	146	<5.00	<2.00	<2.00	<2.00	<2.00
Min $Ca(NO_3)_2$-1	8.2	174	1,324	62.4	201	158	500	120	5.1	<2.00	<2.00	<2.00	<2.00
Min $Ca(NO_3)_2$-2	8.23	153	1,454	61.7	196	155	515	107	9.9	<2.00	<2.00	<2.00	<2.00
Max $CaCl_2$-1	7.4	142	1,436	49.1	201	226	665	67.1	<5.00	<2.00	<2.00	<2.00	<2.00
Max $CaCl_2$-2	7.43	167	1,350	50.9	201	193	689	71.6	<5.00	<2.00	<2.00	<2.00	<2.00
Max NaCl-1	8.31	649	352	69.7	232	196	660	281	<5.00	<2.00	<2.00	<2.00	<2.00
Max NaCl-2	8.56	713	232	70.1	242	170	670	315	<5.00	<2.00	<2.00	<2.00	<2.00
Max $Ca(NO_3)_2$-1	7.43	139	1,356	64.4	185	187	430	68.7	58.2	<2.00	<2.00	<2.00	<2.00
Max $Ca(NO_3)_2$-2	7.51	145	928	64.4	197	175	478	71.7	56.9	<2.00	<2.00	<2.00	<2.00

Table 6-8. pH and trace elements measurements in batch testing 2.

Sample	pH	As	B	Cr	Mo	Se	Sr	V
					ug/L			
4 mM Urea-1	8.49	373	1650	55	173	159	444	196
4 mM Urea-2	8.46	373	1627	53	166	165	426	184
40 mM Urea-1	9.16	735	1723	71	202	235	125	365
40 mM Urea-2	9.18	732	1741	74	205	251	122	374
400 mM Urea-1	9.33	1284	1900	158	247	301	209	688
400 mM Urea-2	9.33	1190	1698	135	217	255	183	609
1:1, 4 mM (CaCl2)-1	8.17	319	1632	53	172	129	431	160
1:1, 4 mM (CaCl2)-2	8.17	316	1705	55	177	112	441	167
1:1, 40 mM (caCl2)-1	7.98	223	1795	59	205	56	467	132
1:1, 40 mM (caCl2)-2	7.96	215	1782	59	203	52	460	134
1:1, 400 mM (CaCl2)-1	7.7	137	1997	62	207	40	1837	74
1:1, 400 mM (CaCl2)-2	7.7	108	2011	64	212	39	1851	81
4:1 400 mM (CaCl2)-1	9.14	702	1608	110	209	85	147	508
4:1 400 mM (CaCl2)-2	9.15	622	1462	91	186	84	159	448
4:1 400 mM (Ca(NO3)2)-1	9.18	982	1777	109	231	99	151	572
4:1 400 mM (Ca(NO3)2)-2	9.2	897	1814	107	235	106	175	575
1:1 400 mM (CaNO3)2)-1	7.5	52	1998	60	220	22	2966	67
1:1 400 mM (CaNO3)2)-2	7.44	42	1824	55	197	14	3161	37

Results of B, Cr, Mo, Se, Sr, and V concentrations versus pH of the solutions in two sets of batch tastings are demonstrated in Figure 6-7 – Figure 6-16.

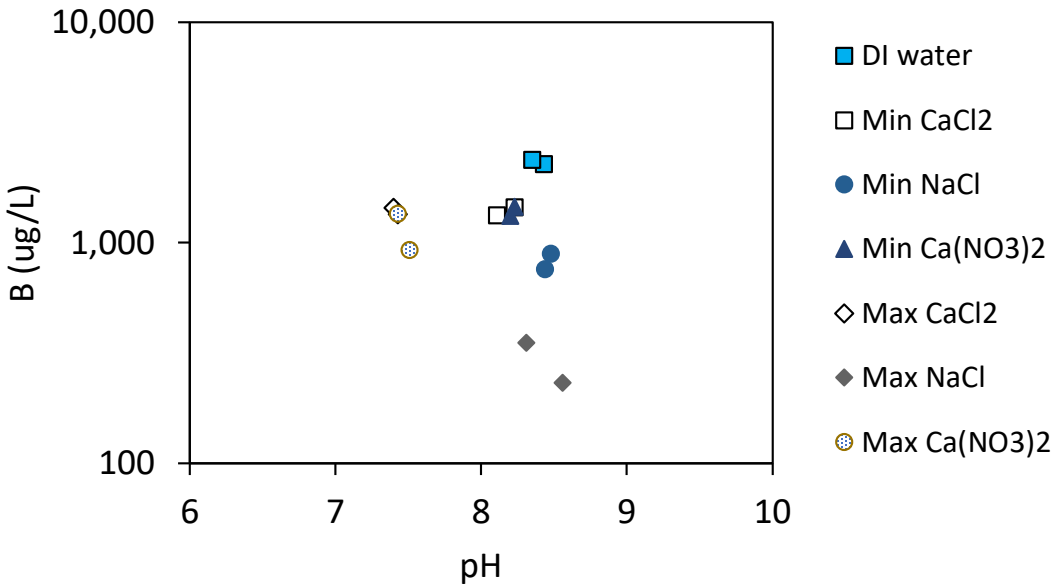

Figure 6-7. [B] vs. pH of the samples in batch testing 1.

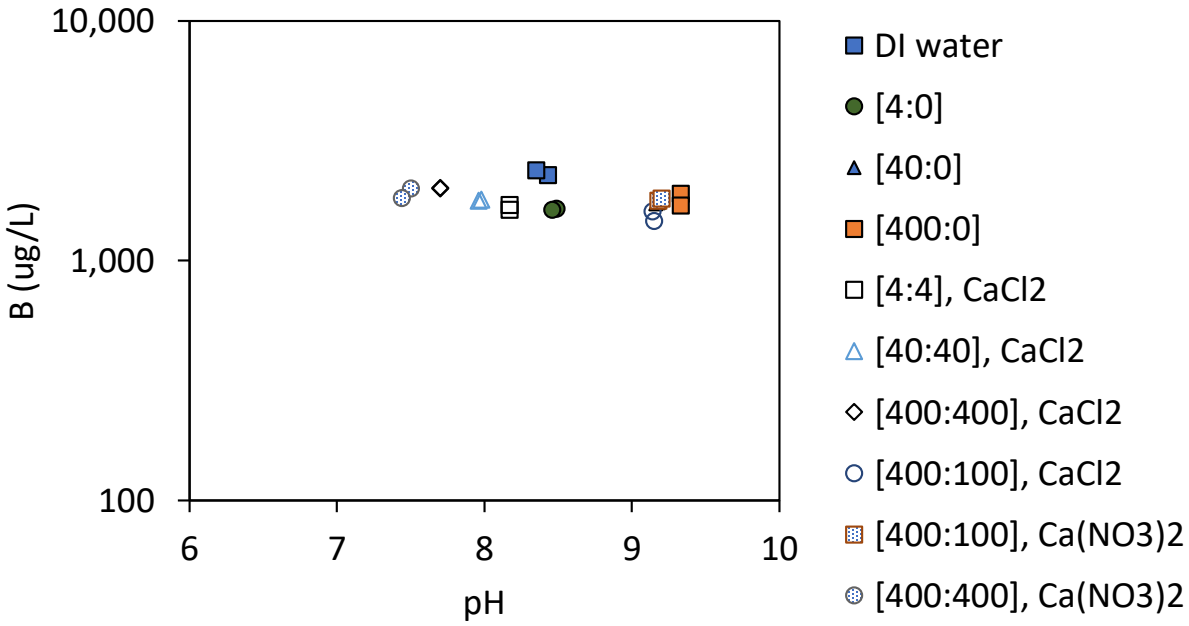

Figure 6-8. [B] vs. pH of the samples in batch testing 2.

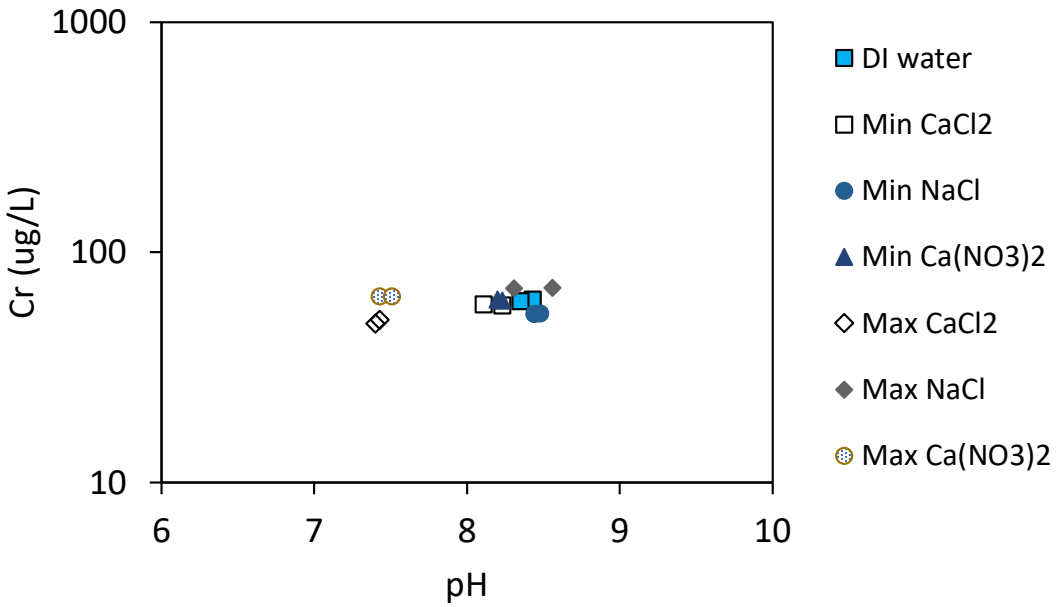

Figure 6-9. [Cr] vs. pH of the samples in batch testing 1.

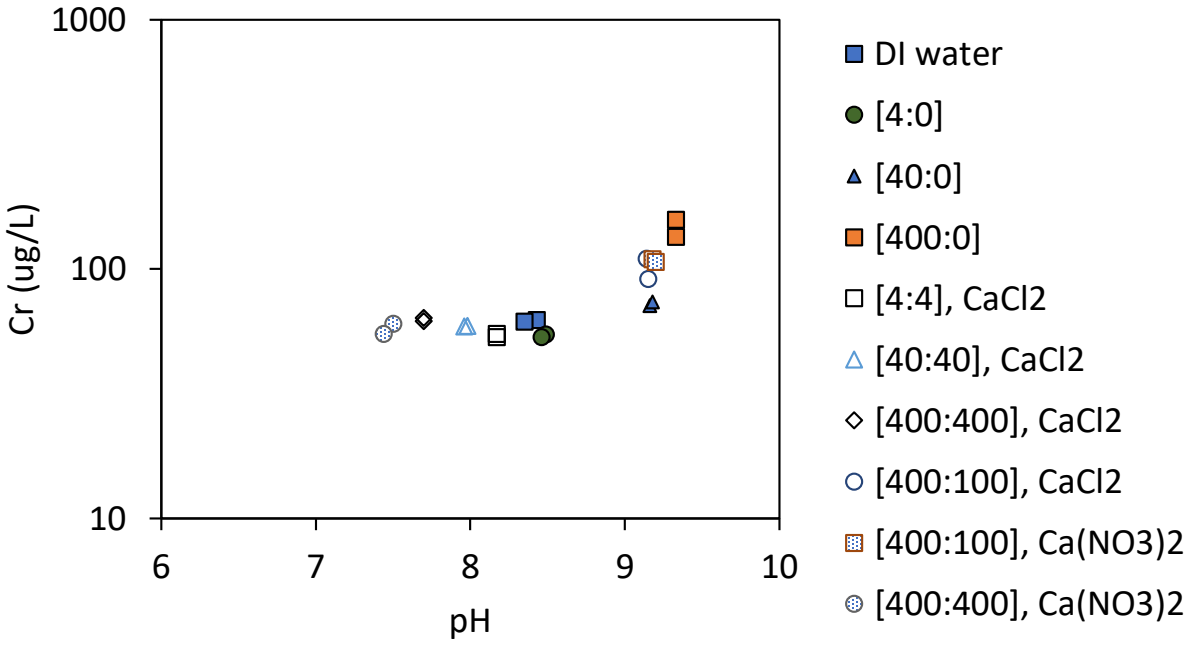

Figure 6-10. [Cr] vs. pH of the samples in batch testing 2.

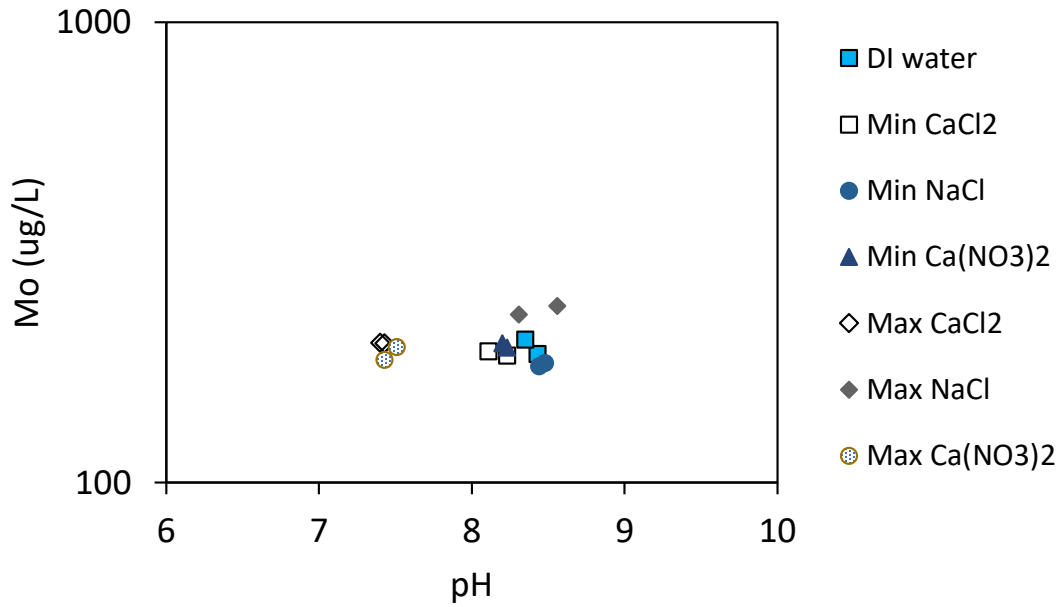

Figure 6-11. [Mo] vs. pH of the samples in batch testing 1.

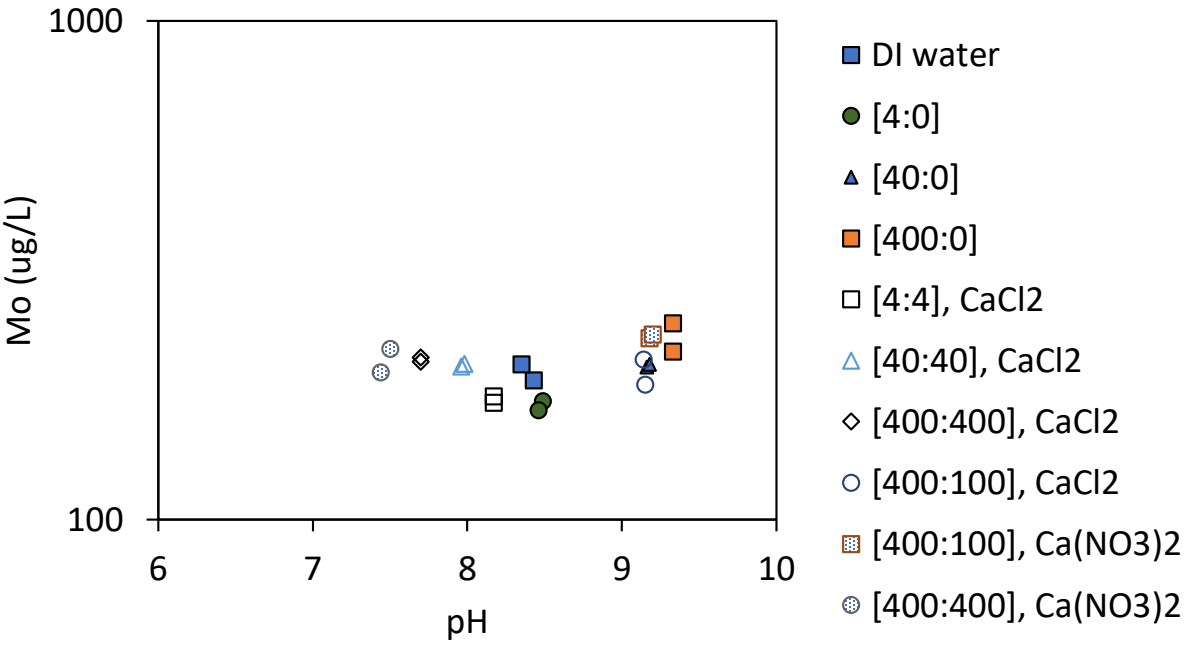

Figure 6-12. [Mo] vs. pH of the samples in batch testing 2.

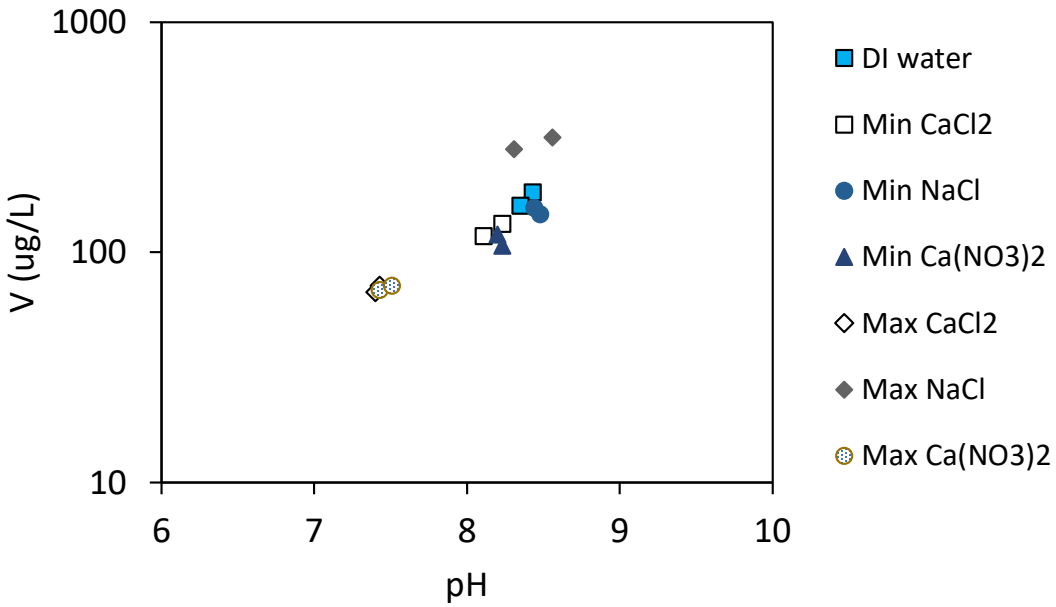

Figure 6-13. [V] vs. pH of the samples in batch testing 1.

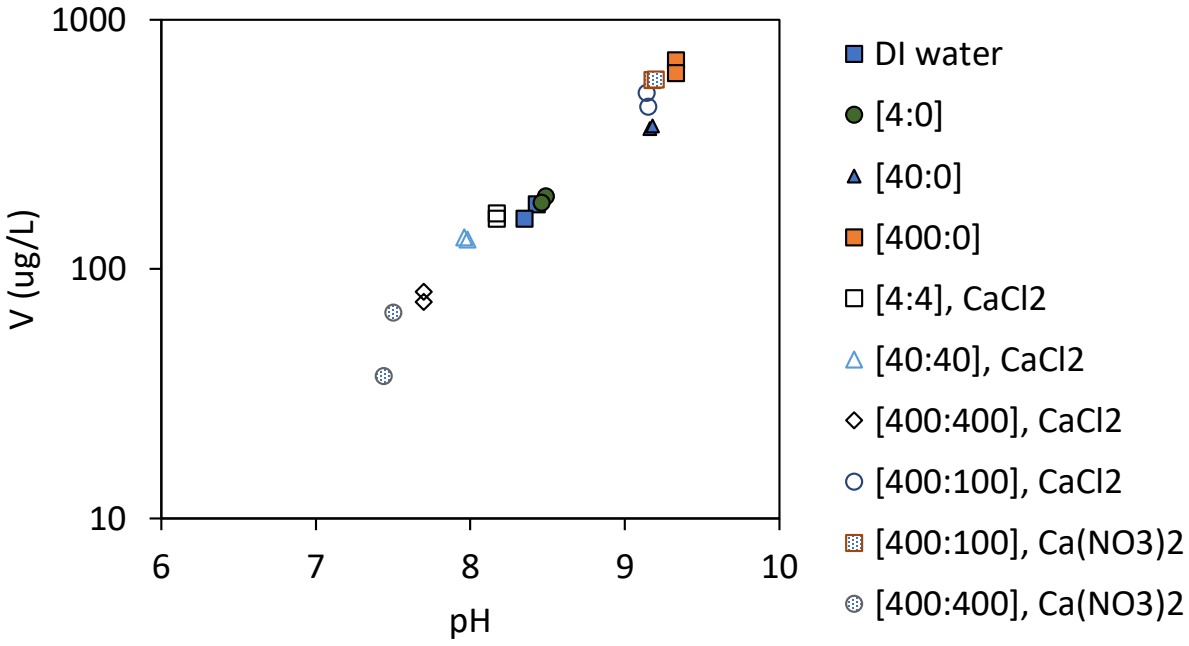

Figure 6-14. [V] vs. pH of the samples in batch testing 2.

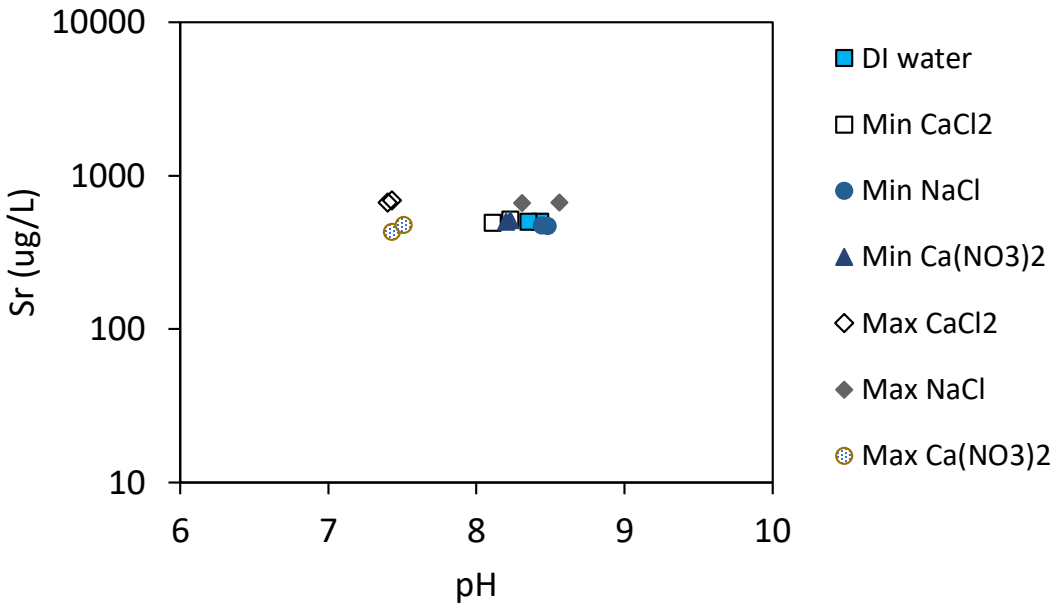

Figure 6-15. [Sr] vs. pH of the samples in batch testing 1.

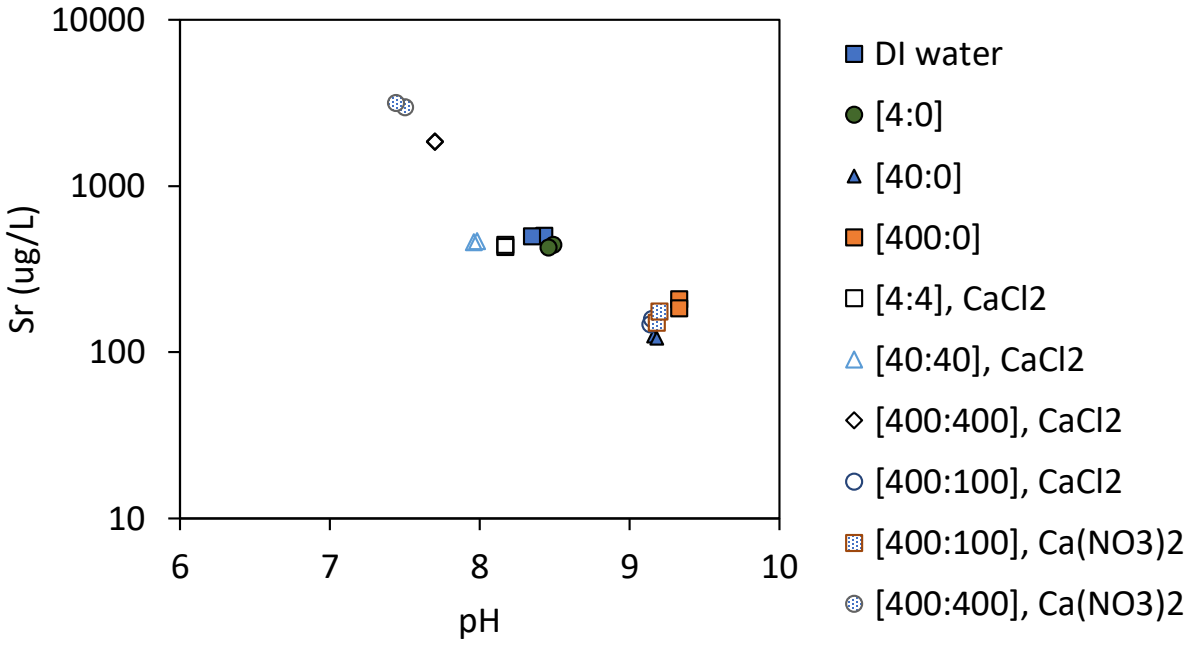

Figure 6-16. [Sr] vs. pH of the samples in batch testing 2.

A summary of observations in batch testing 1 and 2 for each element is presented here:

- Solubility of the boron does not seem to be highly dependent to the pH of the system in the range of this study. The concentration of all the samples except the samples containing NaCl has a [B] above 1000 ug/L. Increasing the [NaCl] decreased the solubility of the B significantly. E.g., maximum NaCl recipe decreased the average [B] from 2327 ug/L in deionized water sample to 292 ug/L in max NaCl recipe. All the samples had a [B] lower than the deionized water sample.
- The [Cr] in all the samples which had a pH between 7 to 9 was in a close range (i.e., between 50 to 70 ug/L). The solubility of Cr increased in the samples, which had 400 ml urea and [1:0], or [4:1] recipes. It indicated increasing the [HU] mobilized Cr. The maximum [Cr] was 158 ug/L in [400:0] recipe.
- The [Mo] did not vary significantly in the samples when the results of batch testing 1 and batch testing 2 were compared. The [Mo] in all the samples were 179 and 249 ug/L, respectively. Minimum NaCl recipe had the minimum [Mo] (i.e., 179 ug/L) and [400:0] recipe had the maximum [Mo] (i.e., 249 ug/L).
- Comparing the [V] Concentrations and [As] in the samples of batch testing 1 and 2 showed similar trends but different values. Increasing the pH of the solution increased the [V]. The average pH and [V] in deionized water sample were 8.39 and 171 ug/L, respectively. For the [400:0] samples, the average pH increased to 9.33 and average [V] raised 648.4 ug/L. The minimum pH and [V] were 7.44 and 37 ug/L in one of the [400:400], $Ca(NO_3)_2$ samples.
- Strontium is a positively charge cation in solution. Increasing the pH level decreased the solubility of this element. [1:0] and [4:1] had the minimum [Sr], and there are two

possible reasons for this reduction; effect of pH and precipitation or co-precipitation of $SrCO_3$. Comparing the results of maximum $CaCl_2$, $Ca(NO_3)_2$ samples with [400,400], $CaCl_2$, and [400,400], $Ca(NO_3)_2$ samples at the same pH level showed lower concentration of strontium in solutions with no hydrolyzed urea.

6.4 Summary and Conclusions

The main objective of this study was exploring the effect of MICP treatment on leaching behavior of arsenic (As) and selenium (Se) from coal ash material. Results are used to explore As and Se adsorption/desorption dependency on the pH level within the context of implementing the MICP process. Modeling in MINTEQ was validated using data reported in literature on arsenic (V) and selenium (IV) adsorption/desorption behavior of fly ashes. The results of validation indicated that the selenium adsorption/desorption behavior of fly ash materials, including the effect of pH can be modeled using MINTEQ.

In order to assess the effect of different salts and MICP treatment on adsorption/desorption of As and Se, batch testing was performed on CA1 material, and different recipes were considered. The studied salts were $CaCl_2.2H_2O$, $Ca(NO_3)_2.4H_2O$, and NaCl. Their concentrations varied between 4 mM to 400 mM to assess the effect of each element separately (i.e., Ca^{2+}, Cl^-). 4:1, 1:1, and 1:0 recipes (i.e., [Urea]:[Ca^{2+}]) were used to examined the effect of MICP treatment in batch testing. The final pH level and concentration of different trace elements in the solution were reported.

Based on the results of this study, the following conclusions are advanced:

1. Different recipes of salts and MICP treatments resulted in different final pHs and arsenic concentrations after 4-24 hrs incubation.

2. Dissolved arsenic concentrations in the batch testing samples were compared with the baseline to see the effect of salts concentration and MICP treatment. All the treated samples with either salt or MICP treatment had concentrations equal or above the baseline curve.
3. These results indicated that arsenic was not immobilized through co-precipitation of the MICP treatment recipes of this study. However, treatment recipe can be designed to decrease the pH of the solution, which would lead to solubility reduction during treatment.
4. Results also indicated that the trend of dissolved selenium concentration in the pH range of 7 and above are the same regardless of the source of the fly ash material. None of the three "background" curves, which were fitted with the results of deionized water samples, was close to the results of the samples with minimum salts concentrations. Therefore, the background curve was not suggested for CA1 material.
5. The results of batch testing using salts and MICP treated recipes showed a variation of selenium concentrations. The results indicated that even low salts concentrations decreased the solubility of the selenium.
6. The comparison of the MICP treated samples and the results of deionized water and salts samples demonstrated that the selenium solubility of these samples is much lower. These results advance the hypothesis that MICP treatment and co-precipitation can decrease desorption of selenium, but to express final statement, further investigation is needed. For this purpose, the effect of pH on solubility of selenium concentration must be studied to ensure the real adsorption/desorption behavior of the studied coal ash.

6.5 References

Ainsworth, C. C., and Rai, D. (1987). "Chemical characterization of fossil fuel combustion wastes: Final report.".

Aurelio, G., Fernandez-Martinez, A., Cuello, G. J., Roman-Ross, G., Alliot, I., and Charlet, L. (2010). "Structural study of selenium (IV) substitutions in calcite." *Chem.Geol.*, 270(1), 249-256.

Benjamin, M. M. (2014). Water chemistry. Waveland Press.

Bhattacharyya, S., Donahoe, R. J., and Patel, D. (2009). "Experimental study of chemical treatment of coal fly ash to reduce the mobility of priority trace elements." Fuel, 88(7), 1173-1184.

Bothe, J. V., and Brown, P. W. (1999). "Arsenic immobilization by calcium arsenate formation." Environ.Sci.Technol., 33(21), 3806-3811.

EPA, U. S. (2003). "National primary drinking water standards." Office of Water, US Environmental Protection Agency.Washington, DC, United States Environmental Protection Agency, .

Fujita, Y., Taylor, J. L., Wendt, L. M., Reed, D. W., and Smith, R. W. (2010). "Evaluating the potential of native ureolytic microbes to remediate a 90Sr contaminated environment." Environ.Sci.Technol., 44(19), 7652-7658.

Gustafsson, J. P. (2013). "Visual MINTEQ version 3.1, department of sustainable development." Environmental Science and Engineering, KTH, Stockholm, .

Hansen, L. D., and Fisher, G. L. (1980). "Elemental distribution in coal fly ash particles." Environ.Sci.Technol., 14(9), 1111-1117.

Huggins, F. E., Senior, C. L., Chu, P., Ladwig, K., and Huffman, G. P. (2007). "Selenium and arsenic speciation in fly ash from full-scale coal-burning utility plants." Environ.Sci.Technol., 41(9), 3284-3289.

Izquierdo, M., and Querol, X. (2012b). "Leaching behaviour of elements from coal combustion fly ash: an overview." International Journal of Coal Geology, 94 54-66.

Jones, D. R. (1995). "The leaching of major and trace elements from coal ash." Environmental aspects of trace elements in coal, Springer, 221-262.

Lecuyer, I., Bicocchi, S., Ausset, P., and Lefevre, R. (1996). "Physico-chemical characterization and leaching of desulphurization coal fly ash." Waste Manage.Res., 14(1), 15-28.

Link, D. D., Walter, P. J., and Kingston, H. M. (1998). "Development and validation of the new EPA microwave-assisted leach method 3051A." Environmental Science and Technology, 32(22), 3628-3632.

Martinez, B. C., DeJong, J. T., Ginn, T. R., Montoya, B. M., Barkouki, T. H., Hunt, C., Tanyu, B., and Major, D. (2013). "Experimental optimization of microbial-induced carbonate precipitation for soil improvement." J.Geotech.Geoenviron.Eng., 139(4), 587-598.

Mortensen, B. M., Haber, M. J., DeJong, J. T., Caslake, L. F., and Nelson, D. C. (2011). "Effects of environmental factors on microbial induced calcium carbonate precipitation." J.Appl.Microbiol., 111(2), 338-349.

Narukawa, T., Takatsu, A., Chiba, K., Riley, K. W., and French, D. H. (2005). "Investigation on chemical species of arsenic, selenium and antimony in fly ash from coal fuel thermal power stations." Journal of Environmental Monitoring, 7(12), 1342-1348.

Praharaj, T., Powell, M. A., Hart, B. R., and Tripathy, S. (2002). "Leachability of elements from sub-bituminous coal fly ash from India." Environ.Int., 27(8), 609-615.

Reardon, E. J., Warren, C. J., and Hobbs, M. Y. (1993). "Reduction of trace element concentrations in alkaline waste porewaters by dedolomitization." *Environ.Sci.Technol.*, 27(2), 310-315.

Silberman, D., and Harris, W. R. (1984). "Determination of arsenic (III) and arsenic (V) in coal and oil fly ashes." Int.J.Environ.Anal.Chem., 17(1), 73-83.

Van der Hoek, Eline E, and Comans, R. N. (1996). "Modeling arsenic and selenium leaching from acidic fly ash by sorption on iron (hydr) oxide in the fly ash matrix." Environ.Sci.Technol., 30(2), 517-523.

Wang, J., Wang, T., Burken, J. G., Chusuei, C. C., Ban, H., Ladwig, K., and Huang, C. P. (2008). "Adsorption of arsenic (V) onto fly ash: A speciation-based approach." Chemosphere, 72(3), 381-388.

Wang, T., Wang, J., Burken, J. G., Ban, H., and Ladwig, K. (2007). "The leaching characteristics of selenium from coal fly ashes." J.Environ.Qual., 36(6), 1784-1792.

Warren, L. A., Maurice, P. A., Parmar, N., and Ferris, F. G. (2001). "Microbially mediated calcium carbonate precipitation: implications for interpreting calcite precipitation and for solid-phase capture of inorganic contaminants." Geomicrobiol.J., 18(1), 93-115.

Xu, Y., Nakajima, T., and Ohki, A. (2001). "Leaching of arsenic from coal fly ashes 1. leaching behavior of arsenic and mechanism study." Toxicological & Environmental Chemistry, 81(1-2), 55-68.

7. Chapter 7: Summary, Contribution, and Future work

7.1 Introduction

Coal ash is a by-product of coal combustion process in power plants. A significant portion of the generated coal ash is disposed of in impoundments and landfills. Gradual deposition of coal ash can induce excessive shear stresses and lead to internal and external structural instabilities. Furthermore, the leaching of trace elements from these materials is a concern especially with respect to the potential of increasing the concentrations in the environment above the drinking water or ecological system standards. Interdisciplinary research has revealed new techniques to modify engineering properties of subsurface materials. Microbial induced calcium carbonate precipitation (MICP) is a bio-mediated process that has shown the potential for improving the engineering properties of soils as well as the potential of immobilizing trace elements (e.g., Sr 90). Work in this thesis was focused on evaluating the effect of MICP treatment on Class-F coal ash as a means of addressing the above mentioned concerns. For this purpose, two different areas are investigated, first, the effect of MICP on engineering properties of coal ash, and second, the effect of MICP on leachable trace elements, specifically arsenic and selenium.

7.2 Summary and general discussion

Factors affecting the chemistry and kinetic reactions of MICP treatment of three coal ash materials (CA1, CA2, and CA3) were investigated. The treatment protocol was developed by performing several column tests on CA1 material. The proposed bio-cementation treatment recipe is a mix of 100 ml of the following chemical solutions (Table 7-1) and 15 ml of the bacteria solution with OD~1.

Table 7-1. Chemical solutions in treatment protocol recipes.

[Urea] (M)	[CaCl2] (M)	NH4Cl (M)
0.4	0.1	0.1
0.4	0.2	0.1

The treatment protocol was applied to the coal ash materials and the monitored specimens' V_S indicated significant cementation level of two of the study fly ashes and slight cementation level of the third. To understand the reason of such a difference in improvement response, the following possible factors were investigated; a) *S. Pasteurii* bacteria activity inhibitors, b) bacteria filtration by coal ash particles c) particle roughness and its effect on calcium carbonate attachment, d) calcium carbonate precipitation inhibitors, and e) nucleation site for calcium carbonate precipitation.

Results indicated that the carbon content of coal ash material showed an important role in calcium carbonate nucleation and precipitation between particles. The results of applying the treatment protocol on the coal ash materials showed the minimal V_S improvement in CA2 while CA1 had the maximum improvement. CA2 had the minimum carbon content, which was 0.5%, and it was 3.4% and 8.6% for CA1 and CA3, respectively. CA3 had higher carbon content in comparison to CA1 while showed less V_S increase per injection. Factors affecting the shear wave velocity of the MICP treated specimens include the effective confinement pressure, calcium carbonate content, particle size distribution, level of grain packing, and particles' morphology. Having coarser particles in material decreases both specific surface area and number of contact points per the same volume of solid. Therefore, less calcium carbonate content is needed to have the same level of V_S increase. For this reason, the results of CA1 and CA3 materials treatment showed different average increase in V_S. The coal ash material CA1 has coarser particle size distribution compared to CA3; V_S increase for CA1 was more than CA3 at the same mass of calcium carbonate precipitation per

injection (e.g., in modified consolidation setup, the magnitude of increase in Vs was 17 m/s and 9 m/s per injection for CA1 and CA3, respectively). It seems that both CA1 and CA3 materials have sufficient carbon content to initiate calcium carbonate nucleation and precipitation, and after that, the particle size distribution was the governing factor for controlling the average V_S increase.

A modified consolidation setup was developed to evaluate the effect of MICP treatment on compressibility parameters of the coal ash materials. This modification added the ability to compute shear wave velocity, to inject the treatment solution into the specimens, and to measure the induced solution pressure during injection. MICP treatment decreased the compressibility of the coal ash materials with such magnitude of reduction larger at the lower levels of applied vertical stress. Increasing the level of stress resulted in decementation, or calcium carbonate bond breakage, with a corresponding reduction of the cementation effect on stiffness or compressibility. Correlations between small strain and large strain parameters were proposed as a means to predict the compressibility of untreated and treated coal ash materials for a given stress level and V_S value. These correlations are based on the study of the two coal ash materials that were successfully cemented. Generalization of such correlations requires further study on the effect of MICP treatment on other coal ash materials.

Chemical equilibrium modeling and experimental batch testing were utilized to study the effect of MICP treatment on the leaching of arsenic and selenium from the tested fly ash. The combined results of modeling and batch testing indicated that MICP treatment could immobilize selenium through co-precipitation. However, it seems that the mechanism was not effective in immobilizing arsenic. One of the main factors affecting the solubility of the trace elements is the pH of the solution. Generally, decreasing the pH level can decrease the solubility of the negatively charged trace elements (e.g., arsenic and selenium) while this reduction increases the solubility of the most

positively charged trace elements (e.g., cadmium and strontium). The level of pH during the MICP treatment process can be controlled by varying the ratio of urea to $CaCl_2$. As long as the [HU] is lower than $[CaCl_2]_{in}$, the maintained pH was low (e.g., the pH of all the specimens in batch testing with [1:1] recipe except [4:4] sample was lower than 8). When the [HU] in the solution was close to or greater than the $[CaCl_2]_{in}$ the pH of the solution increased up to maximum values of 9.3 as was measured during the experimental program. Therefore, designing staged treatment process with controlled pH levels can potentially provide an approach for targeting the solubility of specific trace elements of concern. The treatment protocol to improve the shear stiffness of the coal ash has a ratio of [2:1] (i.e., [Urea:$CaCl_2$]) and [4:1] recipes which led to a pH of 9.3 after hydrolyzing all the urea in the solution. If the goal is to maintain a low pH to decrease solubility of an element of concern, the pH of the solution can be decreased by having a lower the Urea to $CaCl_2$ ratio. The effect of using such low ratio to attain a certain level of shear stiffness improvement is yet to be studied.

7.3 Factors affecting the kinetic of urea hydrolysis via *S. Pasteurii*

7.3.1 Summary

The knowledge and tools to understand the MICP treatment were developed in this chapter. For this purpose, the ureolytic chemical reactions in MICP were modeled to study the effect of different parameters including pH, initial concentrations, and concentration of hydrolyzed urea on the chemical equilibrium state. Electrical conductivity measurements were developed as a monitoring method to assess the kinetics of the MICP reactions after the implementation of proper calibration approach. The effect of population of bacteria and initial concentration of urea is also assessed. An experimental study was designed using a set of column tests and utilizing Ottawa 50-70 sand in

order to investigate the applicability of using electrical conductivity as a monitoring method during the MICP soil stabilization process.

7.3.2 Contributions

The main contributions of this chapter include:

- Based on the results of chemical equilibrium modeling, the correlation between pH, precipitated calcium carbonate, and hydrolyzed urea was found while evaluating different recipes.
- The correlation between electrical conductivity and concentration of hydrolyzed urea was developed, and it was used to introduce the conductivity meter as a monitoring method for different systems.
- The kinetics of hydrolyzing urea with *S. pasteurii* bacteria was investigated using electrical conductivity measurements. The effect of initial substrate (i.e., urea) and *S. pasteurii* cell population on the kinetic of the reaction was explored and compared with the previous studies which were used jack bean enzyme as an urease agent.

7.3.3 Future work

- The correlation between the OD of the solution and *S. pasteurii* cell population is needed to express the results based on cell population instead of the OD. For this purpose, counting plate method can be used.
- The substrate concentration in batch testing was limited to 200 mM, the extent of substrate concentration is of interest to cover the range of urea concentration which is used in MICP treatment. It will also clarify whether the $[U_0]$-initial rate of urea hydrolysis curves reach a plateau while the $[U_0]$ increases.

7.4 Microbial induced calcium carbonate precipitation on coal ash

7.4.1 Summary

In this chapter, the effect of MICP treatment on the coal ash material was investigated. A soil column testing program is performed on coal ash from different power plants. The testing program encompassed the development and optimization of the treatment process. Shear wave velocity, calcium carbonate content, and microscale images are utilized to assess the response of coal ash to the MICP treatment. To optimize the treatment recipe, different approaches were explored, and the best treatment process was recommended. A comprehensive study was performed on the different possible factors potentially affecting the MICP treatment of coal ash including: A) *Sporosarcina pasteurii* bacteria activity inhibitors, B) bacteria filtration by coal ash particles C) particle roughness and its effect on calcium carbonate attachment, D) calcium carbonate precipitation inhibitors, E) nucleation site for calcium carbonate precipitation.

7.4.2 Contributions

- The protocol of MICP treatment on coal was developed after evaluating different methods and recipes, and applied to three coal ash materials with different physiochemical and engineering characteristics.
- Monitoring shear wave velocity during treatment using the developed protocol indicated that the coal ash materials responded differently while treated similarly. The presence and pattern of calcium carbonate was investigated using SEM/EDS analysis.
- The limitation of MICP treatment was identified on one the coal ash materials. Several possible factors affecting the MICP treatment of coal ash were investigated. The

results indicated that carbon content is the dominant factor affecting the MICP treatment of coal ash. The hypothesis is the carbon and carbide material in coal ash can provide the nucleation site for calcium carbonate crystal growth and the lack of this material would inhibit calcium carbonate precipitation.

7.4.3 Future work

- Roughness is one of the factors controlling the attachment of precipitated calcium carbonate on a surface. There were more agglomerated particles in CA1 and CA3 materials compared to CA2 material, which is related to coal combustion and cooling process, and they may provide roughness and nucleation sites for calcium carbonate precipitation. Understanding the effect of agglomerated particles on calcium carbonate precipitation requires further investigations.
- The carbon content of the coal ash showed an important role in calcium carbonate precipitation of coal ash materials. The hypothesis is the carbon and carbide material in coal ash can provide the nucleation site for calcium carbonate crystal growth and the lack of this material would inhibit calcium carbonate precipitation. Confirming this hypothesis needs to be further investigated.
- The treatment protocol was developed and successfully implemented in small scale specimens. The extent of the treatment scale to large scale and field implementation is of interest. There are several possible options for performing this treatment method in the field including: permeation grouting, deep soil mixing, well injection depth extraction (WIDE) but to confirm possibility further investigations are required.

- The development of enzyme induced calcium carbonate precipitation (EICP) treatment protocol for coal ash is a matter of interest. The enzyme size is much smaller than bacteria size, and it can help minimize bio-agent filtration.

7.5 Effect of MICP treatment on engineering properties of coal ash

7.5.1 Summary

The objective of the study presented in Chapter 5 was to experimentally explore the effect of MICP treatment on engineering properties of coal ash material. Compressibility, hydraulic conductivity, and shear wave velocity were the target parameters to be investigated. Traditional odometer testing equipment was modified to provide the ability to inject treatment solution and to measure shear wave velocity. The large-strain and small-strain parameters were extracted from the experimental data for untreated and treated specimens, and a discussion is provided on the level of cementation's effect on different parameters.

7.5.2 Contributions

The following conclusions were advanced based on the results reported in chapter 5;

- The large-strain results demonstrated a reduction in compressibility (C_C and m_v) for treated coal ash in comparison to untreated material. This reduction is more at lower levels of applied vertical stresses.
- Increasing the $CaCO_3$ content of the specimens using MICP treatment increased the shear wave velocity and decreased the void ratio. For the same material, these parameters converged to the same values while the vertical effective stress increased from 24 to 1530 kPa.

- Effect of loading-unloading cycles on decementation (calcium carbonate bond breakage) of MICP treated specimens were evaluated by monitoring shear wave velocities. The resultant shear wave velocity of the second unloading curve for all the treated specimens indicated that the applied level of loading (i.e., σ'_v =1530 kPa) had broken all the cementation bonds or could not break anymore.
- Bio-cementation decreased the initial hydraulic conductivity (k_i) of the studied material, and this reduction was to the extent of 0.05 of initial hydraulic conductivity for maximum level of cementation.
- The effect of MICP treatment on large-strain parameters (i.e., C_C, m_v, k, C_V, m_v) and small-strain parameters (i.e., α, β, α', β') were examined, and the correlation between small-strain parameters (i.e., C_C) and large-strain parameters (i.e., α', β') were determined from experimental data.

7.5.3 Future work

- The effect of bio-cementation and loading-unloading cycles on K_0 of the coal ash is a point of interest. Adding horizontal sensors in oedometer ring can add the ability of monitoring K_0.
- The effect of MICP treatment on shear strength response of coal ash is unknown and need further investigation to better understand its effect on stability of coal ash impoundments.

7.6 Effect of MICP treatment on arsenic and selenium leaching behavior of coal ash

7.6.1 Summary

The objective of chapter 6 was to investigate the effect of MICP process to specifically minimize arsenic and selenium leaching potential. To find an optimized protocol to reduce the concentration of the elements of concerns in leachate, factors affecting the solubility of the elements (e.g., pH and salinity of the solution) and the chemical reactions occurring during MICP treatment were assessed. Chemical equilibrium modeling and batch testing were used to evaluate the effect of pH, salts, and MICP treatment on leaching behavior of arsenic and selenium in a Class-F fly ash.

7.6.2 Contributions

Combining the results of batch testing and chemical equilibrium modeling advanced following contributions;

- The arsenic and selenium adsorption/desorption of fly ash were successfully modeled running chemical equilibrium modeling (i.e., MINTEQ program), and the modeling was calibrated to suggest the backbone pH-[As] curve using results of batch testing.
- MICP treatment did not immobilize arsenic leaching from tested coal ash through co-precipitation. However, the treatment recipe can be designed to decrease the level of pH in solution which corresponds to lower [As] in leachate during treatment.
- Results of batch testing indicated that MICP treatment can decrease the [Se] in leachate through calcium carbonate co-precipitation.

7.6.3 Future work

- The variation of trace elements' concentration of studied fly ash while the pH of the solution is varied can be further investigated performing a batch acidimetric-alkalimetric titration test. These results can be used for suggesting the maximum adsorption densities and also for deriving the adsorption constants for different elements. The backbone pH-[c] curves can be used as the baseline to check the efficiency of treatment recipes.
- The extent of the effect of MICP treatment on mobilization/immobilization of other elements of concern (e.g., chromium, strontium, and boron) is of interest.
- The long term effect of MICP treatment on mobilization/immobilization of trace elements can be explored through a sequential leaching test.

REFERENCES

Ainsworth, C. C., and Rai, D. (1987). "Chemical characterization of fossil fuel combustion wastes: Final report.".

ASTM D 854-00. (2000). "Standard Test for Specific Gravity of Soil Solids by Water Pycnometer." *ASTM International, West Conshohocken, PA*.

ASTM D422-63. (2007). "D422–63 (2007) Standard test method for particle-size analysis of soils." *ASTM International, West Conshohocken.Doi,* 10 1520.

Aurelio, G., Fernandez-Martinez, A., Cuello, G. J., Roman-Ross, G., Alliot, I., and Charlet, L. (2010). "Structural study of selenium (IV) substitutions in calcite." *Chem.Geol.,* 270(1), 249-256.

Bachmeier, K. L., Williams, A. E., Warmington, J. R., and Bang, S. S. (2002). "Urease activity in microbiologically-induced calcite precipitation." *J.Biotechnol.,* 93(2), 171-181.

Bachus, R., and Santamarina, C. (2012). "Geotechnical Properties of Fly ASH and Potential for Static Liquefaction: Volume I–Summary and Conclusions." *EPRI, Palo Alto, CA*.

Bachus, R. C., and Santamarina, J. C. (2014). "Geotechnical Properties and Diagenesis of Ponded Fly Ash." *Geo-Congress 2014: Geo-characterization and Modeling for Sustainability*, Geo-Congress 2014, 326-333.

Benjamin, M. M. (2014). *Water chemistry*. Waveland Press.

Berner, R. A. (1975). "The role of magnesium in the crystal growth of calcite and aragonite from sea water." *Geochim.Cosmochim.Acta,* 39(4), 494504.

Bhattacharyya, S., Donahoe, R. J., and Patel, D. (2009). "Experimental study of chemical treatment of coal fly ash to reduce the mobility of priority trace elements." *Fuel,* 88(7), 1173-1184.

Bothe, J. V., and Brown, P. W. (1999). "Arsenic immobilization by calcium arsenate formation." *Environ.Sci.Technol.,* 33(21), 3806-3811.

Cascante, G., and Santamarina, J. C. (1996). "Interparticle contact behavior and wave propagation." *J.Geotech.Eng.,* 122(10), 831-839.

CCRs Rules. (2015). "Hazardous and Solid Waste Management System; Disposal of Coal Combustion Residuals From Electric Utilities: Final Rule." United States Environmental Protection Agency, Washington, DC.

Cha, M., Santamarina, J. C., Kim, H., and Cho, G. (2014). "Small-strain stiffness, shear-wave velocity, and soil compressibility." *J.Geotech.Geoenviron.Eng.,* 140(10), 06014011.

Clarke, L. B. (1993). "The fate of trace elements during coal combustion and gasification: an overview." *Fuel,* 72(6), 731-736.

Clarke, L. B., and Sloss, L. L. (1992). *Trace elements-emissions from coal combustion and gasification.* IEA Coal Research, .

Daniels, B. L. (2016). "Caution: Hazards Ahead: How the EPA's Refusal to Classify Coal Ash as Hazardous Waste Fuels Environmental and Public Health Concerns." *Vill.Envtl.LJ,* 27 93.

De Leeuw, N. H. (2002). "Molecular dynamics simulations of the growth inhibiting effect of Fe2, Mg2, Cd2, and Sr2 on calcite crystal growth." *The Journal of Physical Chemistry B,* 106(20), 5241-5249.

DeBoer, R. B. (1977). "Influence of seed crystals on the precipitation of calcite and aragonite." *Am.J.Sci.,* 277(1), 38.

DeJong, J. T., Mortensen, B. M., Martinez, B. C., and Nelson, D. C. (2010). "Bio-mediated soil improvement." *Ecol.Eng.,* 36(2), 197-210.

EPA, U. S. (2003). "National primary drinking water standards." *Office of Water, US Environmental Protection Agency.Washington, DC, United States Environmental Protection Agency,* .

Feng, K., and Montoya, B. M. (2015). "Drained shear strength of MICP sand at varying cementation levels." *IFCEE 2015,* 2242-2251.

Feng, K., and Montoya, B. M. (2014). "Behavior of Bio-Mediated Soil in k 0 Loading." *New Frontiers in Geotechnical Engineering,* 1-10.

Fidaleo, M., and Lavecchia, R. (2003). "Kinetic study of enzymatic urea hydrolysis in the pH range 4-9." *Chemical and Biochemical Engineering Quarterly,* 17(4), 311-318.

Fujita, Y., Taylor, J. L., Wendt, L. M., Reed, D. W., and Smith, R. W. (2010). "Evaluating the potential of native ureolytic microbes to remediate a 90Sr contaminated environment." *Environ.Sci.Technol.,* 44(19), 7652-7658.

Giroud, J. P. (2010). "Development of criteria for geotextile and granular filters." *Proceedings of the 9th International Conference on Geosynthetics, Guaruja, Brazil,* 4564.

Greenwood, N. N., and Earnshaw, A. (1984). "Chemistry of the Elements.".

Gustafsson, J. P. (2013). "Visual MINTEQ version 3.1, department of sustainable development." *Environmental Science and Engineering, KTH, Stockholm*.

Hammad, I. A., Talkhan, F. N., and Zoheir, A. E. (2013). "Urease activity and induction of calcium carbonate precipitation by Sporosarcina pasteurii NCIMB 8841." *Journal of Applied Sciences Research,* 9(3), 1525-1533.

Hansen, L. D., and Fisher, G. L. (1980). "Elemental distribution in coal fly ash particles." *Environ.Sci.Technol.,* 14(9), 1111-1117.

Hardin, B. O., and Drnevich, V. P. (1972). "Shear modulus and damping in soils: design equations and curves." *Journal of Soil Mechanics & Foundations Div,* 98(sm7).

Harkness, J. S., Sulkin, B., and Vengosh, A. (2016a). "Evidence for coal ash ponds leaking in the southeastern United States." *Environ.Sci.Technol.,* 50(12), 6583-6592.

Harkness, J. S., Sulkin, B., and Vengosh, A. (2016b). "Evidence for Coal Ash Ponds Leaking in the Southeastern United States." *Environ.Sci.Technol.,* 50(12), 6583.

Huggins, F. E., Senior, C. L., Chu, P., Ladwig, K., and Huffman, G. P. (2007). "Selenium and arsenic speciation in fly ash from full-scale coal-burning utility plants." *Environ.Sci.Technol.,* 41(9), 3284-3289.

Izquierdo, M., and Querol, X. (2012a). "Leaching behaviour of elements from coal combustion fly ash: an overview." *International Journal of Coal Geology,* 94 54-66.

Izquierdo, M., and Querol, X. (2012b). "Leaching behaviour of elements from coal combustion fly ash: an overview." *International Journal of Coal Geology,* 94 54-66.

Jankowski, J., Ward, C. R., French, D., and Groves, S. (2006). "Mobility of trace elements from selected Australian fly ashes and its potential impact on aquatic ecosystems." *Fuel,* 85(2), 243-256.

Jones, D. R. (1995). "The leaching of major and trace elements from coal ash." *Environmental aspects of trace elements in coal,* Springer, 221-262.

Kaniraj, S. R., and Gayathri, V. (2004). "Permeability and consolidation characteristics of compacted fly ash." *J.Energy Eng.,* 130(1), 18-43.

Katz, J. L., Reick, M. R., Herzog, R. E., and Parsiegla, K. I. (1993). "Calcite growth inhibition by iron." *Langmuir,* 9(5), 1423-1430.

Kim, A. G. (2002). "Physical and chemical characteristics of CCB." *Proceedings of Coal Combustion By-Products and Western Coal Mines: A Technical Interactive Forum. Allton, IL: US Department of the Interior, Office of Surface Mining,* 25-42.

Kim, A. G., and Hesbach, P. (2009). "Comparison of fly ash leaching methods." *Fuel,* 88(5), 926-937.

Kutchko, B. G., and Kim, A. G. (2006). "Fly ash characterization by SEM–EDS." *Fuel,* 85(17–18), 2537-2544.

Lebron, I., and Suarez, D. L. (1996). "Calcite nucleation and precipitation kinetics as affected by dissolved organic matter at 25 C and pH> 7.5." *Geochim.Cosmochim.Acta,* 60(15), 2765-2776.

Lecuyer, I., Bicocchi, S., Ausset, P., and Lefevre, R. (1996). "Physico-chemical characterization and leaching of desulphurization coal fly ash." *Waste Manage.Res.,* 14(1), 15-28.

Lin, H., Suleiman, M. T., Brown, D. G., and Kavazanjian Jr, E. (2015). "Mechanical behavior of sands treated by microbially induced carbonate precipitation." *J.Geotech.Geoenviron.Eng.,* 142(2), 04015066.

Link, D. D., Walter, P. J., and Kingston, H. M. (1998). "Development and validation of the new EPA microwave-assisted leach method 3051A." *Environmental Science and Technology,* 32(22), 3628-3632.

Martinez, B. C., DeJong, J. T., Ginn, T. R., Montoya, B. M., Barkouki, T. H., Hunt, C., Tanyu, B., and Major, D. (2013). "Experimental optimization of microbial-induced carbonate precipitation for soil improvement." *J.Geotech.Geoenviron.Eng.,* 139(4), 587-598.

Mayne, P. W., and Kulhawy, F. H. (1982). "Ko- OCR Relationships in Soil." *Journal of the Soil Mechanics and Foundations Division,* 108(6), 851-872.

Mohan, D., and Singh, K. P. (2002). "Single-and multi-component adsorption of cadmium and zinc using activated carbon derived from bagasse—an agricultural waste." *Water Res.,* 36(9), 2304-2318.

Montoya, B. M., DeJong, J. T., Boulanger, R. W., Wilson, D. W., Gerhard, R., Ganchenko, A., and Chou, J. (2012). "Liquefaction mitigation using microbial induced calcite precipitation." *GeoCongress 2012: State of the Art and Practice in Geotechnical Engineering,* 1918-1927.

Mortensen, B. M., Haber, M. J., DeJong, J. T., Caslake, L. F., and Nelson, D. C. (2011). "Effects of environmental factors on microbial induced calcium carbonate precipitation." *J.Appl.Microbiol.,* 111(2), 338-349.

Moulder, J. F. (1995). *Handbook of x-ray photoelectron spectroscopy: a reference book of standard spectra for identification and interpretation of XPS data.* Physical Electronics, Eden Prairie, Minn.

Mullin, J. W. (2001). *Crystallization.* Butterworth-Heinemann, .

Narukawa, T., Takatsu, A., Chiba, K., Riley, K. W., and French, D. H. (2005). "Investigation on chemical species of arsenic, selenium and antimony in fly ash from coal fuel thermal power stations." *Journal of Environmental Monitoring,* 7(12), 1342-1348.

Nijhuis, M., and Kendrick, R. (2014). "Can coal ever be clean." *Retrieved October,* 7 2015.

Poykio, R., Manskinen, K., Nurmesniemi, H., and Dahl, O. (2011). "Comparison of trace elements in bottom ash and fly ash from a large-sized (77 MW) multi-fuel boiler at the power plant of a fluting board mill, Finland." *Energy Explor.Exploit.,* 29(3), 217-233.

Praharaj, T., Powell, M. A., Hart, B. R., and Tripathy, S. (2002). "Leachability of elements from sub-bituminous coal fly ash from India." *Environ.Int.,* 27(8), 609-615.

Reardon, E. J., Warren, C. J., and Hobbs, M. Y. (1993). "Reduction of trace element concentrations in alkaline waste porewaters by dedolomitization." *Environ.Sci.Technol.,* 27(2), 310-315.

Reddy, M. M., and Nancollas, G. H. (1976). "The crystallization of calcium carbonate: IV. The effect of magnesium, strontium and sulfate ions." *J.Cryst.Growth,* 35(1), 33-38.

Rhoades, J. D. (1996). "Salinity: electrical conductivity and total dissolved solids." *Methods of Soil Analysis Part 3—Chemical Methods,* (methodsofsoilan3), 417-435.

Santamarina, J. C., Klein, A., and Fam, M. A. (2001). "Soils and waves: Particulate materials behavior, characterization and process monitoring." *Journal of Soils and Sediments,* 1(2), 130.

Shanahan, C., and Montoya, B. M. (2016). "Erosion Reduction of Coastal Sands Using Microbial Induced Calcite Precipitation." *Geo-Chicago 2016,* 42-51.

Shanahan, C., and Montoya, B. M. "Erosion Reduction of Coastal Sands Using Microbial Induced Calcite Precipitation." *Geo-Chicago 2016,* 42-51.

Shaw, W. H. (1954). "The inhibition of urease by various metal ions." *J.Am.Chem.Soc.,* 76(8), 2160-2163.

Silberman, D., and Harris, W. R. (1984). "Determination of arsenic (III) and arsenic (V) in coal and oil fly ashes." *Int.J.Environ.Anal.Chem.,* 17(1), 73-83.

Styszko-Grochowiak, K., Gołaś, J., Jankowski, H., and Koziński, S. (2004). "Characterization of the coal fly ash for the purpose of improvement of industrial on-line measurement of unburned carbon content." *Fuel,* 83(13), 1847-1853.

Upadhyay, L. S. B. (2012). "Urease inhibitors: A review.".

Van der Hoek, Eline E, and Comans, R. N. (1996). "Modeling arsenic and selenium leaching from acidic fly ash by sorption on iron (hydr) oxide in the fly ash matrix." *Environ.Sci.Technol.,* 30(2), 517-523.

Van Paassen, L. A. (2009). "Biogrout, ground improvement by microbial induced carbonate precipitation." .

Vavouraki, A. I., Putnis, C. V., Putnis, A., and Koutsoukos, P. G. (2008). "An atomic force microscopy study of the growth of calcite in the presence of sodium sulfate." *Chem.Geol.*, 253(3), 243-251.

Walton, W. H., and Butler, W. (2009). "Root Cause Analysis of TVA Kingston Dredge Pond Failure on December 22, 2008." *Vernon Hills*.

Wang, J., Wang, T., Burken, J. G., Chusuei, C. C., Ban, H., Ladwig, K., and Huang, C. P. (2008). "Adsorption of arsenic (V) onto fly ash: A speciation-based approach." *Chemosphere*, 72(3), 381-388.

Wang, T., Wang, J., Burken, J. G., Ban, H., and Ladwig, K. (2007). "The leaching characteristics of selenium from coal fly ashes." *J.Environ.Qual.*, 36(6), 1784-1792.

Warren, L. A., Maurice, P. A., Parmar, N., and Ferris, F. G. (2001a). "Microbially mediated calcium carbonate precipitation: implications for interpreting calcite precipitation and for solid-phase capture of inorganic contaminants." *Geomicrobiol.J.*, 18(1), 93-115.

Warren, L. A., Maurice, P. A., Parmar, N., and Ferris, F. G. (2001b). "Microbially mediated calcium carbonate precipitation: implications for interpreting calcite precipitation and for solid-phase capture of inorganic contaminants." *Geomicrobiol.J.*, 18(1), 93-115.

Whiffin, V. S. (2004). "Microbial CaCO3 precipitation for the production of biocement". Murdoch University, .

Xiao, X., Yang, H., Zhang, H., Lu, J., and Yue, G. (2005). "Research on carbon content in fly ash from circulating fluidized bed boilers." *Energy Fuels*, 19(4), 1520-1525.

Xu, Y., Nakajima, T., and Ohki, A. (2001). "Leaching of arsenic from coal fly ashes 1. leaching behavior of arsenic and mechanism study." *Toxicological & Environmental Chemistry*, 81(1-2), 55-68.

Yun, T. S., and Evans, T. M. (2011). "Evolution of at-rest lateral stress for cemented sands: experimental and numerical investigation." *Granular Matter*, 13(5), 671-683.

Yun, T. S., and Santamarina, J. C. (2005). "Decementation, softening, and collapse: changes in small-strain shear stiffness in k 0 loading." *J.Geotech.Geoenviron.Eng.*, 131(3), 350-358.

APPENDICES

Appendix A: Chemical equilibrium modeling of MICP

The chemical reactions in MICP were modeled using the chemical equilibrium program, MINTEQ 3.1 (Gustafsson 2013). To understand the equilibrium state, equations including mass balances, chemical equilibrium expressions, and a charge balance, proton condition, or total hydrogen (TOTH) were used. In this part, the concentration of all the chemicals to prepare the systems are known, and the final equilibrium condition is the outcome of interest (Benjamin 2014).

The calcium carbonate precipitation in solutions with different initial concentration of $CaCl_2$ ($[CaCl_2]_{in}$) was simulated by titration of hydrolyzed urea. A solution with $[CaCl_2]_{in}$=0.5 M is exemplified to present the steps of MICP modeling herein. The pH of the solution were computed using mass and charge balance equations, and the ionic strength of the solution was selected to be calculated by variation of ions concentrations, the selected options for defining the method of computing pH and ionic strength in MINTEQ program can be found in Figure A1-1. 1 M of CO_3^{2-} and 2 M of NH_4^- are equivalent to 1 M hydrolyzed urea based on Equation 1 in Chapter 3, and these ratios were used to input hydrolyzed urea in the program. Therefore, 0.5 M of Ca^{2+} and 1 M of Cl^- were the inputs of modeling to represent 1 M of $CaCl_2$, as demonstrated in Figure A1-2.

Figure A1-1. Method and input in modeling.

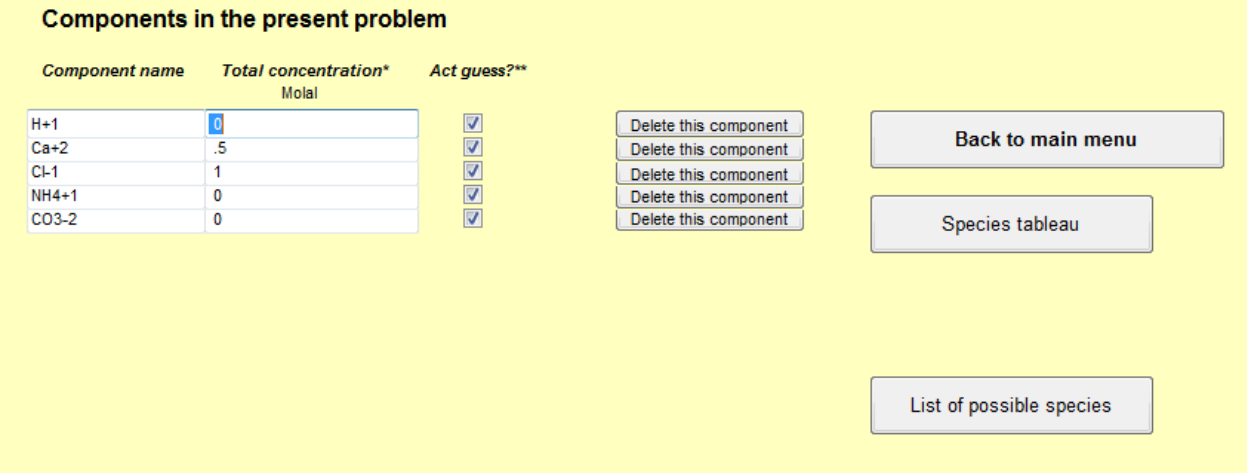

Figure A1-2. Inputs in modeling of MCIP with $[CaCl_2]_{in}$ = 0.5 M.

Different possible solid crystals might precipitate with the existence of Ca^{2+}, CO_3^{2-}, OH^-, and O^{2-}. Their name, formula, and equilibrium Constants are listed in Table 3-1 in Chapter 3. In possible

solid phases in MINTEQ, different possible compositions of $CaCO_3$ solids were defined based on the MINTEQ data base, and they are presented in Figure A1-3.

The range of concentration of hydrolyzed urea was varied between 0 to 1000 mM, and the resultant pH and $CaCO_{3(s)}$ were monitored. For this purpose, the "titration/mixing with a titrant with defined composition" option was selected to vary [HU] in the $CaCl_2$ solution in a close system. The titration option and the defined outputs in the modeling are shown in Figure A1-4. To increase the [HU], 1 L of the solution to be titrated was mixed with 0.001 L (1 mL) of 50 M HU solution (i.e., 50 M CO_3^{2-} and 100 M NH_4^-) in each increment, as demonstrated in Figure A1-5. 21 increments were needed to increase the [HU] of the solution from 0 to 1M. pH, [Calcite], and [NH_4^+] were chosen to be reported in outputs of modeling (Figure A1-4). The [HU] and outputs (i.e., pH, [Calcite], and [NH_4^+]) of MINTEQ modeling for the solution with $[CaCl_2]_{in}$= 0.5 M are presented in Table A1-2. The pH and [$CaCO_{3(s)}$] of the solutions with different $[CaCl_2]_{in}$ were investigated conducting the same chemical equilibrium modeling.

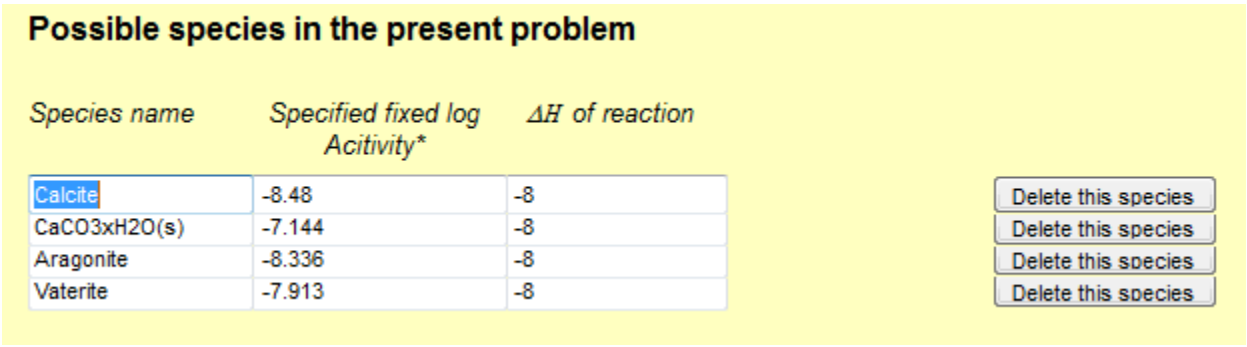

Figure A1-3. Different possible $CaCO_3$ solids in MICP equilibrium modeling and their solid constants.

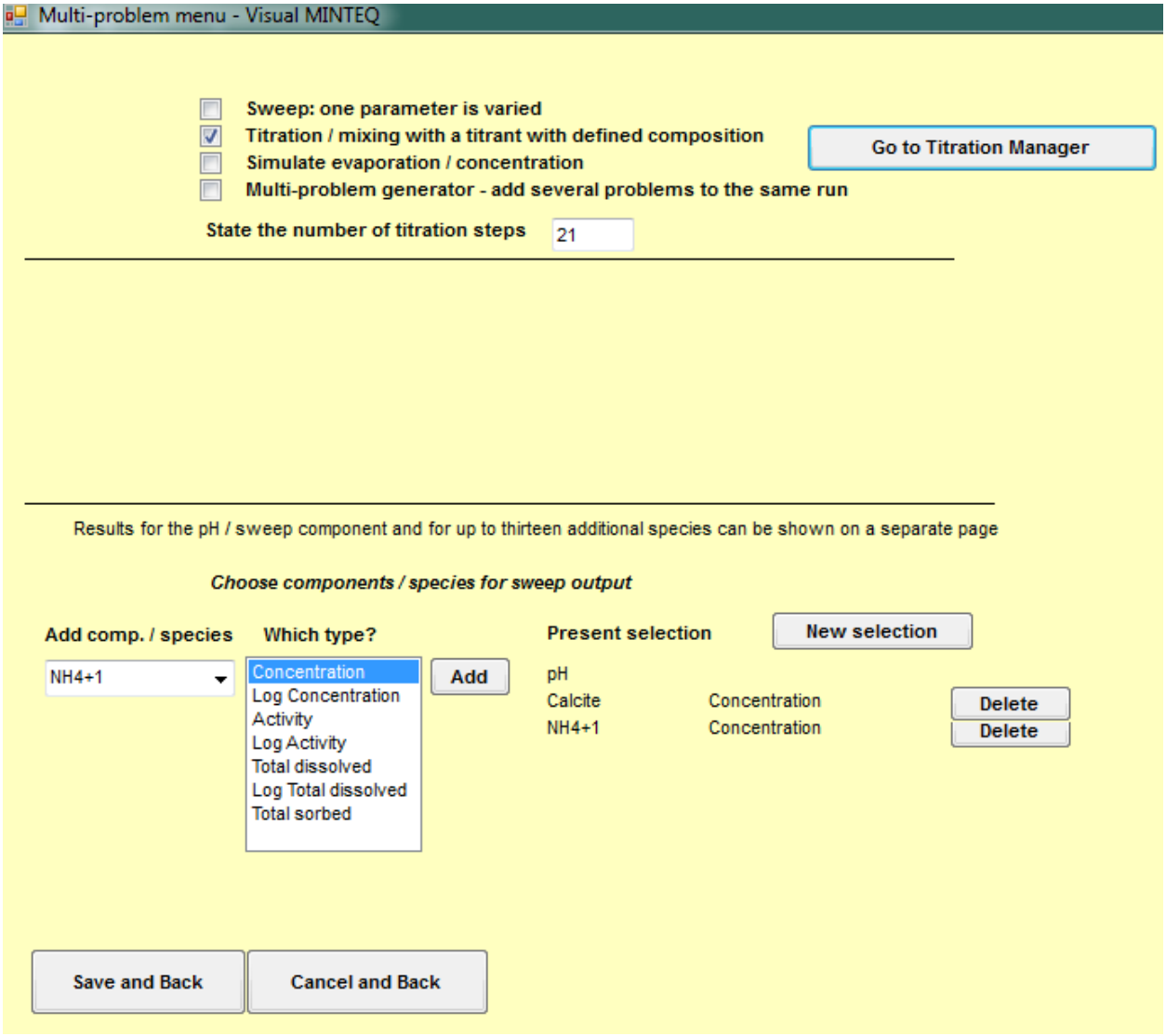

Figure A1-4. Hydrolyzed urea titration and outputs of chemical equilibrium modeling in MINTEQ.

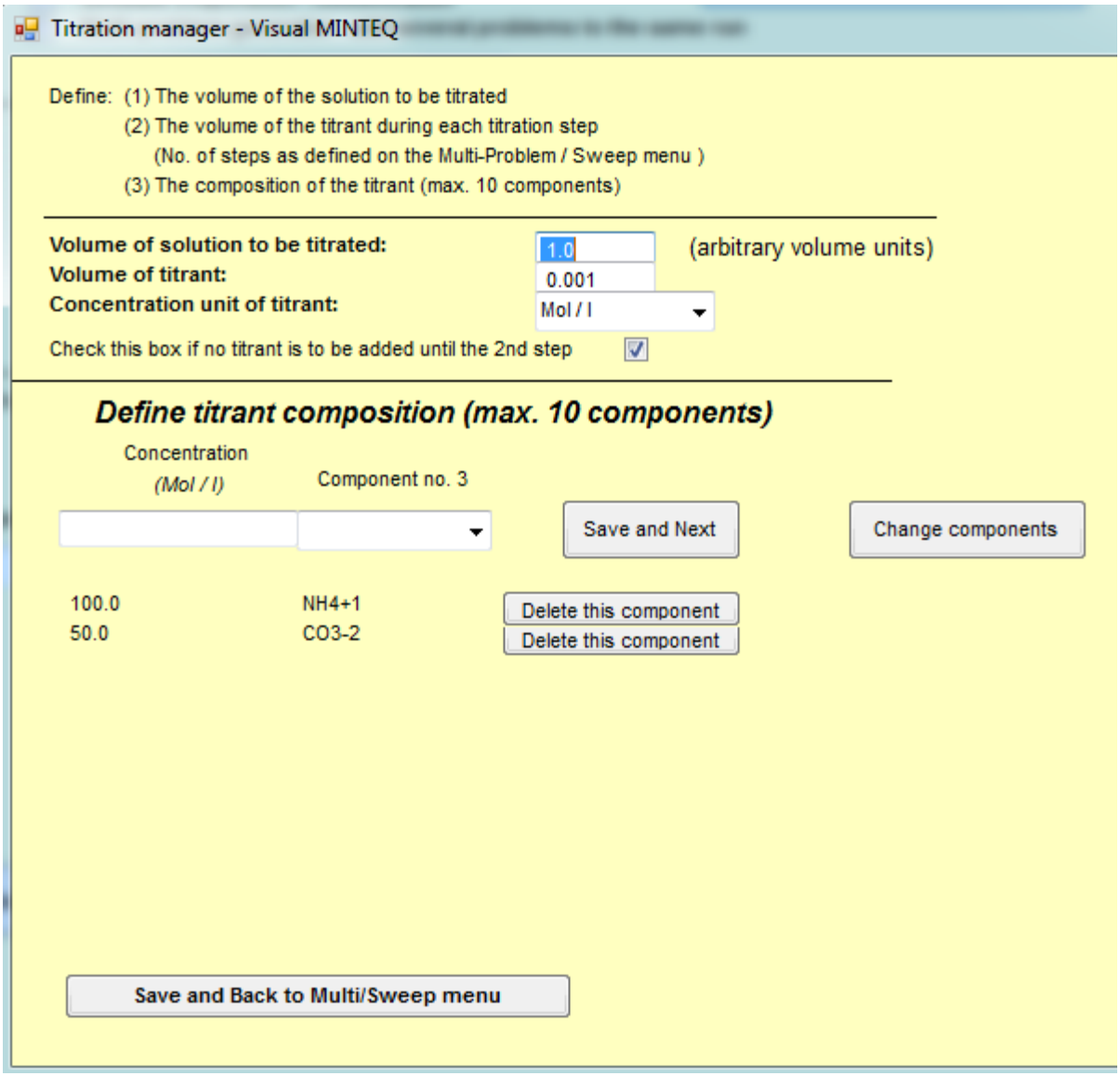

Figure A1-5. Hydrolyzed urea titration in MINTEQ modeling.

Table A1-2. Outputs of MICP modeling for a solution contained $[CaCl_2]_{in}$ = 0.5 M.

Problem number	[HU]	pH	Calcite	NH_4^{+1}
	M	-	M	M
1	0.00	6.75	0.00	0.00
2	0.05	6.82	0.05	0.10
3	0.10	6.71	0.10	0.20
4	0.15	6.66	0.15	0.30
5	0.20	6.63	0.20	0.40
6	0.25	6.62	0.25	0.50
7	0.30	6.63	0.30	0.60
8	0.35	6.66	0.35	0.69
9	0.40	6.70	0.40	0.79
10	0.45	6.81	0.44	0.89
11	0.50	7.22	0.49	0.98
12	0.54	8.12	0.49	1.04
13	0.59	8.40	0.49	1.09
14	0.64	8.55	0.49	1.14
15	0.69	8.65	0.49	1.19
16	0.74	8.73	0.49	1.24
17	0.79	8.79	0.49	1.29
18	0.84	8.84	0.49	1.34
19	0.88	8.87	0.49	1.39
20	0.93	8.91	0.49	1.45
21	0.98	8.94	0.49	1.50

References

Benjamin, M. M. (2014). *Water chemistry*. Waveland Press.

Gustafsson, J. P. (2013). "Visual MINTEQ version 3.1, department of sustainable development." *Environmental Science and Engineering, KTH, Stockholm*.

Appendix B: Adsorption/desorption Modeling

The adsorption/desorption of arsenic (V) and selenium (IV) was modeled using chemical equilibrium modeling in MINTEQ in Chapter 6. The steps for modeling in MINTEQ are explained in this appendix.

The validated model for arsenic in Chapter 6 is exemplified here to explain the conducted steps for adsorption/desorption modeling. The data were collected from a study that was conducted by Wang et al. 2008. The maximum released [As] and maximum site density were reported, respectively, 7.5E-06 mole/gr and 0.6 mg/l based on acidimetric/alkalimetric batch testing. The competitive Langmuir adsorption model, which is a non-electrostatic model, was used to model the solubility of arsenic as a function of pH. There are one adsorbate and multiple adsorbents in competitive Langmuir adsorption model. Equations 1, 2, and 3 demonstrated the pH dependency of different As (V) forms in a solution (Wang et al. 2008), which is in agreement with the MINTEQ database;

$$H_3AsO_4 \Leftrightarrow H_2AsO_4^- + H^+,\ pK_{a1} = 2.26 \quad (1)$$

$$H_2AsO_4^- \Leftrightarrow HAsO_4^{2-} + H^+,\ pK_{a2} = 6.76 \quad (2)$$

$$HAsO_4^- \Leftrightarrow AsO_4^{3-} + H^+,\ pK_{a3} = 11.29 \quad (3)$$

Based on the reported results in Wang et al. 2008 study, considering three adsorption sites resulted in best curve fitting for adsorption of different elements, and one of the adsorption sites was determined to be the only adsorbent of arsenic (i.e., positively charged surface hydroxyl). The adsorption reaction of different arsenic species was expressed as presented in equation 4, 5, and 6 (Wang et al. 2008).

$$SOH_2^+ + H_2AsO_4^- \Leftrightarrow S\text{-}H_2AsO_4 + H_2O;K_{S1} \quad (4)$$

$SOH_2^+ + HAsO_4^{2-} \Leftrightarrow S\text{-}HAsO_4^- + H_2O;\ K_{S2}$ (5)

$SOH_2^+ + AsO_4^{3-} \Leftrightarrow S\text{-}H_2AsO_4 + H_2O;\ K_{S3}$ (6)

The reported values for K_{S1} and K_{S2} were, respectively, 4.4 (or 5.9 kcal mol^{-1}) and 7.9 (or 10.6 kcal mol^{-1}), and the maximum arsenic adsorption density was $7.5x10^{-6}$ mole/(gr ash). At pH of 10 and lower, the AsO_4^{3-} concentration is low, so the adsorption constant of AsO_4^{3-} (i.e., K_{S3}) was not reported. Equation 7 correlates the positively and neutrally charged surface hydroxyl groups and pH (Wang et al. 2008).

$SOH + H^+ \Leftrightarrow SOH_2^+,\ K_H = 10^{3.5}$ (7)

5 gr of fly ash was incubated with 100 ml of the solutions with different additional [arsenic] to investigate the adsorption/desorption of the material. The solution containing 10 mg arsenic was considered to calibrate and validate modeling. 0.142 mM or 10.6 mg/L (i.e., 0.6 mg/L of the maximum released fly ash plus 10 mg/L of additional arsenic) of As (V) was the input component in the program, as presented in Figure A2-1. Figure A2-2 indicates the non-electrostatic model (NEM) and the site concentration were used in the validated model. Higher site density than what was reported in Wang et al. 2008 was used to calibrate modeling regarding the reported data. In this model (i.e., NEM), the neutrally charged surface hydroxyl is the default adsorption site in MINTEQ. Positively charged surface hydroxyl was identified to be the only adsorbent of arsenic in the reported fly ash, Equation 7 was used to correlate the positively and negatively charged surface density and pH of the solution. Figure A2-3 shows the way site densities and pH of the solution were correlated in MINTEQ program. The adsorption reaction of different arsenic species were expressed as presented in equation 4 and 5. In order to define the pH dependency of different arsenic forms' adsorption, these equations were converted to equations 9 and 10 using thermodynamic rules to have neutrally charged hydroxyl site instead of positively charged. Figure

A2-4 and Figure A2-5 present the input values for defining $H_2AsO_4^-$ and $HAsO_4^{2-}$ adsorption on fly ash particles, respectively.

$$SOH + 3H^+ + AsO_4^{3-} - H_2O \Leftrightarrow S\text{-}H_2AsO_4 \text{ , } K_{ads,1} = 10^{25.95} \quad (9)$$

$$SOH + 2H^+ + AsO_4^{3-} - H_2O \Leftrightarrow S\text{-}HAsO_4 \text{ , } K_{ads,1} = 10^{22.69} \quad (10)$$

The pH of the solution was varied in modeling using the sweep option in MINTEQ. For this purpose, the pH of the solution was increased with 0.5 increments in a range of between 2 to 12, the selected sweep options, values and selected outputs (i.e., pH, total dissolved arsenate, and total sorbed arsenate) are presented in Figure A2-6. The resultant outputs of modeling are presented in Figure A2-7.

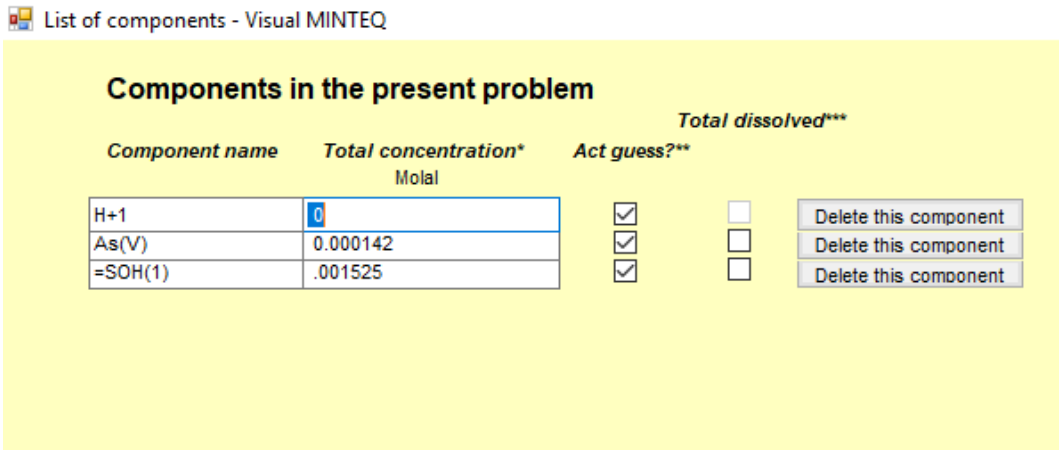

Figure A2-1. Input components for validation model.

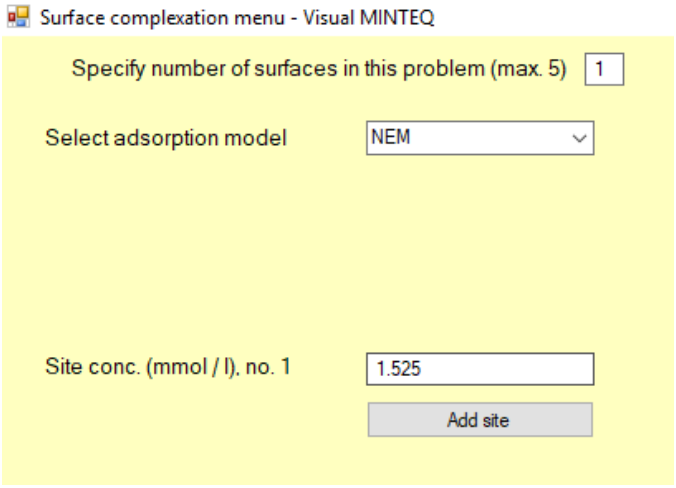

Figure A2-2. Adsorption model and site concentration in arsenic modeling for validation.

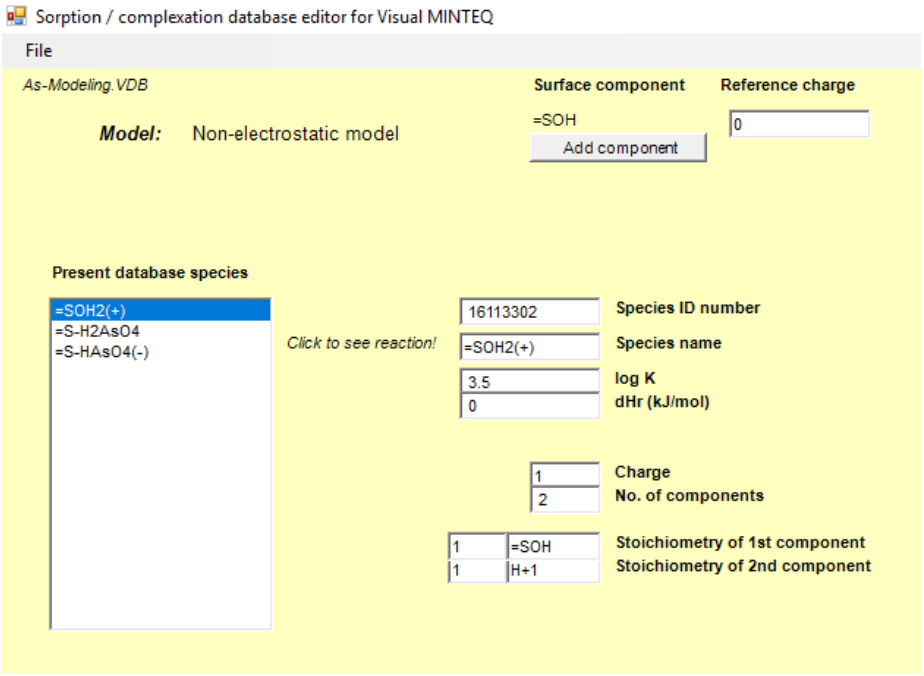

Figure A2-17. Correlation between sites densities and pH in validated model.

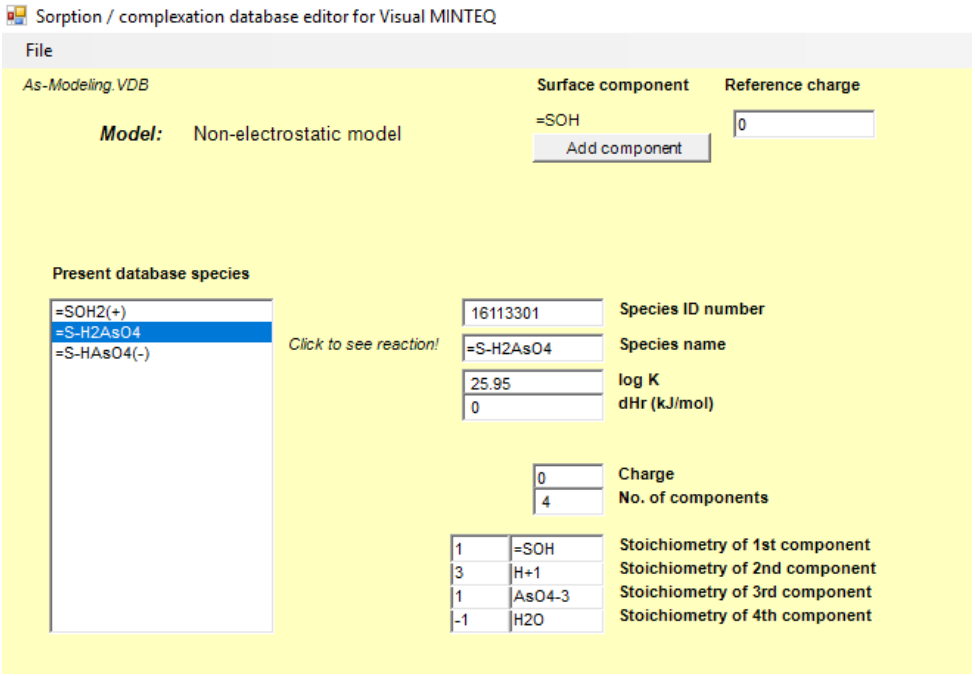

Figure A2-4. Input values for defining adsorption of $H_2AsO_4^-$ on the positively charged hydroxyl groups in validated MINTEQ modeling.

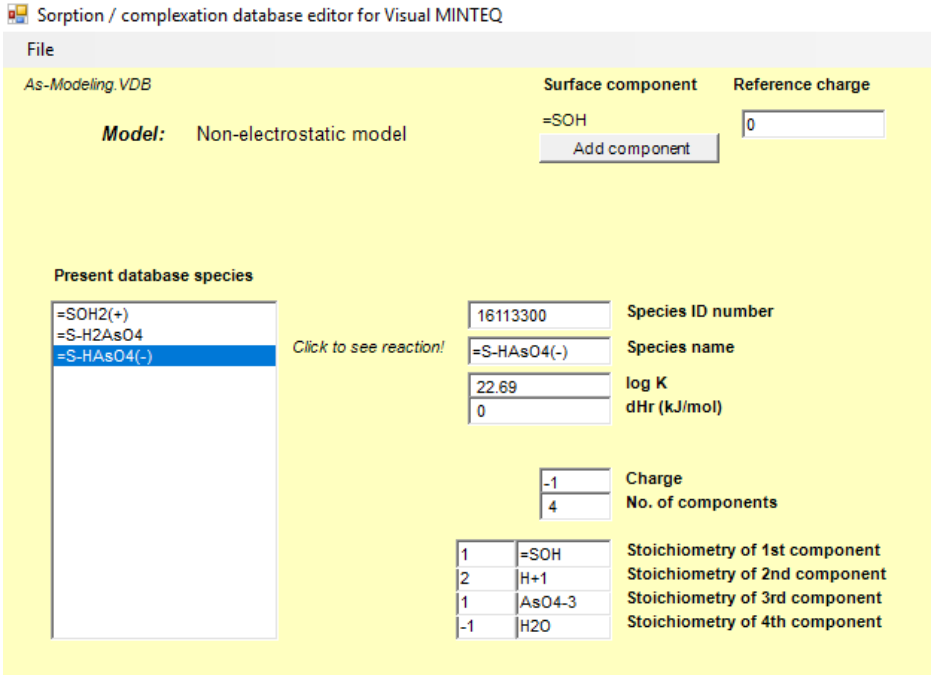

Figure A2-5. Input values for defining adsorption of HAsO42- on the positively charged hydroxyl groups in validated MINTEQ modeling.

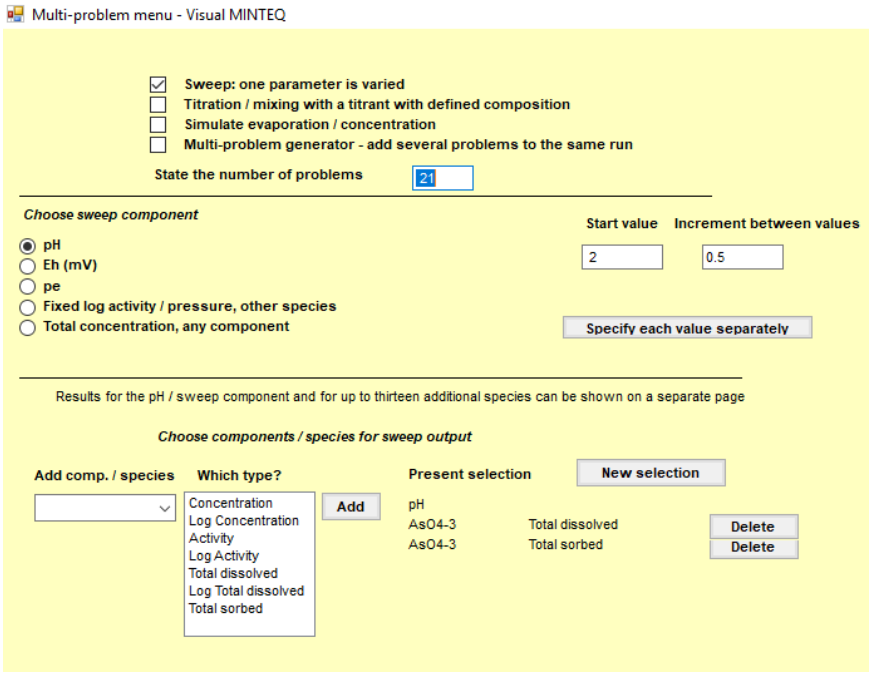

Figure A2-6. pH variation and chosen sweep outputs in modeling.

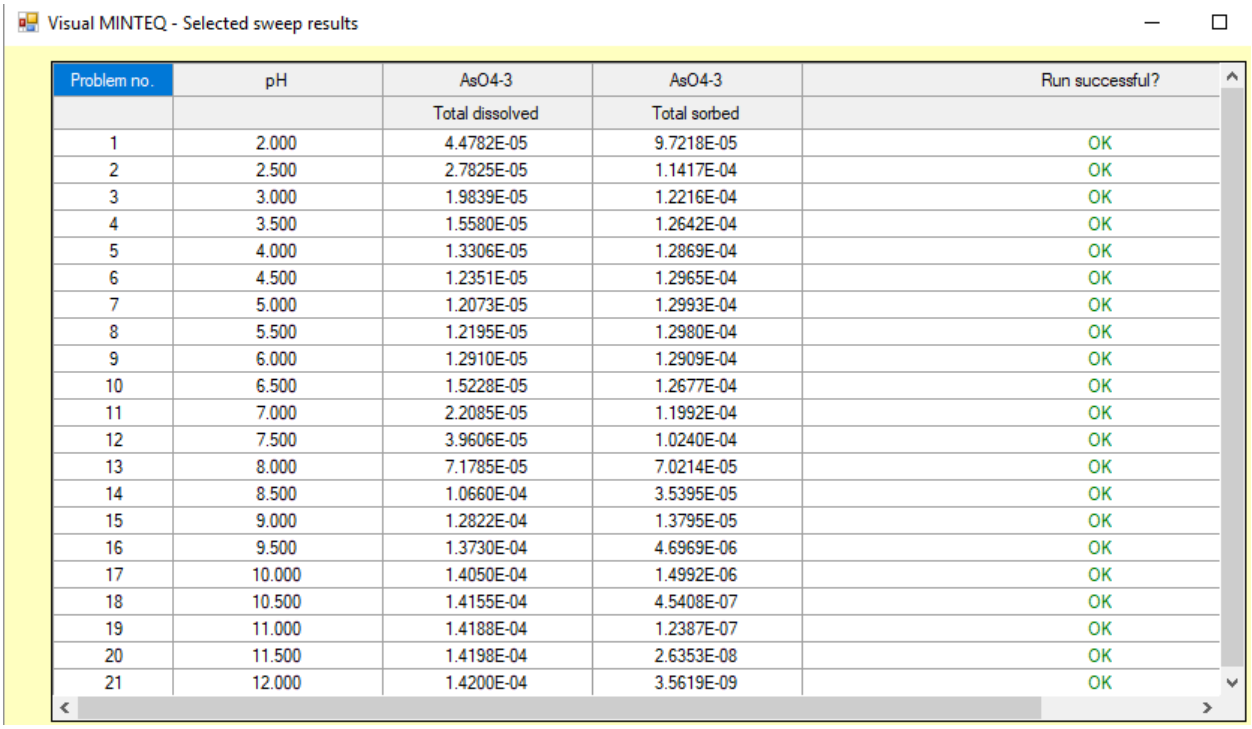

Problem no.	pH	AsO4-3 Total dissolved	AsO4-3 Total sorbed	Run successful?
1	2.000	4.4782E-05	9.7218E-05	OK
2	2.500	2.7825E-05	1.1417E-04	OK
3	3.000	1.9839E-05	1.2216E-04	OK
4	3.500	1.5580E-05	1.2642E-04	OK
5	4.000	1.3306E-05	1.2869E-04	OK
6	4.500	1.2351E-05	1.2965E-04	OK
7	5.000	1.2073E-05	1.2993E-04	OK
8	5.500	1.2195E-05	1.2980E-04	OK
9	6.000	1.2910E-05	1.2909E-04	OK
10	6.500	1.5228E-05	1.2677E-04	OK
11	7.000	2.2085E-05	1.1992E-04	OK
12	7.500	3.9606E-05	1.0240E-04	OK
13	8.000	7.1785E-05	7.0214E-05	OK
14	8.500	1.0660E-04	3.5395E-05	OK
15	9.000	1.2822E-04	1.3795E-05	OK
16	9.500	1.3730E-04	4.6969E-06	OK
17	10.000	1.4050E-04	1.4992E-06	OK
18	10.500	1.4155E-04	4.5408E-07	OK
19	11.000	1.4188E-04	1.2387E-07	OK
20	11.500	1.4198E-04	2.6353E-08	OK
21	12.000	1.4200E-04	3.5619E-09	OK

Figure A2-7. Outputs of the validated adsorption/desorption modeling of arsenic using MINTEQ.

References

Gustafsson, J. P. (2013). "Visual MINTEQ version 3.1, department of sustainable development." *Environmental Science and Engineering, KTH, Stockholm,* .

Wang, J., Wang, T., Burken, J. G., Chusuei, C. C., Ban, H., Ladwig, K., and Huang, C. P. (2008). "Adsorption of arsenic (V) onto fly ash: A speciation-based approach." *Chemosphere,* 72(3), 381-388.